TITLE A STUDY OF MONOCARBON CARBABORANES AND SOME METALLA DERIVATIVES

AUTHOR Michael John Jasstal

INSTITUTION and DATE University of Warwick 1988

A STUDY OF MONOCARBON CARBABORANES AND SOME METALLA DERIVATIVES

by

Michael John Jaastal

A thesis submitted to the University of Warwick in partial fulfilment of the requirements for the degree of Doctor of Philosophy

Department of Chemistry
University of Warwick
Coventry
CV4 7AL

CONTENTS

ACKNOWLEDGEMENT

I am indebted to my wife, Judith, and our children, Nathan, Matthew and Luke for their support, understanding and tolerance of my endeavours.

Special thanks are due to Professor Malcolm G. H. Wallbridge for his unique charm and supervision throughout the period of this work.

I would also like to express my thanks to Dr Nathaniel W. Alcock for teaching me the X-ray crystallographic theory and techniques that have enabled me to carry out the X-ray crystallographic work contained in this thesis. The thrill and experience of producing molecular structures of the compounds that I prepared is much valued.

For much appreciated joviality, thanks are also due to Barry Turner, Andy Edmunds, Tony Parker, Mark Shand, Kevin Buttar, Jim Barker, Lawrence Judd and Richard Whitaker.

The Quota Award from the Science and Engineering Research Council that made this work possible is gratefully acknowledged, as are the efforts of Drs. O. W. Howarth, E. Curzon and A. Harrison (University of Warwick) and Drs. I. Sadler and D. Read (University of Edinburgh) for the recording of n.m.r. spectroscopic data.

A final thank you to Judith for proof reading this manuscript.

DECLARATION

The material contained within this thesis is the findings of independent and original work carried out by the author under the supervision of Professor M. G. H. Wallbridge.

Several portions of the work have been published in the chemical literature and presented at national and international boron chemistry conferences. Details are given in the publications list.

Michael John Jaszta1

August 1988

CONFERENCE PAPERS AND PUBLICATIONS.

CHAPTER 2

PREPARATIVE AND N.M.R. STUDIES ON MONOCARBON CARBABORANES.

A paper presented by Michael J. Jasztal at the Fourth National Meeting of British Inorganic Boron Chemists, INTRABORON IV, Grey College, Durham University, September 24-26, 1984.

A STUDY OF 4-CARBA-ARACHNO-NONABORANE(14) AND THE DERIVED TRIDECAHYDRO-4-CARBA-ARACHNO-NONABORANE(-1) ANION ; STRUCTURE AND C-H BOND ACTIVATION AS SHOWN BY 1- AND 2-D N.M.R.

A paper by O. W. Howarth, M. J. Jasztal, J. G. Taylor and M. G. H. Wallbridge, (Polyhedron, 1985, 4, 1461).

CHAPTER 3

STUDIES ON METALLA DERIVATIVES OF THE MONO CARBON CARBABORANE $CB_9H_{14}^-$.

A paper presented by Michael J. Jasztal at the Fifth National Meeting of British Inorganic Boron Chemists, INTRABORON V, Edinburgh University, September 4-6, 1985.

THE SYNTHESIS AND CRYSTAL AND MOLECULAR STRUCTURES OF SOME TEN VERTEX (MCB$_9$; M = Ru or Os) METALLACARBABORANES; [9,9,9-(CO)(PPh$_3$)$_2$-NIDO-9,6-MCB$_8$H$_{10}$-5-(PPh$_3$)] (M = Ru or Os) and [9,9,9-(η-C$_5$H$_5$)(H)(PPh$_3$)-ARACHNO-9,6-RuCB$_8$H$_{12}$].

A paper by Nathaniel W. Alcock, Michael J. Jasztal and Malcolm G. H. Wallbridge. (J. Chem. Soc., Dalton Trans., 1987, 2793).

CHAPTER 4

THE SYNTHESIS AND CRYSTAL AND MOLECULAR STRUCTURES OF SOME GOLD DERIVATIVES OF CARBANONABORANE(14).

A paper presented by Malcolm G. H. Wallbridge at the Sixth International Meeting of Inorganic Boron Chemists, IMEBORON VI, Bechyne, Czechoslovakia, June 22-26, 1987.

ABSTRACT

The work described in this thesis was carried out to explore the chemistry of carbanonaborane(14), CB_8H_{14}. Incorporation of metal atoms into the molecular framework was of particular interest.

An n.m.r. investigation of the monocarbaboranes CB_8H_{14} and $[CB_8H_{13}]^-$ indicated the presence of unsymmetrical bridging hydrogen atoms in both carbaboranes. More significantly, the endo-hydrogen attached to the carbon atom is involved in exchange with all the three bridging hydrogen atoms in the anion, whereas no such exchange is observed in the neutral precursor.

The reaction of $[MCl(CO)(H)(PPh_3)_3]$ (M = Ru, Os) with $Li[CB_8H_{13}]$ yields the nido-metallacarbaboranes $[(CO)(PPh_3)_2MCB_8H_{10}(PPh_3)]$. Both compounds have a decaborane(14) like cage structure with the 6- and 9-positions occupied by CH and $[M(PPh_3)_2(CO)]$ fragments. Minor products of these reactions have been isolated and characterised as two isomeric chlorinated nido ruthenacarbaboranes and two isomeric closo ruthena- and osmacarbaboranes. A similar reaction with $[Ru(Cl)(\eta\text{-}C_5H_5)(PPh_3)_2]$ yields the arachno species $[(\eta\text{-}C_5H_5)(H)(PPh_3)RuCB_8H_{12}]$ (3). In this case the cage arrangement is similar to that in $[B_{10}H_{14}]^{2-}$ with the 6- and 9- positions substituted by CH_2 and $[RuH(\eta\text{-}C_5H_5)(PPh_3)]$ fragments.

The metalla derivatives isolated from reaction of $Li[CB_8H_{13}]$ with gold reagents, $Au(PR_3)Cl$, were all found to have arachno structures. These auracarbaboranes all have a triple cluster structure consisting of a carbaborane-gold-carbaborane sandwich. The central gold cluster unit consists of either one, two, or seven gold atoms. The heptanuclear gold cluster is the most novel of these auracarbaboranes and displays a different geometry of the central gold cluster to that of the only other known heptanuclear gold cluster.

ABBREVIATIONS

cm^{-1}	-	Wave number (i.r.)
COSY	-	2 dimensional COrrelation SpectroscopY
dppe	-	Bis(diphenylphosphino)ethane, $Ph_2PCH_2CH_2PPh_2$
dppm	-	Bis(diphenylphosphino)methane, $Ph_2PCH_2PPh_2$
dppp	-	Bis(diphenylphosphino)propane, $Ph_2PCH_2CH_2CH_2PPh_2$
diphos	-	Ortho-Phenylenebis(dimethylphosphine), $o\text{-}C_6H_4(P(CH_3)_2)_2$
Et	-	Ethyl group
Hz	-	Hertz
HOMO	-	Highest Occupied Molecular Orbital
i.r.	-	Infra-red
^nJ	-	Coupling constant (Hz), over n bonds (n.m.r.)
L	-	Ligand; electron pair donor
LCAO	-	Linear Combination of Atomic Orbitals
LUMO	-	Lowest Unoccupied Molecular Orbital
min	-	Minutes
M	-	Metal atom
Me	-	Methyl group
M.O.	-	Molecular Orbital
n.m.r.	-	Nuclear Magnetic Resonance
Ph	-	Phenyl group
pm	-	Picometre (m^{-12})
p.p.m.	-	Parts per million (n.m.r.)
R	-	Alkyl group
SEP	-	Skeletal Electron Pair
SEPT	-	Skeletal Electron Pair Theory
thf	-	Tetrahydrofuran
t.l.c.	-	Thin layer chromatography
η	-	η^5 (π) bonding mode of ($\pi^5\text{-}C_5H_5$) to metal atom

KEY FOR STRUCTURAL FIGURES

In order to reduce the complexity of the diagrams of boranes, carbaboranes and metallacarbaboranes clusters contained in Chapter 1 and elsewhere, the following symbols have been used to represent the differing skeletal atoms;

For each of these structural diagrams, reference to the molecular formula (or formulae) provided in the Figure title will assist comprehension of the symbolism used.

In order to achieve clarity in the diagrams of the skeletal structures of the metallacarbaboranes, the ligands bonded to the metal have either been omitted except for the coordinating atom or only partially drawn. The nature of the ligands are given in the Figure title accompanying the diagram.

Whilst the $B-H_{(terminal)}$ hydrogen atoms have been routinely omitted from these diagrams, the endo hydrogens have been included when they are of significance.

The drawings of X-ray structures in Chapters 3 and 4 were produced by computer from the original X-ray solution data files and have been individually labelled.

DEDICATION

To my wife Judith, our children, Nathan, Matthew and Luke

and my mother and father, Kathleen and Henryk.

CHAPTER ONE

CHAPTER 1. INTRODUCTION.

Prior to describing the metallacarbaborane syntheses that form the theme of this thesis, the following brief review of carbaborane and metallacarbaborane chemistry has been made to complement the discussion of these new compounds.

1.1. GENERAL FEATURES OF CARBABORANE CLUSTERS.

The term 'carbaborane' describes a class of compounds related to the boron hydride (borane) clusters by substitution of one or more skeletal boron atoms by carbon atoms. The neutral boranes and anionic boranes characterised by Alfred Stock[1] and the more recently synthesised isoelectronic carbaboranes[2,3] can be classified into the stoichiometries shown in Table 1. Clusters with different stoichiometries to those tabulated are nevertheless isoelectronic, though notable exceptions to this are discussed later. The carbaboranes are derived from the boranes by the notional substitution of a BH group and a hydrogen atom by the isoelectronic CH group, (CH = BH + H$^+$).

In principle any group which is isolobal with a skeletal boron unit can be substituted into the framework to give the corresponding hypothetical heteroborane, though the synthetic route to the compound is normally less easily formulated. Isolobal groups have the same number of 'frontier' bonding orbitals (of the similar symmetry, shape and energy) containing the same number of electrons[4]. Such 'Isolobal Mapping' is of immense value in comparing the vast range of known organic compounds to the known or hypothetical organometallic analogues. An extensive review of the topic was given by Hoffman in

Table 1. Stoichiometry and structural class of the boron hydrides and isoelectronic carbaboranes.

Structural class	Boron hydride	Carbaborane	No of SEP's
Closo	$[B_nH_n]^{2-}$	$C_xB_{n-x}H_{n+2-x}$	n + 1
Nido	B_nH_{n+4}	$C_xB_{n-x}H_{n+4-x}$	n + 2
Arachno	B_nH_{n+6}	$C_xB_{n-x}H_{n+6-x}$	n + 3

Table 2. Heteroboranes which are isoelectronic and isostructural with arachno-$[B_{10}H_{14}]^{2-}$ (13 SEP's)

Heteroborane	Formula	Isoelectronic equivalence
1) Carbaborane[5]	$CB_9H_{13}L$	CH = BH + e^-
2) Azaborane[6]	$[NB_9H_{13}]^-$	NH = BH + H^-
3) Thiaborane[6]	$[SB_9H_{12}]^-$	SH = BH + H^- + H'
4) Platina-borane[7]	$[Pt(PEt_3)_2B_9H_{11}L]$	$Pt(L)_2$ = BH + H^-

Figure 1. Structure of heteroborane clusters isoelectronic with $[B_{10}H_{14}]^{2-}$

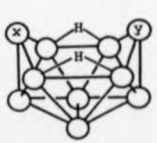

	x	y
1)	CH	B(L)
2)	NH	BH_2
3)	S	BH_2
4)	$Pt(L)_2$	BH(L)

his 1981 Nobel Prize lecture[4].

Heteroboranes containing various main group elements as well as a range of transition metal atoms of suitable oxidation state are known. A relevant series of such compounds is shown in Table 2[5,6,7].

In general, carbaboranes and other heteroboranes, like the boranes, have molecular structures in which the skeletal atoms define the vertices of a range of regular triangular faced polyhedra[8] (see Figure 2). Clusters that deviate from the geometries shown in Figure 2 are few in number, the reasons for which are discussed later. Those clusters that define completely the 'n' vertices of a polyhedron with 'n' skeletal atoms have been designated the structural classification 'Closo'. A significant number of boron based clusters have structures in which one to three vertices of the polyhedra are unoccupied. These 'fragment cages' have been designated the structural classifications, 'Nido', 'Arachno' and 'Hypho' when their 'n' skeletal atoms conform to the polyhedron with (n + 1), (n + 2) and (n + 3) vertices respectively. The relationship between closo, nido and arachno clusters is illustrated in Figure 2, the hypho class is not shown because only a few clusters with such open structures are known.

Williams[8] has noted that in the nido fragment clusters the unoccupied vertex is usually the most highly connected, with adjacent vertices being unoccupied in the more open arachno and hypho clusters.

Carbaboranes with stoichiometries where x = 1 to 4 (See Table 1) and various values of 'n' are known[2,3]. The largest group are the so called dicarbaboranes, where x = 2. The monocarbaboranes, x = 1, are less numerous and the carbon-rich carbaboranes[9], x = 3, 4 less still. Some of the known mono- and di- carbaboranes are tabulated in Tables 3, and 4 respectively, together with a description of the gross

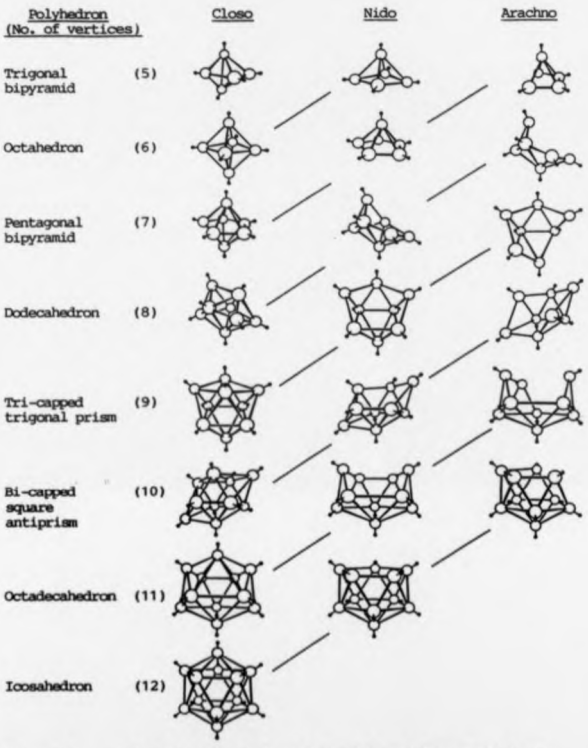

Figure 2. Polyhedral geometries of complete and 'fragment' boron based clusters. (Diagram adapted from reference 10).

(Note: Endo hydrogens not shown since the number and position varies according to the hetero atom content.)

polyhedral geometry and for fragment clusters, the shape of the open face. Note that in some cases there are several carbon positional isomers known, (marked by an asterisk in the tables) and only the known parent carboborane species are given.

A large range of metallacarboboranes, too numerous to tabulate, have been characterised[11,12,13,14], the majority of these are derived from the dicarboboranes. The synthesis and structure of some of these, including some metalla-monocarboboranes are discussed later.

Table 3. Monocarboboranes.

Carborane	Polyhedral** shape	Shape of open face
Closo-CB_5H_7	Octahedron	
Nido-CB_5H_9	Pentagonal bipyramid	Pentagonal planar
Nido-CB_8H_{12}	Bi-capped square antiprism*	Hexagonal chair
Arachno-CB_8H_{14}	Octadecahedron	Hexagonal chair
Closo-$[CB_9H_{10}]^-$	Bi-capped square antiprism	
Nido-$[CB_9H_{12}]^-$	Octadecahedron	Hexagonal boat
Closo-$[CB_{10}H_{11}]^-$	Octadecahedron	
Nido-$[CB_{10}H_{13}]^-$	Icosahedron	Pentagonal planar
Closo-$[CB_{11}H_{12}]^-$	Icosahedron	

(* Carbon positional isomers known, ** Shape of parent polyhedron)

TABLE 4. Dicarbaboranes.

Carbaborane	Polyhedral** Shape	Shape of open face
Closo-$C_2B_3H_5$	Trigonal Bi-pyramid*	
Nido-$C_2B_3H_7$	Octahedron	Square planar
Closo-$C_2B_4H_6$	Octahedron*	
Nido-$C_2B_4H_8$	Pentagonal Bi-pyramid	Pentagonal planar
Closo-$C_2B_5H_7$	Pentagonal Bi-pyramid*	
Closo-$C_2B_6H_8$	Dodecahedron	
Closo-$C_2B_7H_9$	Tri-capped trigonal prism	
Nido-$C_2B_7H_{11}$	Bi-capped square antiprism	Pentagonal buckled
Arachno-$C_2B_7H_{13}$	Octadecahedron	Hexagonal chair
Closo-$C_2B_8H_{10}$	Bi-capped square antiprism*	
Nido-$C_2B_8H_{12}$	Octadecahedron*	Hexagonal boat
Arachno-$C_2B_8H_{14}$	Icosahedron	Hexagonal boat
Closo-$C_2B_9H_{11}$	Octadecahedron	
Nido-$C_2B_9H_{13}$	Icosahedron	Pentagonal planar
Closo-$C_2B_{10}H_{12}$	Icosahedron*	

(* Carbon positional isomers known, ** Shape of parent polyhedron)

1.2. VALENCE BOND APPROACH TO CLUSTER STRUCTURES.

The catenation observed in boron clusters is a direct result of formal electron deficiency. The bonding in the simplest boron hydride, diborane, illustrates this feature. With twelve electrons available for bonding in B_2H_6, only six two-centre two-electron bonds are possible, one less than that required to connect eight atoms. The structure can only be rationalised by including two-electron three-centre hydrogen bridge bonds (B-H-B), a concept originated by Longuet-Higgins[15,16]. The M.O. description of the B-H-B bond is given in Figure 3a.

A systematic rationale for the bonding in boron hydride clusters, based on the extension of the multicentre bonding concept was devised by Lipscomb[17,18,19], the so called 'Topological description'. The essence of this method is the calculation of the number of two and three centre, two-electron bonds required to connect together all of the skeletal atoms using all of the available valence orbitals and electrons. Three centre B-B-B bonds are also used, formulated by the linear combination of three boron atomic orbitals (LCAO) to produce three molecular orbitals in a similar manner to that for the B-H-B three centre bond, as shown in Fig 3b,c.

Two different three centre boron bonds are derivable, namely the 'open' and 'closed' B-B-B bonds. The pi orbital of the center boron atom (a tangential 2p orbital) in the open three centre B-B-B bond replaces the 1s orbital of a hydrogen atom in the B-H-B bond. The symmetry of the open three centre B-B-B bond is such that the electron density resides on the edge of the trangulated cluster, whilst that of the closed three centre B-B-B bond resides in the centre of a triangular face.

a) Three-centre B-H-B bond

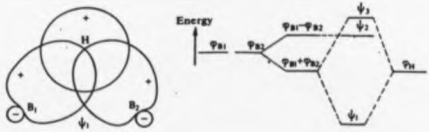

b) Three-centre open B-B-B bond

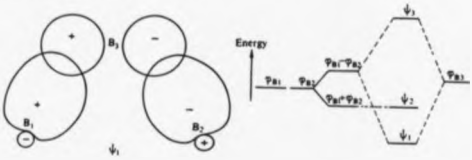

c) Three-centre closed B-B-B bond

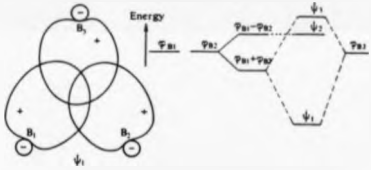

Overlap of atomic orbitals

Energy correlation of molecular orbitals

Figure 3. Molecular orbital diagrams for multicentre bonds, used in the valence-bond description of boron based clusters. (Diagrams reproduced from reference 38)

Possible bonding descriptions are calculated by solving a set of 'equations of balance' to yield one or more 'styx' numbers. Reformulating the general borane stoichiometry as B_pH_{p+q}, the following algebraic equalities relate the number of skeletal electron bond pairs to the necessarily equal total number of two electron skeletal bonds;

$$\text{No of SEP's} = \text{No of skeletal bonds}$$

$$(2p + q)/2 = (s+t+y+x)$$

hence; $\quad s = p - t \quad x = q - s \quad 2y = s - x$

from which a number of possible styx solutions are generated. These numbers, such as the 4220 solution for hexaboranes(10), represent the number of B-H-B bonds, B-B-B bonds, B-B bonds and BH_2 groups respectively, required to depict adequately the bonding in the framework. Each of the possible solutions is evaluated in relation to any symmetry indicated by spectroscopic evidence and by comparison with other known species. Each skeletal atom is assumed to have a terminal exo-polyhedral hydrogen attached.

For hexaboranes(10), the 4220 solution is the most suitable of the alternatives. Arranging the boron atoms as symmetrically as possible, the extra hydrogens are placed around the open face to coincide with the styx description, to yield the topology shown in Figure 4a. This description is only one of a number of canonical resonance structures, that account for the observed symmetry of the molecule, as indicated by the 5 : 1 pattern observed in the ambient temperature ^{11}B n.m.r. spectrum[20]. The rapid bridging hydrogen fluxionality, indicated from the observed ambient temperature n.m.r. spectrum, has been found to be removed at low temperature[21].

a) Topology and molecular structure of B_6H_{10}

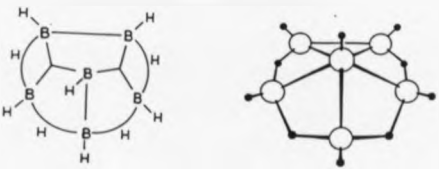

b) Topology and molecular structure of $C_2B_4H_6$

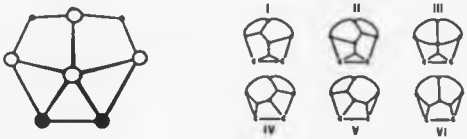

c) Topology of $C_2B_4H_8$ involving 'fractional' three-centre bonding

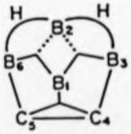

Figure 4. Valence bond description of boranes and carbaboranes.

(Diagrams reproduced from reference 9)

The valence bond description is equally applicable to carbaboranes as shown by comparing the topologies of hexaborane(10) and the isoelectronic dicarbaborane 2,3-dicarbahexaborane(8). The 2240 styx topology of the carbaboranes is fundamentally similar to that of the 4220 topology of the borane, since both have two three centre B-B-B type bonds, albeit a B-B-B and a B-C-B in the carbaboranes. Because of the difference in numbers of endo hydrogens, although the number of electrons remains the same in these analogues, in the carbaboranes there are two fewer B-H-B bridges and consequently two more two centre bonds, as shown in Figure 4b. Nevertheless, the six canonical topologies shown for 2,3-dicarbahexaborane(8), taken as a resonance hybrid give a similar description of the bonding between the apical boron and the basal plane to that of the resonance hybrid of hexaborane(10).

A Self-Consistent Field M.O. treatment of the carbaborane 2,3-dicarbahexaborane(8), has shown that of the six canonical resonance topologies shown in Figure 4.b, the major contributors to the resonance hybrid structure are I and II[22]. The bonding around the basal plane is best described as including a carbon-carbon double bond with one pi bond distorted towards the apical boron, and hence is quite different to the bonding in hexaborane(10) as suggested by the previous simplistic view of the topologies.

A refinement of the valence bond treatment of carbaboranes uses the concept of "fractional" three-centre bonds[23]. An improved valence bond description of $C_2B_4H_8$ using this approach is shown in Figure 4c. A further generalistion has been made by Lipscomb[23], to the effect that the open type of three centre B-B-B bond is not required for the description of boranes, though limited use is found for the valence

description of carbaboranes.

The topological descriptions in Figure 4 show quite clearly that each boron or carbon atom is tetravalent. The diagrams of molecular structure show the apical boron to be six coordinate because it defines only connectivity, regardless of the precise bonding modes involved.

For larger and more symmetrical clusters the valence bond approach is less adequate in accounting for the observed structural symmetry. An alternative approach based on M.O. theory has been developed, as outlined in the next section.

1.3. SKELETAL ELECTRON PAIR THEORY AND RECENT M.O. DESCRIPTIONS.

For electron deficient cluster molecules[24], including carboranes, a structure can be predicted from consideration of the number of skeletal electron pairs available for bonding in the cluster framework[8,11,25,26]. The so called Skeletal Electron Pair Theory (SEPT), originated by K. Wade[25] outlined the following rules[28,29], (also known as 'Wade's Rules');

'For a polyhedral cluster of 'n' atoms, the observed structure will be closo for (n+1) SEP's, nido for (n+2) SEP's and arachno for (n+3) SEP's.'

These rules are compatible with the results of molecular orbital (M.O.) studies of closed and fragment cages. A simple example is the octahedral closo-$[B_6H_6]^{2-}$ system[24]. Each skeletal boron atom contributes three atomic orbitals for skeletal bonding, an sp hybrid and two tangential p orbitals (Figure 5). The overlap of these orbitals (positioned around the surface of a sphere) yields seven bonding M.O.'s, i.e. (n + 1) as shown in Figure 7. The combinations

that produce these M.O.'s are illustrated in Figure 6.

For fragment clusters, such as nido-B_5H_9 and arachno-B_4H_{10} the spatial arrangement of the atoms still generates seven bonding M.O.'s, (n + 2) and (n + 3) respectively. The extra hydrogens ('inner sphere'[19], or 'endo') must be positioned around the open face to retain the symmetry of the skeletal atoms and stabilise the bonding M.O.'s formed. Since closed and fragment polyhedra of 'n' atoms can generate (n + 1), (n + 2) and (n + 3) bonding M.O.'s depending on the symmetry, then a stable system is expected if (n + 1), (n + 2) and (n + 3) skeletal electron pairs are supplied to fill them. It must be noted that whilst these electronic requirements are satisfied by stable species, they only indicate the likely geometry and do not predict that such a compound can be sythesised.

The skeletal electrons are those associated with the inner sphere of boron atoms, hydrogen bridges and the extra hydrogen atoms (endo) of the BH_2 groups. The terminal hydrogens (exo) define the outer sphere.

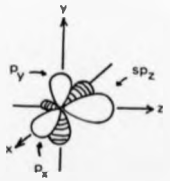

Figure 5. Orbital contribution of BH
(Reproduced from reference 30)

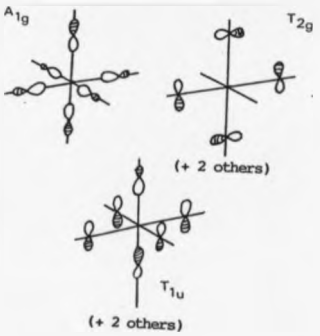

Figure 6. Bonding M.O.'s of $[B_6H_6]^{2-}$.
(Reproduced from reference 30)

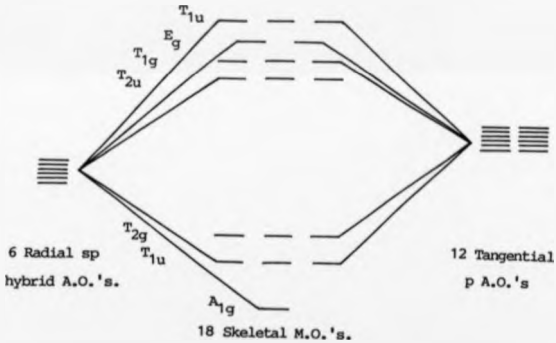

Figure 7. Molecular Orbital diagram for $[B_6H_6]^{2-}$.

Wade's rules apply equally well to formally electron deficient cluster compounds other than the boranes and derivatives, such as the alkali metal alkyls and transition metal carbonyls. For all of these systems the calculation of the electron contribution (e) to the skeleton by a particular skeletal fragment is given by the following formulae, devised by Wade[29],

For a main group element (E), $e = v + x - 2$

For a transitional metal (M), $e = v + x - 12$

where v = number of valence electrons associated with E or M,

x = number of electrons supplied by the exo-polyhedral ligand/s on E or M,

2 = the electrons used to bond the ligand on EL (or EH), or are a lone pair on E,

12 = those electrons used to bond the ligand/s on M and those occupying non-bonding orbitals.

The electron count, (e), for a range of possible skeletal fragments are given in Table 5.

Apparently anomalous values for the electron counts (e) occur for certain cluster moieties of transition metals possessing less than 9 'd' electrons. For example the fragment $Fe(\eta\text{-}C_5H_5)$ is calculated to contribute one electron for cluster bonding. However, the compound $(\eta\text{-}C_5H_5Fe)_2C_2B_6H_8$ has been synthesised[31] and shown to adopt a stable, 10-vertex, closo structure with the iron atoms incorporated into the framework.

MAIN GROUP CLUSTER UNITS (SEP FROM: v + x - 2)

V	Main group element (E)	cluster unit	E (x=0)	EH (x=1)	EH_2 or EL (x=2)
3	B, Al, Ga, In, Tl		1	2	3
4	C, Si, Ge, Sn, Pb		2	3	4
5	N, P, As, Sb, Bi		3	4	5
6	O, S, Se, Te		4	5	6

TRANSITION METAL CLUSTER UNITS (SEP FROM: v + x - 12)

v	T.M. atom (M)	cluster unit	$M(CO)_2$ (x=4)	$M(C_5H_5)$ (x=5)	$M(CO)_3$ (x=6)	$M(CO)_4$ (x=8)
6	Cr, Mo, W		-2	-1	0	2
7	Mn, Tc, Re		-1	0	1	3
8	Fe, Ru, Os		0	1	2	4
9	Co, Rh, Ir		1	2	3	5
10	Ni, Pt, Pd		2	3	4	6

Table 5. Electronic contribution of cluster units.

(Reproduced from Reference 28)

In this case each iron moiety contributes not one but two electrons to the skeletal bonding in order to achieve the required 11 SEP's. Clearly, not all of the exo-polyhedral bonding orbitals of the iron fragment are filled, as signified by the -12 term in the computation.

A modified equation has been proposed by Nishimura[32] for the electron counting in such cases.

$$e = v + x - m + 6$$

The extra term 'm' is the number of electrons normally associated with the metal as an organometallic moiety. Using this equation gives e = 2 for the Fe($-C_5H_5$) unit, since m = 17, producing the required electron pair count of 11 for the observed closo structure, (i.e. n + 1).

Ambiguity in electron counting can arise for apparently simple groups. For example the monocarbaborane $NMe_3CB_5H_{11}$ can be classified as arachno or hypho depending on whether the NMe_3-C-H group is considered to be a skeletal group or a face-edge bridging group (replacing B-H-B). The structures are then isoelectronic with hypho-$[B_6H_{12}]^{2-}$ and arachno-$[B_5H_{10}]^-$ respectively. Though originally reported as hypho[33] a subsequent paper[5] fails to confirm a preferred description.

Grimes[9] points out that the skeletal electron counting theory has only a limited applicability to clusters such as the carbon rich carboranes. In this case SEPT is limited by its assumption that there is complete electron delocalisation over all of the molecule. In clusters such as (η-C_5H_5)Co(CH_3)$C_4B_7H_7$ the significant carbon content results in semi-localised bonding in a portion of the cluster. As a consequence none of the observed geometries of the three isomers of this compound correspond to the twelve vertex fragment based on a regular thirteen vertex polyhedron, (Docosahedron), as predicted by

the SEPT for a 28 electron, (n+2) cluster. In fact seven different non-dodecosahedral geometries have been isolated for twelve atom, 28-electron metallacarbaboranes[9].

A number of other theories concerning the rationalisation of the shape and stability of polyhedral borane and transition metal clusters have been developed more recently. These include Stone's[34] surface vector harmonic analysis and the capping principle developed by Mingos[36], both of which are discussed below. A further refinement of the SEP theory to account for the electron counting in condensed polyhedra has also been developed by Mingos[36], whilst Teo[37] has proposed a modified SEP theory to give an alternative rationalisation of the electron counting schemes developed in the Mingos theories by the introduction of a new skeletal parameter. Both of the latter two theories are concerned mainly with transition metal clusters and are not discussed here.

Stone has developed a new method enabling qualitative description of the M.O.'s of boron hydride or transition metal carbonyl clusters. A brief description of his theory is as follows. Earlier M.O. theory describing cyclic hydrocarbons such as benzene in terms of an 'electron on a ring' were developed by Hoffman to describe cluster compounds in terms of a particle confined to the surface of a sphere. Stone has extended this latter treatment to enable a wave function to be derived from th LCAO's for a number of atoms distributed symmetrically over the surface of a sphere (i.e. a closo system);

$$\psi_{LM}^{\sigma} = \sum \eta_{\sigma} \, Y_{LM}(\Theta\,\phi)$$

where $Y_{LM}(\Theta\,\phi)$ is the surface harmonic

and L = nodal planes and M = -L to L.

This generates a set of 'n' sigma type cluster orbitals from the 'n' cluster atoms. As in other M.O. applications, the energies of these orbitals are expected to increase with the number of nodal planes. Calculations to verify this have shown that the energy of the orbitals is proportional to the average coordination number[34]. Moreover, the energy is minimised by the formation of the maximum number of bonds. This of course is satisfied by a triangulated skeletal geometry, noted earlier as being predominant in the structures of boron hydrides.

The wave function noted above can only be applied to sigma type atomic orbitals and not the pi type nodal p-orbitals present in the BH skeletal fragments. This was solved by determining a function analogous to the previous spherical harmonic which yields a set of vectors parallel to the suface of the sphere at the position of each skeletal atom;

$$V_{LM} = \nabla Y_{LM}(\theta \phi)$$

where ∇ = gradient operator in a given coordinate system.

The direction and magnitude of these vectors (See Figure 8a) are then used to indicate the pi orbital contribution to cluster bonding.

The contours that the surface vector harmonics produce give a qualitative picture of the pi bonding in the cluster. Strongly bonding interactions are indicated where the arrows either reinforce each other or converge. These vector harmonics V_{LM} enable the construction of cluster pi type orbitals from the derived wave functions ϕ^{σ}_{LM}. By rotating the vectors though 90^{O} the complementary pi bonding vectors and wave functions $\bar{V}_{LM}$ and $\bar{\phi}^{\pi}_{LM}$ are obtained. This has the effect of changing the bonding orbitals into antibonding orbitals and vice versa. The 'n' skeletal atoms therefore yield '2n' pi type cluster

a)

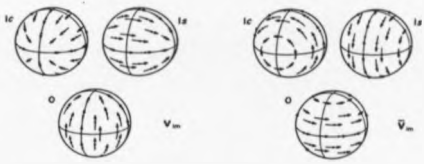

b)

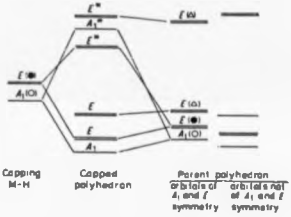

Figure 8. a) Schematic diagram of surface vectors for a closo cluster (Reproduced from reference 34).

b) Idealised M.O. diagram for capping of a symmetrical cluster (Reproduced from reference 35).

orbitals, of which 'n' are bonding. Mixing of the ψ^{σ}_{LM} and ψ^{π}_{LM} orbitals generates in each case a more strongly bonding orbital and a non bonding or antibonding orbital, except when L = 0 i.e. $\psi_{LM} = S$. The net result is that 'n+1' bonding cluster orbitals are generated, thus reinforcing previously noted cluster bonding M.O. descriptions.

Stone has also adapted the surface vector harmonic approach to nido and arachno clusters, the net result of which has similarly agreed with previous M.O. theories that such fragment clusters have the same number of bonding cluster orbitals as that of the parent closo boranes, so long as sufficient stabilisation is provided by protons added to the open face of the cluster.

The term 'Capping Principle' has been coined to describe the observations from M.O. calculations, that a capped polyhedron has the same number of skeletal bonding M.O.'s as the uncapped symmetrical polyhedron. Though applicable to most cluster compounds it is most utilised in the description of metal clusters. The basis of the capping principle as described by Mingos[35] is as follows.

When a symmetrical polyhedron is capped with a M-H fragment (or a B-H fragment), the symmetry of the molecule is lowered to yield a point group with a new principal axis. Redefining the frontier M.O.'s of the parent polyhedron and capping fragment (See Figure 5 for orbitals of the B-H fragment) according to the new symmetry allows their interaction to be analysed using perturbation theory. Thus, only orbitals of the same symmetry are considered to interact, with the strongest interactions produced from M.O. combinations with greatest effective overlap, i.e. from those M.O.'s with similar energy and pseudo-symmetry. In this way the sp_z and $p_{x,y}$ orbitals of the capping fragment will interact most strongly with skeletal M.O.'s of suitable

energy with zero and one nodal planes respectively.

The former interaction results in destabilisation of the capping atom frontier orbital, the effect of which is to reduce the number of skeletal bonding M.O.'s of the capped polyhedron to that of the parent polyhedron. A schematic orbital correlation diagram for the capping of an M_nH_n polyhedron with a M-H fragment is given in Figure 8b.

Though the same skeletal bonding M.O. pattern is often found in clusters with several capping atoms, this is not always the case. In the tri-capped trigonal prismatic cluster geometry, as found for example in $[B_9H_9]^{2-}$, linear combinations of capping frontier orbitals are able to overlap with skeletal antibonding M.O.'s, thereby generating additional bonding M.O.'s in excess of the bonding M.O.'s found in the parent trigonal prismatic cluster.

Whilst the preceding discussion is clearly relevant to the large number of transition metal clusters with capped polyhedral geometries, it also offers an alternative view of the Williams[8] description of nido and arachno borane and carborane clusters alluded to earlier. Thus the description of a nido cluster as having the same number of skeletal bonding M.O.'s as that of the closo polyhedron albeit with one vertex unoccupied is the converse of the Mingos type description of the closo cluster as being a capped nido cluster, the latter obeying the capping principle noted above. A similar description of the relationship between nido and arachno clusters can also be made using the capping principle.

1.4. SYNTHESIS OF CARBABORANES

Carboranes are prepared by the incorporation of carbon atoms into the framework of borane clusters. The boranes are all derived from starting materials such as $LiBH_4$, BF_3 etc. Numerous methods of preparing diborane are available[38], a convenient, high yield preparation being[39],

$$2\ KBH_4 + 2\ H_2PO_3F \longrightarrow B_2H_6 + 2\ KHPO_3F + 2\ H_2$$

Pyrolysis of the diborane then yields a mixture of boranes[40],

$$B_2H_6 \longrightarrow B_4H_{10} + B_5H_9 + B_6H_{10} + B_{10}H_{14}$$

Using varying temperatures and pressures and often in the presence of other reagents, a predominance of one product can be obtained. Decaborane, usually prepared by this method is produced in only 10% yield at 115°C whereas at 150°C in the presence of dimethyl ether the yield is substantially increased to 60%. The preparation and handling of boranes usually require extensive use of vacuum line techniques, since the majority are volatile and air reactive. Decaborane is one exception being relatively air stable, though as with all boron hydrides and derivatives it is toxic.

A variety of methods has been employed to synthesise a particular type of carbaborane. Some of the preparative routes to the mono-, di- and carbon rich carbaboranes are described below.

The small *closo* and *nido* monocarbaboranes are made from the pyrolysis of alkylboranes, as exemplified by the reaction of methyl pentaborane[41]. Alkyl derivatives are accessible from the pyrolysis of

$$\underline{\text{Nido}}\text{-Me-}B_3H_8 \xrightarrow{500^{\circ}C} \underline{\text{Closo}}\text{-}CB_5H_7 + \underline{\text{Nido}}\text{-}CB_5H_9$$

higher alkylated boranes. The products of such thermolytic reactions are often numerous and unpredictable.

The restriction of incorporating only one carbon atom into the borane skeleton negates the use of acetylenes as a general preparative route to monocarboranes (compare to dicarbaboranes synthesis), though several alkylated derivatives of CB_5H_9 have been synthesised by the pyrolysis of 2-butenylpentaborane[42]. The use of an acetylide[43] has the desired effect but results in a C-alkyl derivative.

$$\underline{\text{Nido}}\text{-}B_5H_9 \xrightarrow[2)\ H^{+}]{1)\ MeC{\equiv}CLi} \underline{\text{Nido}}\text{-2-Et-2-}CB_5H_8$$

To avoid the formation of alkyl derivatives the cyanide ion has been successfully used, via nucleophillic attack on decaborane(14) to prepare the known large[44,45] and intermediate[5] monocarboranes (see Figure 9).

$$B_{10}H_{14} \xrightarrow{CN^{-}} [B_{10}H_{13}CN]^{2-} \xrightarrow[2)\ Me_2SO_4]{1)\ H^{+}} \begin{matrix} NMe_3CB_{10}H_{12} \\ + \\ NMe_3CB_9H_{11} \end{matrix}$$

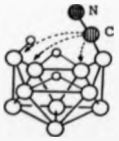

Figure 9. Reaction of decaborane(14) with cyanide.

The CN^- attacks at the least electronegative B(6) or B(9) boron atoms, coordinating as a two electron donor through the carbon atom. The expulsion of a proton gives the arachno-cyano derivative, isolable as the caesium salt. On acidification the nitrile carbon atom interacts with the open face of the cage to give a CB_{10} and CB_9 amino derivative, of which the latter has suffered the loss of a skeletal boron atom. After methylation and separation the amino-carbaboranes can be converted to the parent monocarbaboranes as shown in Figure 10.

Differences in reactivity of similarly functionalised carbaborane clusters is illustrated by the contrast in reaction of $NMe_3CB_{10}H_{12}$ and $NMe_3CB_9H_{11}$ with sodium in thf. The former reaction results only in the removal of the exo-polyhedral amino group, whereas in the latter the deamination is accompanied by a two electron loss to produce the closo-$[CB_9H_{10}]^-$ anion (The C-NMe_3 moiety donates 4 e's for cluster bonding). The expected nido-$[CB_9H_{12}]^-$ anion is synthesised by using sodium in liquid ammonia.

Several of the reactions in Figure 9 are relevant to the work contained in this thesis and are discussed in Chapter 2.

The dicarbaboranes are usually prepared by reaction of boranes with alkynes, giving insertion of two carbon atoms into the framework. The products of such reactions vary according to the conditions employed. The reaction of pentaborane(9) with ethyne for example, gives closo carbaboranes as the major products at higher temperatures[46] and nido carbaboranes at lower temperatures[47].

$$B_5H_9 \xrightarrow{550^oC\ /\ HC{\equiv}CH} C_2B_3H_7 + C_2B_4H_6 + \text{...others}$$

$$B_5H_9 \xrightarrow{200^oC\ /\ \text{ethyne}} C_2B_4H_8 + \text{...others}$$

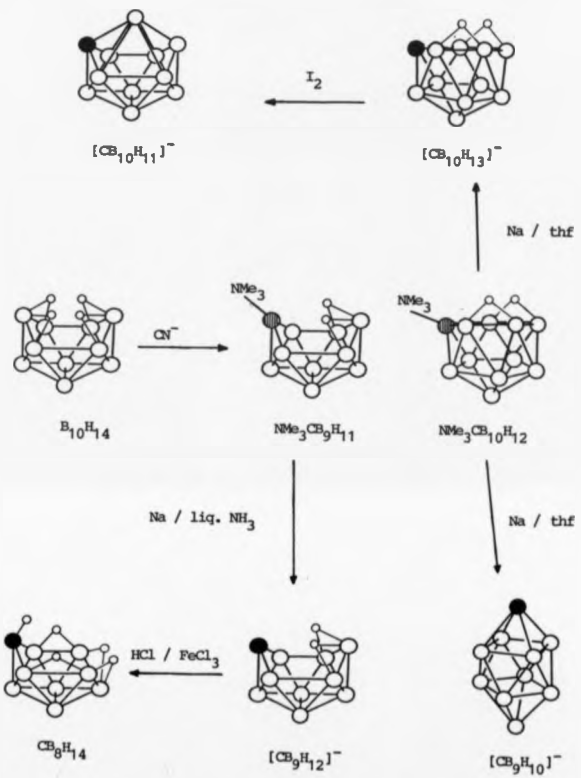

Figure 10. Preparative routes to monocarbaboranes[5,44,45].

Alkyl derivatives are prepared from higher alkynes[48],

$$B_8H_{12} \xrightarrow{\text{2-butyne}} Me_2C_2B_7H_9 + Me_2C_2B_8H_{10}$$

Many of the carbaboranes are accessible via reactions involving lower or higher carbaboranes. Closo dicarbaboranes can be prepared by thermolysis of nido and arachno carbaboranes. The reactions involve either disproportionation[49] or hydrogen loss[50] (or both), as shown in the following examples;

$$C_2B_8H_{12} \longrightarrow C_2B_8H_{10} + H_2$$

$$C_2B_7H_{13} \longrightarrow C_2B_6H_8 + C_2B_8H_{10} + H_2$$

Reaction with diborane can lead to cluster expansion[49].

$$C_2B_6H_8 \xrightarrow{B_2H_6} C_2B_7H_9 + H_2$$

Reaction of Me_3B with nido-2,3 $C_2B_4H_8$ at ambient temperatures gives methylated products with one and two atom expansion[51], $Me_2C_2B_5H_2Me_3$ and $Me_2C_2B_6H_2Me_4$. Pyrolysis of Me_3B at elevated temperatures also gives the former product[52].

Cluster degradation is also a possible route to lower carbaboranes as illustrated by the reaction of $[C_2B_9H_{12}]^-$ with either chromic acid[53] or with formaldehyde in dilute hydrochloric acid[54].

$$[C_2B_9H_{12}]^- \xrightarrow[\text{or HCHO/HCl}]{\text{chromic acid}} C_2B_7H_{13}$$

If this degradation is carried out with a dilute acidic $FeCl_3$ solution, the major product is $C_2B_7H_{11}$[55].

The gas phase mercury sensitised photolysis of carbaboranes has produced boron-boron linked clusters[56], as in the photolysis of 2,4-$C_2B_5H_7$ to yield six isomeric (2,4-$C_2B_5H_6)_2$ clusters, though with other carbaborane species decomposition occurs. The co-photolysis of mixtures leads to low yields of mixed-cage coupled carbaboranes.

The icosahedral ortho-carborane, 1,2-$C_2B_{10}H_{12}$ is prepared by reaction of decaborane with ethyne in the presence of a suitable Lewis base (Et_2S or MeCN)[57,58]. The meta- and para- isomers are then produced by thermal isomerisation[59,60].

$$B_{10}H_{14} \xrightarrow{\text{2 MeCN / ethyne}} C_2B_{10}H_{12} + 2\ H_2$$

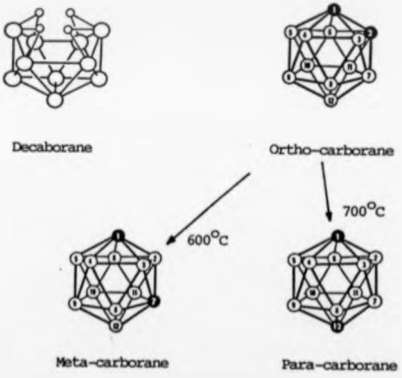

Examples of known tri- and tetracarbaboranes[61,62] are closo-$C_3B_3H_7$ and nido-$C_4B_2H_6$. Though the parent carbaboranes remain unknown, C-alkyl derivatives of C_3B_3, C_4B_4, C_4B_6 and C_4B_8 clusters have been isolated, as have several metalla derivatives[63].

The preparative route to the C_4B_4 carbaboranes involves the coupling of two $[R_2C_2B_4H_5]^-$ units with Fe(II) to form a sandwich complex, which then undergoes air oxidation to yield $R_4C_4B_8H_8$ (Figure 11). The overall process is a four electron oxidation, which has been shown to proceed in thf solution in an intramolecular manner via an intermediate $(R_2C_2B_4H_4)_2Fe_2(thf)_2$ complex[64].

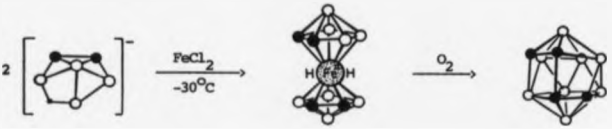

$[(R)_2C_2B_4H_5]^-$ $R_4C_4B_8H_8$

Figure 11. Oxidative fusion reaction to prepare $R_4C_4B_8H_8$.

The oxidative fusion reaction to produce new single clusters is a potentially very useful synthetic tool and not suprisingly an area of current interest.

Such coupling can also be achieved without metal assistance, for example, the tetracarbaborane $C_4B_6Et_{10}$ was synthesised[65] from $K_2[C_2B_3Et_5]$ by oxidation with I_2.

Other attempts at coupling polyhedra by oxidative methods have yielded linked rather than fused dimeric units, such as the chromic acid oxidation[66] of $[C_2B_9H_{12}]^-$ to yield $(C_2B_9H_{11})_2$.

Thermolysis is also a useful route to the carbon rich carbaboranes, as in the gas phase pyrolysis[67] of $C_2B_3H_5$ to obtain nido-$C_4B_7H_{11}$, though as expected other linked carbaboranes are also produced[68].

The photolysis of the nido-$B_4H_8Fe(CO)_3$ in the presence of MeC≡CMe produces as a major product the tetracarbaborane[69] $Me_4C_4B_4H_4$, with minor yields of $Me_6C_6B_4H_4$ and $Me_8C_8B_4H_4$. The insertion of the alkyne molecules is thought to occur via coordination to the metal atom.

1.5. SYNTHESIS OF METALLACARBORANES.

The majority of metallacarbaboranes are prepared by the reaction of metal complexes with neutral or anionic carbaboranes, though their synthesis from boranes has been demonstrated. The currently available synthetic routes can be classified into the following distinct methods:

1) Polyhedral completion of nido carbaborane anions
2) Polyhedral expansion (stepwise or concerted)
3) Oxidative insertion into fragment carbaboranes
4) Polyhedral contraction/degradation
5) Polyhedral replacement/substitution
6) Thermally induced polyhedral rearrangement

A brief review of each of these six synthetic methods is given below.

1.5.1. METALLACARBABORANES FROM POLYHEDRAL COMPLETION OF NIDO CARBABORANE ANIONS.

One of the most widely used synthetic routes to metallacarbaboranes involves the reaction of a carbaborane anion with a metal halide reagent. In this way, Hawthorne was able to synthesise the dianion[70], $[Fe(C_2B_9H_{11})_2]^{2-}$, thereby giving rise to a new area of synthetic chemistry.

The complex is prepared by reaction of nido $[C_2B_9H_{12}]^-$ with NaH and $FeCl_2$. The in situ abstraction of the bridging hydrogen from the carbaborane by NaH forms the dianion $[C_2B_9H_{11}]^{2-}$, which then reacts with the $FeCl_2$. The product was recognised as an analogue of ferrocene from the isolation[71] of the related mixed sandwich complex $[(\eta\text{-}C_5H_5)FeC_2B_9H_{11}]^-$, which was obtained by the addition of an

equivalent of cyclopentadiene to the original reaction mixture (thereby forming $(C_5H_5)^-$ on addition of NaH). Both of these Fe(II) metallacarbaboranes can be easily and reversibly oxidised to the Fe(III) species, in a similar manner to the ferrocene and ferricinium analogues.

The X-ray crystallographic structural analysis of the mixed sandwich Fe(III) complex, shown in Figure 12, confirmed the structural analogy to ferrocene, with one of the cyclopentadiene ligands being replaced with the isolobal carbaborane dianion[72].

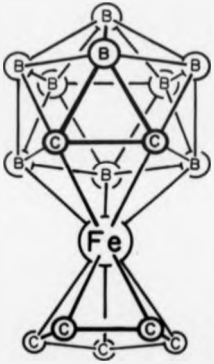

Figure 12. Structure of $[(\eta\text{-}C_5H_5)Fe(C_2B_9H_{11})]$

By coordination to the iron atom, the nido structure of the carbaborane anion is completed to give the closo icosahedral metallacarbaborane. Since the metallacarbaborane product has the same polyhedral geometry (and electron count), with one more vertex occupied than in the precursor the reaction is a polyhedral completion reaction.

As expected the icosahedral structure is distorted due to the longer Fe-B and Fe-C bonds compared to the skeletal B-B and B-C bonds. Notably, the cyclopentadiene ring and pentagonal face of the carbaborane ligand are eclipsed in the mixed sandwich complex, whilst they are staggered in the binary product, (as are the rings in ferrocene[73]).

The isolation of these complexes confirmed the theoretical proposal made by Lipscomb[74], that the bonding orbitals on the pentagonal face of the $[B_{11}H_{11}]^{2-}$ and $[C_2B_9H_{11}]^{2-}$ anions were analogous to those of the cyclopentadiene anion in metallocenes[75], with the five sp^3 orbitals directed to the vacant vertex (See Figure 13).

Binary carbaborane sandwich complexes of a Cr(III)[76], Co(III)[77] and Ni(III)[78] were subsequently synthesised, having analogous structures to the symmetric staggered conformation of the $[Fe(C_2B_9H_{11})_2]^{2-}$ complex[79]. An alternative, 'Slipped' structure was observed for the d^8 and d^9 complexes Cu(II)[80], Cu(III)[80], Ni(II)[80], Rd(II)[81], Au(II)[81] and Au(III)[81]. The d^6 complexes of Ni(IV)[81] and Rd(IV) were found to have a 'cisoid' structure in which the carbon atoms of the two ligands are located on the same side of the complex, though still staggered, as shown in Figure 14.

Several theories have been proposed to explain the slipped structure, in which the metal atom has an electronic configuration

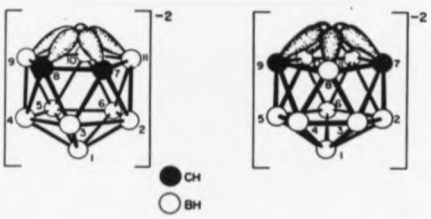

Figure 13. Bonding orbitals in $[C_2B_9H_{11}]^{2-}$.

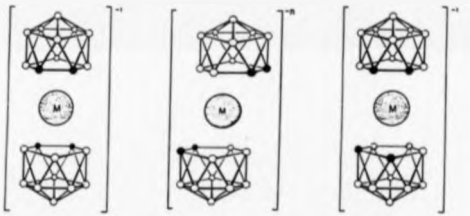

(a) (b) (c)

Figure 14. The symmetric (a), slipped (b) and cisoid (c) sandwich complexes of $[C_2B_9H_{11}]^{2-}$.

greater than eighteen. Originally attributed by Wing[80] to a change in bonding mode from η-5 to the η-3, subsequent comparisons to the Ag(I) and Cu(I) d^{10} benzene complexes were made by Hawthorne and Warren[81], in which the asymmetry of the LUMO of the metal and the HOMO of the ligand disables C_6 symmetry. More recently, Wang[82] suggested that the extra electrons occupy antibonding M.O.'s of the cage, a situation which is compensated for by a change of geometry. The systematic folding of the carbaborane face has been observed and proposed by Wallbridge *et al*[83] as the cause of the slippage.

The reaction of an anionic carbaborane with a metal halide complex has also been successfully applied to other *nido* carbaboranes, as in the preparation of the cobaltacarbaborane[84,85] $[Co(C_2B_7H_9)_2]^{2-}$ from $CoCl_2$ and $[C_2B_7H_{11}]^{2-}$. In the same way that the previous binary complexes could be described as *commo*-icosahedral, the structure of the complex[85] (shown in Figure 15) is a *commo*-bicapped square antiprism, fused at the equatorial cobalt vertex. In this instance the pentagonal face of the carbaborane ligand is puckered. Two isomeric forms of this complex, namely the 6,7-C_2 and 1,6-C_2 isomers are formed when using different refluxing solvents, with a third 1,10-C_2 isomer formed on heating the solid to 315°C.

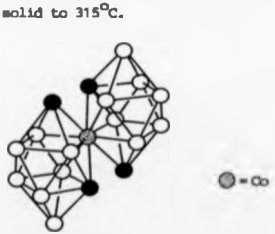

Figure 15. Structure of $[Co(C_2B_7H_9)_2]^-$

1.5.2. METALLACARBABORANES FROM POLYHEDRAL EXPANSION (STEPWISE OR CONCERTED).

The scope of metallacarbaborane synthesis was substantially increased with the discovery of the polyhedral expansion synthesis. This synthetic route enables metal fragments to be inserted into closo carbaboranes to yield closo-metallacarbaboranes with one more vertex than the precursor and two more skeletal electrons, hence the term polyhedral expansion.

The synthesis involves two distinct steps, the first of which is the reduction of the carbaborane with a strong base to produce an intermediate nido carbaborane anion. In the second step, reaction of this anion with an appropriate metal halide reagent generates a closo metallacarbaborane and is analogous to the previously described synthesis. The important difference between polyhedral expansion and the previous synthetic route is that the intermediate nido carbaborane anion need not be isolable, or indeed, overtly stable. The intermediate anion will not necessarily contain any bridging hydrogen atoms, since it results from the opening of a closo cluster in which only terminal hydrogens are present. The inherent instability or reactivity of the intermediate anion without such stabilising facial hydrogen atoms may facilitate reaction with the metal halide reagent used.

The cage opening via cluster reduction that occurs as the first step of the polyhedral expansion reaction is thought to result from the addition of two electrons to an unoccupied molecular orbital, causing a Jahn-Teller type distortion to give the nido structure[86,87]. This change in skeletal geometry is consistant with that implied by 'Wades rules'[29]. The resultant carbaborane anion then reacts with the metal cationic fragment, redressing the electronic balance by donating

the high energy electrons to fill the bonding M.O.'s of the polyhedron with one more vertex.

The first reported example of a polyhedral expansion reaction[88] involved the closo dicarbaborane $C_2B_6H_8$, the structure of which is expanded by the insertion of one or two cobalt cyclopentadienyl fragments. The structures of the precursor and resultant closo metallacarbaborane complexes are shown in Figure 16. The original dodecahedral structure of the carbaborane has been expanded to the nine vertex capped trigonal prism in the monocobalt product[89] and the ten vertex bicapped square antiprism of the dicobalt species[90]. This dicobalta complex was the first example of a heteroborane with a Co-Co linkage (248.9 pm). When the cyclopentadienyl ligand is omitted from the reaction, the closo metallacarbaborane, $[Co(C_2B_6H_8)_2]^-$, is produced[89].

Two important utilizations of the polyhedral expansion synthesis were realised by Hawthorne, namely the application to icosahedral carbaborane precursors to yield thirteen vertex metallacarbaboranes with a so called 'supraicosahedral' geometry, and the application to metallacarbaborane precursors to systematically produce homo- and hetaro-dimetallacarbaboranes.

The first of these advances was accomplished by the polyhedral expansion of the icosahedral closo $C_2B_{10}H_{12}$ to yield[91,92] $(\eta\text{-}C_5H_5)CoC_2B_{10}H_{12}$, which has a closo structure[93] with a docosahedral geometry (1:6:5:1 layers), the nido carbaborane fragment having a slightly puckered hexagonal open face.

The polyhedral expansion of this mono-metallacarbaborane, carried out in an identical manner to the expansion of the neutral carbaborane, yielded amongst other minor products, the first fourteen

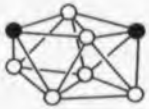

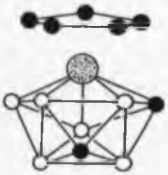

$(\eta\text{-}C_5H_5)CoC_2B_6H_8$

$1,7\text{-}C_2B_6H_8$

1) Sodium in naphthalene

2) $C_5H_5^-Na^+$ / $CoCl_2$

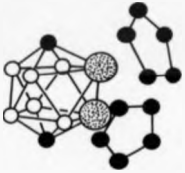

$(\eta\text{-}C_5H_5)_2Co_2C_2B_6H_8$

Figure 16. Polyhedral expansion reaction of $C_2B_6H_8$

vertex metallacarbaborane[94], $(\eta\text{-}C_5H_5)_2Co_2C_2B_{10}H_{12}$. A structure consistent with the spectral data of the dimetallacarbaborane, as shown in Figure 17, is a bicapped hexagonal antiprism, consisting of two staggered 6-membered C-B-B-B-B-B rings capped by $Co(\eta\text{-}C_5H_5)$ fragments. Various analagous fourteen vertex closo dimetallacarbaboranes were subsequently synthesised and their structures ascertained by X-ray crystallography support the proposed structure, as exemplified by the di-iron tetracarbaborane species[95] $(\eta\text{-}C_5H_5)_2Fe_2Me_4C_4B_8H_8$.

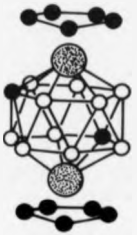

Figure 17. Proposed structure of $(\eta\text{-}C_5H_5)_2Co_2C_2B_{10}H_{12}$.

The first product isolated from the systematic polyhedral expansion of a metallacarbaborane[96] was the dimetallacarbaborane $(\eta\text{-}C_5H_5)Co_2C_2B_8H_{10}$, previously identified as a minor product of the monocobaltacarbaborane preparation. The reduction step of the reaction required three equivalents of sodium naphthenide, the first to reduce Co(III) to Co(II), the second and third for the cage anion production.

The often complex range of products obtained from the polyhedral expansion reaction is illustrated by the insertion of the $Co(\eta\text{-}C_5H_5)$ fragment into $(\eta\text{-}C_5H_5)CoC_2B_7H_9$. From this reaction six products have been characterised[89,97,98], including three isomeric octadecahedral di-cobalta products and an icosahedral tri-cobalta cluster, all formally expansion products. Another product, $(\eta\text{-}C_5H_5)_2Co_2C_2B_5H_7$ results from a combined cluster expansion and degradation, since the product contains one more cobalt atom and one less boron atom than the precusor. In contrast, the analogous polyhedral expansion of $C_2B_5H_7$ afforded amongst other products, the cobaltacarbaboranes $(\eta\text{-}C_5H_5)CoC_2B_6H_8$ and $(\eta\text{-}C_5H_5)_2Co_2B_6H_8$ in which there are more boron atoms than the precursor.

Hetaro dimetallacarbaboranes can also be prepared by polyhedral expansion[99], as shown by the reduction of $(\eta\text{-}C_5H_5)CoC_2B_7H_9$ and reaction with Fe(II) to yield $(\eta\text{-}C_5H_5)_2FeCoC_2B_7H_9$. The octadecahedral eleven vertex structure of this complex (Figure 18), shows the iron and cobalt atoms occupying six and five coordinate positions within the framework, a situation Hawthorne rationalises as reflecting the electron deficiency of the formally d^5 iron atom compared to the d^6 Co(III) vertex.

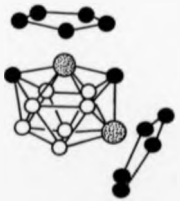

Figure 18. Structure of $(\eta\text{-}C_5H_5)_2FeCoC_2B_7H_9$

The mono-carbon hetaro bimetallacarbaborane species $(\eta\text{-}C_5H_5)_2NiCoCB_7H_8$ obtained from polyhedral expansion of the cobaltacarbaborane anion precursor $[(\eta\text{-}C_5H_5)CoCB_7H_8]^-$, has the expected square-antiprism geometry[100], with the metal atoms adjacent in an equatorial layer.

Another type of polyhedral expansion reaction is known in which the insertion of a metal fragment into the carbaborane is accomplished without an intial reduction step to generate an open cage, the so called 'Concerted polyhedral expansion'. The use of highly nucleophilic zero-valent metal reagents enables insertion into the framework with a net transfer of electrons to the cage, thus satisfying the electronic requirements of the expanded geometry.

The first metallacarbaboranes produced by concerted polyhedral expansion were the icosahedral metallacababoranes[101,102] closo-$(PR_3)PtMe_2C_2B_9H_9$ prepared by the reaction of the zero-valent Pt(0) species, $[Pt(PPh_2Me)_3]$, $[Pt(PEt_3)_3]$ and $[Pt(PMe_3)_2(trans\text{-}stilbene)]$ with closo-$Me_2C_2B_9H_9$. The structure of one of these products (as determined by X-ray crystallography[103,104]) is shown in Figure 19, contrasting the octadecahedral and icosahedral geometries of the precusor and product.

Concerted polyhedral expansion has also been applied to a number of smaller carbaborane precursors. The reaction of $[Pt(PR_3)_2(trans\text{-}stilbene)]$, (R = Me or Et) with closo-$Me_2C_2B_6H_6$ afforded the expected closo platinacarbaborane as the major product[105]. The structure of $(Me_3P)_2PtMe_2C_2B_6H_6$ was found to be a capped trigonal prism, in which the hetaro skeletal atoms occupy all three tetra-hapto capping sites (Figure 20)[106].

Hetaro-dimetallacarbaboranes are accessible by polyhedral

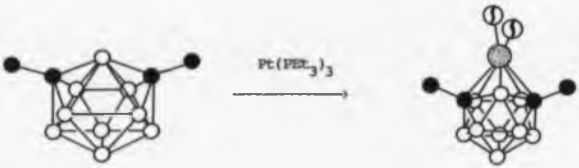

$Me_2C_2B_9H_9$ $(Et_3P)_2PtMe_2C_2B_9H_9$

Figure 19. Concerted polyhedral expansion of $Me_2C_2B_9H_9$

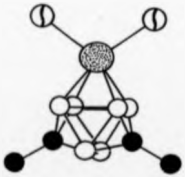

Figure 20. Structure of $(Me_3P)_2PtMe_2C_2B_6H_6$

expansion of closo-metallacarbaboranes. The bimetallacarbaborane $(COD)(\eta\text{-}C_5H_5)NiCoC_2B_8H_{10}$ is thus prepared[107] from the reaction of $Ni(COD)_2$ with $(\eta\text{-}C_5H_5)CoC_2B_8H_{10}$, (COD = cyclo-octa-1,5-diene).

1.5.3. METALLACARBABORANES FROM OXIDATIVE INSERTION INTO FRAGMENT CARBABORANES.

Metallacarbaboranes can also be synthesised by the insertion of metal fragments into nido or arachno carbaboranes. The nido metallacarbaboranes isolated by the reaction with zero valent metal complexes indicate that the reaction is accomplished by the replacement of a bridging hydrogen B-H-B on the open face of the carbaborane precursor. Since the oxidation state of the metal centre is necessarily increased on insertion into the B-H-B bond, the mechanism has been termed 'oxidative insertion'[108,109].

The simple bridging metalla species produced by the initial oxidative addition to a B-H-B bond is in many cases not isolable as such. Often subsequent rearrangement occurs to give the arachno, nido or closo metallacarbaborane product.

An example that illustrates both of these facets of oxidative insertion is the reaction of $[Pt_2(COD)(PEt_3)_4]$ with $R_2C_2B_4H_4$ (R = H or Me)[110]. The platinacarbaborane isolated, μ-4,5-$(Et_3P)_2PtH\text{-}C_2B_4H_6$ has the original nido cluster geometry with a $Pt(PEt_3)_2$ fragment inserted into one of the bridging hydrogen bonds on the face of the carbaborane (Figure 21.a). In this case the product of the oxidative insertion is stable, pyrolysis is required to cause cage closure by the elimination of hydrogen to yield the closo-platinacarbaborane (Figure 21.b)[110,111]. The overall reaction is therefore one of cage completion, since the original nido carbaborane has been transformed into the identical

complete polyhedral geometry by insertion of the metal.

Whilst nido metallacarbaboranes result from the reaction of d^{10} nickel and platinum species with nido carbaboranes, the use of Co(0) species produces closo cages with automatic hydrogen loss[112]. Hence, the reaction of $[Co(PEt_3)_4]$ with the nido carbaboranes $C_2B_7H_{11}$ and $C_2B_8H_{12}$ yield the expected completion products, the closo cobaltacarbaboranes $(Et_3P)_2CoC_2B_7H_9$ and $(Et_3P)_2CoC_2B_8H_{10}$ respectively (Figure 22).

a) μ-4,5-$(Et_3P)_2PtH$-$C_2B_4H_6$ b) $(Et_3P)_2PtMe_2C_2B_4H_4$

Figure 21. Products from a) oxidative insertion of Pt(0) into $R_2C_2B_4H_6$, (R = H) and b) product of pyrolysis, (R = Me).

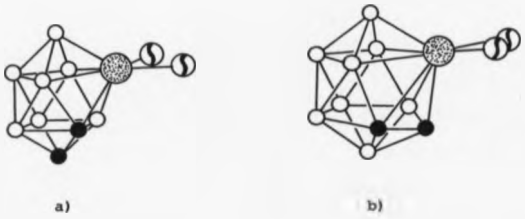

Figure 22. Structures of a) $(Et_3P)_2CoC_2B_7H_9$ and b) $(Et_3P)_2CoC_2B_8H_{10}$.

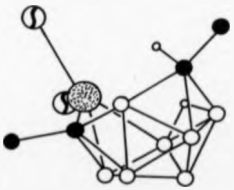

Figure 23. Structure of $(Et_3P)_2NiMe_2C_2B_7H_9$ (Platinum analogue $[(Et_3P)_2PtMe_2C_2B_7H_9]$ also known)

The oxidative addition of Ni(0) and Pt(0) metal reagents into arachno carbaborane cages also yields nido metallacarbaboranes, as exemplified by the reaction of $[Ni(PEt_3)_4]$ and $[Pt(stilbene)(PEt_3)_2]$ with $Me_2C_2B_7H_{11}$ to give the isostructural $(Et_3P)_2NiMe_2C_2B_7H_9$ and $(Et_3P)_2PtMe_2C_2B_7H_9$ complexes[113,114]. These products are therefore the result of a partial cage completion, since the gross polyhedral geometry is unchanged though more fully defined. The initial oxidative insertion, in this case, is reported[114] to occur at one of the skeletal C-H bonds as deduced from spectroscopic observations, though this is not evident from the structure of the final product (Figure 23).

The reaction of Co(0) species with arachno carbaboranes similarly results in spontaneous cage closure, as observed for the reactions with nido carbaboranes. Thus the reaction of arachno-$C_4B_7H_{13}$ with $Co(PEt_3)_4$ produces the closo-cobaltaborane[115] $(Et_3P)_2(H)CoC_2B_7H_9$. This product is similar but not identical to that produced from nido-$C_4B_7H_{11}$. The bicapped square antiprismatic skeletal geometry is found in both, but the presence and absence of a hydrogen attached to the cobalt atom in the former and latter respectively, manifest a different disposition of the cobalt phosphine ligands in each case. Notably, the absence of the hydride in the latter gives a deficient SEP count for the paramagnetic cluster.

The oxidative addition of $Co(PEt_3)_4$ into closo carboranes precursors has been found to result in polyhedral expansion. The cobaltacarbaboranes $(Et_3P)_2CoC_2B_3H_5$ and $(Et_3P)_2(H)CoC_2B_6H_8$ have been prepared from $C_2B_3H_5$ and $C_2B_6H_8$ respectively[112]. The absence and presence of a Co-H function is also observed in these compounds.

1.5.4. METALLACARBABORANES FROM POLYHEDRAL CONTRACTION/DEGRADATION

Polyhedral contraction reactions offer a route to smaller metallacarbaboranes from larger clusters. The degradation is normally induced by the use of a strong base, which removes a skeletal boron atom to yield an intermediate anion. An oxidising agent is then used to effect cage closure.

The base degradation of closo $(\eta\text{-}C_5H_5)CoC_2B_9H_{11}$ results in the removal of one boron vertex to yield $(\eta\text{-}C_5H_5)CoC_2B_8H_{10}$[116]. However, instability of the intermediate carbaborane anion can lead to extensive cage degradation as in the preparation of $[(\eta\text{-}C_5H_5)CoCB_7H_8]^-$ (Figure 24) where the degradation results in the loss of one carbon and three boron atoms[117].

$(\eta\text{-}C_5H_5)CoC_2B_{10}H_{12}$ $[(\eta\text{-}C_5H_5)CoCB_7H_8]^-$

Figure 24. Polyhedral contraction of $(\eta\text{-}C_5H_5)CoC_2B_{10}H_{12}$.

1.5.5. METALLACARBABORANES FROM POLYHEDRAL REPLACEMENT/SUBROGATION

Metallacarbaboranes in which a metal atom has replaced a boron atom from the carbaborane or metallacarbaborane precusor are prepared by a modification of the polyhedral contraction reaction known as the polyhedral subrogation method. Treatment of a closo carbaborane or metallacarbaborane with a strong base to produce an intermediate fragment cluster anion with one or more boron atoms removed (compare with polyhedral contraction) is followed by the introduction of a suitable metal halide reagent thereby enabling replacement of the ejected boron atom with a metal fragment, rather than cage closure by oxidation, as in contraction reactions.

The supraicosahedral dimetallacarbaborane $(\eta\text{-}C_5H_5)_2CoFeC_2B_9H_{11}$ was prepared by polyhedral subrogation[118]. Under similar conditions, the homo-tri-metallacarbaborane $[Co(\eta\text{-}C_5H_5)CoC_2B_9H_{11})_2]^-$ was isolated. The proposed chain like structure of this complex is shown in Figure 25.

1.5.6 METALLACARBABORANES FROM THERMAL REARRANGEMENT OF BORANES CARBABORANES AND METALLACARBABORANES.

The synthetic routes to metallacarbaboranes discussed so far have been successfully employed in a wide range of carbaborane systems whereas the following methods, are relatively less well proven.

Two approaches to the preparation of metallacarbaboranes by thermal reactions have been pursued. The pyrolysis of a metallacarbaborane under vacuum has yielded new dimetallacarbaborane complexes by polyhedral expansion. The first example of the so called 'Thermal metal transfer' reaction[119] afforded amongst other products, the icosahedral bimetallacarbaborane $(\eta\text{-}C_5H_5)Co_2C_2B_8H_{10}$ from the pyrolysis

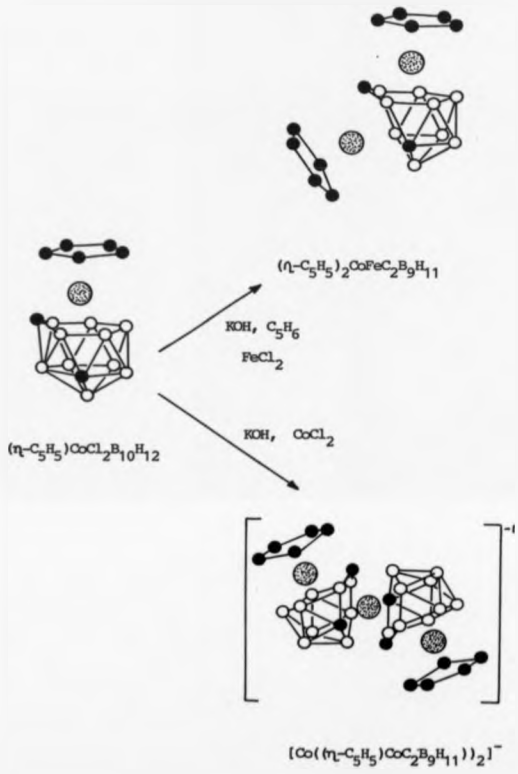

Figure 25. Polyhedral subrogation of $(\eta\text{-}C_5H_5)CoC_2B_{10}H_{12}$.

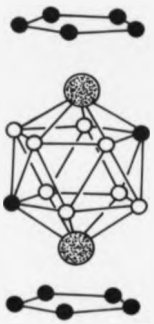

Figure 26. Structure of $(\eta\text{-}C_5H_5)Co_2C_2B_8H_{10}$ synthesised by thermal metal transfer.

pyrolysis of the octadecahedral monometallic precursor $(\eta\text{-}C_5H_5)CoC_2B_8H_{10}$.

An alternative approach demonstrated that thermalisation of *closo* carboborane residues enabled reaction with metal reagents to give new metallacarboboranes by polyhedral expansion. In this way Stone *et al*[120] were able to synthesise $(cod)NiMe_2C_2B_9H_9$ from the pyrolysis of $1,8\text{-}(Me)_2C_2B_9H_9$ and $Ni(cod)_2$.

Similarly, Grimes *et al*[121] isolated the expected expansion product of the thermolysis of $C_2B_5H_7$ and $Fe(CO)_5$, though in this case the major product resulted from polyhedral subrogation (Figure 27).

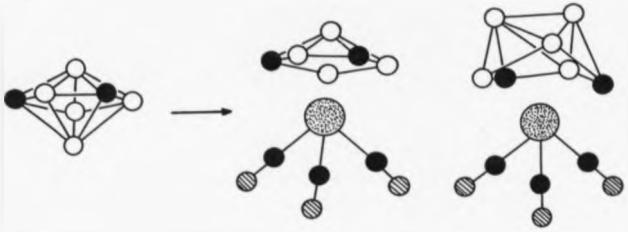

$$C_2B_5H_7 \xrightarrow{Fe(CO)_5} (CO)_3FeC_2B_4H_6 + (CO)_3FeC_2B_5H_7$$

Figure 27. Gas phase subrogation and expansion of $C_2B_5H_7$.

Metallacarbaborane synthesis by simultaneous insertion of a metal and carbon atom into a borane framework was first observed by Meutterties et al[122], in the reaction of the decaborane anion $[B_{10}H_{13}]^-$ and $Mo(CO)_6$. The product $[(CO)_3MoC(O)OCB_{10}H_{10}]^{2-}$, had been formed by incorporation of a molybdenum carbonyl fragment and a carbonyl group into the framework. The latter forms an exo-polyhedral $\lceil$-Mo.C(O).O.C-$\rceil$ ring with a metal bound carbonyl (Figure 28). Similar chromium and tungsten complexes have also been isolated using the respective metal hexacarbonyl reagents.

Figure 28. Structure of $[(CO)_3MoC(O)OCB_{10}H_{10}]^{2-}$.

Metallacarbaboranes have also been prepared directly from the thermal reaction of metallaboranes and alkynes, though these routes are at present very limited. Grimes *et al*[123] adapted the reaction of B_5H_9 and ethyne to the combination of $(\eta\text{-}C_5H_5)CoB_5H_8$ and alkynes to give cobaltacarbaboranes with the general formula $(\eta\text{-}C_5H_5)CoR_2C_2B_4H_4$.

A different approach to metallacarbaborane synthesis employs the metal atom technique, which had previously been demonstrated to be a suitable route to otherwise inaccessible organometallic species[124]. The principle of the adapted method is the co-condensation of thermally generated metal atoms with a borane cluster and an alkyne to produce metallacarbaboranes. The first such reaction[125], using cobalt metal, B_5H_9 and but-2-yne yielded a mixture of mono and di closo cobaltacarbaboranes.

$$B_5H_9 \xrightarrow[\text{Co}]{\text{MeC}\equiv\text{CMe}} \begin{array}{l}(\eta\text{-}C_5H_5)Co\text{:}Me_2C_2B_4H_4\\(\eta\text{-}C_5H_5)_2Co_2Me_2C_2B_3H_3\\(\eta\text{-}C_5H_5)_2Co_2Me_2C_2B_5H_5.\end{array}$$

The main product from the analogous reaction using iron atoms[126] was $(\eta^6\text{-}C_6Me_6)FeMe_2C_2B_4H_4$. Several carbon-rich C_4 metallacarbaboranes were also isolated as minor products, including $(\eta^6\text{-}PhMe)FeMe_4C_4B_5H_5$ and $(\eta^6\text{-}C_6Me_6)FeMe_4C_4B_3H_3$, the structures of which are shown in Figure 29. The former was found to have a nido decaborane like structure, whilst the latter contained an arachno cage with the iron atom in a pentahapto capping skeletal position, coordinated to a CCBBB ring. The very short bond between the remaining two skeletal carbon atoms, 139.2 pm implies a multiple bonding character.

Subsequent research[127] showed that metallacarbaboranes could be prepared under analogous conditions from B_5H_9 and B_6H_{10}, whilst use of $B_{10}H_{14}$ afforded[128] the closo cobaltaborane $(\eta\text{-}C_5H_5)CoB_{10}H_{10}$.

Figure 29. Structures of a) $(\eta^6\text{-}PhMe)FeMe_4C_4B_5H_5$ and b) $(\eta^6\text{-}C_6Me_6)FeMe_4C_4B_3H_3$.

1.6. EFFECTS OF SKELETAL CARBON AND METAL ATOM INCORPORATION.

The carbaboranes and metallocarbaboranes described in the previous sections illustrate two important effects of the incorporation of carbon atoms into the skeleton of a boron hydride framework. Firstly, carbon atoms tend to occupy vertices of low coordination when possible[19,129]. Notably, this effect normally positions the carbon atom on the open face of the fragment clusters or at a low coordinate capping position in the closo species.

Onak[3] has noted that the preference for low coordination is reflected in the relative stabilities of carbaborane isomers. Hence, in the pentagonal bipyramidal $C_2B_5H_7$, a change in coordination of a carbon atom from an equatorial five coordinate position to an apical six coordinate position has been calculated[130] to increase the molecular energy by ~ 200 KJ mol^{-1}. A similar destabilisation of 40 - 150 KJ mol^{-1} is estimated for four and five coordinate carbon in the various trigonal bipyramidal $C_2B_3H_5$ isomers.

A ring capping theory has been proposed[131] which suggests that because of orbital constraints the CH fragment is favoured as the cap on three and four membered rings, whilst the BH fragment is more suitable for capping five membered rings. Thus, the stability of the $C_2B_5H_7$ isomers is predicted to be in the order 2,3 > 1,2 > 1,7 as discussed above. For the icosahedral closo carbaboranes, where the symmetry of the cluster is such that each and every atom caps a 5-membered ring, the capping principle breaks down. Other carbaborane clusters are known where the skeletal carbon occupies a high coordination vertex, though other lower coordination sites are available, such as the octadecahedral closo-$[CB_{10}H_{11}]^-$, in which the carbon is 7-coordinate.

Another feature of carbaborane clusters containing more than one carbon atom in the framework is the preference for mutual separation. A difference in stability of 60 KJ mol^{-1} between the 1,2 and 1,6 isomers of $C_2B_4H_6$ may reflect this propensity, since there is exclusive 5-coordination in this cluster. The rearrangement of the 1,2- isomer to the 1,6- isomer has been experimentally observed.

A simple rule for the prediction of the position of electrophillic or nucleophillic substitution at boron atoms within clusters has been derived from the wealth of M.O. calculations on carbaborane clusters[132]. This rule enables a very approximate relative electronegativity to be assigned to each boron atom within the cluster by means of the following simple dictum; The negative charge on a boron atom decreases on bonding to higher numbers of carbon atoms and for coordination to a given number of carbon atoms the negative charge decreases with higher coordination.

The skeletal carbon atoms are generally the most electropositive atoms of the carbaboranes[130,133,134], contrary to that expected from the normal electronegativies of boron and carbon. Increased electropositivity accompanies increased coordination of the carbon atom.

The bridging hydrogens of fragment carbaboranes are located between boron atoms only. To date no discrete B-H-C or C-H-C bridges have been identified. Another feature of the carbon atom incorporation into borane clusters is exhibited by the tricarbaborane <u>closo</u>-$C_3B_5H_7$. This compound is unique because one of the carbon atoms is without a terminal hydrogen, the so called 'naked carbon'[61,62]. In view of this the high fluxionality observed in its n.m.r. spectra is not suprising.

The incorporation of transition metal atoms into the framework of carbaboranes (or boranes) clusters by the synthetic methods previously

outlined usually yields products that have the polyhedral structures that are readily predicted from the SEPT. In some cases unexpectedly open structures are observed, as noted earlier for the 'slipped' icosahedral carbaborane derivatives $[M(C_2B_9H_{11})_2]^{n-4}$ of the late transition metals, i.e. where M = Ni(II) and Au(III).

Examples of intermediate size metallacarbaboranes with unexpectedly open nido structures were synthesized by Stone et al[105] using Pt(0) reagents. Thus, in addition to the expected closo product obtained from the polyhedral expansion of $Me_2C_2B_6H_6$ the isomeric minor product $(Et_3P)_2PtMe_2C_2B_6H_6$ was also isolated. This product was found to have the gross tricapped trigonal prismatic structure[135] predicted from the closo SEP count. The platinum atom occupies a pentahapto position as a vertex of the trigonal prism (Figure 30). The diamond face B(7).C(8).B(9).Pt(6) was however found to have a non-bonding distance between the boron atoms (defining an edge of the basic trigonal prism), giving a distorted open framework and was therefore denoted as a nido cluster.

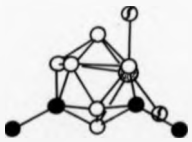

Figure 30. Structure of $(Et_3P)_2PtMe_2C_2B_6H_6$

The analagous reaction of $[Pt(PEt_3)_2(trans\text{-}stilbene)]$, with closo $R_2C_2B_7H_7$ (R = H or Me), afforded only a single product[123, 124]. The structure of $(Et_3P)_2PtMe_2C_2B_7H_7$ as determined by X-ray diffraction[136], showed similar non-bonding interactions giving distortions from the expected square antiprismatic geometry.

A suggested rationale for these observed nido structures involves the adoption of a 16 electron configuration of the Pt(II) species. Stone[137] further suggests that in the nido platinacarbaboranes, only two molecular orbitals of suitable energy and orientation are available for cluster bonding as opposed to the three required for complete incorporation into the closo framework.

In comparison to the open nido square antiprismatic structure of the platinacarbaborane noted earlier, the diferracarbaborane[138] $(\eta\text{-}C_5H_5)_2Fe_2C_2B_6H_8$ has a fully triangulated closo structure that is grossly distorted from the expected square antiprismatic geometry (Figure 31). Of two iron atoms one caps a six membered chair conformation face (C.B.C.Fe.B.B). This compound has 'n' SEP's available for bonding in the framework rather than 'n+1' required for a normal closo structure since each $(\eta C_5H_5)Fe$ fragment only contributes one electron. This type of structure has been designated the title 'hyper-closo' by Hawthorne et al[138,139], another example being the ruthenacarbaborane $(Et_3P)_2RuC_2B_7H_9$.

More recently some analogous metallaborane clusters with similar structural deviations have been prepared by Greenwood et al[140,141], who has assigned to them the term 'iso-closo'. The ten vertex compound $[H(PPh_3)(Ph_2C_6H_4)Ir(B_9H_8)]$ for example has a similar structure to the previously noted ruthenacarbaborane (see Figure 31).

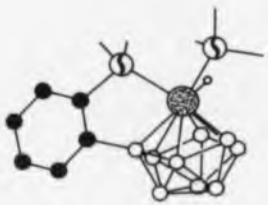

Figure 31. Structure of the 'iso-closo' metallaborane $[H(PPh_3)(Ph_2C_6H_4)Ir(B_9H_8)]$

In addition to the iso-closo ten vertex structure, Greenwood et al have also isolated nine vertex clusters with 'n' SEP counts and unusual iso-closo type structures, an example of which is the iridaborane $(PMe_3)_2HIrB_8H_7Cl$. It has been suggested by Kennedy[142] that in order to achieve the higher connectivity in the iso-closo clusters the metal atom must contributes a further orbital for skeletal bonding, giving four in total. Baker[143] on the other hand prefers to rationalise the structures in terms of the Mingos capping principle[35]. The controversy regarding the description of the bonding in these hyper-closo and iso-closo clusters has recently been focused upon by Mingos et al[144], who have applied Stone's 'Tensor Surface Harmonic Theory'[37] to the ten vertex geometries. The results of these calculations favoured the hyper-closo model adopted by Baker and did not support the proposed contribution of a fourth metal atomic orbital for skeletal bonding.

CHAPTER TWO

CHAPTER 2. ELEVEN, TEN, AND NINE VERTEX MONOCARBON CARBABORANES.

2.1. INTRODUCTION

There is considerable current interest in the formation and properties of cluster molecules, and in particular the rearrangement reactions undergone by such molecular frameworks. One way to study such rearrangements is to label the framework with a substituent atom, for example by substituting a skeletal boron atom with a single carbon atom. These mono-carba-boranes have obvious advantages over disubstituted species, since the presence of only one hetero atom enables its position in the cage to be more easily determined subsequent to reactions in which rearrangement occurs.

An additional attraction of the monocarbaboranes is the fact that they have been much less extensively studied than either the boranes or dicarbaboranes as alluded to in Chapter 1. Transition metal derivatives[44,145], in particular those of intermediate size monocarbaboranes, are similarly less numerous. The main objective of the project was therefore to prepare a number of novel metalla-carbaboranes from these mono carbon substituted borane frameworks, the characterisation of which could potentially elucidate novel features of the cluster reaction mechanisms. In order to achieve the desired goal, the initial work necessarily concentrated on the preparation of the required precursor monocarbaboranes.

The carbaboranes of initial interest were the nine, ten and eleven atom monocarbaboranes produced from the reaction of decaborane and the cyanide ion (See Figures 10 and 32.). This reaction introduces a single carbon atom into the decaborane framework to yield two products, one of which, $(Me_3N)CB_9H_{11}$, has suffered the removal of a

1) Subrogation and expansion

$$B_{10}H_{14} \xrightarrow[2)\ H^+\\ 3)\ Me_2SO_4]{1)\ CN^-} 6\text{-}NMe_3\text{-}6\text{-}CB_9H_{11} + 7\text{-}NMe_3\text{-}7\text{-}CB_{10}H_{12}$$

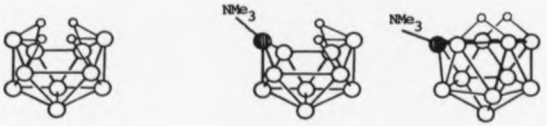

2) De-amination

$$6\text{-}NMe_3\text{-}6\text{-}CB_9H_{11} \xrightarrow[2)\ MeOH\ /\ H_2O]{1)\ Na\ /\ NH_3\ (liq)} [CB_9H_{12}]^-$$

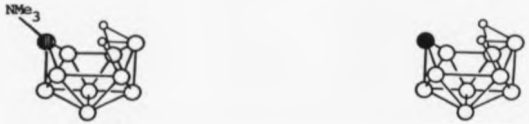

3) Cage degradation

$$[CB_9H_{12}]^- \xrightarrow{FeCl_3\ /\ H^+} CB_8H_{14}$$

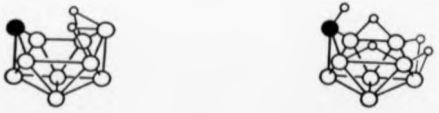

Figure 32. Preparation of carbanonaborane(14) from decaborane(14).

skeletal boron atom. Subsequent de-amination and cage degradation of this subrogation product yields carbanonaborane(14), CB_8H_{14}. This arachno monocarbaborane was of particular interest because of its open polyhedral structure, intermediate size and potential reactivity towards organometallic reagents. Since only closo cobalt, nickel[146,147,148] and iridium[149] derivatives of carbanonaborane(14) and a single nido platinum derivative[150,151] had been previously synthesized and reported, effort was exclusively focused on the transition metal chemistry of this carbaborane.

Preliminary studies on the preparation of these intermediate size monocarbaboranes[5,44,45,149], failed to identify the precise reaction conditions and subsequent work-up procedures. In addition, though structures of the intermediate products have been proposed, they remain tentative and without assignment of the resonances in the ^{11}B n.m.r. spectra. The initial objective of this work was therefore to optimise the yields of the monocarbaborane products from the reaction of decaborane, establishing unequivocally the skeletal structure of each cluster with assignment of the resonances in the ^{11}B n.m.r. spectra where possible.

As a result of the work carried out on the preparation of CB_8H_{14}, carbanonaborane(14), the yields of intermediates have been optimised as far as possible and the preparation simplified by removing the need to carry out an exhaustive chromatographic separation. Most of the isolated intermediates have been characterised by two dimensional (2D) n.m.r. spectroscopy. The anion $[CB_8H_{13}]^-$ has also been prepared by reaction of the parent carbaborane with lithium alkyl reagents and similarly characterised by 2D n.m.r. spectroscopy.

2.2. SYNTHESIS OF INTERMEDIATE SIZE MONOCARBABORANES.

2.2.1. PREPARATION OF 6-NMe_3-6-CB_9H_{11} FROM DECABORANE(14).

The first stage of the preparation of carbanonaborane(14) is the preparation of the monocarbaborane 6-NMe_3-6-CB_9H_{11}. This carbaborane was prepared as a mixture with 7-NMe_3-7-$CB_{10}H_{12}$ in the following way[5]. Decaborane(14) was dissolved in an aqueous solution of sodium cyanide to yield a solution containing the $[6\text{-}NCB_{10}H_{13}]^-$ anion. Treating this solution with hydrochloric acid produced a mixture of two amino-carboranes which were subsequently methylated using Me_2SO_4 and isolated to yield the mixture comprising 6-NMe_3-6-CB_9H_{11} and 7-NMe_3-7-$CB_{10}H_{12}$(see Figure 32 and below).

$$B_{10}H_{14} \xrightarrow[2)\ H^+ \\ 3)\ Me_2SO_4]{1)\ CN^-} 6\text{-}NMe_3\text{-}6\text{-}CB_9H_{11} + 7\text{-}NMe_3\text{-}7\text{-}CB_{10}H_{12}$$

Of these two carbaboranes the first is required to undergo further reaction to yield the monocarbaborane CB_8H_{14}, whilst the latter CB_{10} carbaborane is a less desirable product. It is therefore advantageous to be able to force the ratio of the two carbaboranes obtainable from the reaction of decaborane(14) towards the production of the subrogated CB_9 carbaborane.

In several experiments using acid concentrations ranging from 4 M to 12 M the yield of product mixture was always found to be in the range 21-22g from 20g of decaborane(14). The yields obtained had therefore to be in the range 67-74% based on decaborane used. The lower pessimistic figure is calculated assuming the mixture is only

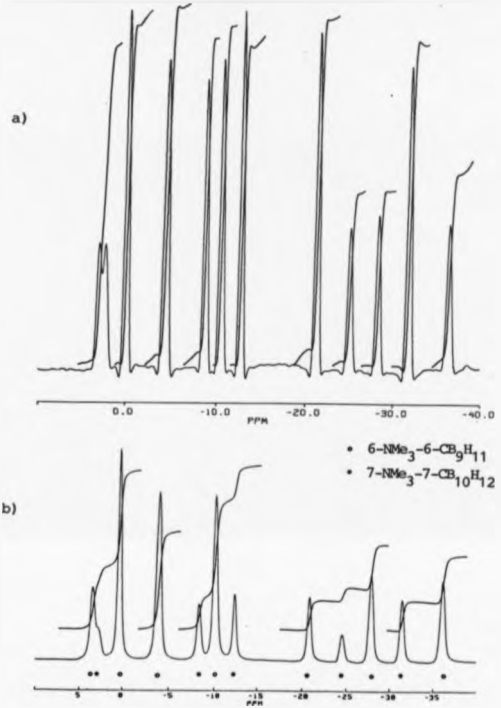

Figure 33. Typical ^{11}B n.m.r. spectra of mixtures of 6-NMe_3-6-CB_9H_{11} and 7-NMe_3-7-$CB_{10}H_{12}$ obtained from cyanide treatment of decaborane(14). Ratios found in these examples to be a) 1.1 : 1 and b) 3.2 : 1 for CB_9:CB_{10} respectively.

NMe_3-7-$CB_{10}H_{12}$ whilst the higher and optimistic figure assumes only $NMe_3CB_9H_{11}$ to be present in the mixture.

Calculation of the ratio of the two products was conveniently obtained from comparison of the integrals for the unique peaks of each component in the 128.8 MHz ^{11}B n.m.r. spectrum of the mixture. Whilst this appears to rely on prior knowledge of the pattern of the n.m.r. spectrum for each component, (information available from the literature[5,44]) it is also accessible from the relative changes in intensity of the various resonances from differing mixtures obtained as seen by comparing the spectra shown in Figure 33. It should be noted that the validity of the measurement of the ratio of the two components in this way was confirmed to be appropriate by chromatographic separation of such reaction mixtures and subsequent component quantification and identification.

Conflicting reports of the ratio of the monocarborane products obtained are given in the literature[5,44]. The molar ratio of the products, $NMe_3CB_9H_{11}$: $NMe_3CB_{10}H_{12}$ is reported by K. Base et al[5] and W. Knoth[44] as 1 : 2 and 7 : 3 respectively. In the former case 'dilute acid' was used, whereas in the latter, 12 molar hydrochloric acid was used in the work up. Since the formation of $NMe_3CB_9H_{11}$ involves the removal of a skeletal boron atom by a degradation reaction one might expect higher acid strength to be favourable. Preparations carried out using varying acid strength (4 molar to 12 molar) have shown no correlation between $NMe_3CB_9H_{11}$ yield and acid strength.

The most important factors effecting the ratio of the CB_9 and CB_{10} products were found to be reaction temperature and time. The optimum yield of 6-NMe_3-6-CB_9H_{11} was obtained if the work-up was carried out with in the following way;

1) Cool the 8 molar acid in an ice-bath to 5°C.

2) Drip the aqueous $[6\text{-}NCB_{10}H_{13}]^-$ into the acid solution solution with stirring over a period of one hour.

3) Stir for at least a further hour allowing the solution to equilibrate to room temperature and to ensure complete reaction, (Indicated by total absence of gas evolution)

Under these conditions the ratio of two carbaborane products $NMe_3CB_9H_{11}$: $NMe_3CB_{10}H_{12}$ was found to be 3.2 : 1.0. This represents a total product yield of 73% and a selectivity to the CB_9 derivative of 56% based on decaborane consumed. These findings obviously confirm and indeed improve upon the findings of W. Knoth. This ratio of products is nearly the reverse of the 1 : 2 ratio quoted by K. Base et al suggesting a fundamental difference in work-up time or temperature.

The noted sensitivity of the reaction to duration of work up time indicated that the CB_9 product may arise from the stepwise degradation reaction of the CB_{10} product rather than from a concerted carbon insertion and boron ejection reaction. This does not however seem to be the case, as prolonged acid treatment of the resultant mixture does not further improve upon the CB_9 product yield.

As noted earlier, of the two carbaborane products $NMe_3CB_9H_{11}$ and $NMe_3CB_{10}H_{12}$, only the former is required for subsequent reaction to ultimately yield CB_8H_{14}. Hence, separation of the two components is required. The use of solvent extraction as a method of separating the two monocarborane products was unsuccessful due to similar solubilities in a range of solvents. Separation by vacuum sublimation also proved unsuccessful.

The separation of the two components is noted[5] by K. Base et al to be achieved using 'dry column chromatography on silica gel in

dichloromethane'. The separation of the two components of the monocarborane product mixture was in fact achieved only by very lengthy and difficult flash column chromatography on silica. The best method for achieving this was to preload the column with the mixture adsorbed onto 40% of its weight of silica. With reasonably large column loadings, some loss of resolution compared to using a solution was observed, though greatly improving the amount of mixture that could be separated in one experiment. Thus 10.6 g of a product mixture shown by n.m.r. spectroscopy to be a 2.3 : 1 mixture of $NMe_3CB_9H_{11}$ and $NMe_3CB_{10}H_{12}$ was separated to give a 4.7 g and 0.8 g of the pure compounds respectively. Only 2% of the material was unaccounted for with the remainder recovered as a middle unseparated fraction. Assuming this fraction to be approximately 50:50 in composition, the chromatographic separation confirms the n.m.r. analysis of the mixture composition.

The 11B{1H} n.m.r. spectra of $NMe_3CB_9H_{11}$ and $NMe_3CB_{10}H_{12}$ obtained are comparable, taking into account differences in chemical shift due to different solvents, to the literature values[5,152]. None of the reported resonances have been assigned to boron atoms in the proposed structures, in both cases. For $NMe_3CB_{10}H_{12}$ a 2D $^{11}B - ^{11}B$ COSY n.m.r. spectrum was obtained and a complete structure - ^{11}B n.m.r. resonance assignment obtained. A 2D study of $NMe_3CB_9H_{11}$ was not undertaken in preference for a study of the parent carborane anion $[CB_9H_{12}]^-$. The n.m.r. studies of these carbaboranes are discussed in Section 2.3.

[Cautionary note : In the preparation discussed it is imperative to ensure that only KOH solution of less than 20% concentration is used to dissolve the dioxinate intermediates otherwise a dramatic fire can occur (see Experimental Section 5.1.2)].

2.2.2. PREPARATION OF $6\text{-}CB_9H_{12}^-$ BY DEAMINATION OF $6\text{-}NMe_3\text{-}6\text{-}CB_9H_{11}$.

The treatment of $NMe_3CB_9H_{11}$ with sodium in liquid ammonia gave on methanolysis the $[CB_9H_{12}]^-$ anion, which was isolated as the tetramethylammonium salt as reported in the literature[5].

$$NMe_3CB_9H_{11} \xrightarrow[2)\ MeOH]{1)\ Na\ /\ NH_3\ (liq)} [CB_9H_{12}]^-$$

The yield of the anion (86%) and the $^{11}B\{^1H\}$ n.m.r. spectrum obtained were comparable to that reported. Disagreement about the structure of the anion noted in the literature has been ratified by a 2D n.m.r. study (Section 2.4) which has provided the complete ^{11}B n.m.r. resonance - structure assignment.

The preparation of $[CB_9H_{12}]^-$ from $NMe_3CB_9H_{11}$ requires lengthy chromatographic separation to obtain the starting material as outlined in Section 2.2.1. This stage of purification has been found to be unnecessary.

Previously reported work[44] has shown that treatment of $NMe_3CB_{10}H_{12}$ with sodium in tetrahydrofuran results in the removal of the exo-polyhedral amino group, whilst similar treatment of $NMe_3CB_9H_{11}$ results in cage closure to give closo-$[CB_9H_{10}]^-$. The de-amination of $NMe_3CB_9H_{11}$ to yield the nido-$[CB_9H_{12}]^-$ is successful under the milder conditions[5] of sodium in liquid ammonia. It therefore seemed likely that under the milder conditions $NMe_3CB_{10}H_{12}$ would be either slow in reaction or totally unreactive.

Using the mixture of carbaboranes from the decaborane / CN^- reaction, de-amination of $NMe_3CB_9H_{11}$ by treatment with sodium in liquid ammonia yielded as expected the $[CB_9H_{12}]^-$ anion whilst the

larger aminocarbaborane $NMe_3CB_{10}H_{12}$ remained unreacted. The solubility of the product anion in water and insolubility of $NMe_3CB_{10}H_{12}$ enabled easy removal of the aminocarbaborane in quantitative amounts and isolation of the product. This preparation also enables confirmation of the ratio of the two components of the original aminocarbaborane mixture by measurement of the isolated aminocarbaborane.

Recently, the Czech group of workers that originally synthesized carbanonaborane(14), CB_8H_{14}, published a method[154] for the isolation of $NH_3CB_9H_{11}$, noting that work on this carbaborane had been hindered by the tedious chromatographic separation of the methylated derivatives. The method described involves the reaction of $NH_3CB_9H_{11}$ with acetone in the presence of hydrochloric acid to form the isopropylidene derivative $6\text{-}Me_2C{=}NH\text{-}6\text{-}CB_9H_{11}$ which is water soluble. The larger CB_{10} amino carbaborane does not react, and being insoluble in water is easily separated from the mixture. The isopropylidene derivative then yields the aminocarbaborane on treatment with dilute solutions of potassium hydroxide and hydrochloric acid. Both this method and that described earlier can be used to obtain pure $[CB_9H_{12}]^-$ for use in the preparation of carbanonaborane(14). Whilst the former isopropylidene method is preferable when the CB_9 aminocarbaborane is required, as for the isolation of other $6\text{-}L\text{-}6\text{-}CB_9H_{11}$ derivatives[150], the latter is preferable for the preparation of carbanonaborane(14) because of the simplicity of the procedure.

2.1.3.2. PREPARATION OF CB_8H_{14} FROM $[CB_9H_{12}]^-$.

The carbaborane CB_8H_{14} was prepared by reaction of $Na[CB_9H_{12}]$ in an acidic solution of $FeCl_3$ as described in the literature[5]. The product was isolated by extraction into a hydrocarbon and purified by

vacuum sublimation.

$$[CB_9H_{12}]^- \xrightarrow{FeCl_3 \,/\, H^+} CB_8H_{14}$$

The yield of product obtained varied from 13% to 31% based on the decaborane(14) used, considerably less than the 80% quoted in the literature[5]. Repeated experiments to improve on the yield showed that slow addition of the acidic $FeCl_3$ solution, extraction into pentane and rapid drying of the extracts over anhydrous $MgSO_4$ gave the best yields. It should be noted that during vacuum sublimation of the product, it is imperative to ensure that all traces of water have been removed and glassware joints are completely air-tight, otherwise a rapid hydrolysis/oxidation reaction occurs which is accompanied by a blue flash of light. In these circumstances, a significant proportion of the product may still be redeemable since the degraded product forms a layer over underlying carbanonaborane(14), which with care can still be purified by sublimation.

The ^{11}B and ^1H n.m.r. spectra obtained for carbanonaborane(14) are in agreement with the reported chemical shifts[5]. Assignment of resonances in both spectra were made from the results of 2D n.m.r. studies (see Section 2.3).

2.1.4. PREPARATION OF $[CB_8H_{13}]^-$ FROM CB_8H_{14}.

In preference to the literature preparation[5] of $[CB_8H_{13}]^-$ by deprotonation of CB_8H_{14} with aqueous K_2CO_3 and isolation as the tetramethylammonium salt, the anion was prepared in ether solution by reaction with stoichiometric ratio of lithium alkyl reagents. In this way undesirable hydrolysis of the precursor was avoided and solutions were compatible with air or moisture sensitive organometallic reagents.

2.3. TWO DIMENSIONAL N.M.R. STUDIES OF CARBABORANE CLUSTERS.

The use of nuclear magnetic resonance spectroscopy (n.m.r.) in the study of boranes and their derivatives has been well documented[14, 155]. More recently two dimensional (2D) homo and hetaro nuclear chemical shift correlation spectroscopy[156,157] (COSY) data have also been shown to be useful in providing additional structural information. A description of n.m.r. spectroscopy as applied to boron hydrides is given in Appendix II.

The application of homonuclear 2D ^{11}B n.m.r. techniques have been utilised by Grimes[158] and others[159] to elucidate boron hydride cluster connectivity. The spectra produced exhibit diagonal symmetry with cross peaks due to scalar spin-spin coupling, indicating adjacent nuclei (see Appendix II for a more detailed description). Boron atoms connected by a bridging hydrogen have been found, in general, not to give rise to such coupling[158,159]. This is explained in terms of the negligible electron density along the B-B vector predicted in the theoretical description of three-centre bridging hydrogen bonds. However, some exceptions have been noted[158], as in nido-2-$(C_5H_5)CoB_4H_8$ and nido-$[C_6(Me)_6]Fe(C_2H_3)_2C_2B_3H_5$, wherein the observation of a coupling between boron atoms connected by a bridging hydrogen is proposed to be due to increased delocalisation of bonding in the basal plane of these two clusters.

These 2D n.m.r. techniques have been applied to several of the nine, ten and eleven vertex monocarbaboranes prepared during the course of this work in order to extend the current knowledge of the type of results to be expected using these techniques. The results are discussed in the following sections.

2.3.2. A 2D NMR STUDY OF NIDO-$NMe_3CB_{10}H_{12}$.

The skeletal electron count for this monocarbaborane is 13 SEP's indicating a nido structure based on an icosahedron. The 1:2:2:2:1:2 pattern observed in the ^{11}B n.m.r. spectrum (labelled a-f in Figure 34) is as previously noted[44], consistent with this type of structure.

The 2D ^{11}B COSY spectrum obtained is shown in Figure 35. From the couplings observed in this spectrum and taking into account the two-fold ratio of the resonances 'b', 'c', 'd' and 'f', the total skeletal connectivity is deduced to be as shown in Figure 36a. Some features of this connectivity-structure deduction are explained as follows.

In the proton coupled ^{11}B n.m.r. spectrum, the doublets of resonances 'c' and 'd' exhibit fine structure due to coupling of bridging hydrogens. Because resonances 'c' and 'd' arise from four boron atoms the coupling cannot be due to BH_2 groups. The absence of a cross peak between 'c' and 'd' only indicates that they are not bonded directly but does not rule out the possibility of connection via a bridging hydrogen.

The 'b-b' and 'd-d' connection has to be assumed, since coupling between equivalent atoms is not observable. The carbon atom is positioned so as to retain the observed symmetry, giving the total connectivity corresponding to the structure shown. This confirms the suggested structure of $NMe_3CB_{10}H_{12}$ previously reported[44] (See Figure 36b).

The deshielding effect of the carbon atom on neighbouring boron atoms is clearly illustrated by the down-field shift of the resonances assignable to the boron atoms B(8,11) and B(2,3), compared to those of the B(9,10) and B(4,6) boron atoms. In contrast to this effect, the

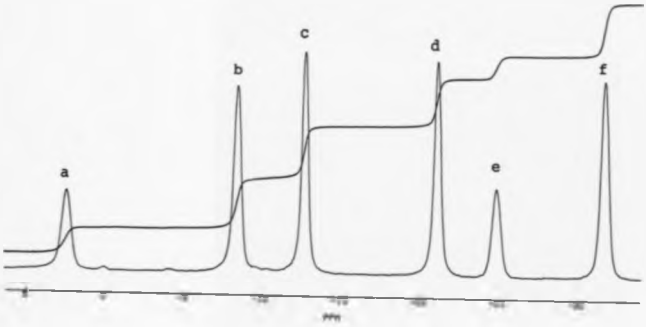

Figure 34. ^{11}B $\{^{1}H\}$ n.m.r. spectrum of $NMe_3CB_{10}H_{12}$

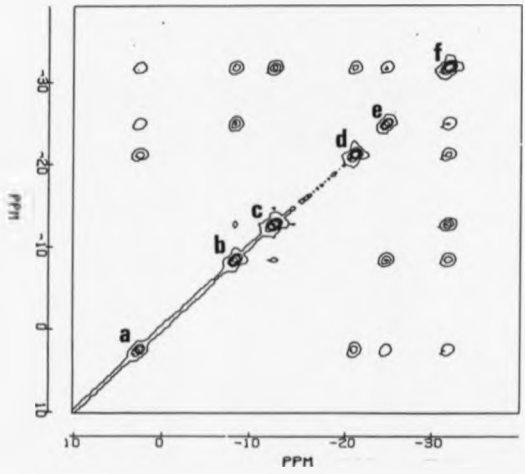

Figure 35. 2D ^{11}B COSY n.m.r. of $NMe_3CB_{10}H_{12}$

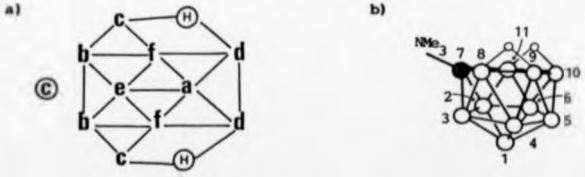

Figure 36. a) Connectivity and b) structure of $NMe_3CB_{10}H_{12}$

lowest field resonance, arising from one of the two unique boron atoms, is assignable to the B(5) boron atom. Not only is this boron atom not adjacent to the skeletal carbon atom but it occupies a position as far removed from it as is possible within the framework, a position usually described as 'antipodal' relative to the carbon atom.

This relationship is more easily envisaged by viewing the structure of $NMe_3CB_{10}H_{12}$ as an icosahedron with the C(7) and B(5) atoms as the polar vertices, i.e. antipodal, with the missing vertex of the nido structure being absent from one of the tropical planes. Of course other atom combinations may also be described as antipodal, for example B(4) and B(11) or B(6) and B(8).

Similar deshielding effects are observed for the resonances of boron atoms adjacent and antipodal to the carbon atoms in the icosahedral closo dicarbaboranes[155]. In the ortho-dicarborane isomer, illustrated below, the boron atoms B(9,12) antipodal to the carbon atoms C(1,2) produce the lowest field resonance in the ^{11}B n.m.r. spectrum. In this instance, however, of the six boron atoms adjacent to the carbon atoms the two that are adjacent to both carbon atoms, B(3,6), give rise to the highest field resonance, an apparently diamagnetic (upfield) shift.

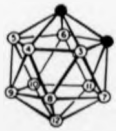

Structure of ortho-$C_2B_{10}H_{12}$.

2.3.2. A 2D NMR STUDY OF NIDO-$[CB_9H_{12}]^-$.

W. Knoth[44] and K. Base et al[5] have proposed a decaborane type stucture for the $[CB_9H_{12}]^-$ anion with the bridging hydrogens in the position shown in Figures 37a and 37b respectively. This disagreement about the position of the bridging hydrogens has been solved by a 2D n.m.r. study, which has also provided the complete ^{11}B n.m.r. resonance assignment.

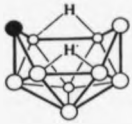

a)

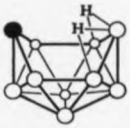

b)

Figure 37. Proposed structures of the $[CB_9H_{12}]^-$ anion.

The skeletal electron count for the $[CB_9H_{12}]^-$ anion gives 12 SEP's indicating a nido structure based on an octadecahedron, analogous to decaborane(14). The 2:1:2:2:1:1 pattern observed in the ^{11}B n.m.r. spectrum (labelled a-f in Figure 38) is consistent with the predicted structure. The cross peaks observed in the 2D ^{11}B COSY spectrum of $[CB_9H_{12}]^-$ (Figure 39) indicates the fundamental cluster connectivity to be as shown in Figure 40a.

In the ^{11}B n.m.r. spectrum resonances 'b' and 'd' (ratio 1:2) exhibit small couplings attributable to bridging hydrogens, thus indicating that the bridging hydrogens are located in the position proposed by Base et al[5]. A complete n.m.r. resonance structure

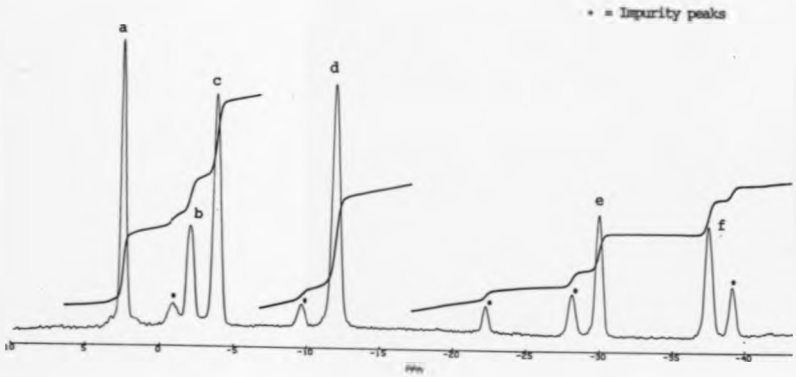

Figure 38. $^{11}B\{^{1}H\}$ n.m.r. spectrum of the $[CB_9H_{12}]^-$ anion.

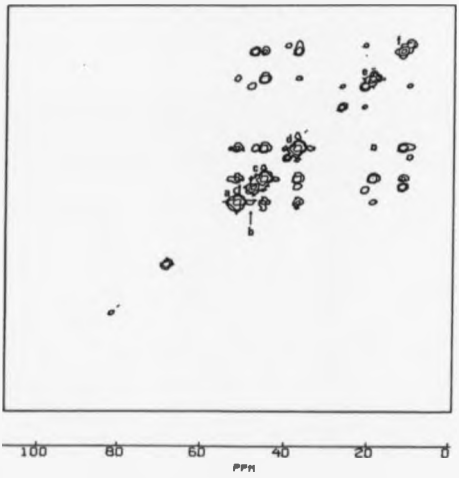

Figure 39. 2D ^{11}B COSY n.m.r. spectrum of the $[CB_9H_{12}]^-$ anion.

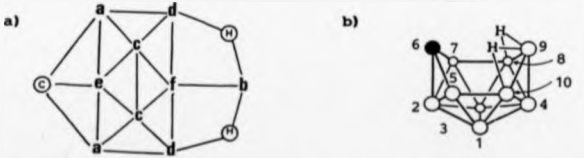

Figure 40. a) Connectivity and b) structure of the $[CB_9H_{12}]^-$ anion.

assignment is therefore derived by comparing Figures 38, 40a and 40b.

One unusual feature of the ^{11}B COSY spectrum is the observation of a strong 'a'-'d' coupling and a weak 'b'-'d' coupling. The former coupling is indicative of boron atoms directly connected thus discounting the Knoth type structure, whilst the latter weak coupling appears to arise from boron atoms connected by bridging hydrogens. This of course is contrary to the previous findings[158,159] including the ^{11}B COSY spectrum of $NMe_3CB_{10}H_{12}$ described earlier. The observation of coupling between B-H-B boron atoms in $[CB_9H_{12}]^-$ was the first indication that such couplings could be obtained and indeed perhaps were characteristic of a B-H-B-H-B apical skeletal fragment.

By comparing the ^{11}B n.m.r. spectra of the isoelectronic clusters, $B_{10}H_{14}$ and $[CB_9H_{12}]^-$ (Figure 41) the deshielding effect of the carbon atom can be clearly seen by a relative displacement downfield (~10 p.p.m.) of the B(5,7) and B(2) boron resonances in the carbaborane, due to the position of the boron atoms adjacent to the carbon atom and a similar diamagnetic shift of the approximately antipodal boron atom to high field as noted in the previous discussion.

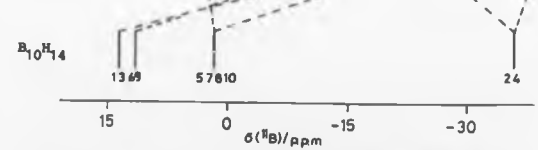

Figure 41. Stick diagram showing correlation between the ^{11}B n.m.r. spectra of $B_{10}H_{14}$ and $[CB_9H_{12}]^-$.

2.3.3. A 2D NMR STUDY OF CB_8H_{14}.

The application of Wade's rules to the neutral monocarborane, CB_8H_{14}, leads to a predicted arachno structure based on a octadecahedron[29]. The absence of the most highly connected vertex and one adjacent vertex, as indicated by Williams' rules[8], with the four bridging hydrogens positioned symmetrically in the open face of the cluster, yields the predicted structure, as shown in Figure 42.

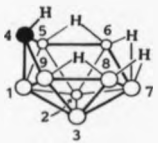

Figure 42. Proposed structure of CB_8H_{14}.

The ^{11}B n.m.r. spectrum of CB_8H_{14} contains five resonances (relative intensities 1:1:2:2:2, denoted a-e in Figure 44.). This pattern is of course compatible with the proposed structure as noted by Base *et al*[5] and Dolansky *et al*[162]. A complete assignment of the ^{11}B resonances has been proposed by Base *et al* based upon both $J(B\text{-}H_{(bridge)})$ couplings and experience of chemical shifts in related systems[162,163], as follows:

B(7), 17.0 p.p.m.; B(1), -3.7 p.p.m.; B(5,9), -6.3 p.p.m.

B(6,8), -34.9 p.p.m.; B(2,3), -41.1 p.p.m.

From the ^{11}B COSY spectrum recorded for CB_8H_{14} (Figure 44) two alternative assignments of skeletal connectivity are possible, as shown

Correct skeletal connectivity

Alternative connectivity

Figure 43. Alternative skeletal connectivities of CB_8H_{14}.

in Figure 43. The two possible assignments arise because of the high symmetry of the carborane. In the 2D ^{11}B n.m.r. experiment the carbon atom is 'invisible' giving a false additional two-fold symmetry to the framework. Similar difficulties in assignment have been noted in the ^{11}B COSY of the icosahedral 1,2- and 1,7- $C_2B_{10}H_{12}$ isomers[158]. The correct structure of CB_8H_{14} may be deduced by examining the ^1H n.m.r. spectra obtained with selective ^{11}B decoupling as shown in Figure 45.

The fully coupled ^1H n.m.r. spectrum consists of a series of quartets at lower field arising from the $B-H_{(terminal)}$ bonds, while at higher field there are two resonances (-0.13 and -2.06 p.p.m.) from the CH_2 group, and two broad resonances (centred at -0.64 and -3.76 p.p.m.) from the two sets of bridging hydrogen atoms. These four higher field resonances have been previously reported, but not the complete ^1H spectrum, and no assignment of individual sets of bridging hydrogens exists[11,12].

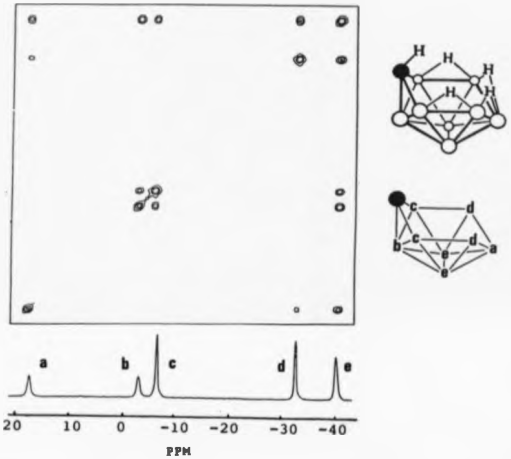

Figure 44. 2D ^{11}B COSY n.m.r. spectrum of CB_8H_{14}.

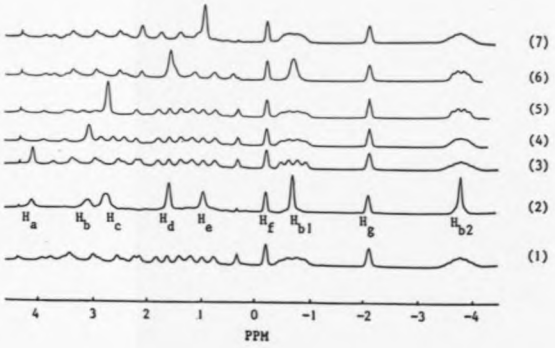

Figure 45. $^{1}H\text{-}\{^{11}B_{selective}\}$ n.m.r. spectra of CB_8H_{14}
(1) Fully coupled, (2) Broad band decoupled, and (3-7) Selective decoupling at ^{11}B frequencies B_a to B_e respectively.

Though the broad band decoupled spectrum gives little information, selective decoupling at resonance 'a' (assigned as in Figure 44) partially decouples the set of bridging hydrogens at -0.64 p.p.m., while the same treatment at resonance 'b' only decouples the terminal proton at 3.17 p.p.m. On decoupling at resonance 'c' one of the CH resonances becomes sharpened, indicating that the resonance is assignable to the boron atoms B(5,9) adjacent to the carbon atom. The same effect does not result from decoupling at the ^{11}B frequency of resonance 'd'.

The unambiguous skeletal connectivity is therefore deduced as shown in Figure 43, with the ^{11}B n.m.r. resonances being assigned to the cluster boron atoms as follows;

a=B(7), b=B(1), c=B(5,9), d=B(6,8) and e=B(2,3).

This assignment derived from spectroscopic probing of cluster connectivity agrees with that proposed by Base *et al*[162,163] from empirical observations.

Using the above information, the complete assignment of the resonances in the ^1H n.m.r. spectrum of CB_8H_{14} is as follows;

Terminal: H_a=$H_{B(7)}$, 4.20 p.p.m.; H_b=$H_{B(1)}$, 3.17 p.p.m.; H_c=$H_{B(5,9)}$, 2.83 p.p.m.; H_d=$H_{B(6,8)}$, 1.66 p.p.m.; H_e=$H_{B(2,3)}$, 1.0 p.p.m.

Bridging: H_{b1}=$H_{B(6,8)-B(7)}$, -0.6 p.p.m.; H_{b2}=$H_{B(5,9)-B(6,8)}$, -3.7 p.p.m..

C-H : H_f=$H_{\underline{exo}}$, -0.1 p.p.m.; H_g=$H_{\underline{endo}}$, -2.0 p.p.m..

The $^1H_{(terminal)}$ resonances follow the same pattern as in the ^{11}B n.m.r. spectrum.

As was found for $[CB_9H_{12}]^-$, closer inspection of the ^{11}B COSY spectrum reveals that a coupling between B(6,8) and B(7) is observed, though they are connected by a bridging hydrogen. This is in contrast to the absence of coupling between B(5,9) and B(6,8), which are also

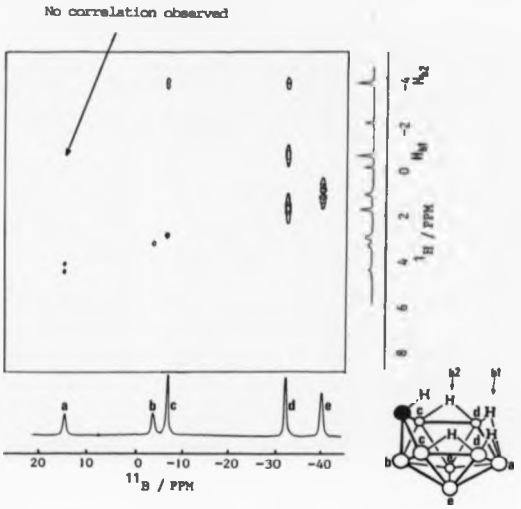

Figure 46. ^{1}H-^{11}B Correlation map of $CB_8H_{14}^-$.

connected by bridging hydrogens.

The theoretical justification for the absence of such coupling is based on an ideal symmetrical bridging hydrogen bond where there is negligible electron density along the B-B vector. In an unsymmetrical

bridge there may be significant electron density along the B-B vector, enabling scalar spin-spin coupling. These results indicate therefore that CB_8H_{14} contains two distinctly different types of bridging hydrogen atoms. Further evidence in support of this proposal is seen in the ^1H-^{11}B shift correlation map (Figure 46). The correlations between the ^{11}B resonances and the resonances due to the attached hydrogen atoms are as shown.

All of the hydrogen resonances are readily assignable and are in agreement with that deduced above. The high field symmetrical bridging hydrogens exhibit coupling to c[B(5,9)] and d[B(6,8)] as expected. The lowfield resonance due to the proposed unsymmetrical bridging hydrogens give an observable coupling to d[B(6,8)] only and not to a[B(7)]. From this information the bridging group is deduced to be displaced towards the d[B(6,8)] boron atoms. Similar conclusions have been reached following theoretical CNDO/2 calculations[162].

Corroborating evidence for the unsymmetrical bridge is provided by the $^1H\{^{11}B_{selective}\}$ n.m.r. spectra (Figure 45). Decoupling at both c[B(5,9)] and d[B(6,8)] resonance frequencies has an identical effect upon the highfield bridging hydrogen resonance, compatible with that expected for a symmetrical bridge. In comparison, decoupling at the d[B(6,8)] frequency, results in a near-singlet resonance for the lowfield bridging hydrogen resonance, whereas decoupling at the a[B(7)] frequency has considerably less effect. The differential effect of selective decoupling reflects a larger association of the d[B(6,8)] boron atoms with the bridging hydrogen atom compared to that of the a[B(7)] boron atom, as expected for an unsymmetrical bridging hydrogen displaced closer to the a[B(6,8)] boron atoms. The refined structure is therefore as shown in Figure 44.

2.3.4. A 2D NMR STUDY OF $[CB_8H_{13}]^-$ ANION.

The $^{11}B\{^1H\}$ n.m.r. spectrum of the anion $[CB_8H_{13}]^-$ is similar to that of the neutral CB_8H_{14} showing five resonances (relative intensities 2:1:1:2:2, denoted a - e in Figure 47), indicating that symmetry of the framework is preserved on deprotonation, in agreement with the model proposed by Base[5].

The highest field resonance e, shows the largest $J(B\text{-}H_{(bridge)})$ coupling, and can be assigned to the B(6,8) pair of boron atoms. Further assignments cannot be made with confidence from this spectrum alone, since the relative chemical shifts of the resonances have changed substantially compared with those from CB_8H_{14}. To date the complete assignment of the ^1H and ^{11}B resonances for the anion has not been established.

The connectivity in the skeleton of the anion is derived in a similar manner to that used for the neutral precursor, namely, from the ^{11}B COSY spectrum (Figure 47) and a series of $^1H\text{-}\{^{11}B_{(selective)}\}$ spectra to give the following ^{11}B n.m.r. resonance assignments:

a=B(5,9), 4.0 p.p.m.; b=B(7), -3.9 p.p.m.;c=B(1), -21.5 p.p.m.;
d=B(2,3), -30.4 p.p.m.; e=B(6,8), -35.2 p.p.m.

Notable features of the ^{11}B COSY spectra of the neutral CB_8H_{14} and the anionic $[CB_8H_{13}]^-$ are now evident, as follows. Firstly, in the anion, a strong coupling is observed between B(5,9) and B(6,8), which is absent in the neutral precursor, suggesting the symmetrical bridges in CB_8H_{14} are now unsymmetrical in $[CB_8H_{13}]^-$. Secondly, for the three boron atoms B(6,8) and B(7) in the anion, now connected by a single unique bridging hydrogen, a weak coupling is still observed, and is a clear indication of significant electron density along the B-B vector in this four-centre bond. Thirdly, an unexpected reduction in the

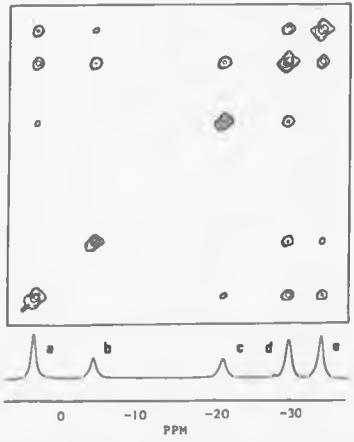

Figure 47. ^{11}B COSY of $[CB_8H_{13}]^-$ anion.

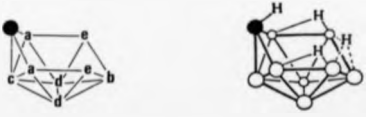

a) b)

Figure 48. a) Connectivity and b) structure of the $[CB_8H_{13}]^-$ anion.

observed coupling between B(1) and B(5,9) of the anion is also found, which is presumably produced by the shift of electron density on the open face of the cluster towards the B(6,8) positions, resulting in a reduced electron density between those boron atoms adjacent to the carbon atom.

From the assignment of the ^{11}B n.m.r. resonances for the neutral CB_8H_{14} and anionic $[CB_8H_{13}]^-$ noted above the order of the resonances has changed in a way that confirms the electron density shift, such that the lowest-field resonance is now attributable to the relatively less electronegative boron atoms B(5,9) adjacent to the carbon atom, though the major factor may be the relative up-field shift of the B(7) boron atom due to the reduction in coordination.

The practical difficulties involved in the preparation of the anion, namely the elimination of hexane residues from the lithium butyl solution, lead to impurity peaks in the ^1H spectrum. However, assignment of the lowfield resonances from the terminal hydrogen atoms was made possible by a series of difference spectra produced by subtracting the spectra obtained by selective ^{11}B decoupling from the fully decoupled spectrum.

The impurities do not interfere with the more important upfield CH_2 and bridging hydrogen resonances, which appear as two singlets (C-H), a distorted quartet and a broad multiplet, of ratio 1:1:2:1 respectively. The unique bridging hydrogen resonance, at highfield, is complex because of the coupling to three boron atoms. The distorted quartet resonance is due to greater coupling to the B(6,8) boron atoms than to the B(5,9) boron atoms in the unsymmetrical bridge. The complete assignment of the resonances in the ^1H n.m.r. spectrum of $[CB_8H_{13}]^-$ is as follows;

Terminal: H_a=$H_{B(5,9)}$, 3.93 p.p.m.; H_b=$H_{B(7)}$, 3.05 p.p.m.; H_c=$H_{B(1)}$, 2.52 p.p.m.; H_d=$H_{B(2,3)}$, 1.44 p.p.m.; H_e=$H_{B(6,8)}$, 1.29 p.p.m.;
Bridging: H_{b1}=$H_{B(5,9)-B(6,8)}$, -1.04 p.p.m.; H_{b2}=$H_{B(6,8)-B(7)}$, -2.0 p.p.m..
C-H : H_f=H<u>exo</u>, 0.34 p.p.m.; H_g=H<u>endo</u>, -0.36 p.p.m..

The $^1H_{(terminal)}$ resonances again follow the same pattern as in the ^{11}B n.m.r. spectrum.

Confirmation of the unsymmetrical nature of both types of hydrogen bridge is provided by subtraction spectra. A significant effect on both bridging resonances is observed by decoupling at the e[B(6,8)] frequency, whilst decoupling at a[B(5,9)] and b[B(7)] frequencies has only a marginal effect on both bridging hydrogen resonances. The refined structure of the anion, $[CB_8H_{13}]^-$, to show the unsymmetrical bridging groups is shown in Fig 48.

In order to exemplify further the presence of unsymmetrical bridging hydrogens in the anion a ^1H-^{11}B correlation map was recorded (Figure 49). The expectation was, from the results of the ^1H-^{11}B correlation map obtained for CB_8H_{14} that couplings for both bridging hydrogens in the anion would be observed since they are both unsymmetrical. Unfortunately the map obtained was found to include a number of false reflected peaks due to quad imaging. Despite efforts to eliminate this effect using instrumental methods these anomalous peaks (annotated on Figure 49) remained, thereby reducing the reliability of the remaining couplings and the value of the experiment.

It is noteworthy that the highfield <u>endo</u>-CH resonance has a broader linewidth (50 Hz) than either the <u>exo</u>-CH resonance (24 Hz) of the anion, or the <u>endo</u>-CH resonance (33 Hz) in the neutral precursor.

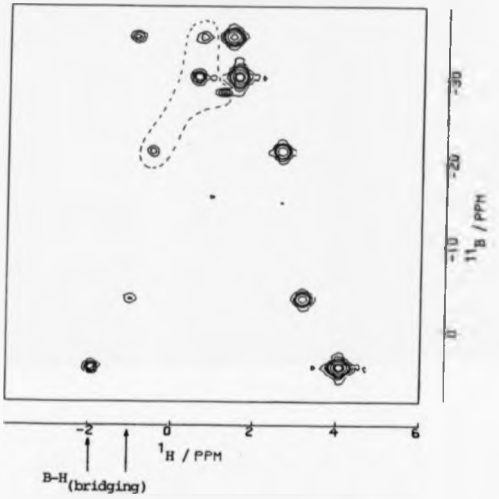

Maximum of nine correlations expected.
Eight of these are observed.
The anomalous peaks are enclosed in a dotted line

Figure 49. ^{1}H-^{11}B correlation map for the $[CB_8H_{13}]^-$ anion.

When the ^{1}H n.m.r. resonance of either of the bridging hydrogens are stimulated at their own resonance frequency, saturation transfer to the other bridging hydrogen resonance and endo-CH resonance is observed, causing signal enhancement. The spectrum obtained is shown in Figure 51 as a subtraction plot of the ordinary ^{1}H spectrum from the enhanced spectrum (Figure 50). The stimulation of the high field endo-CH resonance causes similar saturation transfer to the three bridging hydrogens yielding an identical spectrum to that shown in Figure 51.

Only the high field endo-CH resonance experiences this effect, not the low field exo-CH. Thus stimulation of the low field CH resonance does not result in saturation transfer and resonance enhancement. To eliminate any suspicion that the transfer is due to the close proximity of these resonances, the saturation experiment was carried out using the lowest field terminal hydrogen resonance. The spectrum obtained (Figure 52) clearly exhibits no saturation transfer to other resonances.

The saturation transfer experiments strongly suggest that the endo-CH hydrogen, and all three bridging hydrogens, are in exchange at room temperature. The exo-CH hydrogen is not involved in the exchange process. Similar saturation transfer experiments on CB_8H_{14} showed that the neutral precursor does not exhibit such exchange.

Line width broadening observed during variable temperature n.m.r. studies yields a very approximate activation energy for this process of 50 kJ mol^{-1}. The removal of a proton has therefore significantly activated the open face of the cluster, including the endo-hydrogen on the carbon atom. While fluxional behaviour of bridging hydrogen atoms in boranes and carbaboranes is well established, the observation of

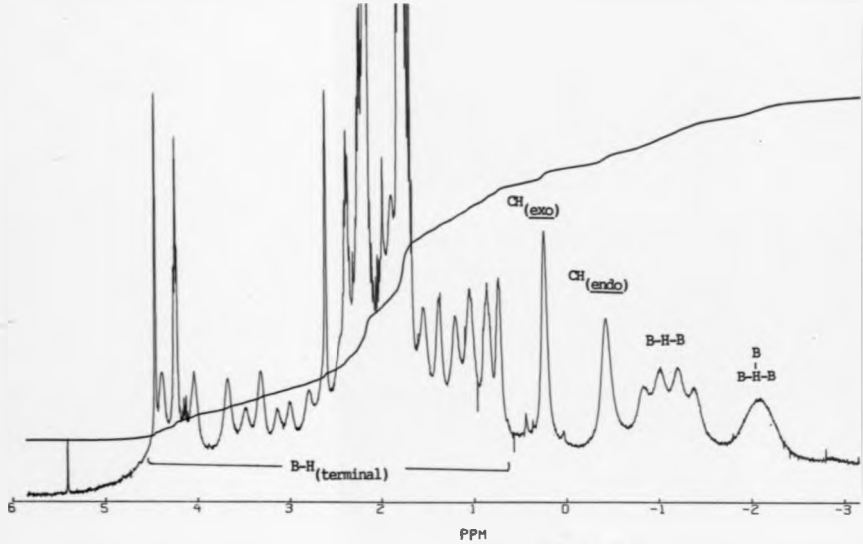

Figure 50. ^{1}H n.m.r. spectrum of the $[CB_8H_{13}]^-$ anion.

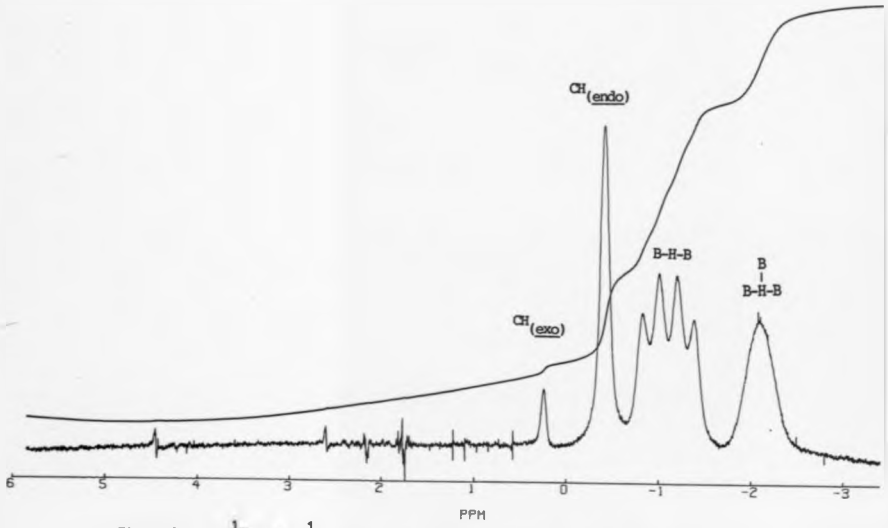

Figure 51. $[^1H_{(sat)} - {}^1H]$ n.m.r. subtraction spectrum for specific saturation of the bridging or endo CH hydrogens in the $[CB_8H_{13}]^-$ anion.

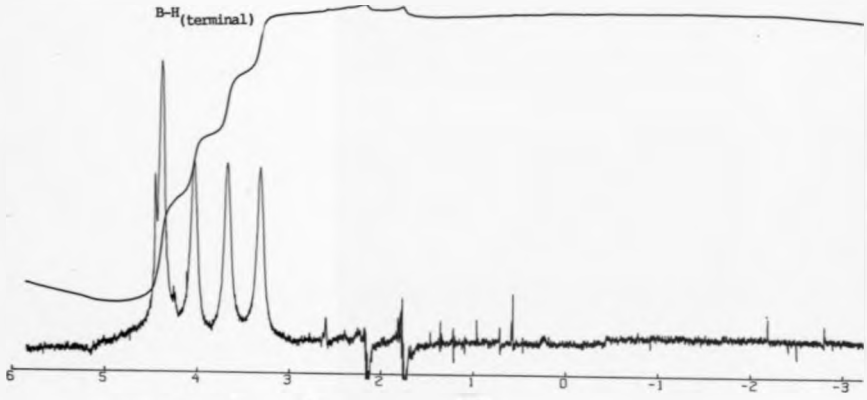

Figure 52. $[^1H_{(sat)} - {}^1H]$ n.m.r. subtraction spectrum for specific saturation of the lowest field $BH_{(terminal)}$ hydrogen in the $[CB_9H_{13}]^-$ anion.

such a process incorporating a single endo-C-H hydrogen atom appears to be a novel feature.

During the early stages of the previously described study of CB_8H_{14}, an attempt was made to deuterate the carbaborane in order to assist the spectral analysis and assignment. The initially observed spectra of the product were found to be inconsistent with the envisaged straightforward substitution process and the experiment was abandoned. The later discovery of the hydrogen exchange process in the $[CB_8H_{13}]^-$ anion, led to a re-examination of this deuteration experiment.

The deprotonation-deuterolysis method previously used, involving condensation of DCl gas onto isolated $Li[CB_8H_{13}]$ was found to be unsatisfactory. An alternative approach was therefore adopted, which consisted of deprotonation of the neutral precursor in $(C_2D_5)_2O$ followed by hydrolysis with excess D_2O.

Since hydrogen exchange occurs in the anion, it was expected that repeated deprotonation and deuterolysis would yield successive deuterated product in which the endo-CH and both bridging hydrogen n.m.r. resonances are similarly reduced in intensity compared to the remaining exo CH resonance. Unfortunately, when each product was analysed, such stepwise reduction in resonance integral was not obtained beyond the first treatment due to gross product degradation, possibly as a result of excessive manipulation.

An interesting result was however obtained by comparing the n.m.r. spectrum of the deuterated product after a single treatment and that obtained after five successive treatments followed by product purification by sublimation. The ^1H n.m.r. spectra of both of these products showed identical reductions in the $CH_{(endo)}$ and $BH_{(bridging)}$ resonances compared to the $CH_{(exo)}$ resonance (see Figure 53b).

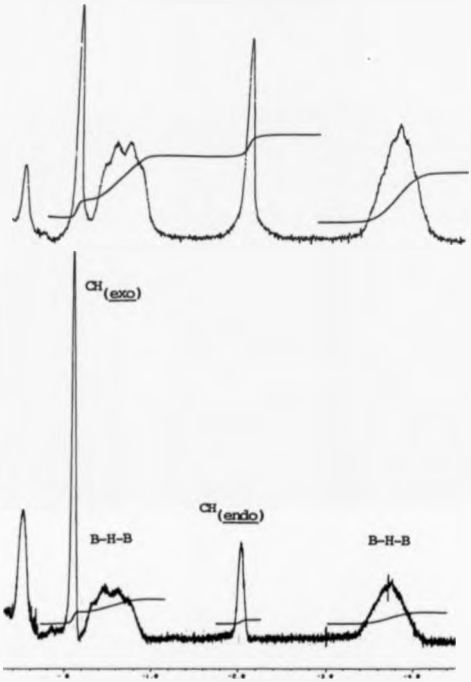

Figure 53. ^{1}H n.m.r. spectra of a) CB_8H_{14} and b) CB_8H_{14} after five deprotonation-deuterolysis cycles. (Note only the relevant high-field portion of each spectrum is shown).

The observed ^1H n.m.r. resonance integration ratio of $CH_{(exo)}$:$BH_{(bridging)}$:$CH_{(endo)}$:$BH_{(bridging)}$ thus changed from 1:2:1:2 respectively in the original CB_8H_{14} sample to 1:1:0.3:1 in the deuterated product.

Two aspects of this experiment require clarification. Firstly, deuterium exchange between CB_8H_{14} and D_2O alone was not observed without prior deprotonation, and secondly, the previously described resonance saturation experiments showed no exchange between terminal and bridging BH hydrogens, thus eliminating the need to consider these processes as contributing factors.

The observed deuteration ratio of the $CH_{(endo)}$ and $BH_{(bridging)}$ hydrogens therefore shows, of the five endo hydrogen sites in the neutral carbaborane, a higher selectivity towards deuteration of the $CH_{(endo)}$ hydrogen. Whilst this could be interpreted as an indication that protonation of the anion can occur at the skeletal carbon atom as opposed to the presumed reprotonation at the triangular B(6,7,8) face of the anion, it more likely reflects a stronger primary isotope effect for the $CH_{(endo)}$ hydrogen than for the $BH_{(bridging)}$ hydrogen. Thus on protonation of the anion, scrambling of the endo hydrogens around the face to form the neutral carbaborane is effected by a stronger $C\text{-}D_{(exo)}$ bond than the $B\text{-}D_{(bridging)}$ bond. The slower exchange of the more strongly bound C-D deuterium thus resulting in a greater reduction of the $CH_{(exo)}$ resonance in the ^1H n.m.r. spectrum.

Having investigated the $[CB_8H_{13}]^-$ anion, attempts to produce and identify the di-anion by further removal of a proton were made. This proved to be unsuccessful, possibly due to the observed insolubility of the product in a range of solvents, or more likely the probable cage degradation expected on further activation of the open cluster face.

CHAPTER THREE

CHAPTER 3. TEN VERTEX RUTHENIUM AND OSMIUM MONOCARBON CARBABORANES (CLOSO, NIDO AND ARACHNO MCB_8 FRAMEWORKS, M = Ru, Os)

3.1. INTRODUCTION

A large number of ten vertex polyhedra containing metal and boron atoms in the framework have been synthesised[12,164]. Though a variety of structures have been identified, most of these ten atom clusters adopt a nido structure, based on nido-decaborane(14), wherein the metal atom occupies one of the apical B(6,9) vertices (see Figure 54). Examples of such metallaboranes are the tungsten[165], rhenium[166], ruthenium, osmium[165] and iridium[167] derivatives of the general formula $(L_xH_yM)B_9H_{13}$ characterised by Greenwood et al and the manganese and rhenium derivatives characterised by Gaines et al[168] (see Table 6).

Isomers of the nido-6-substituted $[MB_9]$ metalladecaborane derivatives have been isolated in which the metal atom either occupies another vertex on the open face of the cluster or, more rarely, one of the vertices of the butterfly basal plane, i.e. one of B(1,2,3,4) shown in Figure 54. The two cobaltaborane isomers isolated by Grimes et al[169,170] and Sneddon et al[171] and the recently synthesised ruthenaboranes[172] given in Table 6 illustrate this feature.

In addition to the large number of nido $[MB_9]$ clusters characterised, various other ten vertex metallaboranes have been synthesised, such as the closo $[MB_9]$[173], and bimetallic $[M_2B_8]$ nido[174] and arachno[175] clusters noted in Table 6.

A reasonable number of metalladicarbadecaborane derivatives $[MC_2B_7]$ have also been isolated[103,176,177,178,179], some of which are also shown in Table 6.

In comparison to the number and variety of metalladecaboranes and metalladicarbadecaborane derivatives known, the range of ten

Type	Compound	Observed Structure	Hetero Atom Position
$[MB_9]$	$(PMe_2Ph)_3H_2WB_9H_{13}$	Nido	W(6)
	$(PMe_2Ph)_3HReB_9H_{13}$	Nido	Re(6)
	$(PMe_2Ph)_3RuB_9H_{13}$	Nido	Ru(6)
	$(PMe_2Ph)_3OsB_9H_{13}$	Nido	Os(6)
	$(PMe_2Ph)_2HIrB_9H_{13}$	Nido	Ir(6)
	$[(CO)_3MnB_9H_{13}]^-$	Nido	Mn(6)
	$[(CO)_3ReB_9H_{13}]^-$	Nido	Re(6)
	$(C_5H_5)CoB_9H_{13}$	Nido	Co(5)
	$(C_5H_5)CoB_9H_{13}$	Nido	Co(2)
	$(C_6Me_6)RuB_9H_{13}$	Nido	Ru(1)
	$(C_6Me_6)RuB_9H_{13}$	Nido	Ru(2)
	$(PhMe_2P)_2NiB_9H_7Cl_2$	Closo	Ni(1)
$[M_2B_8]$	$(C_5Me_5)_2Co_2B_8H_{12}$	Nido	Co(6,9)
	$(C_5Me_5)_2Co_2B_8H_{12}$	Nido	Co(5,7)
	$(PhMe_2P)_4Pt_2B_8H_{10}$	Arachno	Pt(6,9)
$[MC_2B_7]$	$[(C_5H_5)CoC_2B_7H_{11}]^-$	Nido	C(6,2), Co(7)
	$[(C_5H_5)CoC_2B_7H_{11}]^-$	Nido	C(6,7), Co(8)
	$[(C_5H_5)CoC_2B_7H_9]^-$	Closo	C(1,10), Co(2)
	$[(C_6H_6)RuC_2B_7H_{11}]^-$	Nido	C(5,6), Ru(2)
	$[(C_6Me_3H_3)FeC_2B_7H_9]^-$	Closo	C(1,6), Fe(2)
	$[(C_6Me_3H_3)FeC_2B_7H_{11}]^-$	Nido	C(9,10), Fe(6)
	$[(Et_3P)Pt(MeC_2)B_7H_7]^-$	Nido	Pt(10)

Table 6. Some examples of ten atom metallaboranes $[MB_9]$, dimetallaboranes $[M_2B_8]$ and metalladicarbaboranes $[MC_2B_7]$ derivatives.

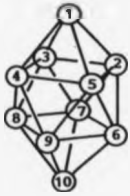

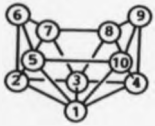

Figure 54. Skeletal numbering schemes for ten vertex closo and nido clusters.

Type	Compound	Observed Structure	Hetero Atom Positions
$[MCB_8]$	$(C_6H_4PPh_2)(PPh_3)IrC(OH)B_8H_6(OMe)$	Iso-nido	C(10), Ir(7)
	$(PPh_3)PtCB_8H_{12}$	Nido	C(6), Pt(9)
	$[(C_5H_5)CoCB_8H_9]^-$	Closo	C(1), Co(6)
	$[(C_5H_5)NiCB_8H_9]^-$	Closo	C(1), Ni(10)
	$[(PPh_3)_2HIrCB(PPh_3)B_7H_8]^-$	Closo	C(10), Ir(2)
$[M_2CB_7]$	$(C_5H_5)_2Ni_2CB_7H_8$	Closo	C(1), Ni(6,7)
	$(C_5H_5)_2CoNiCB_7H_8$	Closo	C(1), Co(2), Ni(10)
	$(C_5H_5)_2CoNiCB_7H_8$	Closo	C(1), Co(6), Ni(8)
	$(C_5H_5)_2CoNiCB_7H_8$	Closo	C(1), Co(6), Ni(10)
	$(C_5H_5)_2CoNiCB_7H_8$	Closo	C(1), Co(6), Ni(9)

Table 7. The known metallacarbadecaboranes derivatives.

vertex systems containing only a single carbon and metal atom, i.e. the $[MCB_8]$ metallacarbaboranes, are limited in number, and further examples are required before bonding and structural trends become apparent.

The derivatives synthesised to date, listed in Table 7, incorporate metal fragments from the cobalt and nickel groups, and include *nido* compounds containing iridium[180] and platinum[150,151], and *closo* species with cobalt[146,147,181], nickel[146,147,148] and iridium[149]. In addition *closo* bimetallic species containing either two nickel atoms[146,147], or a nickel and cobalt atom[182,183] (four isomers identified) are also known.

The *arachno* carbaboranaborane(-1) anion $[CB_8H_{13}]^-$ is now well characterised[5,184](See Chapter 2, Section 3.4 and Figure 48b.); it is isoelectronic with the borane anion $[B_9H_{14}]^-$ and the dicarbaborane $C_2B_7H_{13}$, and possesses the same framework structure albeit with the expected differences in distibution of the hetaro atom(s) and *endo* hydrogens about the open face of the cluster.

Since both of these isoelectronic borane and dicarbaborane clusters have been successfully utilised in the preparation of a number of the metalla derivatives noted in Table 6, it was desirable to test the suitability of the monocarbaborane anion as a precursor for the preparation of the related $[MCB_8]$ clusters. In particular, to attempt to expand the range of such clusters beyond those noted in Table 7, by preparation of *nido* and if possible, *arachno* derivatives, since the known $[MCB_8]$ clusters have predominantly *closo* structures.

The reaction of $[CB_8H_{13}]^-$ with several ruthenium and osmium phosphine halide compounds has yielded a number of *closo*, *nido* and *arachno*-$[MCB_8]$ compounds, as described in the following sections.

3.2 THE VERTEX NIDO-AND ARACHNO METALLACARBABORANES $(MCB_9$ FRAMEWORKS, M = Ru, Os)

THE SYNTHESIS AND CRYSTAL AND MOLECULAR STRUCTURES OF $[9,9,9\text{-}(CO)(PPh_3)_2\text{-}NIDO\text{-}9,6\text{-}MCB_8H_{10}\text{-}5\text{-}(PPh_3)]$. ((1) M=Ru; (2) M=Os), AND $[9,9,9\text{-}(\eta\text{-}C_5H_5)(H)(PPh_3)\text{-}ARACHNO\text{-}9,6\text{-}RuCB_8H_{12}]$ (3).

The reaction of the arachno-anion $[CB_8H_{13}]^-$ with the ruthenium halide reagent $[RuCl(CO)(H)(PPh_3)_3]$ in refluxing benzene yielded the nido-ruthenacarbadecaborane $[(CO)(PPh_3)_2RuCB_8H_{10}(PPh_3)]$, (1), as the major product. This compound was obtained in 54% yield as a red crystalline solid, after purification by preparative t.l.c. using dichloromethane and light petroleum as the eluent. The idealised equation for the formation of this product is as follows;

$$Li[CB_8H_{13}] + [RuCl(CO)(H)(PPh_3)_3] \longrightarrow [(CO)(PPh_3)_2RuCB_8H_{10}(PPh_3)] + 2\,H_2 + LiCl$$
(1)

The corresponding osmium compound $[(CO)(PPh_3)_2OsCB_8H_{10}(PPh_3)]$, (2), was obtained in 34% yield by a similar procedure, and was isolated as an orange crystalline solid.

The n.m.r. spectra of both (1) and (2) are consistant with three open cluster structures as shown in Figure 55, where the metal atom is coordinated into the triangular portion of the open face of the arachno-carbaborane, to yield the ten vertex decaborane-like framework. Thus the ^{11}B spectrum of (1) shows seven of the eight expected resonances for an asymmetrically substituted framework, with one resonance integrating to a two-fold ratio, due to coincidental

overlap (see Figure 56). The ^{1}H n.m.r. spectrum exhibits resonances due to seven $B\text{-}H_{(terminal)}$ hydrogens, two inequivalent B-H-Ru protons at higher field, a single C-H proton and the aromatic hydrogens of the triphenylphosphine ligands. The ^{31}P n.m.r. spectrum shows three resonances of which two are assignable to the $Ru(CO)(PPh_3)$ fragment and one to the cage substituted triphenylphosphine group. The presence of a metal carbonyl group is indicated by an infrared absorption at 1965 cm^{-1}. The n.m.r. data obtained for compounds (1) and (2) are collated in Table 8.

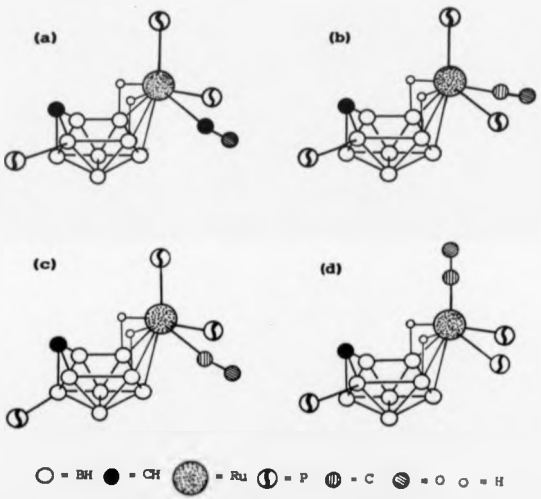

Figure 55. Alternative structures for the nido metallacarbaboranes (1) and (2).

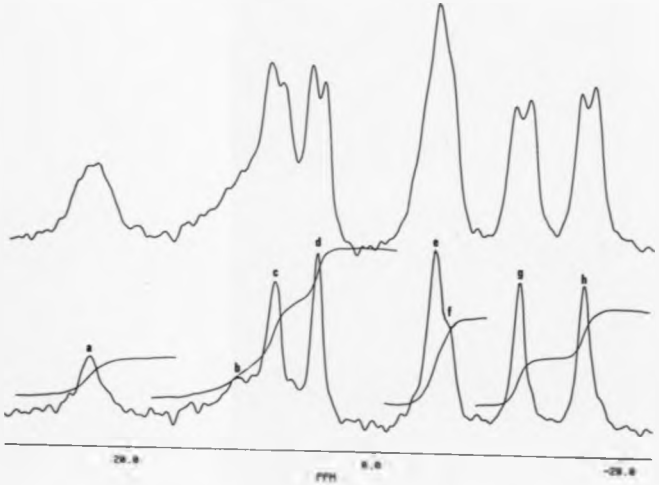

Figure 56. The ^{11}B and $^{11}B\{^1H\}$ n.m.r. spectra for compound (1).

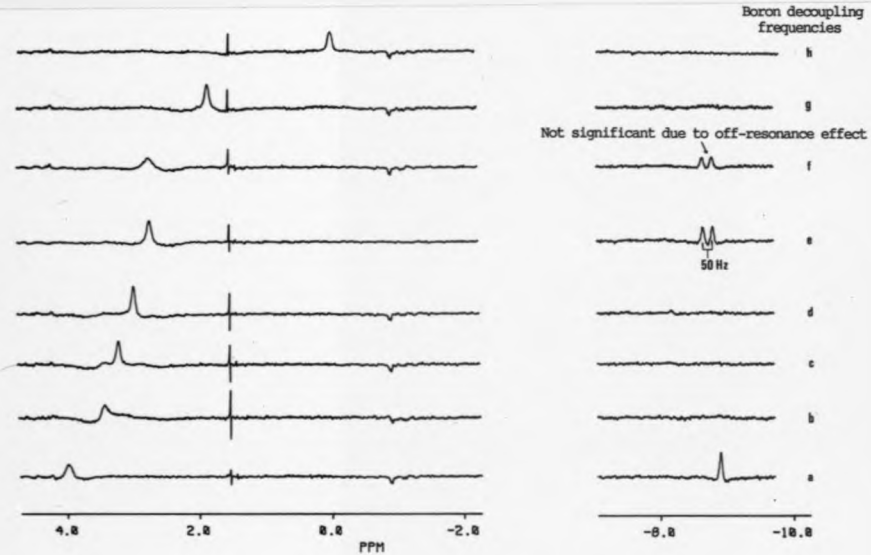

Figure 57. Series of selectively boron decoupled proton spectra for compound (1), presented as $^{1}H\{^{11}B_{(selective)}\}-^{1}H$ subtraction spectra, (Boron decoupling frequencies as annotated.).

BORON-11 AND PROTON N.M.R. DATA

Tentative Assignment	Compound(1)		Compound(2)	
	^{11}B (p.p.m.)	^{1}H (p.p.m.)	^{11}B (p.p.m.)	^{1}H (p.p.m.)
8	23.2	3.98	18.4	4.57
7	11.1	3.43	11.0	3.35
1,3	8.2	3.22	6.9	3.77
1,3	4.8	2.98	2.8	3.53
5	-4.8	B-P	-6.0	B-P
10	-4.8	2.73	-6.5	3.29
2,4	-11.6	1.83	-13.5	2.90
2,4	-16.8	0.02	-23.7	-0.23
C(6)-H(exo)	6.0		6.1	
B(8)-H-M(9)	-8.9		-8.9	
B(10)-H-M(9)	-8.72		-8.67	
PPh_3		6.9-7.5		6.9-7.7

PHOSPHORUS-31 N.M.R. DATA

Tentative Assignment	Compound(1) (p.p.m.)	Compound(2) (p.p.m.)
$M(PPh_3)_{axial}$	50.1	18.8
$M(PPh_3)_{equatorial}$	39.3	10.4
$B-(PPh_3)$	8.8	8.8

Table 8. Boron-11, proton and phosphorus-31 n.m.r. data (p.p.m.) for the nido metallacarbaboranes (1) and (2).

The correlation of the n.m.r. resonances to the predicted structure for compounds (1) and (2) were made as follows, considering specifically the assignments made for the ruthenacarbaborane (1).

A series of selectively ^{11}B decoupled ^{1}H spectra shows each of the seven boron resonances to be associated with a terminal hydrogen (see Figure 57 and Table 8). The ^{11}B resonance with a two-fold integral is also found to be associated with only a single hydrogen, thus indicating the overlapping of a B-H and B-P resonance.

Selective decoupling of the ^{11}B resonances at -4.8 p.p.m. and 23.2 p.p.m. resolves the two high field hydride resonances (-8.72, -8.9 p.p.m.) in the ^{1}H spectrum into a doublet and singlet respectively. The high-field shift of these resonances indicates their coordination to the ruthenium atom, whilst resolution on boron decoupling indicates they also bridge to the adjacent boron atoms on the open face of the cluster. Broad band ^{31}P decoupling further resolves the low field hydride doublet resonance into a singlet, $^{2}J(^{31}P\text{-}Ru\text{-}^{1}H) \sim 50$ Hz. The coupling constant is of the order previously reported for such a trans coupling[185], and thus enables unambiguous assignment of the B(8,10) resonances and the hydride resonances that bridge these boron atoms to the ruthenium atom.

A further effect of broad band ^{31}P decoupling is the removal of a small coupling displayed by the C-H resonance, $^{3}J(^{31}P\text{-}B\text{-}C\text{-}^{1}H) \sim 12.5$ Hz, reasonably indicating phosphine substitution at one of the B(2) or B(5,7) boron atoms adjacent to the carbon atom of the assumed 9,6-$RuCB_8$ decaborane-like structure.

The comparison of ^{11}B shifts of (1) with those of the carbaborane $[CB_9H_{12}]^-$ and the isoelectronic ruthenaborane $(CO)(PPh_3)_2(CO)RuB_9H_{11}(PPh_3)$ analogue[11], does not enable definite

assignment of the substitution position to be made, although the asymmetry of the ^{11}B n.m.r. spectrum does favour B(5,7) substitution, as proposed for the borane analogue noted above. The substituted boron atom was subsequently confirmed to be B(5) from the X-ray structure determination of compound (1), thus enabling the previously noted B-P resonance to be unambiguously assigned as B(5), though the ^{31}P coupling is unresolved.

Of the remaining five unassigned resonances, the resonance at 11.1 p.p.m., is far broader than the rest, indicating that it may be due to the remaining boron atom on the open face of the cluster, B(7). Such correlation of resonance between ^{11}B linewidth and cluster position has been noted by Greenwood *et al*[185].

The four remaining ^{11}B resonances are therefore attributable to the B(1,2,3,4) atoms. Though unambiguous assignment is not possible in this instance, tentative assignment can been deduced from comparison of ^{11}B shielding patterns of (1) with those of decaborane(14)[155]. Subsequent spectroscopic data obtained for similar substituted *nido*-ruthenacarbaborane species (compounds (4) and (5) discussed in Section 3.2) has provided support for the assignments given in Table 8.

Of the three resonances in the ^{31}P spectrum at 50.1, 39.3 and 8.8 p.p.m. respectively, the two low-field resonances both show a small doublet coupling $^{2}J(^{31}P\text{-}Ru\text{-}^{31}P)$ - 25 Hz, consistent with a *cis* disposition of the two phosphine substituents on the ruthenium centre. The resonance at 39.3 p.p.m. also shows the *trans* coupling observed for the lower field hydride resonance in the ^{1}H n.m.r. spectrum and is therefore assignable to the equatorial phosphine. The highfield resonance, being a broad unresolved quartet, is assigned to the cage substituted phosphine.

The ^{11}B, ^{1}H and ^{31}P n.m.r. spectra of (2) are very similar to those of (1). A minor point of interest is that of the three resonances in the ^{31}P n.m.r. spectrum, at 18.8, 10.4 and 8.8 p.p.m. respectively, the B(cage)-P resonance occurs with exactly the same shift in both (1) and (2). The other two resonances each show a cis coupling [$^{2}J(^{31}P\text{-}Os\text{-}^{31}P)$ - 10 Hz], with the equatorial phosphine having the additional trans coupling [$^{2}J(^{1}H\text{-}Os\text{-}^{31}P)$ - 44 Hz].

Of the four possible asymmetric structures shown in Figure 55, type (d) is eliminated since spectroscopic evidence shows only one of the metal bound phosphines is trans to the hydride atoms. All of the structures (a) to (c) are thus consistent with the observed n.m.r. data and are therefore the alternative postulated structures for the ruthenium and osmium carbaboranes (1) and (2). It is incorrect to assume that structure (c) would be unlikely to produce the observed deviations from a 1:1:2:2:2 pattern in the ^{11}B n.m.r. spectra as expected of a symmetric molecule because the asymmetry is solely due to the disposition of the ruthenium bound ligands. The ruthenaborane, $[(CO)(PPh_3)_2RuB_9H_{13}]$[185], for example, exhibits asymmetric shifts of the ^{11}B n.m.r. resonances of equal magnitude to those found for compound (1) regardless of the absence of a cage substituent.

The available spectroscopic data are unable to differentiate between the three alternative structures for compounds (1) and (2). In an attempt to discriminate between structures (a), (b) and (c), the ^{11}B COSY n.m.r. spectrum was obtained. Unfortunately, because of the wide linewidth of the resonances observed for this ruthenacarbaborane, the experiment was unsuccessful. Similar failure of this technique was experienced for all other metallacarbaboranes prepared during the course of this work, with the exception of those auracarbaboranes

described in Chapter 4.

In order to deduce the position of the cage phosphine substituent with respect to the metal exo-polyhedral ligands, and because structural parameters were required for comparative purposes with the arachno compound (3) described below, X-ray diffraction studies of both (1) and (2) were undertaken, the details of which are given in Chapter 5.

Compounds (1) and (2) are isomorphous and adopt a nido ten vertex cluster structure, with the carbon and metal atoms in the 6- and 9-positions respectively, with the phosphine cage substituent in the 5-position (Figure 58 shows the ruthenium compound). All skeletal atoms were located, with the presence and position of the bridging and terminal hydrogens being inferred from the n.m.r. data as discussed above. The position of the carbon atom was inferred from the observed bond distances and the thermal parameter behaviour. The skeletal bond distances for both compounds (1) and (2) are given in Figures 59 and 60 respectively, with a comprehensive list given in Chapter 5.

The phosphine substituent is found to be syn with respect to the carbonyl ligand on the ruthenium atom, due probably to a steric requirement. The metal bound phosphines are mutually cis, one being trans to a bridging hydrogen as predicted from the n.m.r. data. Both enantiomers of this chiral molecule are present within the unit cell, as indicated by the centrosymmetric space group.

All bond lengths are within the ranges found in previous metallacarbaborane structures. The most notable feature is the short bond distance of ~ 155 pm between the cage carbon and adjacent boron atoms B(5,7) in the open face of the cluster, compared with that

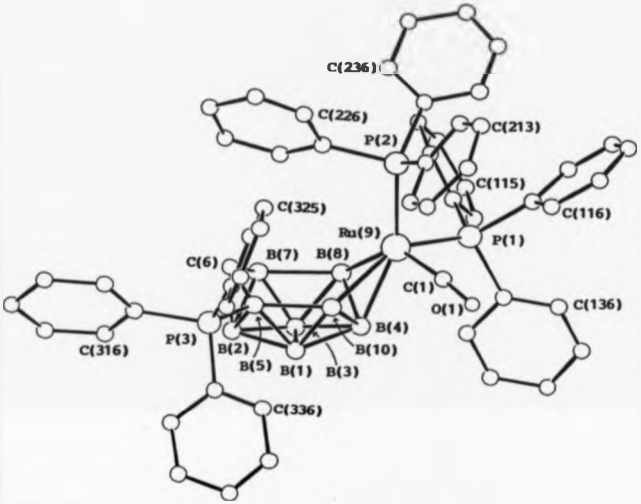

Figure 58. Drawing of the X-ray crystallographically determined molecular structure of the ruthenacarbaborane nido-[9-(CO)-9,9-$(PPh_3)_2$-9,6-$RuCB_8H_{12}$-5-(PPh_3)] (1). (Osmium analogue not illustrated but is essentially identical)

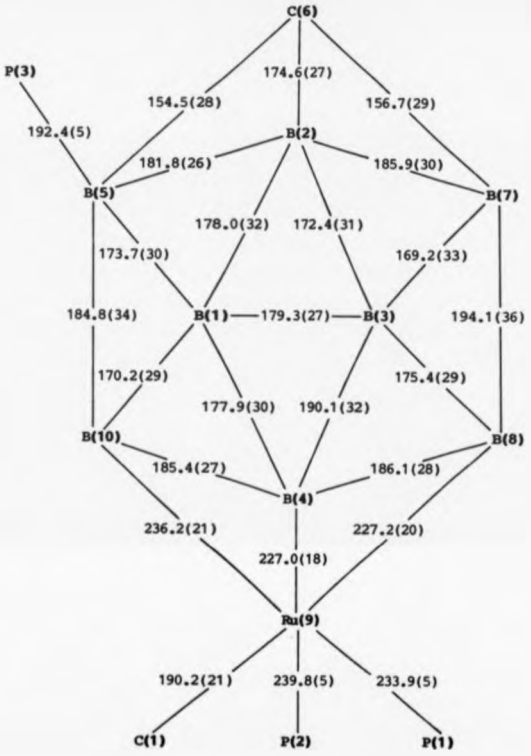

Figure 59. Skeletal interatomic distances (pm), with standard deviations in parenthesis, for the ruthenacarbaborane nido-[9-(CO)-9,9-$(PPh_3)_2$-9,6-$RuCB_8H_{12}$-5-(PPh_3)] (1).

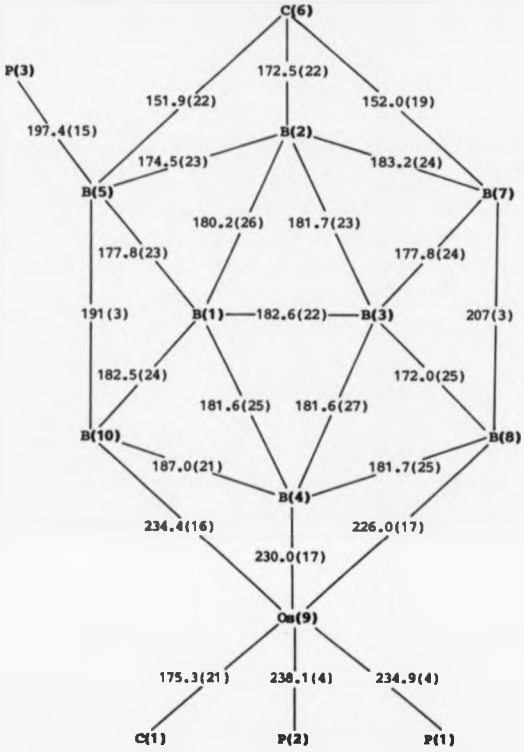

Figure 60. Skeletal interatomic distances (pm), with standard deviations in parenthesis, for the osmacarbaborane nido-[9-(CO)-9,9-$(PPh_3)_2$-9,6-$OsCB_8H_{12}$-5-(PPh_3)] (2).

of - 175 pm to the boron atom B(2) in the basal plane. This may indicate an sp^2 like bonding mode for the C-H group, directed more towards the open face of the cluster, with the tangential p orbital involved in bonding to the basal boron atom. The axial phosphine shows a Ru-P distance some 5 pm longer than that for the cis phosphine ligand.

The coordination geometry at the ruthenium atom is that of a distorted octahedron, with the Ru-P(2) and Ru-B(4) being the axial vectors, with Ru-P(1), Ru-CO, Ru-H(8,9), and Ru-H(9,10) vectors lying in the downward distorted equatorial plane.

The isomorphous osmacarbaborane (2) shows no gross deviations in skeletal geometry or interatomic distance compared to that observed for the ruthenium compound (1). The same pattern in bonding at the carbon-boron and metal-phosphine vectors is also found. The B(cage)-P(3) distance is marginally shorter in (1) than in (2). The carbon of the carbonyl group is some 15 pm closer to the osmium atom than is found in the ruthenium analogue. However, other distances around the osmium atom mirror the pattern and magnitude found in the ruthenium analogue.

A formal electron count where the metal atom provides two electrons and three orbitals for the skeletal bonding, as Ru(II)/Os(II), gives the twelve SEP's required for a nido structure based on the octadecahedron[29]. The metal atoms thus adopt an 18 electron configuration with a quasi-octahedral geometry, the three bonding orbitals in the cluster being largely associated with the two bridging hydrogen atoms between B(8) and B(10) and the metal, with the other one being more involved in the metal-B(2) bond. This cluster is an analogue of the recently reported[185] ruthenium(II) borane

$[(CO)(PPh_3)_2RuB_9H_{11}(PPh_3)]$; the need for the presence of the phosphine on the cage in (1) and (2) to provide the extra skeletal electron is clearly apparent. Further comparisons of the two structures with the arachno compound are given below.

The arachno $[(\eta\text{-}C_5H_5)(H)(PPh_3)RuCB_8H_{12}]$, (3), was obtained as yellow crystals in 67% yield from the action of $[CB_8H_{13}]^-$ on $[RuCl(\eta\text{-}C_5H_5)(PPh_3)_2]$ in a diethyl ether-benzene solvent mixture. In comparison with the previous reaction to form the nido ruthenium and osmacarbaboranes (1) and (2), which was complete in under one hour, this reaction required two days at reflux before the carbaborane reagent was completely depleted. This slower reaction rate might be expected to result from the lower refluxing temperature of the ether-benzene mixture employed in the latter reaction compared to the benzene reflux temperature used in the former. This however conflicts with the observation that negligible reaction was observed when benzene was used as the solvent.

A possible pathway to compound (3) may involve the formation of a cationic ruthenium species followed by metathesis with concomitant loss of a phosphine ligand from the ruthenium centre.

$$[RuCl(\eta\text{-}C_5H_5)(PPh_3)_2] \longrightarrow [Ru(\eta\text{-}C_5H_5)(PPh_3)_2]^+ + Cl^-$$

$$Li[CB_8H_{13}] + [Ru(\eta\text{-}C_5H_5)(PPh_3)_2]Cl \longrightarrow [(\eta\text{-}C_5H_5)(H)(PPh_3)Ru(CB_8H_{12})] + LiCl + PPh_3$$

Thus, the observation of an improved reaction rate when a diethyl ether-benzene solvent mixture is used, compared to benzene alone, may reflect the better solvation of the dissociated ions formed from the

ruthenium precursor dissociation step in the more polar solvent mixture.

The structure of (3) cannot be deduced unambiguously from the ^{11}B n.m.r. data. Though less likely than the favoured 9,6- substituted decaborane(14) like structure, subsequently confirmed by X-ray crystallographic analysis, a 10,5- (or even 8,5) subrogated framework as found for the $[(\eta\text{-}C_5H_5)C_2B_7H_{11}]$ cluster[187], would in principle, be expected to yield the observed n.m.r. behaviour.

Whilst the presence of the $[RuH(\eta\text{-}C_5H_5)(PPh_3)]$ fragment renders the eight cage borons inequivalent, there is in this case also, a coincidental overlap of two resonances since only seven resonances are observed (See Figure 61 and Table 9). The thirteen hydrogens were detected in the ^1H n.m.r. spectrum, and identified as arising from eight terminal B-H, two bridging B-H-B, two C-H, and one Ru-H protons. The protons of the cyclopentadienyl group and the phosphine ligand are also observed, while the ^{31}P n.m.r. spectrum shows a single resonance as expected, at 39.3 p.p.m. The hydride resonance from the Ru-H bond exhibits two couplings, one from the adjacent phosphorus atom of the phosphine ligand, which occupies a position cis to the hydride $[^2J(^{31}P\text{-}Ru\text{-}^{31}P) = 29$ Hz]. With reference to the found 6,9 substituted cluster structure, the other smaller coupling arises from a three bond coupling to a terminal B-H proton on either the B(8) or B(10) atoms bonded to the metal in the open face of the cluster. The coupling $[^2J(H\text{-}Ru\text{-}B\text{-}H) \sim 5$ Hz] is removed by selective decoupling of the three terminal B-H resonances near + 2.5 p.p.m., although the off-resonance effect did not allow the unambiguous identification of the precise beta-hydrogen involved. In addition decoupling ($^1B\text{-}^1H$) of the lower field bridging B-H-B atom causes a sharpening of the Ru-H resonance,

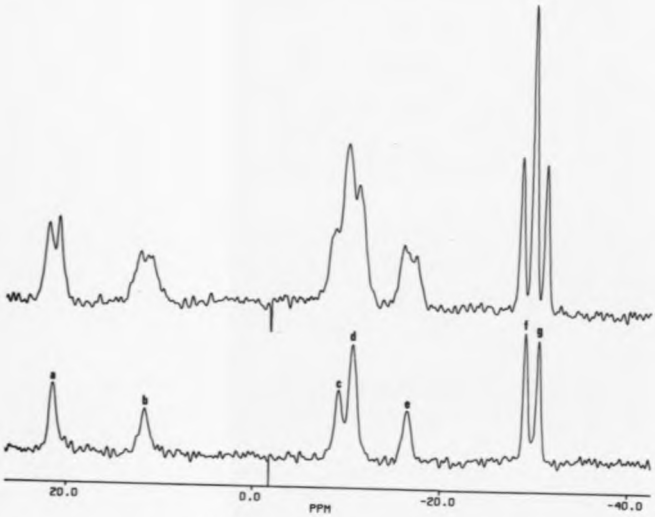

Figure 61. ^{11}B and $^{11}B\{^{1}H\}$ n.m.r. spectra of compound (3).

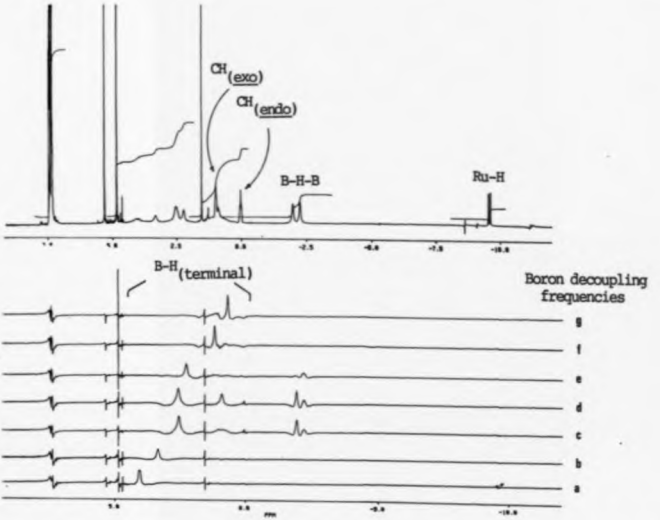

Figure 62. Series of selectively boron decoupled proton spectra for compound (3), presented as $^{1}H(^{11}B_{(selective)})-^{1}H$ subtraction spectra, (Boron decoupling frequencies as annotated).

BORON-11 AND PROTON N.M.R. DATA

Tentative Assignment	^{11}B (p.p.m.)	^{1}H (p.p.m.)
4	20.8	4.1
2	11.0	3.3
10	-9.9	2.5
5,7	-11.3	2.54
5,7	-11.3	0.9
8	-17.2	2.2
1,3	-29.8	1.2
1,3	-31.2	0.7
C(6)-H(exo)		1.0
C(6)-H(endo)		0.1
B(5)-H-B(10)		-2.0
B(7)-H-B(8)		-2.3
Ru(9)-H		-9.5
PPh_3		7.3-7.5
(η-C_5H_5)		4.8

PHOSPHORUS-31 N.M.R. DATA

Tentative Assignment	^{31}P (p.p.m.)
$Ru(PPh_3)_{equatorial}$	57.1

Table 9. Boron-11, proton and phosphorus-31 n.m.r. data (p.p.m.) for the arachno ruthenacarbaborane (3).

whereas the same operation with the high field bridging B-H-B has comparatively little effect. These observations are compatible with the Ru-H being disposed to one side of the open face of the cluster, and, while the Ru-H hydrogen was not detected in the crystal structure analysis, the relative positions of the (C_5H_5) and PPh_3 ligands around the metal centre suggest that the hydrogen is located as shown in Figure 63. The high field C-H resonance is also sharpened on decoupling (^1H-^1H) the bridging B-H-B protons, and thus arises from the endo-C-H while the lowfield C-H resonance is due to the exo-C-H proton.

The effects of selective ^{11}B and ^1H decoupling on the ^1H n.m.r. spectrum allows correlation of the ^{11}B and ^1H spectra, and some limited assignments of the resonances (see Table 9). For example, a series of selectively ^{11}B decoupled ^1H spectra show each boron atom to be associated with a terminal hydrogen. Selective decoupling of the ^{11}B resonances at -9.9(1B), -11.3(2B), and -17.2(1B) p.p.m. sharpens the resonances from the bridging hydrogens at -2.0 and -2.3 p.p.m., thus assigning the former as the four boron atoms in the open face of the cluster. More specifically, decoupling of the ^{11}B resonance at -11.3 p.p.m. sharpens both of the proton resonances (B-H-B) at -2.0 and -2.3 p.p.m., strongly suggesting that this resonance is due to the two boron atoms B(5,7), since of the four boron atoms in the open face, these are the two most likely to possess similar chemical and electronic environments, in the absence of any endo-cage substitution. As expected, decoupling of the ^{11}B resonances at -9.9 and -17.2 p.p.m. sharpens the bridging proton resonances at -2.0 and -2.3 p.p.m. respectively, and are assigned to B(8,10) atoms. The observed sharpening of the Ru-H resonance on decoupling the low field bridging

hydrogen (-2.0 p.p.m.), as noted above, does however identify the lower field ^{11}B resonance (-9.9 p.p.m.) as being due to the B(10) atom. Furthermore, the three resonances at -9.9, -11.3 and -17.2 p.p.m. are broader than the others appearing in the spectrum, and the assignments therefore also reinforce the earlier observations[13] that the boron atoms in the open face of the decaborane-like skeleton usually give rise to broader resonances and vice-versa. Of the four remaining boron resonances, those at -29.8 and -31.2 p.p.m. are tentatively assigned to B(1,3) atoms because of their similar environment within the cluster. Decoupling the ^{11}B resonance at 20.8 p.p.m results in a slight sharpening of the resonance from the Ru-H proton, and this resonance has therefore been assigned to B(4). By elimination the remaining B(2) position has been assigned to the resonance at 11.0 p.p.m.

The structure of (3) determined by a single-crystal X-ray diffraction study is shown in Figure 63, with the skeletal bond distances given in Figure 64, (see also Chapter 5). All skeletal atoms were located except for the hydride on the ruthenium atom, its position being inferred from spectroscopic evidence. This deduction is confirmed by the substantial difference between the P(1)-Ru(9)-B(8) and P(1)-Ru(9)-B(10) angles [89.8(2) and 111.9(1)^{o}] which clearly indicate that the metal hydrogen bond is on the same side of the metal as B(10).

The overall geometry of the cluster resembles that of the arachno-$[B_{10}H_{14}]^{2-}$ anion, as indicated by the position of the two bridging hydrogens on the open face of the cluster, and the CH_2 group at the apical vertex.

The geometry around the ruthenium metal is approximately

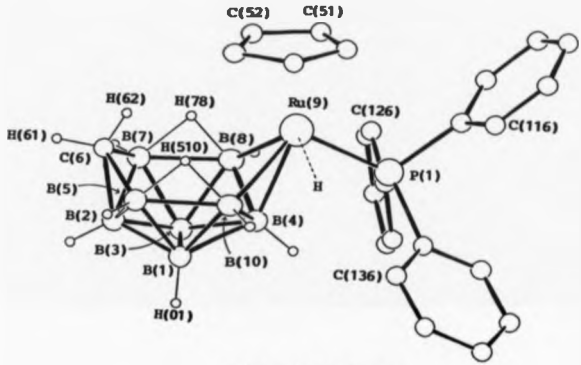

Ru-H hydride indicated
from n.m.r. spectroscopy.

Figure 63. Drawing of the X-ray crystallographically determined molecular structure of the ruthenacarbaborane arachno-[9-(η-C_5H_5)-9-(H)-9-(PPh_3)-9,6-$RuCB_8H_{12}$] (3).

Figure 64. Skeletal interatomic distances (pm), with standard deviations in parenthesis, for the ruthenacarbaborane *arachno*-[9-(η-C_5H_5)-9-(H)-9-(PPh_3)-9,6-$RuCB_8H_{12}$] (3).

dodecahedral with the carborane ligand and cyclopentadienyl ligands both occupying three coordination sites. The remaining two coordination sites are occupied by the phosphine and hydride ligands. The increase in coordination number of the ruthenium metal in this compound compared to that in the nido ruthenacarbaborane (1), results from the loading of the metal with the cyclopentadienyl ligand in addition to the phosphine, carbaborane and hydride groups.

All inter-atomic distances are in the expected range, though differences between the gross geometry of this arachno cluster and the nido compounds (1) and (2) are found. The presence of a CH_2 group on the open face of the cluster is indicative of the arachno class of carbaboranes. The inter-atomic distances from the carbon atom to adjacent boron atoms have a more even distribution than those found in the nido clusters (1) and (2), with the shortest bond now found to be that to B(2) in the basal plane. The angular disposition of B(2), H(61) and H(62) about the carbon is approximately tetrahedral. This can be interpreted as an sp^3 hybridised carbon with strong bonds to the two attached hydrogens and B(2), with the fourth orbital involved in bonding to the adjacent borons B(5,7) on the open face.

The fundamental difference in cluster geometry, expected from a Wade type of structural classification[29] between the nido metalla-carbaborane compounds (1) and (2), and the arachno metallacarbaborane (3) is their conformity to eleven and twelve vertex polyhedra respectively, namely the octadecahedron and icosahedron. Though small, such differences in geometry should manifest itself in the length and breadth of the open face of the cluster, since in the two cases the open face should be so disposed as to accommodate one and two unoccupied vertices respectively. However, because of the overwhelming

size of the metal atom in both types of compound such differences are not observed at or around the metal vertex, both with regard to length and breadth of the open face. However, the width of the arachno cluster (3), B(5) to B(7), is some 25 pm wider than in nido compounds (1) and (2). Such a widening is expected in an arachno ten atom cluster due to conformation of the open face to the icosahedral structure less two pentahapto vertices, compared to the more condensed eleven vertex nido octadecahedral structure in which one six coordinate vertex is unoccupied.

The structure of compound (3) is clearly similar to either the arachno-$[B_{10}H_{14}]^{2-}$ anion, with the CH_2 and metal vertices subrogating the two $[BH]^{2-}$ vertices, or the dicarbaborane analogue, arachno -6,9--$C_2B_8H_{14}$, with one of the CH_2 vertices subrogated by the $Ru(H)(\eta-C_5H_5)(PPh_3)$ fragment.

The compound (3) presents an interesting problem with regard to the usual electron counting procedure. If the ruthenacarbaborane (3) is considered to be an arachno cluster, (26e; 13 SEP's), this infers that the carbaborane ligand $[CB_8H_{12}]$ can be considered to be a hypho cluster, thus also having an SEP count of thirteen, indicating a 4- charge. The oxidation state of the ruthenium metal centre is thus indicated to be is Ru(VI), from coordination of the cyclopentadienyl ligand, hydride and notionally $[CB_8H_{12}]^{4-}$ carbaborane ligand. The Wade type calculation of the electron contribution of the $Ru(H)(\eta-C_5H_5)(PPh_3)$ fragment to cluster bonding is also found to be four electrons, thus agreeing with the proposed oxidation state.

This description is however based on the consideration of the Ru-H hydride as being an exo-metal bound ligand not participating in the cluster bonding or contributing to the skeletal electron count.

If however this metal hydride is considered to be an endo cluster hydrogen, then the two electrons associated with it account for two of the four donated by the ruthenium fragment thus indicating a Ru(IV) oxidation state. In other words, the $Ru(\eta\text{-}C_5H_5)(PPh_3)$ fragment contributes three electrons to skeletal bonding, with a twenty-six SEP count achieved from the twenty-three electrons of the $[CB_8H_{13}]^{3-}$ carbaborane ligand, which includes the electron from the endo hydrogen associated with the metal vertex. The ruthenium metal is now seen to have a Ru(IV) oxidation state by coordination of the cyclopentadienyl ligand and $[CB_8H_{13}]^{3-}$ carbaborane ligand. This latter description of the ruthenium oxidation state and electronic contribution is prefered, since the $Ru(H)_{endo}(\eta\text{-}C_5H_5)(PPh_3)$ fragment of compound (3) is clearly analogous to the $[BH_{(endo)}H_{(exo)}]^-$ vertex of the arachno-$[B_{10}H_{14}]^{2-}$ anion as noted earlier.

The rationalisation of the electronic contribution of metal bound endo hydrogens is not a new problem, and has been discussed previously as in the case of the arachno $[(HIrB_8H_{12})(CO)(PMe_3)_2]$[188], where the $Ir\text{-}H_{(endo)}$ proton contributes to the cluster electron count, although no bonding interaction with the cluster is observed. The same situation is apparent for compound (3), where there is no observation of a cluster bonding interaction of the $Ru\text{-}H_{(endo)}$ hydrogen, thus indicating that it functions as a BH_2 type endo hydrogen as opposed to a $Ru\text{-}H_{(bridging)}\text{-}B$ hydrogen.

An interesting comparison (Figure 65) can be made between the ^{11}B n.m.r. spectra of compounds (1) and (3) and those of the isoelectronic boron hydrides $B_{10}H_{14}$ and $[B_{10}H_{14}]^{2-}$ respectively. The most immediate observation of the trends within these four sets of spectra, is the reversal of the B(1,3) and B(2,4) shifts between the

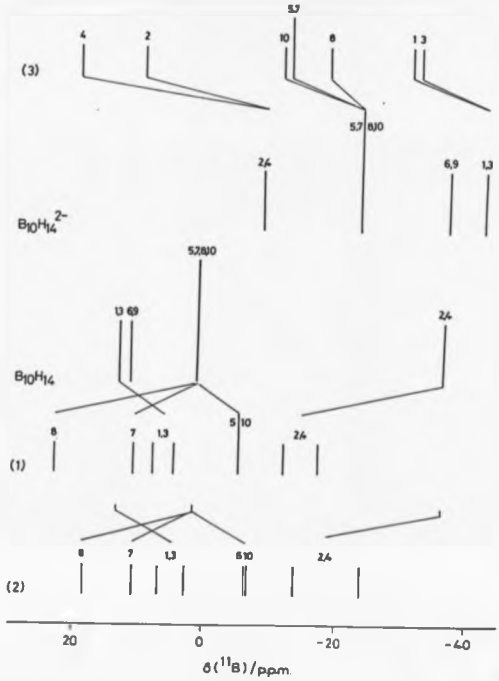

Figure 65. Stick diagram of the ^{11}B n.m.r. spectra of nido-$B_{10}H_{14}$ and arachno-$[B_{10}H_{14}]^{2-}$ and their correlation to the spectra of the isoelectronic and isostructural metallacarbaboranes, nido-[5-(PPh_3)-9-(CO)-9,9-(PPh_3)$_2$-9,6-$RuCB_8H_{10}$] (1), nido-[5-(PPh_3)-9-(CO)-9,9-(PPh_3)$_2$-9,6-$OsCB_8H_{10}$] (2) and arachno-[9-(C_5H_5)-9-(H)-9-(PPh_3)-6,9-$RuCB_8H_{12}$] (3).

nido and arachno clusters, and moreover the general agreement in pattern between the borane and hetaro-borane examples within each structural classification. Clearly, this agreement is more easily seen in the compound (3), where there is no endo cage substitution, adding to the asymmetry of the cluster. The high field shift of the B(2,4) and B(1,3) resonances in the nido and arachno compounds respectively, is further evidence of the observation[163] that a boron atom which connects two boron atoms that are bridged by a hydrogen atom on the open face will have high field shifts. In the case of (1) and (2), whilst no bridging hydogen is present to indicate such an effect at B(2), the distribution of the electron density within the cage presumably mirrors the B_9 analogues (see Table 6), where there are indeed such B-H-B bridges.

A notable down field shift observed in the nido compounds (1) and (2), is that of the resonance due to the boron atom B(8). From the comparison of the ^{11}B n.m.r. shifts for $B_{10}H_{14}$ and $[CB_9H_{12}]^-$ the substitiution of the carbon into the decaborane(14) skeleton is observed to produce an upfield shift of 13.8 p.p.m. for the B(8) resonance, indicating this effect, if additive, is substantially modified by more dominant effects in the ruthenacarbaborane. Two other structural features of the position of the B(8) atom within the framework which may account for this observation are apparent. Firstly, it is approximately antipodal to the exo phosphine substituent on B(5) and secondly it is adjacent to the ruthenium atom.

The tendancy for $B-H_{(terminal)}$ proton resonances to mirror the pattern found for the ^{11}B shifts of the boron atoms to which they are attached has been long established as a feature of borane and carbaborane clusters[155]. The proton-boron-11 correlation plot for the

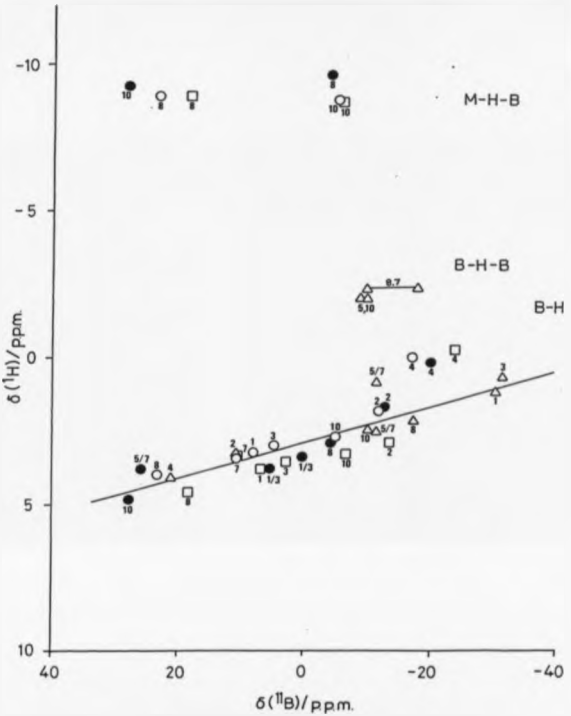

Figure 66. Proton-boron-11 shielding correlation plot for *nido*-[9-(CO)-9,9-$(PPh_3)_2$-9,6-$RuCB_8H_{12}$-5-(PPh_3)] (1) (○), *nido*-[9-(CO)-9,9-$(PPh_3)_2$-9,6-$OsCB_8H_{12}$-5-(PPh_3)] (2) (□) and *arachno*-[9-(C_5H_5)-9-(H)-9-(PPh_3)-6,9-$RuCB_8H_{12}$] (3) (△) and *nido*-[9-(CO)-9,9-$(PPh_3)_2$-9,6-RuB_9H_{11}-5-/7-(PPh_3)][185] (●).

compounds (1), (2) and (3) shown in Figure 66 illustrates this property.

Greenwood *et al* have noted that the slope of the line obtained from such a plot is normally about 16:1 ($^{11}B : ^{1}H$) for a number of [MB_9] *nido* decaboranyl species[166,185], providing the anomalous shifts exhibited for the B(4) resonances are excluded. Assignment of the B(4) resonance is thus assisted by this trend, [Note: B(4) here is equivalent to B(2) in 6-MB_9 derivatives].

The same pattern of shift correlation is observed for compounds (1), (2) and (3), Figure 66, with a slope of 16:1 found for both the *nido* and *arachno* complexes. The distribution of shifts for the ruthenacarbaborane (1) deviate less from the line than do the analogous ruthenaborane shifts. The previously noted anomalous B(4) shifts are also apparent for compound (1). The correlation is seen to hold irrespective of the environment of the participating boron atoms, excepting the previously noted B(4) position, as shown by comparing the *nido* and *arachno* compounds (1) and (3).

The grouping of similar resonances in such correlation plots for related [MB_9] decaboranyl species[140] has been ascribed to parallels in the cluster electronic structure. In comparing the assignments of the resonances for the ruthenacarbaborane (1) and analogous ruthenaborane species in Figure 67, an apparent mis-match occurs in the grouping for the B(8) and B(10) resonances.

Some confusion exists about the assignment in the resonances for the 5-/7- substituted ruthenaborane species [$(CO)(PPh_3)_2RuB_9H_{11}(PPh_3)$]. In the paper describing this compound[185] the numbering scheme presented with the proposed structure does not correspond with the numbering used in the presentation of the n.m.r. data, the numbering

schemes appear to be enantiomeric. The identity of the lowfield ^{11}B resonance (28 p.p.m.) has been confirmed[189] to be that of the boron atom attached to the hydride (-9.26 p.p.m.), trans to the equatorial phosphine, the latter displaying the expected $^2J(^{31}P\text{-}Ru\text{-}^1H)$ coupling as published[185]. This corresponds to B(10) in the scheme employed here for the 6-carba-9-metalla decaboranyl derivatives. This is clearly in contrast to that found for compound (1), where the lowfield resonance is that of the boron atom attached to the hydride trans to the carbonyl ligand, as described earlier.

Clearly, even though an addendum has been published[189] to clarify the earlier mistaken publication[185], there remains the possibility that the differences in resonance assignment between the ruthenacarbaborane $[(CO)(PPh_3)_2RuCB_8H_{10}(PPh_3)]$ (1), and the ruthenaborane $[(CO)(PPh_3)_2RuB_9H_{11}(PPh_3)]$[185,189], is due to a wrong assignment in the latter. There may however, be another explanation, as follows.

The two compounds differ in respect to the 6- position by the interchange of a CH and BH_2 group, with the latter comprised of one terminal and one bridging hydrogen atom (to one of the adjacent B(5,7) boron atoms). A further possible difference is that of the phosphine substitution site. Whilst in the ruthenacarbaborane (1) the substitution occurs at B(5), syn to the Ru-(CO) group, in the ruthenaborane analogue differentiation between the syn and anti sites, B(5) and B(7) respectively, has not been made.

The ^{11}B n.m.r. shifts of the three $[MB_9]$ ruthenadecaborane analogues[185] $[(CO)(PPh_3)_2RuB_9H_{13}]$, $[(CO)(PPh_3)_2RuB_9H_{11}(PPh_3)]$ and, $[(PPh_3)_2HRuB_9H_{12}(PPh_3)]$ which are the unsubstituted, the (5- or 7-) and 10- phosphine substituted products respectively, have the B(8), B(10) and B(8) resonances at lower field respectively, in relation to

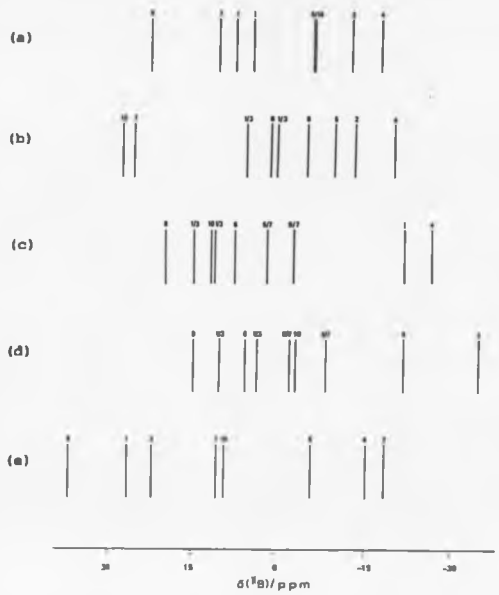

Figure 67. Stick diagram of the ^{11}B n.m.r. spectra of:

(a) Nido-[9-(CO)-9,9-$(PPh_3)_2$-9,6-$RuCB_8H_{10}$-5-(PPh_3)] (1)

(b) Nido-[9-(CO)-9,9-$(PPh_3)_2$-9,6-RuB_9H_{11}-5-/7-(PPh_3)]

(c) Nido-[9-(CO)-9,9-$(PPh_3)_2$-9,6-RuB_9H_{13}

(d) Nido-[9-(H)-9,9-$(PPh_3)_2$-9,6-RuB_9H_{12}-10-(PPh_3)]

(e) Nido-[9-(CO)-9,9-$(PPh_3)_2$-9,6-RuB_9H_{11}-5-(PPh_3)] .

(Data for (b)-(d) taken from references 185 & 189. The B(6) resonance in the predicted spectrum (e) is not attainable.)

the alternative resonance of the B(8,10) pair. The shift observed for the ruthenacarbaborane (1) follows that of the non-substituted and the B(10) substituted analogues (the first and third compounds given above), with the modification that the shift difference is much larger.

A possible pattern of these shifts is therefore that the B(8) resonance is at lower field than the B(10) by virtue of its position approximately trans to the Ru-(CO) group. The larger shift of the B(8) for the ruthenacarbaborane (1) is then a possible effect of the antipodal B(5)-PPh_3 group. If the latter effect is large than in the 5-/7- substituted ruthenaborane analogue the observed reversal in the B(8,10) resonance position may result from the overriding effect of a B(7)-PPh_3 group antipodal to the B(10) boron atom.

Though this pattern suggests that the phosphine substitution in the borane analogue of (1), $[(CO)(PPh_3)_2RuB_9H_{11}(PPh_3)]$[185] may be at the 7- position, it is conceivable that the differences in the ^{11}B n.m.r. spectra are solely attributable to the CH and BH_2 interchange

A line diagram of the relevant ^{11}B n.m.r. spectra of these ruthenadecaboranyl species is given in Figure 67. Included also is the spectrum predicted for the 5-PPh_3 ruthenaborane by the additive effect of substitution of $[Ru(PPh_3)(CO)]$ and $[B(5)-PPh_3]$ into decaborane(14). The relevant shifts were obtained by comparison of the spectrum of compound (1) to that of the $[CB_9H_{12}]^-$ anion, though this spectrum must be viewed with the knowledge that such a gross approximation of additive effects has not been found to be generally applicable.

3.3 CHLORINATED NIDO-RUTHENACARBABORANES ($RuCB_8$ FRAMEWORKS): THE SYNTHESIS AND CRYSTAL AND MOLECULAR STRUCTURES OF [9,9,9-(CO)(PPh_3)$_2$-NIDO-9,6-$RuCB_8H_9$-3-Cl-5-(PPh_3)] (4) AND [9,9,9-(CO)(PPh_3)$_2$-NIDO-9,6-$RuCB_8H_9$-7-Cl-5-(PPh_3)] (5).

A minor product of the reaction of [RuCl(CO)(H)(PPh_3)$_3$] with Li[CB_8H_{13}] is a chlorinated derivative of the previously discussed nido ruthenacarbaborane (1). The product is formulated as [9,9,9-(CO)(PPh_3)$_2$-nido-9,6-$RuCB_8H_9$-3-Cl-5-(PPh_3)] (4), where the decaborane(14) like framework has the 6- and 9- positions substituted by CH and [Ru(PPh_3)$_2$CO] fragments and has the phosphine and chlorine exo substituents at the 5- and 3- positions respectively.

A further chlorinated product can be produced by treatment of the nido compound (1) with halogenated solvents (e.g. CH_2Cl_2) and is formulated as [9,9,9-(CO)(PPh_3)$_2$-nido-9,6-$RuCB_8H_9$-7-Cl-5-(PPh_3)] (5).

A similar range of n.m.r. measurements have been obtained for the two chlorinated ruthenacarbaboranes (4) and (5) as was required for the characterisation of compound (1), (shown in Table 10). Since the correlation of the observed n.m.r. data to the proposed structures (verified by X-ray crystallography) follows much the same reasoning as described earlier for compound (1) a full analysis is not required here. However, several interesting features of the observed ^{11}B n.m.r. spectra are discussed below after the following structural discussion, and are of interest with respect to the relative effects of substituents on the chemical shifts of the cage atoms.

The cluster boron-11 and proton resonances of compounds (4) and (5) are consistent with a nido structure analogous to that of the ruthenacarbaborane (1). The B(8,10) resonances are readily assigned

BORON-11 AND PROTON N.M.R. DATA

Tentative Assignment	Compound(4)		Tentative Assignment	Compound(5)	
	^{11}B (p.p.m.)	^{1}H (p.p.m.)		^{11}B (p.p.m.)	^{1}H (p.p.m.)
8	21.5	4.12	8	24.5	3.95
3	14.8	B-Cl	7	18.4	B-Cl
1	9.8	3.62	1	10.1	3.29
7	9.8	3.57	3	5.5	3.10
10	-1.8	2.91	10	-4.7	2.71
5	-4.7	B-P	5	-9.2	B-P
2	-12.4	1.78	2	-11.6	2.11
4	-17.2	-0.17	4	-18.8	-0.01
C(6)-$H_{(exo)}$		5.3			5.5
B(8)-H-Ru(9)		-8.9			-8.5
B(10)-H-Ru(9)		-8.67			-8.7
PPh_3		6.9-7.7			6.9-7.5

PHOSPHORUS-31 N.M.R. DATA

Tentative Assignment	Compound(4) ^{31}P (p.p.m.)	Compound(5) ^{31}P (p.p.m.)
$Ru(PPh_3)_{axial}$	49.2	50.4
$Ru(PPh_3)_{equatorial}$	41.4	39.0
B-(PPh_3)	10.5	8.0

Table 10. Boron-11, proton and phosphorus-31 n.m.r. data (p.p.m.) for the nido metallacarbaboranes (4) and (5).

from sharpening of the bridging B-H-Ru proton resonances in selective $^{1}H\{^{11}B\}$ decoupling experiments. The identification of a BH(terminal) hydrogen on B(8,10) also eliminates the possibility of exo substitution at these skeletal boron atoms. The presence of a correlation at the B(2) and B(4) resonance group in the proton-boron-11 shift correlation plot (see Figure 68) for compounds (1), (4) and (5), also reasonably eliminates substitution at these boron atoms, as well as allowing a tentative assignment for these positions.

The exo phosphine substituent is therefore indicated to be positioned at the B(5) or B(7) boron, as was found for the non-chlorinated derivative, with the exo chlorine position indicated to be attached to the B(1), B(3) or B(5,7) boron atoms. The disposition of the two exo substituents (PPh_3 and Cl) relative to each other and the orientation of the ligands on the ruthenium atom is similarly unobtainable from the n.m.r. data. The asymmetry imposed by the second substituent at the positions noted above, would in principle enable the ligands on the metal to adopt the opposite orientation to that found in compound (1), without this being apparent from the n.m.r. data. However, assuming the same structure as that found for compound (1), the alternative structures for compounds (4) and (5) are the B(1), B(3) or B(7) chloro-substituted products. Since the exo phosphine could be in a syn or anti position with respect to the Ru-(CO) ligand (i.e. B(5)-PPh_3 or B(7)-PPh_3) there are six possible structures, indistinguishable from the n.m.r. data alone.

In order to determine unambiguously the geometry of the metal-ligand fragment, its disposition with respect to the carbaborane cage and the distribution of exo phosphine and chlorine substituents in the nido-ruthenacarboranes (4) and (5), each has been characterised

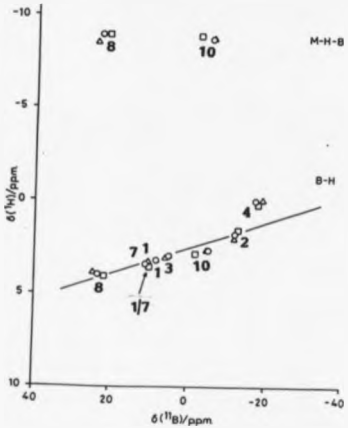

Figure 68. Proton-boron-11 shielding correlation plot for nido-[9-(CO)-9,9-$(PPh_3)_2$-9,6-$RuCB_8H_{10}$-5-(PPh_3)] (1) (○), nido-[9-(CO)-9,9-$(PPh_3)_2$-9,6-$RuCB_8H_9$-3-Cl-5-(PPh_3)] (4) (□) and nido-[9-(CO)-9,9-$(PPh_3)_2$-9,6-$RuCB_8H_9$-7-Cl-5-(PPh_3)] (5) (△).

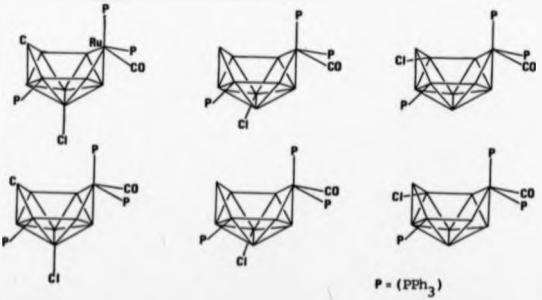

Figure 69. Schematic diagrams of the six possible structures of the compounds (4) and (5) indicated from n.m.r. evidence.

by single-crystal X-ray diffraction analysis. Drawings of the crystallographically determined molecular structures of (4) and (5) and diagrams of the skeletal bond distances are given in Figures 70-73, with other crystallographic details given in Chapter 5.

The crystal molecular structures of the ruthenacarbaboranes (4) and (5) consist of the predicted nido 6,9-MCB_8 decaboranyl framework with the cluster phosphine substituent on the B(5) boron atom, as was found for compound (1), with the further similarity that, regardless of the position of the chlorine substituent, the exo phosphine is syn with respect to the metal carbonyl group. This of course eliminates three of the possible isomeric structures postulated above. Of the remaining 1-, 3- and 7- chloro substituted isomers postulated, the ruthenacarbaboranes (4) and (5) are identified as 3-Cl and 7-Cl derivatives respectively.

Notably, the least symmetrical isomer in terms of ligand distribution, the 1-Cl product is not found. The synthesis of the 7-Cl isomer from the parent ruthenacarbaborane (1) is thus seen to proceed without perturbation of the metal environment.

The replacement of a terminal hydrogen with a chlorine atom does not affect the number of skeletal electrons available for bonding in the framework, hence the ruthenacarbaboranes (4) and (5) are both 18 electron d^6 Ru(II) complexes, with the metal contributing three orbitals and two electrons to the cage, with the metal centre possessing a quasi-octahedral bonding geometry, as postulated for the isoelectronic parent compound (1).

The rather large e.s.d's associated with the inter-atomic distances derived from the crystal structure analysis of the chloro-ruthenacarbaboranes (4) and (5) limit the discussion of their

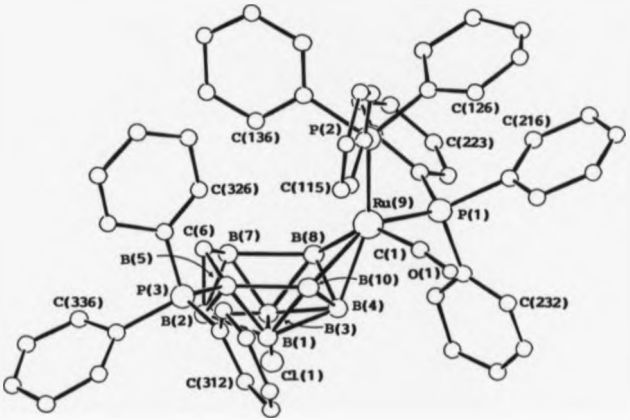

Figure 70. Drawing of the X-ray crystallographically determined molecular structure of the ruthenacarbaborane *nido*-[9-(CO)-9,9-$(PPh_3)_2$-9,6-$RuCB_8H_9$-3-Cl-5-(PPh_3)] (4).

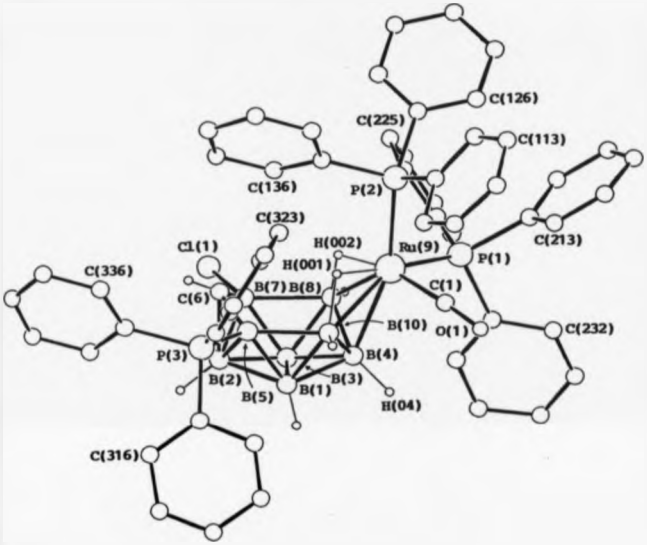

Figure 71. Drawing of the X-ray crystallographically determined molecular structure of the ruthenacarbaborane nido-[9-(CO)-9,9-$(PPh_3)_2$-9,6-$RuCB_8H_9$-7-Cl-5-(PPh_3)] (5).

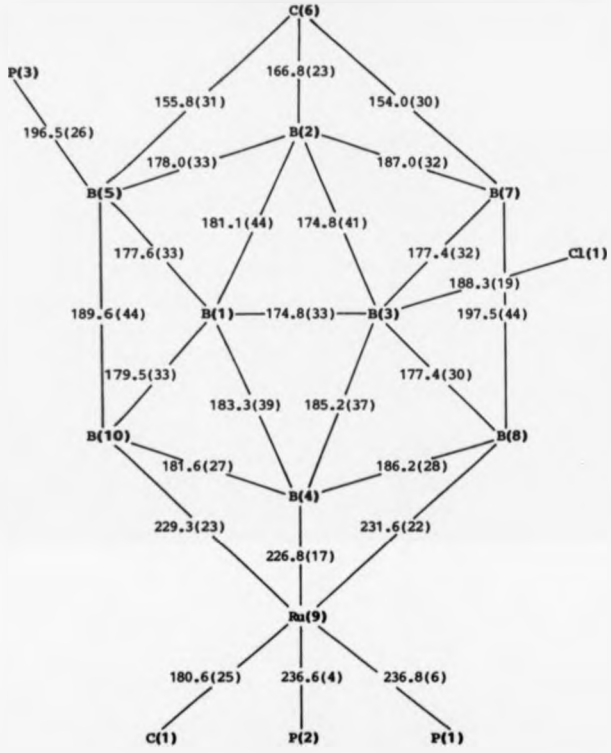

Figure 72 Skeletal interatomic distances (pm), with standard deviations in parenthesis, for the ruthenacarbaborane nido-[9-(CO)-9,9-$(PPh_3)_2$-9,6-$RuCB_8H_9$-3-Cl-5-(PPh_3)] (4).

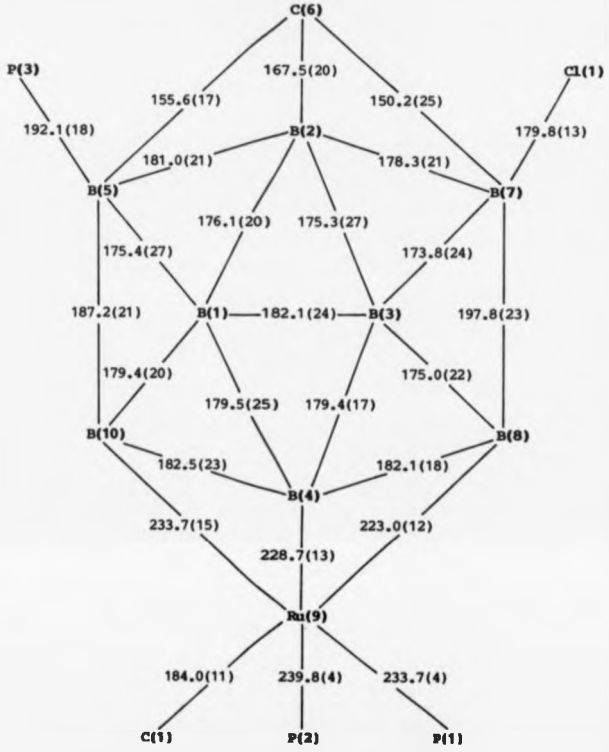

Figure 73. Skeletal interatomic distances (pm), with standard deviations in parenthesis, for the ruthenacarbaborane nido-[9-(CO)-9,9-(PPh_3)$_2$-9,6-$RuCB_8H_9$-7-Cl-5-(PPh_3)] (5).

variation with respect to the parent compound (1). With reference to compounds (4) and (5), the skeletal B-B distances are found to range from 173.8(24) pm to 197.8(23) pm, and are thus within the range found for the non-chlorinated species. A similar pattern of longer B-B distances for the B(7)-B(8) bond, anti to the Ru-(CO) ligand is observed, though again the difference from the skeletal norm is not as pronounced as that found in the nido-$[MB_9]$ decaboranyl species. The B(5)-B(10) distances are also somewhat smaller than the B(7)-B(8) distances as found previously.

The most notable feature of the skeletal interatomic distances of the chloro derivatives (4) and (5), in comparison to the parent compound (1), is that the substitution of a chlorine atom for a hydrogen atom in both the 3- and 7- positions has only a marginal effect upon the general pattern of skeletal distances. Discernible variations occur for several bonds to the B-Cl boron atoms, though they are only of ~3 pm, which is comparable to the e.s.d.'s observed.

As discussed in Section 3.1, the cluster boron-11 and proton n.m.r. resonances of compounds (1) and (2) are consistent with the crystallographic molecular structures obtained and are readily assigned via peak multiplicity, selective sharpening of bridging proton resonances and by comparison to those of decaborane(14), as shown in Figure 65. The similar data obtained for compounds (4) and (5) allow the unambiguous identification of the B(3) and B(7) resonances by virtue of the absence of a correlating terminal hydrogen resonance in the proton spectrum. Whilst the B(1,3) resonances for compounds (1) (2) and (5) can be identified with two resonances in each case, they are not unambiguously identifiable. For compound (4) the B(3) resonance is identified as noted above, but the B(1) and B(7)

resonances overlap, therefore preventing separate characterisation. The tentative assignment of the B(7) resonance in compounds (1) and (2) was made purely on the basis of the linewidth, which is not an entirely satisfactory method, since its position in the spectrum is very close to those resonances assigned to the B(1,3) boron atoms.

The ^{11}B n.m.r. resonances of the substituted boron atoms in the 3-Cl and 7-Cl subtituted $B_{10}H_{13}Cl$ species[190,191] show a downfield shift of 9.5 and 9.1 p.p.m. respectively compared to the parent $B_{10}H_{14}$ cluster, along with a range of lesser down and upfield shifts for the other skeletal boron atoms. Comparison of these downfield shifts found for the chloro-decaboranes with the B(3)-Cl and B(7)-Cl resonance shifts identified for the ruthenacarbaboranes (4) and (5) reasonably indicate the order of the resonances in the non-chlorinated parent ruthenacarbaborane (1) as B(7):B(1):B(3), as shown in Figure 74. This of course agrees with the assignment for B(7) on the basis of linewidth noted earlier. The respective downfield shifts are thus 10.0 and 7.3 p.p.m. in the 3- and 7- chlororuthenacarbaboranes (4) and (5), the latter being somewhat less than the 9 p.p.m. found in $B_{10}H_{13}Cl$ derivatives.

Some ambiguity arises because the B(7) downfield shift could be 10.2 p.p.m. giving the alternative B(1):B(7):B(3) assignment for the ruthenacarbaborane (1) (see Figure 74.), whilst still retaining the 10.0 p.p.m. downfield shift for B(3). The -2 p.p.m. difference is of the order found for the lesser changes in chemical shift identified for resonances of other non-substituted skeletal atoms in the chloro-decaboranes. In the present work a suitable method for correlating all of the observed chemical shift changes of the ruthenacarbaboranes characterised with those of the chloro-decaborane clusters has been

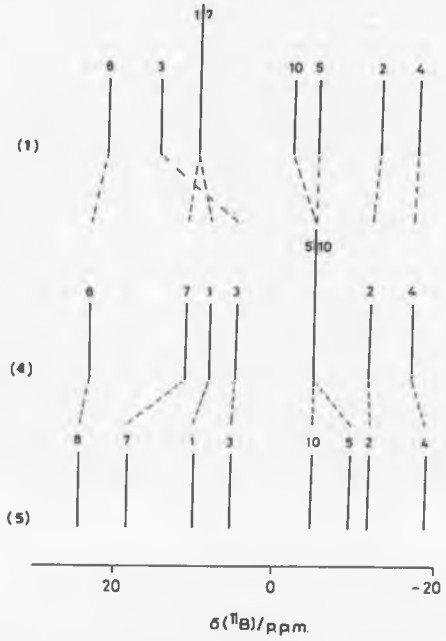

Figure 74. Stick diagram of the ^{11}B n.m.r. spectra of nido-[9-(CO)-9,9-$(PPh_3)_2$-9,6-$RuCB_8H_9$-5-(PPh_3)] (1), nido-[9-(CO)-9,9-$(PPh_3)_2$-9,6-$RuCB_8H_8$-3-Cl-5-(PPh_3)] (4) and nido-[9-(CO)-9,9-$(PPh_3)_2$-9,6-$RuCB_8H_8$-7-Cl-5-(PPh_3)] (5).

devised, namely a ^{11}B-^{11}B shift correlation plot (not to be confused with the spectroscopic COSY technique). Plotting the ^{11}B resonance chemical shifts for the non-substituted species (X-axis), i.e. decaborane(14) and the ruthenacarbaborane (1), against those of the substituted complex (Y-axis), i.e. 3-Cl (or 7-Cl) decaborane and the 3-Cl ruthenacarbaborane (4) [or compound (5)] gives the diagram shown in Figure 75. By joining the points assigned to similar atoms, the plot readily displays all of the information required to correlate the changes in chemical shift between the two analogous sets of non-substituted and substituted complexes. Clearly if the shift changes are precisely additive then all lines joining similar atoms would be parallel to the diagonal. Deviations from this parallel thus either indicate a wrong assignment or the non-additivity of the shifts, depending on the magnitude of the deviation. The displacement of the lines above or below the diagonal depend upon the magnitude of the changes in the chemical shift involved.

One immediate problem of such a plot is finding all three of the compounds required to compare with the compound under inspection. In these cases, recourse has to be made to the normal one-to-one method of comparison.

The diagram shown in Figure 75, clearly shows that the changes in chemical shift for the 3-Cl and 7-Cl ruthenacarbaboranes are additive in a fashion similar to that found for the analogous decaborane species. The downfield shift of the B(3) and B(7) resonances are clearly seen to be the most significant and additive. For the 7-Cl ruthenacarbaborane (5), the upfield shift of the B(5) resonance is also noted to be significant, but clearly an expected shift as judged by the parallel correlation observed.

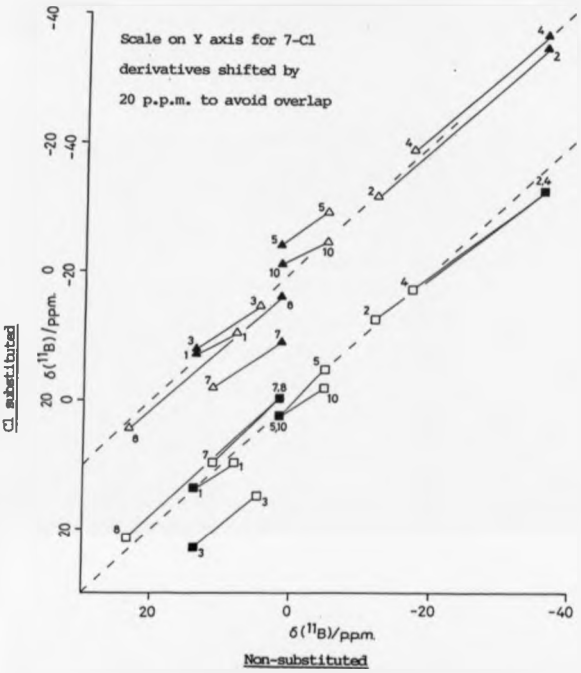

Figure 75. ^{11}B-^{11}B shift correlation plot for the cluster couples $[(PPh_3)_2RuCB_8H_9(PPh_3)]$ (1) against $[(PPh_3)_2RuCB_8H_9Cl(PPh_3)]$ (4), (5) and $B_{10}H_{14}$ against Cl-$B_{10}H_{13}$. (■ = 3-Cl-$[B_{10}]$; ▲ = 7-Cl-$[B_{10}]$; and □ = 3-Cl-$[RuCB_8]$; △ = 7-Cl-$[RuCB_8]$).

The correlations for the B(7) and B(1,3) resonances in the 7-Cl and 3-Cl ruthenacarbaboranes suggest the correct assignment is B(7):B(1):B(3) as noted earlier. Alternative assignments give poorer agreement, as judged from the respective alternative plots. The correlation of the B(2) and B(4) resonances thus supplements the strong evidence provided by the unusual shifts of the B(4) resonance in the proton-boron-11 correlation plots (Figures 66 and 68).

In an attempt to cross-check the validity of the devised ^{11}B-^{11}B shift correlation method of comparing n.m.r. shifts for substituted species the technique was applied to the following couples $B_{10}H_{14}$ / 2-Cl-$B_{10}H_{13}$ and the rhenaborane analogues $[(PMe_3Ph)HReB_9H_{13}]$ / $[2\text{-Cl-}(PMe_3Ph)HReB_9H_{12}]$, using data taken from the literature[192,193]. The ^{11}B-^{11}B shift correlation plot is shown in Figure 76, in which there is an overall agreement of the resonances assignment and shift pattern, with the major shift readily seen as that of the chlorine subtituted 2- position. However, one noticeable digression from this pattern is the correlation for one of the B(8,10) resonances of the rhenaborane derivative, which is near perpendicular to, rather than parallel to, the diagonal norm, immediately arousing suspicion. This resonance could be brought into the expected trend by displacement to a shift similar to the other component. An examination of the proton-boron-11 shift correlation plot contained within the paper from which this data was obtained suggests that the shift value of +2.1 p.p.m. has been mis-typed in the relevant data section and should in fact be -2.1 p.p.m. Clearly an erroneous displacement of a resonance by 4.2 p.p.m. is of significance and may on inspection be detected. By checking the data using the ^{11}B-^{11}B shift correlation method the mistake is easily identifiable.

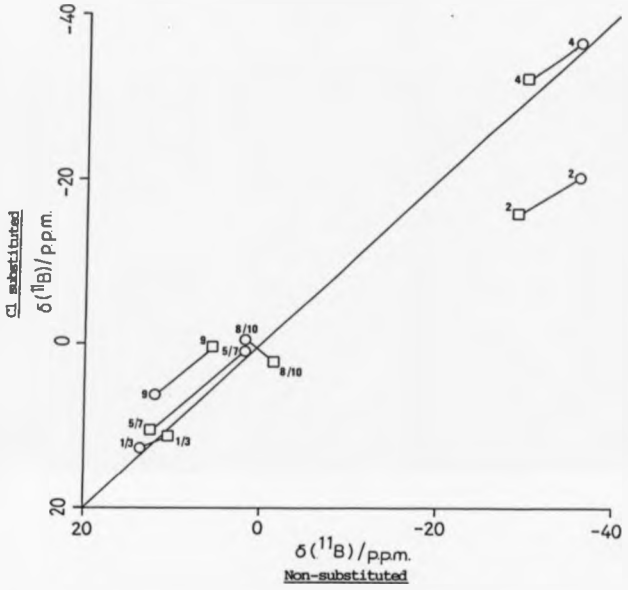

Figure 76. ^{11}B-^{11}B shift correlation plot for the cluster couples $[(PMe_3Ph)HReB_9H_{13}]$ against $[2\text{-}Cl\text{-}(PMe_3Ph)HReB_9H_{12}]$ and $B_{10}H_{14}$ against $2\text{-}Cl\text{-}B_{10}H_{13}$, where (○) = $2\text{-}Cl\text{-}[B_{10}]$ and (□) = $2\text{-}Cl\text{-}[ReB_9]$.

3.4. CLOSO METALLACARBABORANES (MCB_8 FRAMEWORKS, M = Ru, Os). THE SYNTHESIS AND CRYSTAL AND MOLECULAR STRUCTURES OF [2,2,2-(CO)(PPh$_3$)$_2$-CLOSO-2,1-RuCB$_8$H$_8$-10-(PPh$_3$)] (6) AND [2,2,2-(CO)(PPh$_3$)$_2$-CLOSO-2,1-OsCB$_8$H$_8$-3-(PPh$_3$)] (7).

From the reaction of arachno-$[CB_8H_{13}]^-$ with the ruthenium halide derivative $[RuCl(CO)(H)(PPh_3)_3]$ in benzene, in addition to the previously discussed nido derivatives, compounds (1), (4) and (5) (Sections 3.1 and 3.2), a further product (6), formed in ~3% yield was isolated by t.l.c. as an orange crystalline solid and characterised by spectroscopy and single-crystal X-ray diffraction analysis as closo-$[(CO)(PPh_3)_2RuCB_8H_8(PPh_3)]$ (6). The idealised equation for its formation is :

$$Li[CB_8H_{13}] + [RuCl(CO)(H)(PPh_3)_3] \longrightarrow [(CO)(PPh_3)_2RuCB_8H_8(PPh_3)] + 3H_2 + LiCl$$

It is interesting that in contrast, the corresponding osmium compound $[(CO)(PPh_3)_2OsCB_8H_8(PPh_3)]$, (7) , was a major product of the analogous reaction of $[OsCl(CO)(H)(PPh_3)_3]$ with $Li[CB_8H_{13}]$, being obtained as a yellow crystalline solid in 26% yield.

The n.m.r. data for compounds (6) and (7) are given in Table 11. The ^{11}B n.m.r. spectrum of (6) shows five resonances, with a 1:1:2:2:2 integration ratio (see Figure 77). The ^1H n.m.r. spectrum of (6) indicates a closed cluster geometry, since there is an absence of resonances attributable to endo bridging hydrogens, B-H-B, M-H-B or M-H functions. The four highest field boron resonances are found to be associated with $B-H_{(terminal)}$ hydrogens as shown by a series of

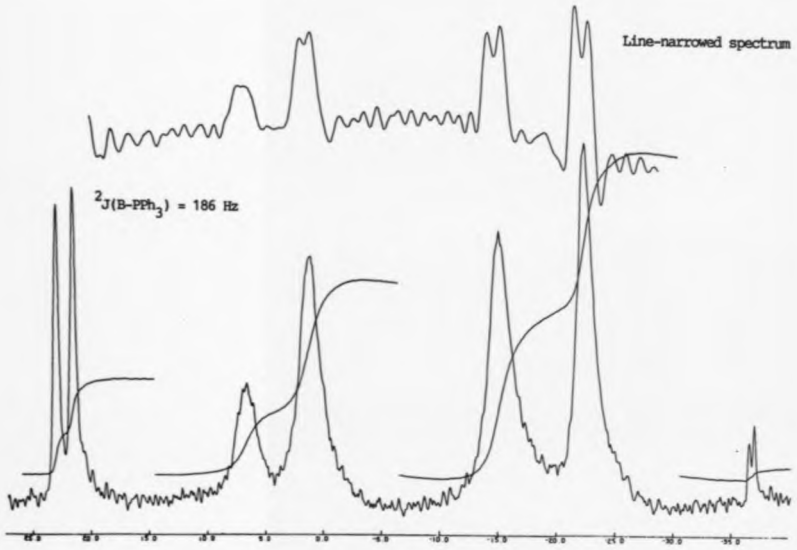

Figure 77. The ^{11}B n.m.r. spectrum of compound (6).

BORON-11 AND PROTON N.M.R. DATA

Integral Ratio	Compound(6) ^{11}B (p.p.m.)	Compound(6) ^{1}H (p.p.m.)	Integral Ratio	Compound(7) ^{11}B (p.p.m.)	Compound(7) ^{1}H (p.p.m.)
1	21.8	B-P	1	42.3	6.52
1	8.0	2.78	1	0.2	2.54
2	1.1	2.64	1	-4.2	1.44
2	-15.2	0.24	1	-8.1	2.67
2	-22.9	0.28	1	-17.4	0.65
			1	-23.1	B-P
			1	-28.6	-1.02
Assignment			1	-30.1	-1.32
C(6)-$H_{(exo)}$		5.1			4.4
PPh_3		7.0-7.9			6.9-7.7

PHOSPHORUS-31 N.M.R. DATA

Assignment	Compound(6) ^{31}P (p.p.m.)	Compound(7) ^{31}P (p.p.m.)
M(PPh_3)	40.7	7.8, 3.5
B-(PPh_3)	Not observed*	Not observed*

Table 11. Boron-11, proton and phosphorus-31 n.m.r. data (p.p.m.) for $[(CO)(PPh_3)_2RuCB_8H_8(PPh_3)]$ (6) and $[(CO)(PPh_3)_2OsCB_8H_8(PPh_3)]$ (7).

[* B-PPh_3 resonances not observed, though the presence of cage bound phosphine ligands was indicated by $^{2}J(^{31}P-^{11}B)$ couplings in the ^{11}B n.m.r. spectrum (see text).]

selectively ^{11}B decoupled ^{1}H n.m.r. spectra, the results of which are given in Table 11. The boron atom producing the lowfield resonance in the ^{11}B spectrum does not have an attached terminal hydrogen atom, as judged from a similar decoupling experiment. The doublet observed for this resonance, in both the ^{11}B and $^{11}B(^{1}H)$ spectrum of (6), is indicative of a boron atom with a phosphine ligand attached, the observed coupling of $^{2}J(^{31}P-^{11}B) \sim 185$ Hz is of the expected magnitude. The integration ratio of aromatic proton resonances to other cluster proton resonances is consistent with the presence of three triphenyphosphine ligands. Since a B-PPh_3 group has been reasonably indicated the remaining two must be bound to the ruthenium atom. The ^{31}P n.m.r. spectrum shows only one resonance at 40.6 p.p.m. attributable to these two metal bound triphenylphosphine ligands. The cage bound phosphine resonance was not observed. The infrared spectrum confirms the presence of a carbonyl group on the ruthenium atom, $\nu(CO)max = 1925\ cm^{-1}$ indicating the metal fragment to be $Ru(PPh_3)_2(CO)$. From spectroscopic evidence, the ruthenacarbaborane (6) can be reasonably formulated as closo-$[(PPh_3)_2(CO)RuCB_8H_8(PPh_3)]$.

The mirror plane symmetry possessed by (6) as suggested by the integration pattern of the ^{11}B resonances is compatible with only three possible substitution patterns, as shown in Figure 78, (a to c), based on the predicted bi-capped square antiprismatic geometry in which the framework is notionally tri-substituted (X = CH, $Ru(PPh_3)_2(CO)$, B-PPh_3). Restricting the carbon atom position to occupy a low coordinate polar vertex yields the six possible structural conformations for the ruthenacarbaborane (6), [Figure 78, (d) to (i)]. Notably, of these six alternatives, four are isomers of structural type (c). The six alternative structures embrace all three possible

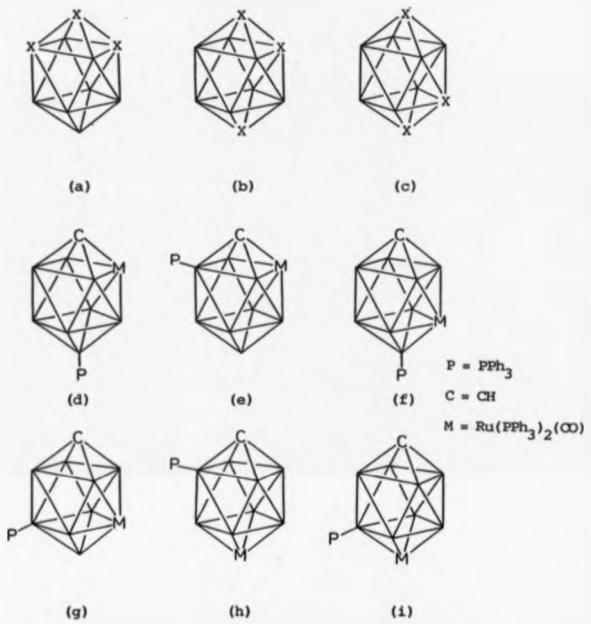

Figure 78. (a)-(c) Possible isomeric structural types for notionally symmetrically tri-substituted ten vertex closo clusters, $MCB_7(B\text{-}L)$. (d) - (i) Structural modifications for compound (6), assuming tetrahapto carbon atom.

metal positions in which the ruthenium can occupy the polar site or a vertex in one of the two tropical belts. Two possible phosphine substitution sites are then dictated by the observed symmetry. For a structure containing the metal in a tropical belt, the phosphine can only be at the polar vertex or trans to the metal in the same tropical belt. For the derivative in which the metal occupies the polar vertex the cage phosphine can be positioned on either tropical belt.

The assumption that the carbon atom will occupy a polar vertex is consistent with the observed site preference for carbon atoms within other heteroboranes clusters (Section 1.6) and more specifically is as found in the two structurally verified closo-MCB_8 derivatives noted earlier[146,147,181]. However, structures in which the carbon atom is pentahapto, though unlikely, cannot be totally ruled out from consideration. In this instance, a further six alternative structural modifications are produced (not illustrated), corresponding to three pairs of type (a), (b) and (c) in which the metal and cage phosphine are interchanged.

The available spectroscopic evidence is unable to distinguish between the structural isomers discussed above, and for this reason, the X-ray crystal structure of (6) was obtained. Though a symmetrical disposition of the metal bound phosphine and carbonyl ligands (with respect to the cage) is presumed in order to maintain the observed mirror plane symmetry, their exact orientation is also not evident from the spectroscopic data.

The details of the crystallographic study of (6) are given in Chapter 5. A drawing of the closo-ruthenacarbaborane (6) is shown in Figure 79. The molecular structure is found to be that of a bicapped square antiprism in which the carbon atom is tetrahapto, occupying a

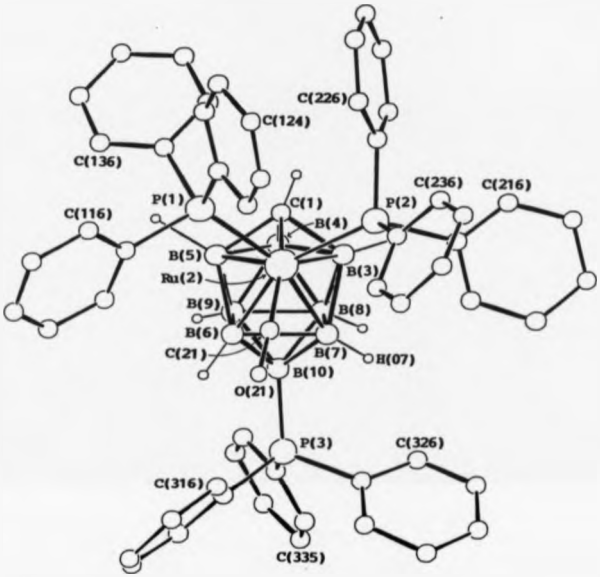

Figure 79. Drawing of the X-ray crystallographically determined molecular structure of the ruthenacarbaborane [2,2,2-(CO)(PPh_3)$_2$-*closo*-2,1-$RuCB_8H_8$-10-(PPh_3)] (6).

polar vertex. The ruthenium atom is situated adjacent to the carbon atom in the upper tropical belt with the cage bound phosphine substituted on to the polar boron atom.

A Wade type electron count for the ruthenacarbaborane (6) gives 22 electrons (11 SEP's) for skeletal bonding, with the ruthenium atom contributing three orbitals and two electrons. The closo structure predicted by the 'n+1' SEP count is consistent with the observed molecular geometry. The ruthenacarbaborane (6) can thus be regarded as an 18 electron d^6 ruthenium(II) complex.

The disposition of the phosphine and carbonyl ligands on the metal is observed to be as predicted, with the carbonyl lying on the pseudo mirror plane as defined by the C(1), Ru(2), B(10) and B(4) atoms. This mirror plane is not a crystallographically observed symmetry element, rather its presence is inferred in solution by n.m.r. spectroscopy, a less exacting structural probe. Not surprisingly, the sterically demanding triphenylphosphine ligands on the metal are directed towards the nearest point of steric relief, with the aromatic rings suitably staggered to reduce intra-molecular contacts. The distorted octahedral geometry of the ligands around the metal is defined by the approximately mutually perpendicular bonding vectors to the phosphorus and carbon atoms, (P(1), P(2), C(1) and C(21)), the latter two defining the axial vectors. The bonding vectors from the metal to the equatorial plane of the carbaborane residue accounts for the remaining distorted cis octahedral equatorial vectors. The bonding angles around the ruthenium atom are given in Table 12, with a more comprehensive list given in Chapter 5.

The structure of the closo-ruthenacarbaborane (6) is of the type (d) shown in Figure 78, and related to that observed for the closo

Table 12. Inter-bond angles at ruthenium atom (°) for [2-(CO)-2,2-$(PPh_3)_2$-*closo*-2,1-$RuCB_8H_8$-10-(PPh_3)] (6), (Standard deviations in parenthesis).

P(1)-Ru(2)-P(2)	96.9(1)	P(1)-Ru(2)-C(21)	91.0(3)
P(2)-Ru(2)-C(21)	98.0(3)	C(1)-Ru(2)-P(1)	96.0(1)
C(1)-Ru(2)-P(2)	99.2(2)	C(1)-RU(2)-C(21)	160.5(3)
C(1)-Ru(2)-B(3)	41.3(4)	C(1)-Ru(2)-B(5)	43.0(4)
C(1)-Ru(2)-B(6)	81.0(3)	C(1)-Ru(2)-B(7)	81.1(4)
B(3)-Ru(2)-B(7)	47.4(4)	B(5)-Ru(2)-B(6)	46.5(4)
B(3)-Ru(2)-B(5)	67.9(4)	B(6)-Ru(2)-B(7)	49.6(4)

iridacarbadecaborane[149] $[(PPh_3)_2(H)IrCB_8H_8(PPh_3)]$ (type (f)) by the interchange of the polar C-H and B-P fragments, or alternatively, the displacement of the metal site from the lower to upper tropical plane.

The ruthenacarbaborane (6), is also structurally similar to the cobaltacarbaborane[146,147,181] $(\eta\text{-}C_5H_5)CoCB_8H_9$, with the carbon and metal fragments in similar skeletal positions. In the cobalt derivative there is no cage substituted boron atom. In contrast, the analogous nickel complex[148], $(\eta\text{-}C_5H_5)NiCB_8H_9$, has the carbon and metal fragments in the upper polar and lower tropical sites respectively (as in the iridium complex), though this isomer has been observed to rearrange to the more stable isomer with the metal in the lower polar vertex[146,147]. Whilst these iridium and metallocene derivatives are not iso-structural with the ruthenacarbaborane (6), they are the only

closo ten-vertex [MCB_8] species known.

The skeletal inter-atomic distances found for compound (6) are comparable to those observed in the related closo cobaltacarbaborane cluster, $(\eta\text{-}C_5H_5)CoCB_8H_9$[181], as shown in Table 13, (see also Chapter 5). The skeletal distances are found to be in the following order of magnitude;

metal > tropical > equatorial > lower polar > upper polar

This trend is also observed in both the cobaltacarbaborane $(\eta\text{-}C_5H_5)CoCB_8H_9$, as seen from inspection of Table 13, and the parent borane anion $[B_{10}H_{10}]^{2-}$, where the tropical, equatorial and polar B-B distances are 186, 181 and 173 pm respectively[193].

Differences in magnitude of B-B skeletal distances between the parent borane anion and the ruthenacarbaborane (6) are surprisingly modest in view of the large size differential between the boron and ruthenium atom. The shorter distances of the polar carbon to the tropical boron atoms are as expected for a C-B distance, being comparable to those found in other ten vertex metallacarbaborane species, one example being $[6,6\text{-}(Et_3P)_2\text{-}1,2,6\text{-}C_2CoB_7H_9]$[128].

Two interesting features of the ruthenacarbaborane (6) skeletal B-B distances are apparent from comparison to those of the cobalt derivative. Firstly, there is the similarity of the polar boron distances regardless of the presence or otherwise of an exo bound phosphine ligand. Clearly the two and three electron contribution to skeletal bonding of the B-H and B-PPh_3 fragments is delocalised around the closo framework, since the bonding capability of each appears to be identical. Secondly, systematically shorter equatorial bonds are

Table 13. Comparison of skeletal interatomic distances (pm) for [2,2,2-(CO)(PPh_3)$_2$-closo-2,1-$RuCB_8H_8$-10-(PPh_3)] (6) and [2-(η-C_5H_5)-closo-2,1-$CoCB_8H_9$]$^{-(*)}$. (Standard deviations in parenthesis), (*) Data taken from reference 181.

Compound	(6)	(η-C_5H_5)$CoCB_8H_9$		(6)	(η-C_5H_5)$CoCB_8H_9$
Upper polar vertex					
C(1)-M(2)	211.5(10)	190(1)	C(1)-B(3)	157.2(17)	157(2)
C(1)-B(4)	161.8(13)	158(1)	C(1)-B(5)	163.8(14)	157(1)
Upper tropical plane					
M(2)-B(3)	231.0(12)	210.6(8)	M(2)-B(5)	232.3(11)	213.1(9)
B(3)-B(4)	184.5(17)	178(2)	B(4)-B(5)	187.2(18)	183(1)
Equatorial plane					
M(2)-B(6)	232.5(9)	210.6(9)	M(2)-B(7)	230.2(11)	208.0(9)
B(3)-B(7)	185.3(15)	185(1)	B(3)-B(8)	185.8(13)	181(2)
B(4)-B(8)	175.5(18)	171(1)	B(4)-B(9)	176.1(16)	174(1)
B(5)-B(6)	183.5(16)	180(1)	B(5)-B(9)	185.2(15)	179(1)
Lower tropical plane					
B(6)-B(7)	194.2(16)	183(1)	B(6)-B(9)	182.5(16)	182(1)
B(7)-B(8)	187.1(16)	184(1)	B(8)-B(9)	185.4(14)	178(1)
Lower polar vertex					
B(10)-B(6)	168.8(15)	166(1)	B(10)-B(7)	169.8(13)	170(1)
B(10)-B(8)	167.3(15)	166(1)	B(10)-B(9)	167.9(18)	167(1)

observed for the B(4)-B(8) and B(4)-B(9) vectors in both the ruthenium and cobalt complexes, in each case of at least 3 pm from the mean distance. Since the metal and exo-polyhedral ligands are different in each, this common effect must arise from either the substitution of the carbon atom into the polar vertex, or more likely the presence of a skeletal metal fragment at the vertex roughly antipodal to this triangular face.

A similar absence of endo hydrogen resonances in the spectroscopic data obtained for the osmacarbaborane (7) (Table 11) also indicates a closed cluster geometry for this compound. In this case eight individual resonances are observed in the ^{11}B n.m.r. spectrum (Figure 80), immediately indicating an asymmetric molecular structure. Seven of the eight boron resonances are found to be associated with a B-H(terminal) hydrogen as shown by a series of selectively ^{11}B decoupled ^{1}H n.m.r. spectra, whilst the boron resonance at -23.1 p.p.m. gives a coupling of $^{2}J(^{31}P-^{11}B)$ ~ 126 Hz and is attributable to a boron atom with an attached phosphine ligand. The ^{31}P n.m.r. spectrum shows two resonances at 3.47 and 7.83 p.p.m. respectively. These resonances show a small coupling due to the cis disposition of two inequivalent phosphine ligands on the osmium atom $^{2}J(^{31}P-Os-^{31}P)$ ~ 10 Hz. The expected resonance for the cage bound phosphine was not observed, probably because of the combination of low concentration and multiplicity of the signal due to coupling from the attached boron atom. The presence of a metal bound carbonyl ligand is confirmed by an infrared absorption at 1900 cm^{-1}.

In contrast to the substitution pattern predicted for the ruthenacarbaborane (6), the eight individual resonances observed in the ^{11}B n.m.r. spectrum of the osmacarbaborane (7) indicate the

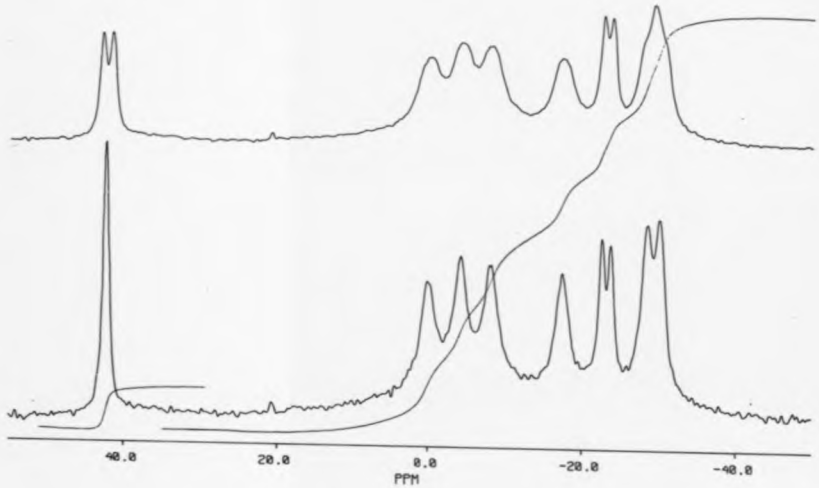

Figure 80. The $^{11}B\{^{1}H\}$ and ^{11}B n.m.r. spectra of compound (7).

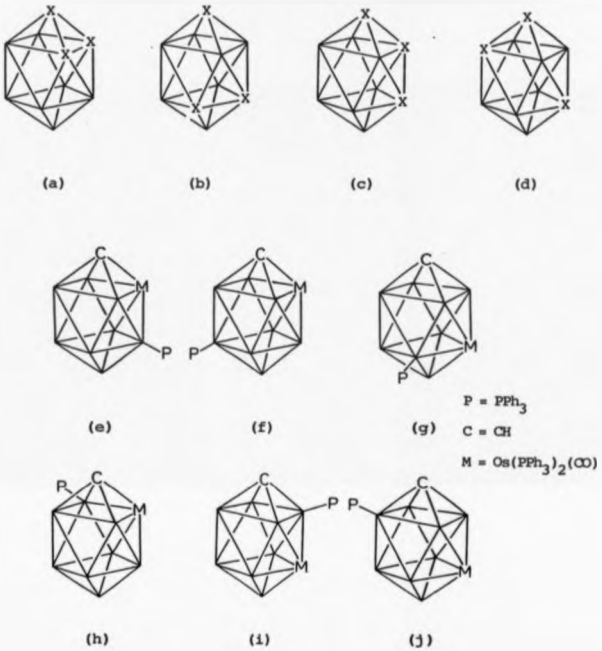

Figure 81. (a)-(c) Possible isomeric structural types for notionally asymmetrically tri-substituted ten vertex closo clusters, X_3B_7. (d)-(i) Possible structures for compound (7), assuming tetrahapto carbon.

disposition of the hetero atoms to be one of the four notionally asymmetrically tri-substituted bicapped square antiprismatic geometries, as shown in Figure 81, (a) to (d). Assuming the carbon atom occupies a tetrahapto vertex, for reasons noted earlier, gives six possible structures, [Figure 81, (e) to (j)], consistent with the spectroscopic data observed for the osmacarbaborane (7).
In all six alternative structures, each has a polar B-H vertex, in comparison to the possible polar B-H, B-P and $Ru(L_3)$ fragments of the symmetric structures postulated for the ruthenacarbaborane (6). The six structures are then composed of the various antipodal and cis dispositions of the B-P and $Os(L_3)$ fragments in the tropical planes.

As noted earlier, a structure including a pentahapto CH group whilst rather unlikely, cannot be totally disregarded, since there is no evidence to confirm its absence. Furthermore the asymmetric disposition of the symmetric $OsPPh_3(CO)$ fragment with respect to the cage could, in principle, produce an asymmetric structure from those symmetric isomers containing a mirror plane noted in Figure 81. It is however, unlikely that the gross changes in the ^{11}B spectrum of the osmacarbaborane (7) compared to that of the ruthenacarbaborane (6), would result solely from a such a rotation of exopolyhedral metal bound ligands.

The hydrogen attached to the cage carbon exhibits a small coupling to the cage bound phosphine, $^3J(^{31}P\text{-}B\text{-}C\text{-}^1H) \sim 5$ Hz, which is removed on phosphorus decoupling. This reasonably locates the cage bound phosphine as adjacent to the carbon atom in the upper tropical plane, hence discounting the possibility of structural types (e), (f) and (g), shown in Figure 81, though the position of the metal atom within the framework is not ascertainable from spectroscopic evidence.

In contrast, the iridacarbaborane closo-[(H)$(PPh_3)_2IrCB_8H_8(PPh_3)$][149], has a hydride on the metal atom which shows a 12 Hz coupling from the adjacent cage bound phosphine, hence locating this phosphine at a position adjacent to the metal atom. The iridium complex was found to have a structure corresponding to that shown in Fig 81(f), where the metal is in the lower tropical plane. The combination of these observed C-H and M-H couplings to a cage phosphine, would potentially identify unambiguously the structural type shown in Figure 81(h) if isolated.

In order to ascertain which of the postulated structures is adopted [Figure 81(h), (i) or (j)], the osmacarbaborane (7) has been characterised by single-crystal X-ray diffraction analysis, the details of which are given in Chapter 5.

An Ortep diagram of the molecular structure of the closo osmacarbaborane is given in Figure 82. Note that there are three isomeric cluster units in the asymmetric unit as shown. The fundamental structure is as predicted, being a bicapped square antiprismatic cage structure with the carbon atom occupying a tetra-hapto polar vertex. The position of the osmium atom in a tropical vertex adjacent to the carbon coincides with that found for the ruthenacarbaborane (6), and is similarly different to that observed for the iridium analogue. The position of phosphine substitution is as predicted, in the upper tropical plane. In keeping with the asymmetry indicated by spectroscopic evidence, the phosphine is necessarily mutually cis to both the carbon and osmium atoms.

Unlike the nido ruthenium and osmium carbaborane derivatives from the reaction of $[CB_8H_{13}]^-$ and the respective metal halide derivative, which were found to be isomorphous, the closo derivatives

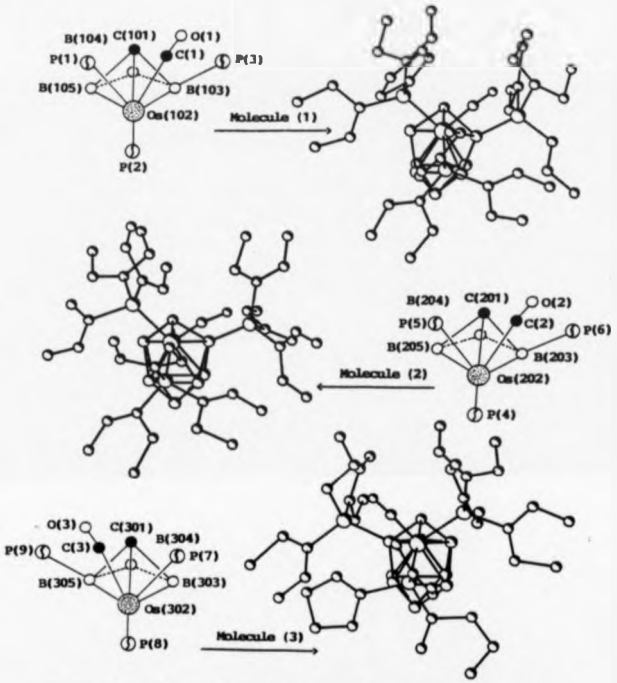

Figure 82. Drawing of the X-ray crystallographically determined molecular structure of the osmacarbaborane [2,2,2-(CO)$(PPh_3)_2$-*closo*-2,1-$OsCB_8H_8$-3-(PPh_3)] (7) showing the three molecules of the crystallographic asymmetric unit. (Skeletal numbering analogous to that for compound (6))

are not. Furthermore, the closo osmacarbaborane (7) has a substantially larger crystallographic asymmetric unit than the ruthenium derivative containing three isomeric cluster units, giving a total atom count of 207, excluding hydrogen atoms. As a result, computational limitations (noted in Chapter 5) have restricted the refinement of this crystal structure to an R factor of 0.14. The detailed bond lengths and angles obtained must therefore be considered with regard to this low degree of refinement. The skeletal bond lengths are given in Table 14.

The three molecules in the asymmetric unit of closo-[3-(PPh_3)-2,2,2-(CO)(PPh_3)$_2$-2,1-$OsCB_8H_8$] all conform to the geometry described above, with variations in skeletal inter-atomic distances, but more noticeably differ in the rotational alignment of the triphenylphosphine ligands about the P-cage vectors. Whilst this is of consequence crystallographically, it will have no bearing on the expected, or indeed observed, spectroscopic data, since such rotational freedom is probably manifest in the solution structure. The observed dissymmetry between molecules in the asymmetric unit may be a function of crystal packing and is thus of minor interest.

In contrast to the mirror plane symmetry of the ruthenacarbaborane (6), the osmacarbaborane (7) is asymmetric because of the tropical position of the cage bound phosphine. A further asymmetric centre exists due to the disposition of the triphenylphosphine and carbonyl ligands on the osmium atom. In this case the orientation of the ligands has been rotated by 120 degrees in comparison to that observed in the ruthenium analogue to yield the rotational form in which the carbonyl ligand is adjacent to the cis B-PPh_3 group with one of the phosphine ligands aligned with the Os(2)-C(1)-B(4)-B(10) plane.

The osmacarbaborane (7) is isoelectronic with the ruthenium analogue, having 11 SEP's (n+1) for skeletal bonding, with the 18 electron d^6 osmium(II) metal atom contributing three orbitals and two electrons. The coordination geometry at the osmium atom is also that of a distorted octahedron with the skeletal carbon and trans phosphine ligand forming the axial vectors. The equatorial bonding vectors are to the cis phosphine and carbonyl ligands, and the lower tropical plane of the carbaborane ligand.

Table 14. Skeletal interatomic distances (pm) for the three molecules of the asymmetric unit of the osmacarbaborane [2,2,2-(CO)$(PPh_3)_2$-closo-2,1-$OsCB_8H_8$-3-(PPh_3)] (7).

Molecule	1	2	3
Upper polar vertex			
C(M01)-Os(M02)	217.3	218.1	210.3
C(M01)-B(M03)	174.9	173.6	151.4
C(M01)-B(M04)	158.8	159.0	168.5
C(M01)-B(M05)	168.8	150.5	157.1
Upper tropical plane			
Os(M02)-B(M03)	235.0	248.8	237.2
Os(M02)-B(M05)	233.8	231.4	239.9
B(M03)-B(M04)	191.7	189.2	180.3
B(M04)-B(M05)	192.3	177.9	171.1

Table 14 continued

Equatorial plane			
Cm(2)-B(M06)	240.1	236.9	228.2
Cm(2)-B(M07)	230.4	230.0	245.1
B(M03)-B(M07)	179.1	202.1	192.7
B(M03)-B(M08)	175.5	176.5	184.1
B(M04)-B(M08)	178.7	187.2	177.6
B(M04)-B(M09)	182.4	161.0	185.4
B(M05)-B(M06)	185.2	174.5	187.0
B(M05)-B(M09)	190.4	190.6	177.1
Lower tropical plane			
B(M06)-B(M07)	186.2	203.0	211.2
B(M06)-B(M09)	194.2	182.8	190.1
B(M07)-B(M08)	193.7	203.5	199.9
B(M08)-B(M09)	199.5	202.7	209.9
Lower polar vertex			
B(M10)-B(M06)	166.1	171.0	182.8
B(M10)-B(M07)	175.5	184.0	196.6
B(M10)-B(M08)	167.1	179.4	192.3
B(M10)-B(M09)	167.2	172.2	170.4

(Note; M refers to the respective molecule 1-3.
Standard deviations are omitted because the
structure refinement is incomplete, see Chapter 5)

CHAPTER FOUR

CHAPTER 4 TEN VERTEX GOLD MONOCARBON CARBABORANES. MONO-, DI-, AND TRIPLE-DECKER CLOSO-ARACHNO-FRAMEWORKS $[L_yAu_x(CB_8H_{12})_2]$ WHERE Y = 1, 2, 7 AND L = PHOSPHINE LIGAND.

4.1. INTRODUCTION

Metalla derivatives of CB_8H_{14} have now been synthesised using transition metals from all three triads of Group VIII[146-149,180]. Apart from the oxidative insertion of zero valent platinum to yield the platinacarbaborane $(PPh_3)_2PtCB_8H_{12}$[150,151] the rest of these derivatives, including those ruthenium and osmium clusters described in Chapter 3 of this thesis, were prepared from the reaction of a suitable transition metal halide reagent with the carbaborane anion $[CB_8H_{13}]^-$. These reactions produce closo, nido and arachno metallacarbaboranes in which the metal is incorporated into the framework of the carbaborane precursor and is accompanied by rearrangement or loss of bridging hydrogens.

In contrast, from the research of transition metal carbonyl cluster chemistry, it has been found that the bridging hydrogens in such clusters can be replaced, without subsequent intra-molecular rearrangement, by the isolobal $Au-PR_3$ group, the theoretical justification for which was developed by Hoffmann[194]. The gold derivatives $[Co_3Fe(\mu_3\text{-}AuPPh_3)(CO)_{12}]$ and $[Os_4Fe(\mu\text{-}H)_3(\mu\text{-}AuPEt_3)(CO)_{12}]$ in which the gold phosphine fragments bridge a Co_3 face and Os-Os edge respectively are thus derived from the hydrido parent compounds $[Co_3Fe(\mu_3\text{-}H)(CO)_{12}]$[195] and $[Os_4Fe(\mu_3\text{-}H)_4(CO)_{12}]$[196]. The most popular gold reagents used for these reactions are of the type $[ClAuPR_3]$[195] or $[MeAuPR_3]$[197,198].

Few auraboranes and auracarbaboranes clusters have been previously synthesised in comparison to the diverse range of other transition

metal derivatives known[12,164]. The pentaborane[199] and dicarbollide[200,201] derivatives, $PPh_3AuB_5H_8$ and $[Au(C_2B_9H_{11})_2]^-$, exemplify the different possible mode of gold atom coordination to a borane framework. In the former, the gold phosphine fragment replaces a bridging hydrogen on the open face of the cluster, retaining the original structural geometry, whilst in the latter cluster the gold atom, free of its original ligands, is fully incorporated into the nido carbaborane skeleton to yield a commo-closo sandwich complex.

In order to further exemplify the interaction of gold reagents with carbaborane frameworks, the reactions of several gold-phosphine reagents with CB_8H_{14} and its derived anion were studied. The principal goal of this was to discover whether replacement of one or more bridging hydrogen atoms in the intermediate sized carbaborane cluster occurs with or without further incorporation of the gold atom or atoms into the cluster framework.

The reactions of CB_8H_{14} and $[CB_8H_{13}]^-$ with the gold reagents $ClAuPPh_3$, $MeAuPPh_3$, $ClAuP(cyclo\text{-}C_6H_{11})_3$, $MeAuP(cyclo\text{-}C_6H_{11})_3$ and $Au_2Cl_2(dppm)$ were found to yield the six auracarbaborane products shown in the reaction scheme overleaf, (auracarbaboranes (8) to (13)).

From the initial n.m.r. data obtained for these products, prior to full structural characterisation, it was clear that the gold fragments had been incorporated into the cluster framework to yield arachno derivatives rather than products in which the gold fragment replaced a single bridging hydrogen. The target of the investigation thus changed to structural characterisation of these apparently complex products. At least differentiation between the structural features of the major and minor products isolated was desired.

The major product isolated from the reaction of the mononuclear

REACTION 1 Mononuclear Gold Reagents.

CB_8H_{14} + $MeAuPR_3$

or

$[CB_8H_{13}]^-$ + $ClAuPR_3$

Major Product $[Au(CB_8H_{12})_2]^-$ $[Au(PR_3)_2]^+$ (see Section 4.2)

(8) R = Ph ; (10)* R = (Cyclo-C_6H_{11})$_3$

Minor Product $[(CB_8H_{12}Au)(AuPPh_3)_5(AuCB_8H_{11})]$ (see Section 4.3)

(9) and (11)* R = Ph only

REACTION 2 Dinuclear Gold Reagent

$[CB_8H_{13}]^-$ + $Au_2Cl_2(dppe)$

Major Product $[(CB_8H_{12})_2Au_2(dppe)]$ (see Section 4.4)

(12)*

Minor Product $[Au(CB_8H_{12})_2]^-$ $[Au_x(dppe)_y]^+$ (see Section 4.4)

(13)

(8-13) = Auracarbaborane numbering scheme used in text.

* = Structure confirmed by X-ray crystallography.

gold reagents was the mononuclear commo auracarbaborane anion, $[Au(CB_8H_{12})_2]^-$ (8,10), in which both the ligands on the gold atom have been replaced by the carbanonaborane ligand $[CB_8H_{12}]^{2-}$. The counter cation has been identified as the linear bisphosphine complex $[Au(PR_3)_2]^+$. A minor product of this reaction was also identified as the heptanuclear commo auracarbaborane $[(CB_8H_{12}Au)(AuPPh_3)_5(AuCB_8H_{11})]$ (11), a novel cluster in several respects.

The products isolated from the reaction of the dinuclear gold phosphine complex $Au_2Cl_2(dppe)$ similarly incorporate the metal atom into the cluster framework. In this instance however, the equivalent of the unobserved intermediate product from the above reaction was isolated as the main product, that is, the carbaborane-gold-phosphine complex $[(CB_8H_{12})_2Au_2(dppe)]$ (12). The minor product of the reaction was found to be the previously identified commo auracarbaborane anion, $[Au(CB_8H_{12})_2]^-$, and was observed to be readily formed from the dinuclear auracarbaborane by the loss of the chelating phosphine ligand. In this instance the identity of the counter cation was not established.

During the course of this work, Welch et al[202] has published the preliminary results from analogous studies of the reactions of gold-phosphine reagents with decaborane(14). The main product isolated was found to be the hexanuclear commo auraborane $[Au_6(B_{10}H_{12})_2(PEt_3)_4]$. This product, a triple cluster of gold and boron, has a similar gross structure to the heptanuclear commo auracarbaborane (11) prepared during this work, albeit with the basic differences in borane sub-cluster composition and orientation and number of gold atoms incorporated into the gold sub-cluster. Further comparison of these two triple clusters is given in Section 4.3.

4.2 A-COSMO-AURACARBABORANE ANION $[Au(CB_8H_{12})_2]^-$. THE SYNTHESIS OF $[Au(CB_8H_{12})_2]^-$ $[Au(PR_3)_2]^+$ (R = C_6H_5 (8) ; cyclo-C_6H_{11} (10)) AND THE CRYSTAL AND MOLECULAR STRUCTURE OF $[(9,6\text{-}Au(CB_8H_{12})_2)_2]^-$ $[Au(P(cyclo\text{-}C_6H_{11})_3)_2]^+$ (10).

The reaction of an equimolar mixture of arachno CB_8H_{14} with $MeAu(PPh_3)$ in diethyl ether at room temperature, gives a red solution which quickly deepens in colour. Despite the intensity of this colouration, the ^{11}B n.m.r. spectrum of this mixture showed that the yield of product was insignificant compared to the unreacted carbaborane present. The addition of a further two molar equivalents of the gold reagent was found to reduce the surplus carbaborane content of the reaction mixture, giving a corresponding increase in yield of the major product, with the carbaborane being completely depleted by reaction of a further three-fold equivalence of the gold reagent. The ^{11}B n.m.r. spectra of the 1:3 and 1:6 reaction mixtures are shown in Figure 83. The latter spectrum clearly shows the resonances of the major product with those of one or more minor products visible as minor peaks. A similar reaction was observed to occur between the arachno carbaborane anion $[CB_8H_{13}]^-$ and $AuCl(PPh_3)$, as observed by ^{11}B n.m.r. spectroscopy and t.l.c.

Two compounds, auracarbaboranes (8) and (9), were isolated from the reaction mixture by preparative scale t.l.c. Both products were red coloured solids, though the major product auracarbaborane (8) was much deeper in hue.

The ^{11}B n.m.r. spectrum of auracarbaborane (9) (Figure 84b) shows three groups of resonances with an approximate 2:1:5 integration ratio. If this reflected a single carbaborane fragment within the

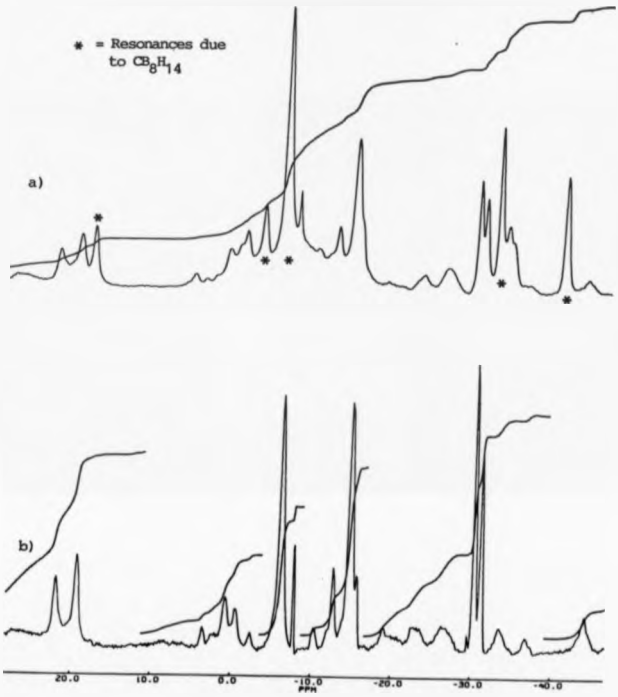

Figure 83. ^{11}B n.m.r. spectra of reaction mixtures containing a) 1:3 CB_8H_{14} : $MeAuPPh_3$ and b) 1:6 CB_8H_{14} : $MeAuPPh_3$

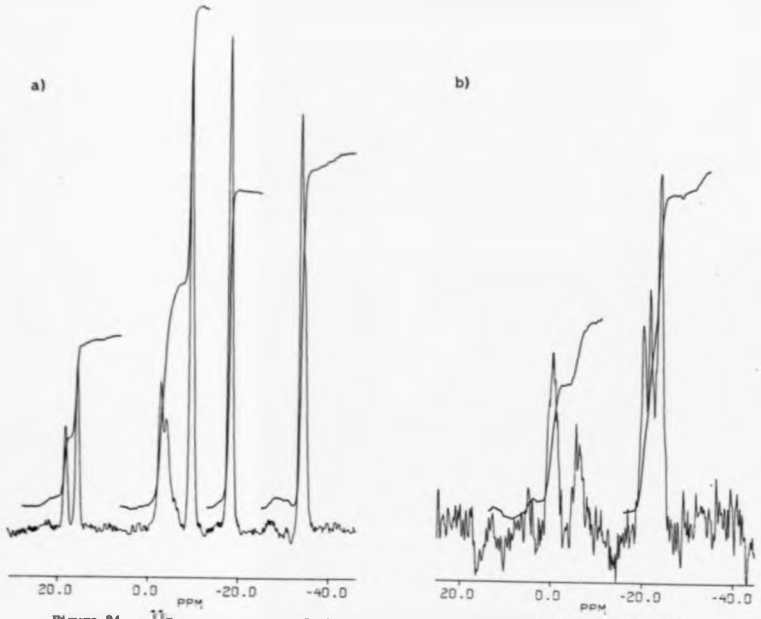

Figure 84. ^{11}B n.m.r. spectra of a) auracarbaborane (8) and b) auracarbaborane (9).

molecule than the latter group of resonances would presumably be composed of three resonances in a 1:2:2 ratio. Since the latter is clearly composed of more than three resonances, the inference is that two carbaborane fragments (or more) are responsible for the observed spectrum, giving a weighted integration ratio of 4:2:10. The ^{1}H n.m.r. spectrum obtained showed the presence of aromatic protons and two types of BHB bridging hydrogens.

Further investigation of auracarbaborane (9) was not pursued because of the very small amounts of material available and the apparent instability of the compound, (crystals grown under an inert atmosphere were observed to darken over a period of days).

Attention was focused on the major product of the reaction, auracarbaborane (8). The ^{11}B n.m.r. spectrum of this compound was originally observed to contain eight resonances in an approximate 1:1:1:1:4:4:2:2 integration ratio, which resembled the overlapping of two 1:1:2:2:2 type spectra with the middle two resonances superimposed (Figure 84a). The proton spectrum similarly indicated the presence of two symmetrical carbaborane residues, by virtue of the presence of two sets of BHB and CH_2 resonances (both $CH_{(\underline{exo})}$ and $CH_{(\underline{endo})}$, distinguished by their shift and multiplicity). The ^{31}P n.m.r. spectrum obtained showed only one resonance.

The initial spectroscopic data obtained were consistent with a molecule in which there are two carbaborane cages in differing coordination environments, presumably linked by a number of gold fragments, each retaining the mirror plane symmetry of the carbaborane precursor.

Compound (8) was thus reasonably formulated as an $(CB_8H_{12})_2Au_x(AuPPh_3)_y$ derivative. Potentially, either one or two

$AuPPh_3$ groups could replace both of the bridging hydrogen atoms on the triangular face of C_8H_{14}. Indeed, the integration ratio of aromatic to cluster hydrogen resonances indicated the presence of three or four PPh_3 groups, hence supporting numerous possible formulations involving gold aggregation complexes where $x + y > 2$, consistent with two carbaborane residues in differing symmetrical coordination environments. The simplest of these would be a triple cluster comprised of a central trigonal array of gold atoms, attached to which are two carbaborane residues, one fused to an edge by coordination to two gold atoms, the other linked by the remaining gold atom. Larger central gold sub-units could thus also be envisaged, having the same symmetry properties. In these, the extra gold vertices would be occupied by $AuPPh_3$ fragments, as found in a range of hetero gold clusters.

The orientation of the carbaborane residues with respect to each other, must be in an anti or syn conformation in order to retain mirror plane symmetry in each carbaborane residue, assuming a similar symmetry within the central gold sub-unit. The alternative staggered orientation of the carbaborane residues removes any symmetry.

In order to ascertain the number of gold phosphine fragments incorporated into the carbaborane precursor and their relative and skeletal disposition, an X-ray diffraction study of compound(8) was undertaken. Verification of the observed n.m.r. data was also desirable. Unfortunately, numerous crystals of compound (8) were assessed for suitability in an X-ray study and found to be either non diffracting or twinned.

Though repeated attempts to recrystallise compound (8) from a range of solvents failed to produce suitable crystals for an X-ray

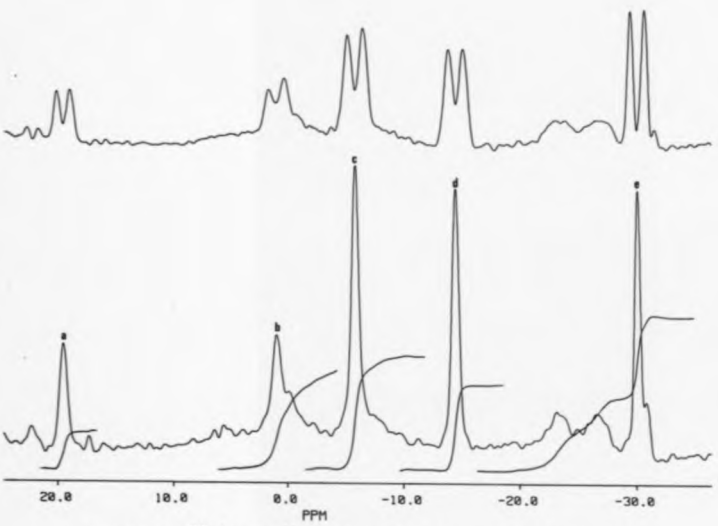

Figure 85. $^{11}B\{^{1}H\}$ and ^{11}B n.m.r. spectra of auracarbaborane(8) after purification by repeated recrystallisation.

study, two important results were obtained. Firstly, material crystallised for the purpose of an X-ray study was later found to produce an ^{11}B n.m.r. spectrum with a 1:1:2:2:2 pattern corresponding to one of the previous observed 1:1:2:2:2 spectra overlapping to give a 1:1:1:1:4:4:2:2 pattern (See Figure 85). This therefore implied that the material isolated as auracarbaborane(8) consisted of two discrete compounds that had not been separated by t.l.c. Further chromatographic experimentation did not however resolve the material.

The second important result of the recrystallisation of compound (8) was the isolation of another novel auracarbaborane complex, a heptanuclear gold triple cluster, auracarbaborane (11). A detailed description of the structural features of this novel cluster is given in Section 4.3.

Whilst progressing with the X-ray diffraction analysis of auracarbaborane(11) further reactions of CB_8H_{14} with gold phosphine reagents were investigated. The reaction of the cyclohexylphosphine analogue of $MeAuPPh_3$, i.e. $MeAuP(cyclo\text{-}C_6H_{11})_3$, with CB_8H_{14} was undertaken for the following reasons. The prime reason was to establish whether a product different to auracarbaborane(8) would result from the reaction of a gold reagent with a more sterically demanding phosphine ligand, and if so whether characterisation of this product would in any way assist in elucidation of the nature of the auracarbaborane (8) which still remained uncharacterised.

If the reaction yielded the cyclohexylphosphine analogue of auracarbaborane(8), as indicated by n.m.r. spectroscopy, then perhaps crystals suitable for an X-ray diffraction study could be obtained, thus enabling the characterisation of both the triphenylphosphine and tricyclohexylphosphine gold carbaborane clusters.

The reaction of arachno CB_8H_{14} with excess MeAuP(cyclo-C_6H_{11})$_3$ in diethyl ether at room temperature, gave a pink solution which yielded amongst other products the yellow compound auracarbaborane(10) on t.l.c. work up. The $^{11}B\{^1H\}$ n.m.r. spectrum of auracarbaborane (10) (Figure 86) contains eight resonances in an approximate (1:1):(1:1):(4):(4):(2:2) integration ratio. Those signals grouped in parenthesis are of similar chemical shifts. The most significant feature of this spectrum is the fact that it is nearly identical to that obtained for auracarbaorane(8). In both spectra the eight resonances appear to result from the overlapping of 1:1:2:2:2 type spectra and in fact taking into account a difference in shift due to either referencing or solvent effects, both spectra have identical shifts for every resonance. This clearly indicated that the auracarbaboranes (8) and (10) were analogous compounds.

Though described earlier as a 1:1:1:1:4:4:2:2 spectrum, i.e. the overlapping of two 1:1:2:2:2 spectra, the integration ratio of the eight resonances is not that expected for a 1:1 overlap but nearer to 1:2. This ratio would in principle indicate that the auracarbaborane (10) contains three CB_8 cluster units, two of which are in identical environments.

Though additional spectroscopic data was obtained for auracarbaborane (8) and thus may be of use in characterisation of the analogous auracarbaboranes (8) and (10), discussion of this information is more usefully made after the following description of the X-ray crystallographic structure determination of auracarbaborane (10).

In contrast to the previous experience of crystal twinning found for auracarbaborane (8), crystals of the tricyclohexylphosphine derivative auracarbaborane (10), of suitable quality for X-ray

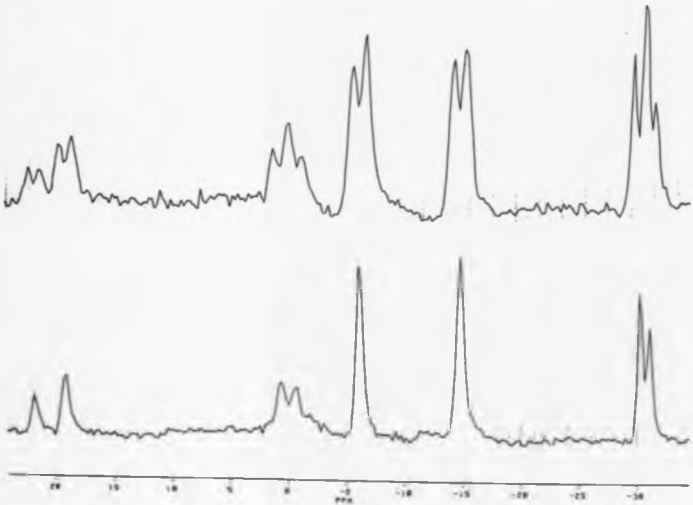

Figure 86. The ^{11}B and $^{11}B\{^1H\}$ n.m.r. spectra of auracarbaborane(10).

diffraction analysis, were obtained by the solvent diffusion method. A full account of the X-ray crystallographic structure determination of the auracarbaborane (10) is contained in Chapter 5. Compound (10) crystallised in space group $P\bar{1}$, with two discrete molecules identified in the asymmetric unit. The simplest of these was the cationic species $[Au(P(C_6H_{11})_3)_2]^+$. The Au(I) phosphine cation has a linear P-Au-P axis as shown in the drawing of the X-ray crystallograpic molecular structure of this cation (Figure 87). The linearity of the complex is not unexpected, since a linear geometry has been found for other triphenylphosphine gold complexes[203] including $[Au(PPh_3)_2]^+[Au(MNT)_2]^-$ where MNT is maleonitriledithiolate. Gold complexes with the stoichiometry $[(PPh_3)Au(L-L)]$, where $[L-L]^{2-}$ is a bidentate chelating ligand, were originally believed to contain Au(II), but are now recognised to be mixed valence Au(I)/Au(III) complexes, $([Au(PR_3)_2][Au(L-L)_2])$, hence their description as pseudo-gold(II) compounds.

The most notable feature of the structure of the tricyclohexylphosphine gold(I) cation of auracarbaborane (10) is that the cyclohexyl rings on the phosphine ligands are eclipsed with respect to each other. Whilst this conformation is observed in the solid state structure, in solution the phosphine ligands are free to spin around the P-Au-P axis to include all the alternative staggered conformations.

The second and most important molecule in the asymmetric unit of auracarbaborane (10), characterised as the counter anion, was the cosmo-auracarbaborane $[(CB_8H_{12})_2Au]^-$. The structure of the anion essentially comprises two $[CB_8H_{12}]^{2-}$ carbaborane ligands coordinated to a central cosmo-gold atom. The overall positive charge thus corresponds to an Au(III) oxidation state for the central gold atom.

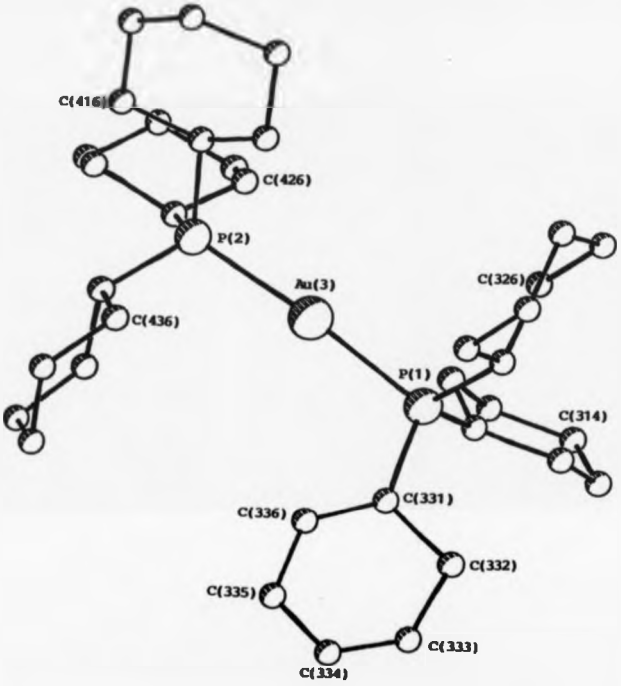

Figure 87. Drawing of the X-ray crystallographically determined molecular structure of $[AuP(cyclo\text{-}C_6H_{11})_2]^+$, the cation component of auracarbaborane (11), $[(CB_8H_{12})_2Au]^-$ $[AuP(cyclo\text{-}C_6H_{11})_2]^+$.

The refinement of the anion was complicated by the presence of two alternative commo-gold positions and two alternative carbaborane cluster orientations. The structure of the anion including all of the located skeletal atoms is shown in Figure 88. This molecular drawing is clearly incorrect in terms of the stoichiometry of the anion formulation and requires some explanation. The following description of the resultant structure is accompanied by a number of schematic diagrams to aid discussion (Figure 89).

Consider the anion as consisting of two carbaborane units and one gold atom. One of the carbaborane cluster units was refined as a CB_8 unit in a particular orientation (Figure 89a). The central gold atom was thus found and refined at the coordinates corresponding to the 9- position in the decaborane like framework (Figure 89b). A second gold atom position was also identified and refined in a similar manner to the first position (Figure 89c). Both of the gold positions were therefore assigned half occupancies, giving a whole occupancy for the combined position. The second carbaborane unit was in fact found to be in two orientations with respect to the other carbaborane ligand, namely the syn and anti configuration (Figure 89d). Because both of the second carbaborane cluster units gave approximately equal refinement, the skeletal atoms of each carbaborane were also assigned half occupancies (giving a whole occupancy for each atom of the disordered carbaborane ligand). The syn and anti carbaborane conformations thus correspond to one of the alternative gold atom positions (Figure 89a).

To clarify the original molecular drawing of the auracarbaborane (10) anion, (Figure 88), the unravelled molecular drawings of the syn and anti conformations of $[(CB_8H_{12})_2Au]^-$ are given in Figure 90.

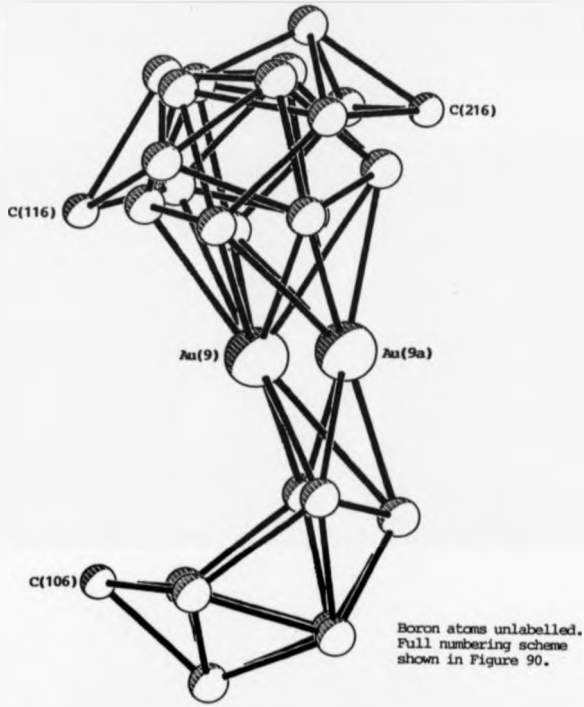

Figure 88. Drawing of the X-ray crystallographically determined molecular structure of $[(CB_8H_{12})_2Au]^-$, the anionic component of the auracarbaborane (10), $[(CB_8H_{12})_2Au]^-$ $[AuP(cyclo\text{-}C_6H_{11})_2]^+$.

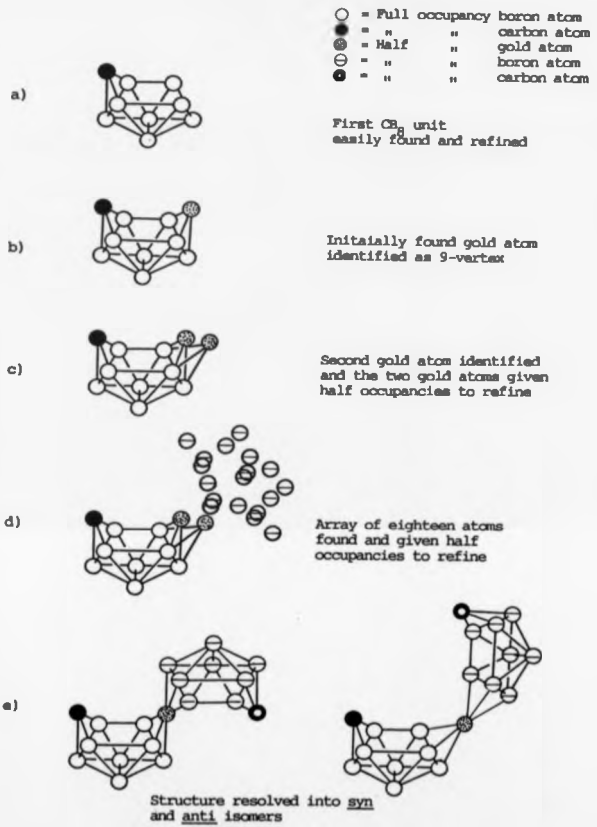

Figure 89. Schematic diagrams of $[(CB_8H_{12})_2Au]^-$ showing those atoms refined with crystallographic fractional occupancies.

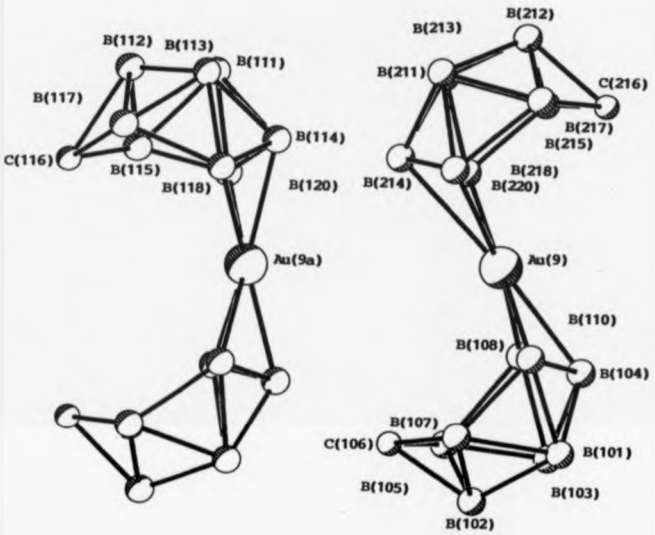

Figure 90. Drawing of the X-ray crystallographically determined molecular structure of the syn and anti conformations of $[(CB_8H_{12})_2Au]^-$, the anionic component of the auracarbaborane (10).

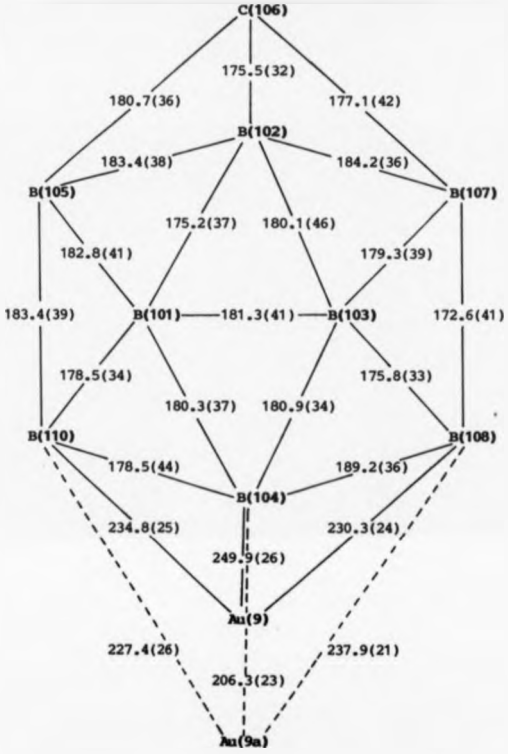

Figure 91. Skeletal distances (pm) for ordered 'CB_8' sub-unit of the auracarbaborane anion $[(CB_8H_{12})_2Au]^-$ (10).

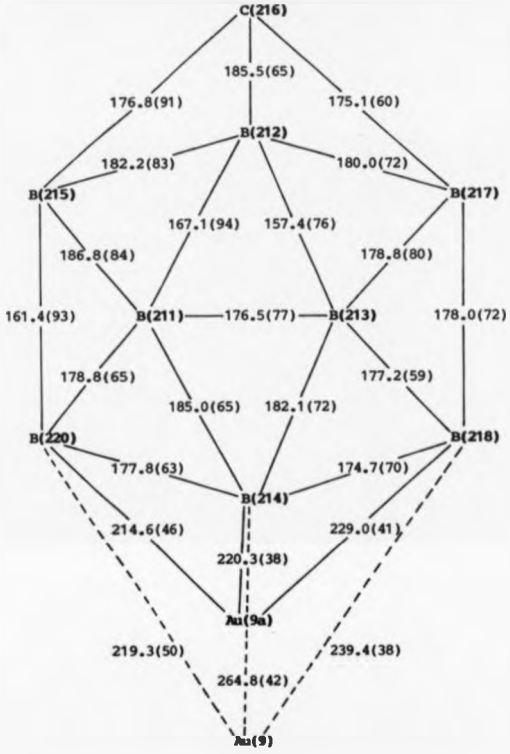

Figure 92. Skeletal distances (pm) for disordered 'anti-CB_8' sub-unit of the auracarbaborane anion $[(CB_8H_{12})_2Au]^-$ (10).

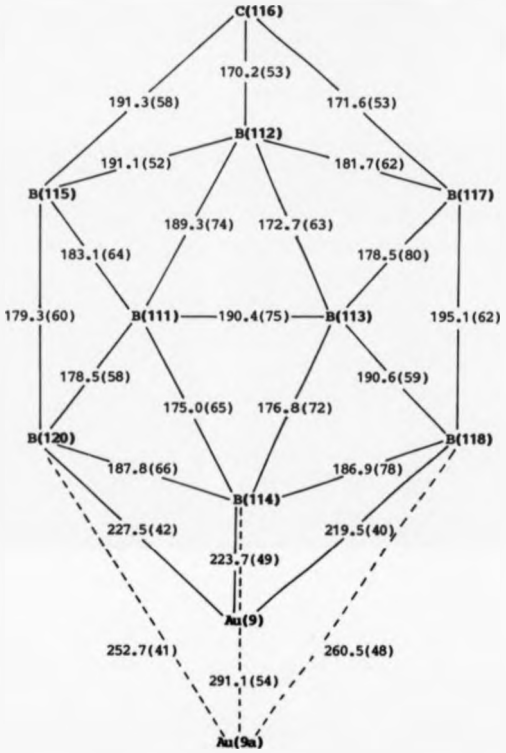

Figure 93. Skeletal distances (pm) for disordered 'syn-CB_8' sub-unit of the auracarbaborane anion $[(CB_8H_{12})_2Au]^-$ (10).

From the spectroscopic data obtained on auracarbaboranes (8) and (10), and X-ray crystallographic data on the latter, the main product of the reaction of CB_8H_{14} with $MeAuPR_3$ reagents has been shown to be the mixed valence gold salt $[(PR_3)_2Au]^+ [Au(CB_8H_{12})_2]^-$. The structure of the tricyclohexylphosphine derivative was established by X-ray crystallography and shown to consist of linear Au(I) cation, $[((cyclo\text{-}C_6H_{11})_3P)_2Au]^+$ and a cosmo Au(III) auracarbaborane anion $[Au(CB_8H_{12})]^-$. The anion was found to be present in two isomeric conformations, in which the two carbaborane sub-clusters are coordinated to the central gold atom in an anti or syn orientation. In both isomers the gold atom occupying the cosmo vertex has a pseudo square planar coordination geometry.

The inter-atomic distances found for the ordered $[CB_8]$ sub-unit of the auracarbaborane (10) anion (see Figure 91) are within the ranges observed for the previously characterised ruthanacarbaboranes (see Chapter 3). Those observed for the disordered syn and anti $[CB_8]$ sub-units show greater variance from the expected range (see Figures 92 and 93), including several excessively long and short distances of ~195 pm and ~158 pm. These distances do however have to be considered in conjunction with both the apparent crystal disorder and the observed standard deviations of 4-8 pm.

The anion of auracarbaborane (10), $[(CB_8H_{12})Au(CB_8H_{12})]^-$, has 92 valence electrons as calculated for a cosmo polyhedron according to the Mingos[37] electron counting rules for condensed polyhedra.

The presence of two isomeric forms of auracarbaborane anion $[(CB_8H_{12})_2Au]^-$ in auracarbaborane (10), and by analogy also for auracarbaborane (8), correlates with the n.m.r. spectroscopic evidence obtained on these products noted earlier. Thus the observed

1:1:1:1:1:4:4:2:2 pattern of the ^{11}B n.m.r. spectra of auracarbaboranes (8) and (10) shown in Figures 84a and 86 respectively arise from the overlapping of the 1:1:2:2:2 spectrum for each of the isomeric carbaborane anions. Note that identification of each 1:1:2:2:2 spectrum (annotated in Figure 86) is derived from the relative intensities of each resonance in these spectra, made possible by the presence of unequal amounts of each isomer. These assignments are confirmed by the spectrum of the single isomeric form of auracarbaborane (8) isolated by repeated recrystallisation (Figure 85). Unfortunately the assignment of each 1:1:2:2:2 ^{11}B n.m.r. spectrum to a particular isomer is not possible from the data obtained, though one might suspect that the anti isomer would be the preferred conformation and thus be responsible for the 1:1:2:2:2 spectrum of greatest intensity in the observed spectra (see Figure 86).

The presence of terminal hydrogens on each of the boron atoms of the $[CB_8H_{12}]$ sub-cluster within the $[(CB_8H_{12})_2Au]^-$ anion and the presence of two identical bridging hydrogens on the open face was confirmed by a series of $^1H(^{11}B_{select})$-^1H subtraction spectra obtained on the isolated isomer of auracarbaborane (8) (Figure 94). The observed correlation of the bridging hydrogens to two resonances of two-fold intensity clearly indicates that the bridging hydrogens connect the B(7,8) and B(5,10) boron atoms, as expected for the arachno configuration. The assignment of the resonances in the ^{11}B and ^1H n.m.r. spectra of auracarbaboranes (8) and (10) were then deduced from comparison with the shifts observed for the arachno ruthenacarbaborane (3) (see Chapter 3). The n.m.r. spectra assignments for the isomeric mixture of auracarbaborane anions $[(CB_8H_{12})_2Au]^-$ and further n.m.r. data including an ^{11}B COSY spectrum is presented in Section 4.4.

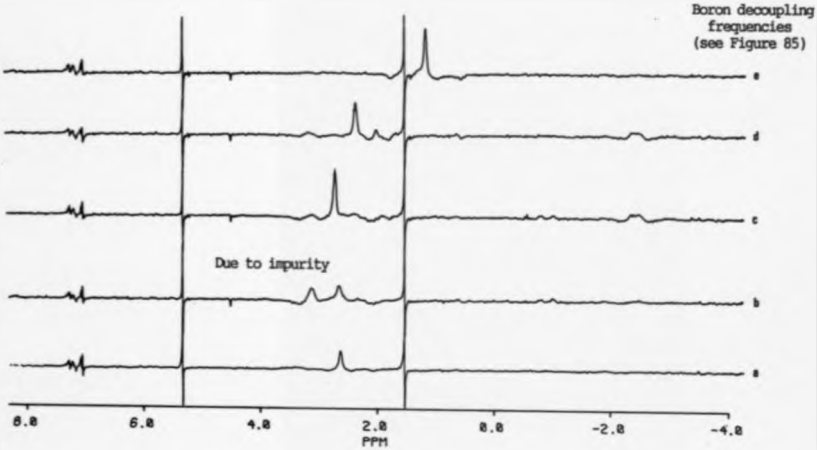

Figure 94. Series of selectively boron decoupled proton spectra for auracarbaborane (8) after purification by repeated recrystallisation, ($^{1}H\{^{11}B_{(select)}\}$-$^{1}H$ spectra). (Boron decoupling frequencies as annotated).

where the isolation of the same commo auracarbaborane anion from a stable intermediate gold complex is discussed.

Since the work contained in this thesis was completed Welch et al[204,205] have published further results of analogous work with decaborane(14). From this work the major product was identified as the mono bridge substituted product (cyclo-$C_6H_{11})_3PAuB_{10}H_{13}$[204]. In addition, two auraborane anions were isolated[205], namely $[(B_{10}H_{12})Au(B_{10}H_{12})]^-$ and $[(B_{10}H_{12})Au(B_{10}H_{13})]^{2-}$ (see Figure 95).

The structure of the auraborane(1-) anion, $[(B_{10}H_{12})Au(B_{10}H_{12})]^-$, was found to be similar to the anti conformation of auracarbaborane (10) described above albeit with an overall nido commo cluster geometry containing $B_{10}H_{12}$ ligands rather than arachno commo cluster geometry

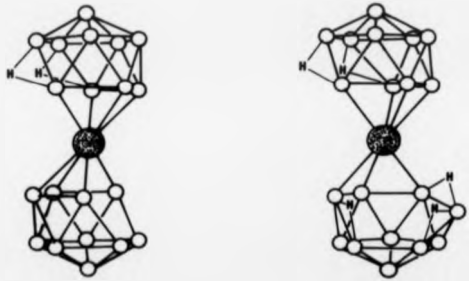

a) b)

Figure 95. Structures of the auraborane anions[205]
a) $[(B_{10}H_{12})Au(B_{10}H_{12})]^-$ and b) $[(B_{10}H_{12})Au(B_{10}H_{13})]^{2-}$.

containing CB_8H_{12} ligands of auracarbaborane (10). In contrast to auracarbaborane (10) the syn conformation was not observed for the decaborane analogue.

The structure of the auraborane(2-) anion, $[(B_{10}H_{12})Au(B_{10}H_{13})]^{-}$, as determined by X-ray crystallography, was shown to consist of a nido $(B_{10}H_{12}Au)$ sub-cluster fused at the gold vertex to an arachno $(AuB_{10}H_{13})$ sub-cluster. The auraborane(2-) anion thus differs from the auraborane(1-) anion by the addition of a hydride ion, which contributes by providing a further overall negative cluster charge and a third bridging hydrogen atom on the open face of the arachno sub-cluster.

In view of the observed difficulties in refinement of the auracarbaborane X-ray structure, it seems reasonable to question whether a similar dianion consisting of arachno and hycho sub-cluster units may be present in auracarbaborane (10). This is however, discounted for the following reasons. Firstly, if the auracarbaborane (10) was a dianion, then one would expect to identify two $[(PR_3)_2Au]^{+}$ cations for each cosmo carbaborane anion in the X-ray crystallographic study. This was not observed. Secondly, the addition of a further endo hydrogen to the CB_8H_{12} fragment would be expected to reduce the symmetry of the cluster and therefore produce an ^{11}B n.m.r. spectrum very different from the overlapping 1:1:2:2:2 pattern observed. If the possibility of one carbaborane fragment being coordinated to the cosmo gold atom via a B-Au-B bridge is considered, thereby retaining an arachno sub-cluster structure, the additional bridging hydrogen could be accommodated on the open face of the cluster but this would again reduce the symmetry of the cluster with the above consequences in the expected ^{11}B n.m.r. spectrum.

4.3 A HEPTANUCLEAR AURACARBABORANE TRIPLE CLUSTER. THE SYNTHESIS AND CRYSTAL AND MOLECULAR STRUCTURE OF $[(CB_8H_{12}Au)(AuPPh_3)_5(AuCB_8H_{11})]$ (11).

The major product isolated from the reaction of $MeAuPPh_3$ with CB_8H_{14} has been identified as the mononuclear *cosmo*-auracarbaborane species $[Au(CB_8H_{12})_2]^-$ $[AuP(cyclo\text{-}C_6H_{11})_2]^+$ (8) (see Section 4.2). In contrast, Welch *et al*[202] have found that the reaction of decaborane(14), $B_{10}H_{14}$, with $MeAuPEt_3$ yielded the hexanuclear triple cluster $(B_{10}H_{12})_2Au_6(PEt_3)_4$ as the major product. The objective of both of these reactions was to synthesise a gold derivative of the borane cluster by replacement of a single bridging hydrogen atom on the open face of the borane cluster with the isolobal $AuPR_3$ fragment. The major product of both reactions has clearly resulted from a more complex substitution, above and beyond a single hydrogen replacement yielding clusters with skeletal metal atoms of high coordination.

Welch *et al*[202,204] have isolated the bridge substituted product [*nido*-μ-5,6-$(AuP(cyclo\text{-}C_6H_{11})_3$-$B_{10}H_{13}]$ using the more sterically demanding gold phosphine, $MeAuP(cyclo\text{-}C_6H_{11})_3$. Since the product of the analogous reaction of CB_8H_{14} with the tricyclohexylphosphine gold reagent has been shown to yield a mononuclear *cosmo* auracarbaborane anion (Section 4.2), the products obtainable from the reaction of boranes or carbaboranes with gold phosphine reagents would appear to be sensitive to the boron cluster geometry, the gold phosphine used and the reaction conditions employed. The existence[205] of $[(B_{10}H_{12})Au(B_{10}H_{12})]^-$, the decaborane analogue of the isolated *cosmo* auracarbaborane anion, was not known during the course of this work.

From a ligand point of view the less sterically demanding

arachno carbaborane CB_8H_{14} is more likely to be able to coordinate to a single gold atom to form a disubstituted product than is the nido decaborane fragment. However, given that the condensation of further $[AuPR_3]$ fragments is so readily observed in the decaborane reaction it would seem likely that under the conditions employed for the reaction of $MeAuPPh_3$ and CB_8H_{14} (i.e. a five-fold excess of the gold reagent) a minor product involving some further gold condensation would be produced. This in fact has proven to be the case.

During the attempts to grow crystals of auracarbaborane (8) for X-ray analysis, in addition to the previously noted isomeric purification, crystals of another product auracarbaborane (11) were obtained. Mistakenly believed to be crystals of auracarbaborane (8), i.e. the triphenylphosphine analogue of auracarbaborane (10), one was found to be suitable for X-ray analysis and was subjected to a full crystallographic structure determination. Unfortunately the origin of auracarbaborane (11) is not clear, so discussion of the possibilities is deferred until after the following description of the found structure.

A drawing of the crystal and molecular structure found for the auracarbaborane (11) is shown in Figures 96 and 97 with diagrams of skeletal distances given in Figure 98. The structure of the auracarbaborane (11) essentially comprises two $[CB_8]$ cluster units sandwiching a central heptanuclear $[Au_7]$ cluster. The metal cluster core consists of five $[Au(PPh_3)]$ fragments and two gold atoms Au(2) and Au(5) ligated by the carborane clusters. The geometry is best described as a capped trigonal bipyramid with an edge bridging $[Au(PPh_3)]$ group. Hence Au(2), Au(5) and Au(3) define the trigonal equatorial plane, with Au(4) and Au(1) the polar positions.

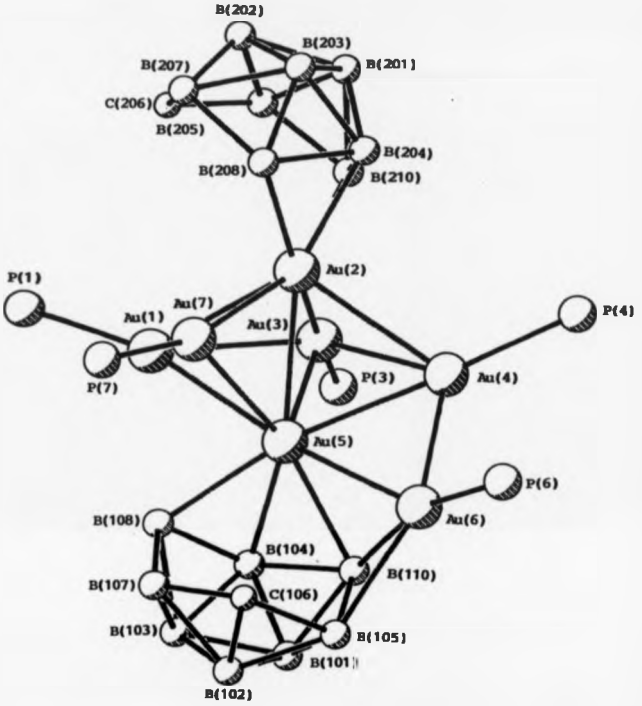

Figure 96. Drawing of the crystal and molecular structure of auracarbaborane (11), $[(CB_8H_{12}Au)(AuPPh_3)_5(AuCB_8H_{11})]$. (Phenyl rings of PPh_3 ligands omitted for clarity)

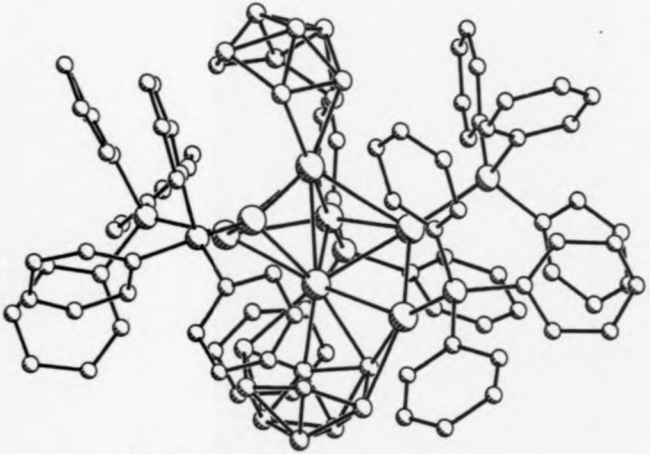

(For atom identification see Figure 96)

Figure 97. Drawing of the crystal and molecular structure of auracarbaborane (11), $[(CB_8H_{12}Au)(AuPPh_3)_5(AuCB_8H_{11})]$.

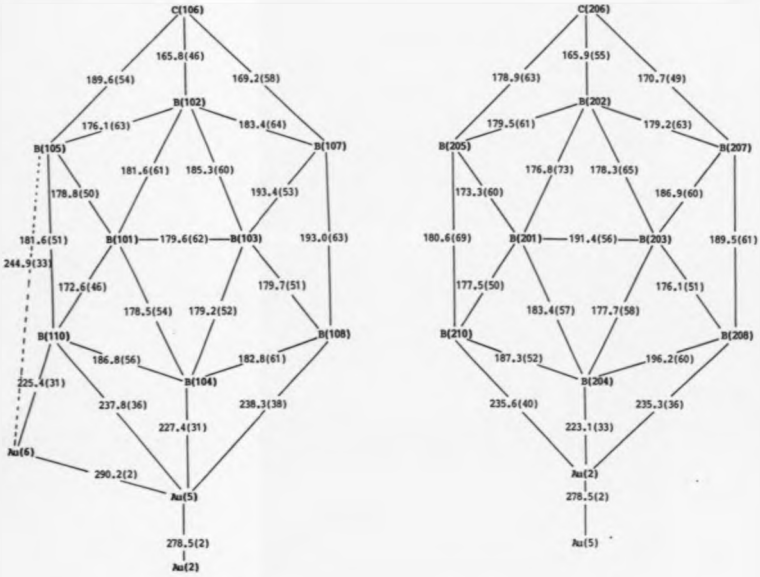

Figure 98. Skeletal distances (pm) for first and second '$AuCB_8$' sub-units of $[(CB_8H_{12}Au)(AuPPh_3)_5(AuCB_8H_{11})]$ (11).

Au(1)-Au(2)	282.5(2)	Au(1)-Au(3)	296.9(2)
Au(1)-Au(5)	272.4(2)	Au(1)-Au(7)	293.2(2)
Au(2)-Au(3)	269.7(2)	Au(2)-Au(4)	288.3(2)
Au(2)-Au(5)	278.5(2)	Au(2)-Au(7)	265.7(2)
Au(3)-Au(4)	299.3(2)	Au(3)-Au(5)	284.9(2)
Au(4)-Au(5)	271.2(2)	Au(4)-Au(6)	285.0(2)
Au(5)-Au(6)	290.2(2)	Au(5)-Au(7)	293.9(2)
Au(1)-P(1)	228.3(10)	Au(3)-P(3)	228.4(8)
Au(4)-P(4)	232.4(9)	Au(6)-P(6)	229.7(9)
Au(7)-P(7)	230.3(10)		

Table 15. Inter-atomic Au-Au and Au-P distances (pm) for the central heptanuclear gold core of $[(CB_8H_{12}Au)(AuPPh_3)_5(AuCB_8H_{11})]$ (11).

Compound	Arachno-(11)	Arachno-(3)	Nido-(1)
B(5)-C(6)	178.9(63)	171.2(9)	154.5(28)
C(6)-B(7)	170.7(49)	173.6(10)	156.7(29)
B(7)-B(8)	189.5(61)	186.3(11)	194.1(36)
B(8)-M(9)	235.3(36)	231.6(5)	227.2(20)
M(9)-B(10)	235.6(40)	230.3(6)	236.2(21)
B(10)-B(5)	180.6(69)	190.4(9)	184.8(34)
C(6)-B(2)	169.5(55)	166.0(7)	174.6(27)

Table 16. Comparison of inter-atomic distances (pm) around open face of nido and arachno ruthenacarbaboranes (1) and (3) and the auracarbaborane (11) (M = Ru, Au).

The $Au(PPh_3)$ fragment Au(7) caps the Au(1)(2)(5) face, with Au(6) bridging the Au(4)-Au(5) edge.

Each of the two carbaborane residues is coordinated via the triangular portion of the open face to a polar gold atom of the central gold cluster. One of the carbaborane sub-units is coordinated by a further gold atom, namely the edge bridging gold atom Au(6), which is coordinated to B(10S) and B(11O) on the square open face of the carbaborane sub-unit. The position of Au(6) clearly removes any symmetry within the central gold sub-cluster and also between the two carbaborane sub-clusters. The two carbaborane ligands are in a staggered orientation, approximately perpendicular with respect to each other.

The inter-atomic distances observed around the open face of the auracarbaborane units, in particular the C(6) to B(2,5,7) distances, are consistent with an arachno cluster structure, by comparison to the distances observed for the nido and arachno ruthenium $[CB_8]$ derivatives (1) and (3), (see Table 15). Though hydrogen atoms were not located in the crystal structure determination, the forementioned distances reasonably indicate the presence of a CH_2 skeletal fragment in each carbaborane cluster.

A similar lack of crystallographic and spectroscopic evidence for the presence or otherwise of bridging hydrogen atoms on the open face of the carbaborane sub-units is not solved by examination and comparison of the inter-atomic distances around the open face of the auracarbaborane (11), since the observed B(5)-B(10) and B(8)-B(7) distances of the nido and arachno ruthenacarbaboranes have not been found to be characteristic. However, given that a CH_2 group is indicated, such a fragment is associated only with arachno

carbaboranes, and thus indicates the presence of bridging hydrogens positioned on the square portion of the open face of each carbaborane sub-unit, i.e. B(107)-H-B(108), B(205)-H-B(210) and B(207)-H-B(208). Presumably, there is no bridging hydrogen at B(105)-H-B(110), since this site is occupied by the bridging Au(6)PPh_3 fragment. The alternative nido formulation for this sub-cluster, in which a single endo hydrogen is incorporated as a CH_2 group, in preference to a CH and BHB bridge is not a feature observed in other carbaborane clusters.

The fundamental triple cluster arrangment of the auracarbaborane (11) is similar to the recently reported[202] hexanuclear triple cluster $[(B_{10}H_{12}Au)(AuPEt_3)_4(AuB_{10}H_{12})]$, in that the structure comprises two borane type units sandwiching a central gold atom cluster, though they differ greatly in the nature of the two sub-cluster composition (see Figure 99a).

Apart from the obvious differences between the $[CB_8]$ and $[B_{10}]$ residues in each of the triple clusters, in the auracarbaborane (11), there are seven, as opposed to six, gold atoms within the central gold cluster. The central gold cluster of the auraborane complex is described as having a radially compressed octahedral geometry[202], with a symmetrical square array of four $AuPPh_3$ fragments around the $B_{10}Au$-AuB_{10} axis. This contrasts to the rather less symmetrical disposition of the five $AuPPh_3$ fragments of the auracarbaborane (11). The axial gold separation (i.e. the interatomic distance between the gold atoms coordinated to borane ligands) in the auracarbaborane (Au(2)-Au(5) = 278.5(2) pm) is some 13 pm shorter than that found in the auraborane,(291.88(16) pm). This axial compression is consistent with the difference between an octahedral and pentagonal bipyramidal type geometry, where coordination of a further equatorial atom causes

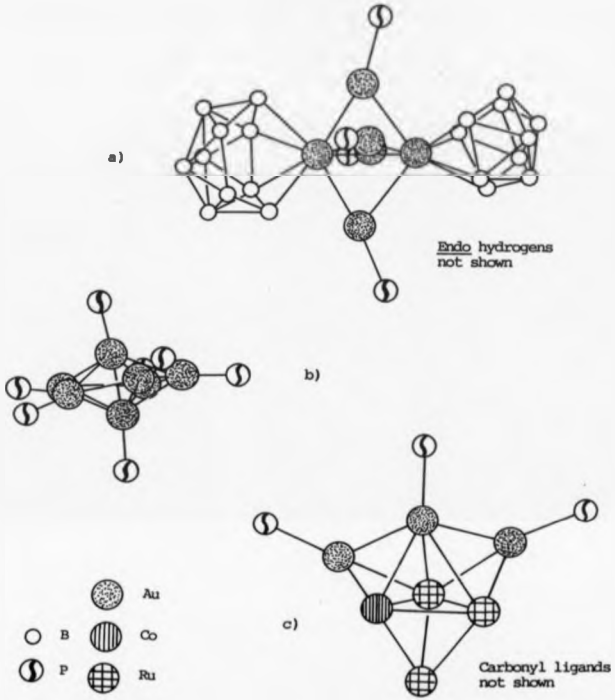

Figure 99. Drawings of the molecular structures of;

a) $[(B_{10}H_{12}Au)(AuPEt_3)_4(AuB_{10}H_{12})]$ [202]

b) $[Au_7(PPh_3)_7]^+$ [206]

c) $[Au_3CoRu_3(CO)_{12}(PPh_3)_3]$ [207].

the equatorial belt to become expanded and consequentially the axial distance reduced.

Whilst the gold cluster geometry of the heptanuclear auracarbaborane (11) outlined above is correctly described in terms of a capped and edge bridged trigonal bipyramid, alternative descriptions as condensed tetrahedra or distorted pentagonal bipyramid are found to be useful in comparison with geometries adopted by other heptanuclear metal clusters.

Of the wide range of metal clusters known the heptanuclear compounds are less well represented, in particular only one homo-heptanuclear gold cluster has been isolated, namely $[Au_7(PPh_3)_7]^+$, which has been shown to have a pentagonal bipyramidal structure[206] (Figure 99b). Other homonuclear seven atom clusters all have capped-octahedral geometries, as typified by $Rh_7(CO)_{16}$ and $Os_7(CO)_{21}$ and are therefore unrelated to the auracarbaborane structure. The gold containing hetaro-heptanuclear metal clusters characterised have conformed to a structure based on a bi-capped trigonal bipyramid, as exemplified by $[Au_3CoRu_3(CO)_{12}(PPh_3)_3]$[207] (see Figure 99c.)

In this example the structure is reasonably predictable since the original M_3M' cluster conforms to the same structure, albeit including the bridging hyride vertices. Direct replacement of the bridging hydride atoms with $[AuPPh_3]$ units yields the heptanuclear species, with the increased metal content. In this instance the edge bridging hydride ligands of the parent species are replaced by face bridging $AuPPh_3$ fragments. Other related hetaro-hepta-nuclear compounds show a similar gross structure, one example being, $[Au_3Ru_3(\mu_3\text{-}COMe)(CO)_9(PPh_3)_3]$[198], where the seventh metal position is occupied by the triple bridging carbyne.

	a	b	c
Axial	278.5(2)	258(2)	
Radial	265.7(2)-293.9(2)	274(2)-290(2)	262-272
Peripheral	285.0(2)-299.3(2)	287(2)-300(2)	280-310
Au-P	228.4(10)-232.4(9)	222(6)-238(6)	

Table 17. Comparison of Au-Au distances (pm) of a) $[Au_7]$ core unit of auracarbaborane (11), b) $[Au_7(PPh_3)_7]^+$ [206] c) distances found in high nuclearity gold clusters[212].

The bicapped-trigonal bipyramidal structure adopted by these metal clusters differs from that observed for the auracarbaborane (11) in the position of the two capping/bridging fragments, as shown by comparing Figures 99c and 96. In the hetaro cluster, the capping fragments are adjacent on one side of the trigonal equatorial plane whilst in the auracarbaborane they lie either side of the plane.

Of the three structural conformations observed for heptanuclear metal clusters, the auracarborane $[Au_7]$ geometry is most easily derived from the pentagonal bipyramidal geometry found for $[Au_7(PPh_3)_7]^+$. The notional unlinking of one gold vertex in the pentagonal equatorial plane of the latter, causing it to be edge bridging, yields the structure of the auracarbaborane metal core cluster.

The observed gold-gold distances found for the heptanuclear core of the auracarbaborane (11) (Table 17a) are comparable to the radial and peripheral distances observed for other polynuclear gold clusters (Table 17c), where the latter are generally found to be 10-30 pm longer than the former. The Au-Au interatomic distances found for auracarbaborane (11) show a longer radial bond distance range similar

to that of $[Au_7(PPh_3)_7]^+$ (Table 17b). The axial Au-Au distance of the auracarbaborane (11) is some 20 pm longer than that found in $[Au_7(PPh_3)_7]^+$, indicating a less compressed pentagonal bipyramidal structure, presumably resulting from the unlinking of Au(6), one of the members of the pentagonal equatorial belt.

Whilst the bond angles of the slightly puckered equatorial pentagonal Au_5 belt of $[Au_7(PPh_3)_7]^+$ (106.3-109.4(0.4)^o) conform to that expected for a regular pentagon (108^o) and indeed to the tetrahedral angle (109^o), those of the auracarbaborane are compressed to ~104^o, also possibly as a result of the unlinking of the Au(6) gold vertex from the pentagonal belt.

Another significant difference between the auracarbaborane (11) and $[Au_7(PPh_3)_7]^+$ is the orientation of the phosphine ligands. In the latter, the phosphine-gold vectors are directed approximately towards the centre of the pentagonal bipyramid (a quasi tetrahedral disposition), whilst in the auracarbaborane (11), the Au-PPh_3 vectors are approximately co-linear with a radial Au-Au vector, yielding an overall disposition of phosphine ligands alternating in a one-up, one-down fashion around the equatorial belt.

The large cone angle of the PPh_3 ligand (Tolman cone angle[208] = 145^o; Mingos cone angle[209] = 111^o) does not appear to adversely affect the orientation of the phosphine ligands in the pentagonal bipyramidal $[Au_7(PPh_3)_7]^+$ cluster. In the auracarbaborane, the presence of the carbaborane ligands and displacement of the Au(6) vertex to an edge bridging position does not appear to be any more sterically demanding than the triphenylphosphine ligands of the $[Au_7(PPh_3)_7]^+$ cluster, hence, steric hinderence is not thought to be the dominant factor in the ancalolous phosphine disposition observed in the auracarbaborane.

Centrally directed phosphine ligands are found for a range of homo and hetero gold clusters. However, the alternative radial disposition is found in some smaller gold clusters, such as $Fe(CO)_4(AuPPh_3)_2$[210] and $V(CO)_5(AuPPh_3)_3$[211], where the phosphine ligands are co-linear with the V-Au and Fe-Au vectors respectively. This feature has been explained in terms of 'supplementary bonding', in which the peripheral bonding is considered only to be a weak interaction, consistent with the longer Au-Au distances. This arises because the $AuPR_3$ fragment has available for skeletal bonding a single low lying sp^{σ} hybrid orbital and two relatively high lying p^{π} tangential orbitals. The high gold s-p promotional energies and small $6p^{\pi}-6p^{\pi}$ overlap integrals[212,213] therefore dictate that the latter play a reduced role in cluster bonding.

These peripheral Au-Au distances are comparable to the inter-molecular distances linking dinuclear gold complexes in the solid state. One example of this is $[Au_2(S_2CNBu_2)_2]_n$, where the intra- and inter-molecular distances are 279 and 302-340 pm respectively[214]. For $Fe(CO)_4(AuPPh_3)_2$ the Au-Au distance of 302.8(1) pm is also of a similar magnitude[209]. The bonding in this complex has been described as intermediate between two cis Au-Fe two-centre two-electron bonds and a three-centre two-electron bond[213].

For auracarbaborane (11), the implication of this theory is that the strongest bonding contribution of the $AuPPh_3$ fragments of the central gold cluster is directed along the Au-PPh_3 axis towards the relevant cosmo gold atom. One would therefore expect to find these $Au_{(cosmo)}$-$AuPPh_3$ distances to be the shortest within the cluster. Thus from the observed orientation of the phosphine ligands in auracarbaborane (11) (shown in Figure 96) the gold-gold interatomic

distances Au(1)-Au(5), Au(2)-Au(3), Au(2)-Au(7), and Au(4)-Au(5) would be expected to be the smallest and indeed reference to Table 15 shows this to be the case.

As noted earlier, the origin of auracarbaborane (11) is not clear. Because the n.m.r. spectra originally obtained for auracarbaborane (8) were thought to be due to this heptanuclear complex no further work was carried out on this product, with the end result being that insufficient time was available to investigate once the true identity of auracarbaborane (8) as $[(Ph_3P)_2Au]^+[Au(CB_8H_{12})_2]^-$ had been established.

Since this compound was obtained from the recrystallisation of auracarbaborane (8) two possibilities exist. Firstly, the heptanuclear auracarbaborane (11) is derived from a complex degradation/aggregation reaction of the mononuclear *closo*-auracarbaborane (8) which occured during its recrystallisation from dichloromethane. A second possibility is that auracarbaborane (11) is in fact the previously identified minor product auracarbaborane (9) (see Section 4.2). Of these two possibilities the latter is favoured, since the isolation of the major product by t.l.c. could have suffered from entrainment of the minor product auracarbaborane (9). The ^{11}B n.m.r. spectrum shown in Figure 84 does correlate to that expected for a cluster species involving at least two carbaborane fragments, further favouring the co-identity of auracarbaboranes(9) and (11).

The possible formulation of the auracarbaborane (11) as an anionic species is excluded by virtue of its synthesis in the absence of a suitable stabilising cation, i.e. preparation from CB_8H_{14} and $MeAuPPh_3$. The presence of a gold counter cation is clearly discounted by its absence from the crystal structure determination.

4.4 A BINUCLEAR AURACARBABORANE 'A' FRAME COMPLEX. THE SYNTHESIS AND CRYSTAL AND MOLECULAR STRUCTURE OF $[(dppe)(AuCB_8H_{12})_2]$ (12).

The gold (I) phosphine reagent $ClAu(PPh_3)$, has been shown to react with the carbanonaborane anion $[CB_8H_{13}]^-$ yielding the mononuclear cosmo auracarbaborane (8) $[(CB_8H_{12})Au]^-$ $[(AuPPh_3)_2]^+$. Evidence of further gold fragment condensation was provided by the characterisation of the heptanuclear triple cluster auracarbaborane (11). The structural aspects of this heptanuclear $[Au_7]$ cluster were discussed in Section 4.3 with brief reference to its novelty in contrast to the number of other known homonuclear gold-phosphine $[Au_n]$ clusters. The isolation of this heptanuclear species, an odd number of gold atoms in both senses of the word, raises the question of whether other triple clusters could be synthesised where 'n' is more representative of the foresaid gold-phosphine cluster series. A corollary to this question is whether species with $n < 7$ would be structurally indicative of the stepwise formation of the heptanuclear species. In particular, would the $[Au_6]$ cluster have an octahedral geometry as observed for the borane triple-cluster or a capped trigonal bipyramidal structure. The geometry of the $[(CB_8)Au_8(CB_8)]$ species is also of interest in order to identify the stepwise growth pattern.

In the heptanuclear $[Au_7]$ auracarbaborane (11), the coordination of the two carbaborane ligands to the central gold sub-unit is via one and two gold atoms. For a hypothetical auracarbaborane triple cluster with an even number of gold atoms, would the carbaborane residues be similarly asymmetrically coordinated ?

In order to synthesise an even-numbered polynuclear gold triple cluster a binuclear gold complex was deemed to be a suitable reagent. The use of a reagent containing two gold atoms linked via a bidentate bridging phosphine ligand may lead to products containing at least one Au_2 core unit or multiples of this unit, $[Au_2]_n$.

The reaction of the gold (I) reagent Cl_2Au_2(dppe) with the carbanonaborane anion $[CB_8H_{13}]^-$ was therefore undertaken. Whilst any potential stepwise condensation of this phosphine bridged gold complex is clearly not directly analagous to that of the mononuclear gold complex, other interesting aspects of the condensation process were potentially discernible. Clearly, the most significant effect to be established was the effect on cluster geometry of the restraining bridging phosphine ligand. The semi-unlinking of the bridging phosphine from in the vicinity of the condensation reaction also offered the possibility of products resulting from exo-polyhedral -B-Au-P-CH2-CH2-P- borocycle formation.

The choice of reagent was therefore limited to a number of binuclear gold complexes of the type XAuL-LAuX where X is a halide and L-L a bidentate phosphine ligand, such as $Ph_2PCH_2PPh_2$ (dppm) or $Ph_2PCH_2CH_2PPh_2$ (dppe). Of these two phosphine ligands dppe offers two advantageous features. Firstly dppe is a more stable chelating ligand. The comparison of the rhodium complexes [RhCl(CO)(L-L)] illustrate this feature since a monomeric complex is found when L-L = dppe and dimeric when L-L = dppm[215]. This effect may assist the unlinking of one gold atom from the binuclear complex for cluster aggregation and possibly promote gold cation formation.

More importantly, of these two bridging phosphine ligands dppe was favoured due to the structural flexibilty of the possible six

membered Au-P-C-C-P-X heterocycle, where X = Au^{+} or B, over the five membered heterocycle possible from dppm.

The reaction of a 1:2 mixture of Au_2Cl_2(dppe) with $Li[CB_8H_{13}]$ in diethyl ether at room temperature afforded yellow crystals of compound (12) and a red solid, compound (13). The reaction of the carbaborane anion $[CB_8H_{13}]^-$ with excess of the gold reagent under similar experimental conditions did not result in the formation of any new products, as indicated by identical t.l.c. analysis.

The ^{11}B n.m.r. spectrum of auracarbaborane (12) gave eight discernable resonances of equal integration (Figure 100 and Table 18), thus indicating an asymmetric framework which of course could result from either asymmetric metal insertion, exo cage substitution or asymmetry of the metal fragment.

None of the ^{11}B resonances exhibited any ^{31}P coupling, thus eliminating phosphine substitution on the cage boron atoms, whether by ligand transfer or by exo-cyclic ring formation. The two high-field resonances were appreciably narrower than those at lower field and were of similar shape, as was found for the arachno ruthenacarbaborane (3). A series of selectively ^{11}B decoupled ^{1}H n.m.r. spectra showed each of the eight boron resonances to be associated with a terminal hydrogen (see Figure 101 and Table 18), thus confirming the absence of any type of exo substitution.

The presence of bridging BHB hydrogens is indicated by two resonances in the $^{1}H(^{11}B)$ n.m.r. spectrum at -1.62 and -2.73 ppm. The shift of these signals are indicative of bridging hydrogen atoms connecting two boron atoms on the open face of a $[CB_8]$ or $[MCB_8]$ cluster as opposed to the metal-hydride type MHB bridging hydrogens connecting the inserted metal atom to the open face or the cluster framework.

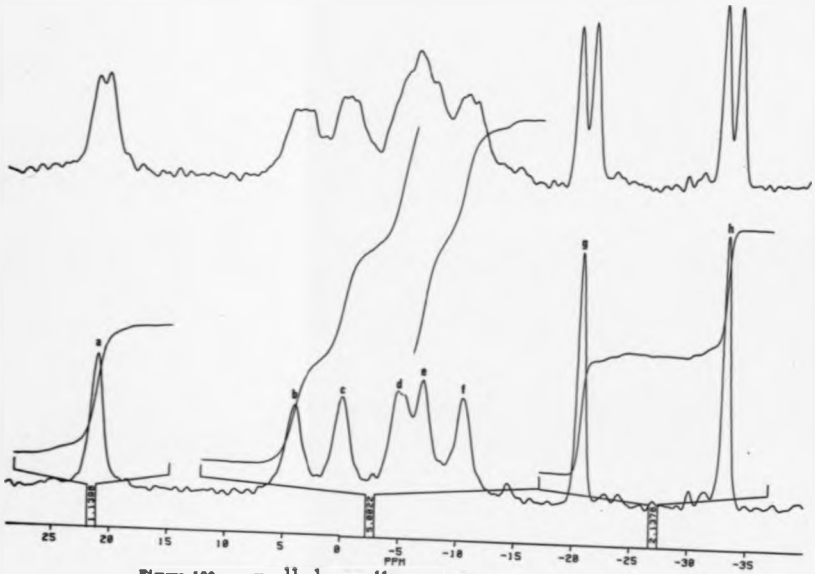

Figure 100. The $^{11}B\{^{1}H\}$ and ^{11}B n.m.r. spectra for auracarbaborane (12).

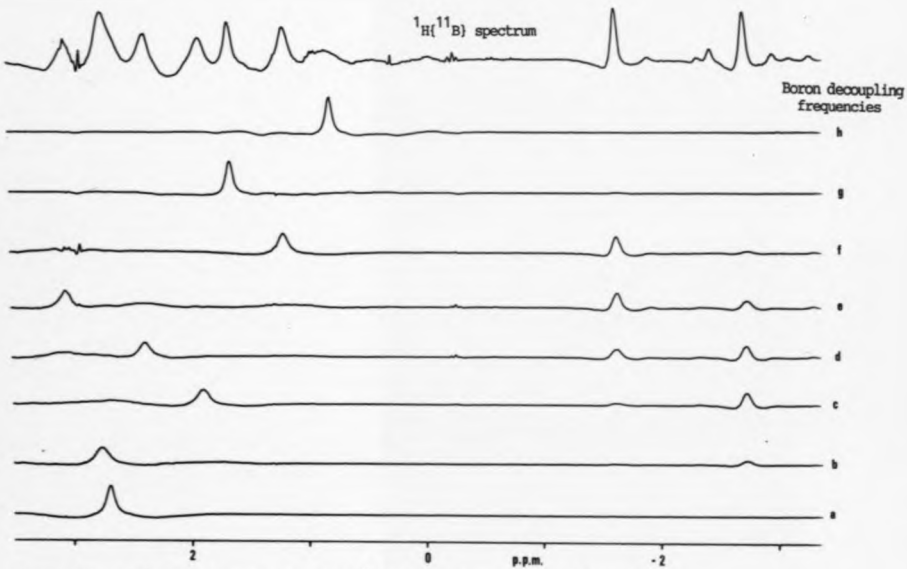

Figure 101. Selectively Boron-11 decoupled ^{1}H n.m.r spectra for auracarbaborane (12), presented as subtraction spectra.

BORON-11 AND PROTON N.M.R. DATA

Tentative Assignment	^{11}B (p.p.m.)	^{1}H (p.p.m.)
4	21.1	2.69
2	4.1	2.76
5,7	0.0	1.90
	-4.8	2.39
8,10	-7.0	3.06
	-10.5	1.21
1,3	-20.7	1.67
	-33.2	0.83
C(6)-$H_{(exo)}$		0.97
C(6)-$H_{(endo)}$		-0.23
B(5)-H-B(10)		-1.62
B(7)-H-B(8)		-2.73
CH_2 of P-CH_2-CH_2-P		- 3
$P(C_6H_5)_2$		7.2-7.6

Table 18. Proton and boron-11 n.m.r. data for auracarbaborane (12).

Gold ligands not shown

(a) (b)

Figure 102. Possible coordination sites of gold fragment to the carbaborane cluster in auracarbaborane (12).

The shifts are thus more akin to the B-H-B shifts observed in the arachno ruthenacarbaborane (3) than those found for the nido ruthenacarbaborane (1). Furthermore, the selectively ^{11}B decoupled ^{1}H n.m.r. spectra showed each of these bridging hydrogens to be associated with two boron atoms, thus assigning them to four different boron atoms on the open face of the carbaborane residue.

The pattern and integration ratio of the other resonances observed in the $^{1}H\{^{11}B\}$ n.m.r. spectrum confirmed the presence of one dppe ligand and two carbaborane cages. The ratio of the aromatic resonances of the dppe ligand to the two BHB resonances, $CH_{(exo)}$ and $CH_{(endo)}$ resonances was found to be approximately 20:2:2:2:2 as required by four phenyl groups of one dppe ligand and two CH_2 fragments and four BHB hydrogen atoms of two arachno carbaborane clusters. The aliphatic CH_2 resonances of the dppe ligand $(Ph)_2P-CH_2-CH_2-P(Ph)_2$ overlay a terminal B-H resonance and therefore elude integration. The highfield CH resonance is found to be sharpened on broad band ^{11}B decoupling indicating that this resonance couples to an adjacent boron atom, thus assigning it to the endo position, as was found for the $CH_{(endo)}$ hydrogen in the arachno ruthenacarbaborane (3).

From spectroscopic evidence the auracarbaborane (12) is reasonably formulated as $(CB_8H_{12})_xAu_y(dppe)_z$, where $x : z = 2 : 1$ and $x + z = 3, 6$ .. etc. Whether the asymmetry of the auracarbaborane (12), as illustrated by the ^{11}B n.m.r. spectrum, is a result of an asymmetric gold insertion position within the framework (see Figure 102a) or the asymmetric configuration of the carbaborane and phosphine residues around the gold atom or atoms (Figure 102b) is not accessible from the spectroscopic data.

The insertion of ruthenium and gold fragments into the arachno

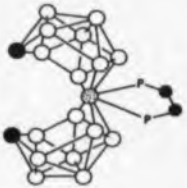

(a)

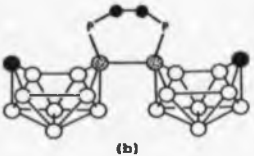

(b)

(c)

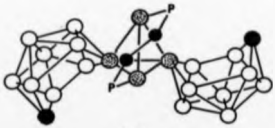

(d)

Figure 103. Possible structures for the auracarbaborane (12) $(CB_8H_{12})_xAu_y(dppe)_z$. For (a) - (d) y = 1,2,3,4.

CB_8 framework has been shown to occur exclusively at the 9- position (see ruthenacarbaboranes (1), (3) and auracarbaborane (11)). In each case the symmetric framework is rendered asymmetric by the exo-metal ligand disposition (and exo-cage substitution). Hence, the insertion of the gold fragment into the square portion of the arachno $[CB_8H_{13}]^-$ carbaborane was thought to be unlikely (Figure 102a), the favoured structure being an 9,6-$AuCB_8$ type (Figure 102b). If the carbon atom was involved in coordination of the gold atom, a different distribution of the endo hydrogens might be expected, perhaps a BH_2 group with the two bridging hydrogens as C-H-B and a B-H-B groups. In addition to the fact that a C-H-B bridging hydrogen group has not to date been characterised in any carbaborane cluster, n.m.r. data obtained clearly discounts this possibility.

The value of 'y' in the formulation postulated for the auracarbaborane (12) is not obtainable from the spectroscopic evidence. As seen from the structure of the heptanuclear auracarbaborane (11), gold phosphine reagents can be incorporated into the CB_8 carbaborane framework with or without phosphine elimination.

Thus it was conceivable that gold insertion into the CB_8 framework could result in an aggregation product in which the Au : dppe ratio (y : z) was not 2 : 1. In principle 'y' could range from one to four. The schematic structures of the clusters that conform to the postulated stoichiometry are shown in Figure 103a-d.

Of those shown, the binuclear gold complex (b) is clearly the most likely product, since its formation is easily visualised as the metathesis by dissociation of chloride and coordination of the carbaborane with elimination of hydrogen and concommitant gold-gold bond formation.

The formation of the mononuclear complex (Figure 103a) containing a gold atom coordinating a chelating phosphine ligand, must involve amongst other processes, the breaking of an Au-P bond with the elimination of the gold atom. In the formation of the heptanuclear auracarbaborane (11), the reverse occurs, namely the gold atom is incorporated with the phosphine eliminated. Presumably, the driving force for this is the coordination of a carbaborane residue to the gold atom. One might therefore expect the formation of another [$AuCB_8$] product in stochiometric amounts if the mononuclear cluster was the major product. Could this be the compound (13) ? (evidence noted later disproves this possibilty). The mononuclear gold complex does however appear to be very sterically crowded, and therefore less favoured. Though high, the coordination number of the conjuncto-gold atom is not excessive in comparison to that observed in the heptanuclear auracarbaborane (11). Both the tri- and tetranuclear complexes (Figure 103c,d) are less sterically demanding and contain lower coordinate gold atoms.

For all the postulated structures a-d (except b), their formation would clearly be accomplished only via a complex aggregation process. Whilst this process would probably be no more complicated than that which led to the formation of the heptanuclear auracarbaborane (11), the simpler mechanism outlined above for the formation of the binuclear complex is favoured.

A further attribute of the binuclear gold complex is the lower coordination of the cosmo-gold-phosphine atoms, as observed in the heptanuclear auracarbaborane (11), where the degree of coordination of the gold atom to other gold atoms within the gold sub-cluster is reduced by the coordination of a phosphine ligand and conversely, is increased by its elimination.

The predicted formulation of the auracarbaborane (12) is therefore $(CB_8H_{12})_2Au_2(dppe)$, corresponding to the structure (b) shown in Figure 103.

In order to confirm the structure of the auracarbaborane (12) an X-ray crystal structure determination was undertaken. Definitive proof of the formation of a gold-gold bond would thus be provided, with the additional structural information regarding the conformation of the six membered ⌐Au-P-C-C-P-Au¬ ring.

The structure of the auracarbaborane (12) as determined by an X-ray diffraction study is shown in Figure 104. The structure is as predicted, a gold-carbaborane triple cluster with a binuclear gold sub-unit. Two $[CB_8]$ carbaborane clusters are ligated to the two gold atoms of the precursor thereby replacing the chlorine atoms with the resultant formation of an Au-Au bond. An alternative description is that of an 'A' frame auracarbaborane. The six-membered auracyclic ring ⌐Au-P-C-C-P-Au¬ is seen to adopt a twisted chair conformation in the solid state.

The orientation of the carbaborane and phosphine ligands coordinated to the gold atoms is such that a two-fold rotation axis intersects the auracyclic ring in the perpendicular direction, between the Au-Au and CH_2-CH_2 bonds. This equivalence is not crystallographically perfect, though it does of course concur with the spectroscopic

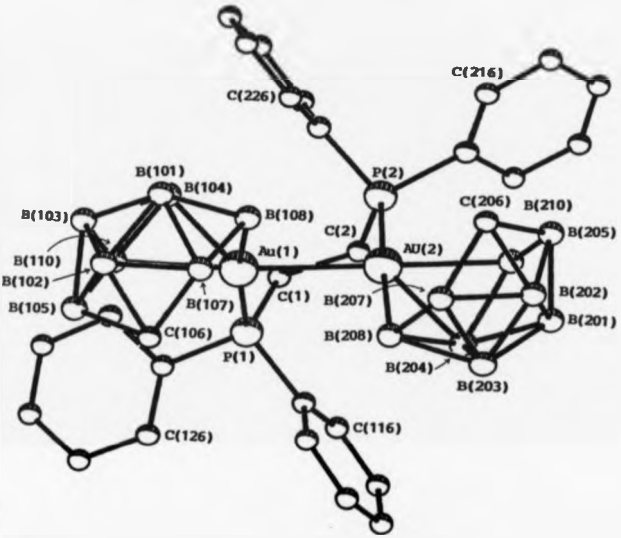

Figure 104. Drawing of the X-ray crystallographically determined molecular structure of the auracarbaborane $(CB_8H_{12})_2Au_2(dppe)$ (12).

evidence, in that both CB_8 residues are magnetically equivalent and give rise to one set of ^{11}B n.m.r. resonances.

For any one of the $AuCB_8$ frameworks, the asymmetry of the exo-gold ligands causes each of the eight skeletal boron atoms to be magnetically inequivalent, thus accounting for the observed asymmetry of the ^{11}B n.m.r spectrum.

As mentioned above, the conformation of the auracyclic ring is that of a twisted chair. As with any other cyclohexane analogue, several other conformations are possible, ie. boat, twist boat, etc. In order to assess the relevance of the adopted conformation the alternatives require some discussion.

Considering the chair conformer in which the phosphorus atoms are considered the apical atoms, the presence of the aromatic rings of the phosphine in the apical positions inhibits the adoption of the boat conformation, since they would clearly interact in this sterically crowded isomer.

An alternative view of the auracyclic ring is that one CH_2 group and one $AuCB_8$ group form the apical vertices. In this conformer, the flipping over of the CH_2 vertex would lead to a bottom heavy ring, with a rather unhindered CH_2 apex. The flipping over of the $AuCB_8$ vertex would in addition possibly lead to greater steric interaction between the carbaborane residues.

In all of the boat conformations discussed, the sterically demanding phosphine and carbaborane ligands clearly cause greater steric interaction, thus favouring the chair conformer. The formation of the twisted conformation may result from crystallographic packing forces or further steric relief gained by encroaching on the rather sterically unhindered CH_2 vertices or indeed a combination of both.

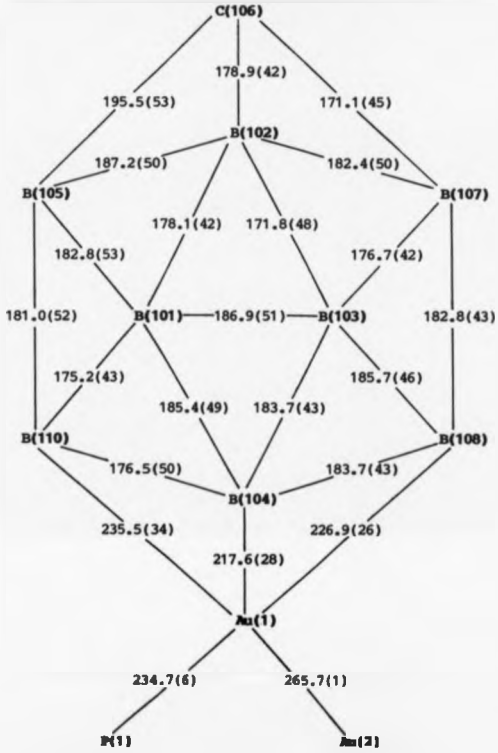

Figure 105. Skeletal distances (pm) for first '$AuCB_8$' sub-unit of $(CB_8H_{12})_2Au_2(dppe)$ (12).

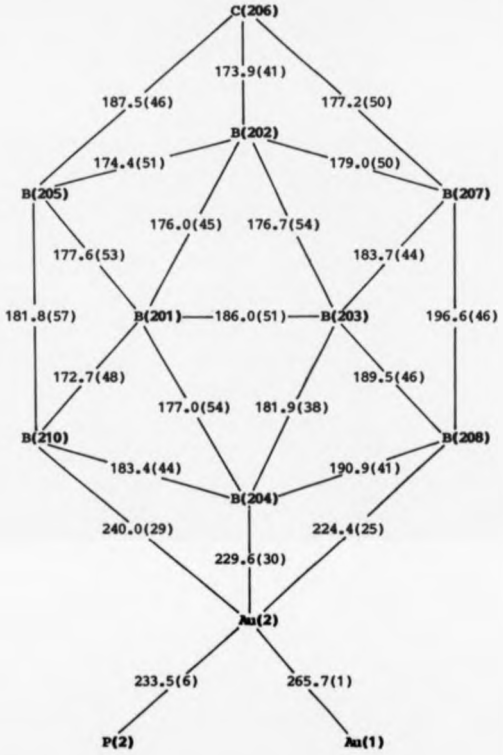

Figure 106. Skeletal distances (pm) for second '$AuCB_8$' sub-unit of $(CB_8H_{12})_2Au_2(dppe)$ (12).

The observed Au-Au distance of 2.657(1) is far shorter than that generally found in binuclear gold(I) complexes and more comparable to that observed in gold(II) complexes[206,213,216];

Au(I)	$[Au_2Cl_2(dppm)_2]$	296 pm
	$[Au_2(dppm-H)_2]$	288 pm
	$[Au_2(Et_2PCH_2CH_2S)_2]$	310 pm
	$[Au_2(Et_2P(CH_2)_2)_2]$	303 pm
	$Au_2(S_2CNPr_2)_2$	276 pm
Au(II)	$Au_2Cl_2(CH_2PEt_2CH_2)_2$	260 pm

The above gold-gold distances therefore reinforce the proposal of an Au(II) oxidation state for the auracarbaborane (12), in accord with the coordination of a $[CB_8H_{12}]^{2-}$ ligand. The diamagnetic nature of the auracarbaborane, as evident from the normal line width of the ^{11}B n.m.r. spectra obtained is accomplished by the formation of the gold-gold bond, thus spin pairing the paramagnetic $5d^9$ Au(II) metal electrons.

Each gold atom has a stable sixteen electron configuration made up of the eleven valence shell electrons with the additional electrons provided by two from the coordinated phosphine, one from the gold-gold bond and two electrons from the neutral CB_8H_{12} carbaborane ligand. Each gold atom provides two electrons and three orbitals for bonding in the auracarbaborane skeleton.

The observed arachno structure of the auracarbaborane (12) is thus maintained even though the gold atoms only contribute enough electrons for a formal nido electron count, as was found for the arachno ruthenacarbaborane (3).

The observed skeletal inter-atomic distances are shown in Figures 105 and 106, with the full crystallographic data contained in Chapter 5. The skeletal inter-atomic distances, particularly those around the open face of the carborane units, are consistent with an arachno cluster structure, by comparison to the distances observed for the nido and arachno ruthenium [CB_8] derivatives (1) and (3), as shown in Table 19.

In both carbaborane sub-units of the auracarbaborane (12) the C(6)-B(5) distance is abnormally long (188 and 195 pm) compared to that found in the arachno ruthenacarbaborane (3) (173 pm).

Compound	(12) Arachno- $(CB_8H_{12})_2Au(dppe)$ (pm)	(3) Arachno- $CB_8H_{12}RuCp(PPh_3)$(H) (pm)	(1) Nido- $CB_8H_{10}Ru(PPh_3)_2(CO)$ (pm)
B(5)-C(6)	196(5) , 188(5)	171(1)	155(3)
C(6)-B(7)	171(5) , 177(5)	174(1)	157(3)
B(7)-B(8)	183(4) , 197(5)	186(1)	194(4)
B(8)-M(9)	227(3) , 224(3)	231.6(5)	227(2)
M(9)-B(10)	236(3) , 240(3)	230.3(6)	236(2)
B(10)-B(5)	181(5) , 182(6)	190.4(9)	185(3)

Table 19. Comparison of inter-atomic distances around open face of nido and arachno ruthenacarbaboranes (1) and (3) and the auracarbaborane (12).

The second product, auracarbaborane (13), isolated from the reaction of $[CB_8H_{13}]^-$ with $Cl_2Au_2(dppa)$ was interesting for a number of reasons. Firstly, the observed n.m.r. spectra were similar to the spectra obtained for the previously characterised commo auracarbaboranes (8) and (10) and secondly, auracarbaborane (13) was observed to be formed when a dichloromethane solution of the binuclear auracarbaborane (12) was left to stand at room temperature for two days.

The observed ^{11}B n.m.r. spectrum of auracarbaborane (13) exhibited eight resonances (labelled a-h in Figure 108) which again had the appearance of being due to two overlapping 1:1:2:2:2 spectra. In fact the resonances of this spectrum were identical in shift and pattern to those in the ^{11}B n.m.r. spectra obtained for auracarbaboranes (8) and (10), though there were slight differences in relative integration ratio (compare Figures 108 and 84). This did however indicate that auracarbaborane (13) also consisted of the commo auracarbaborane anion $[(CB_8H_{12})_2Au]^-$ previously characterised.

As noted earlier, comparison of the relative integration ratio of the two sets of 1:1:2:2:2 resonances found in the ^{11}B n.m.r. spectrum of auracarbaboranes(10) and the single 1:1:2:2:2 spectrum of auracarbaborane (8) isolated by repeated recrystallisation (Figure 85) enabled the eight resonances of the complex spectrum to be separately identified with individual 1:1:2:2:2 spectra of the syn and anti isomers as follows; (a:d:e:f:h) and (b:c:e:f:g), (see Figures 86 and 108).

The $^1H\{^{11}B_{(selective)}\}$ n.m.r. spectra of auracarbaborane (13), shown in Figure 109, shows that each of the boron atoms responsible for the eight ^{11}B n.m.r. resonances has a terminal hydrogen atom attached. Note that as well as the syn and anti conformations of the

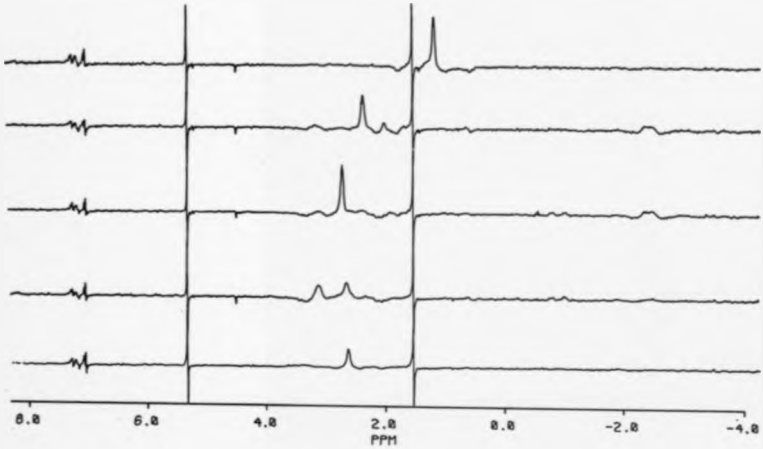

Figure 107. Series of selectively boron decoupled proton spectra for auracarbaborane (8) after purification by repeated recrystallisation, ($^{1}H\{^{11}B_{(select)}\}$-$^{1}H$ spectra). Figures 107 and 94 are identical. (Boron decoupling frequencies as annotated).

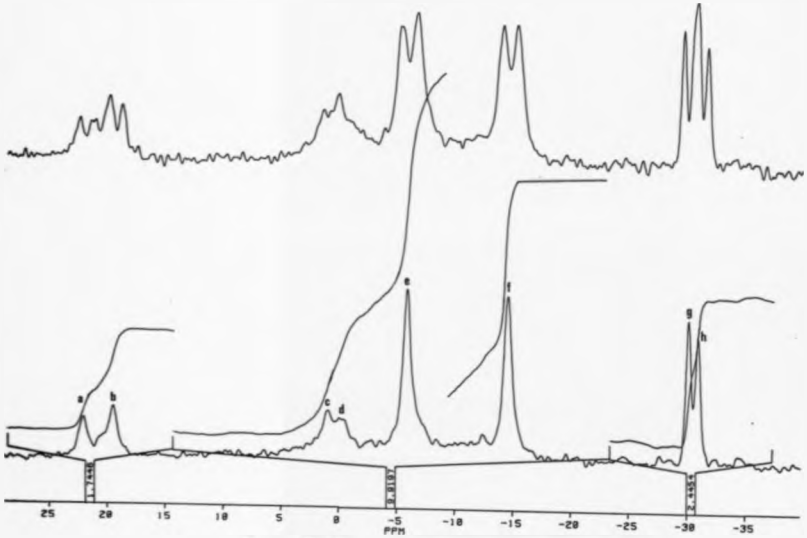

Figure 108. ^{11}B and $^{11}B\{^{1}H\}$ n.m.r. spectra of auracarbaborane (13).

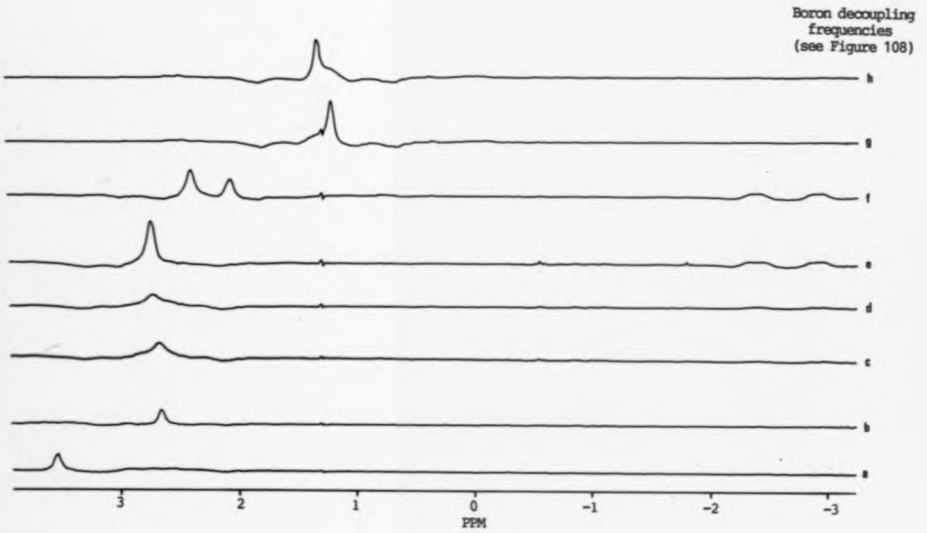

Figure 109. Series of selectively boron decoupled proton spectra for auracarbaborane (13), presented as $^{1}H\{^{11}B_{(selective)}\}-^{1}H$ spectra, (Boron decoupling frequencies as annotated.).

BORON-11 AND PROTON N.M.R. DATA

Tentative Assignment (Syn or Anti)		^{11}B (p.p.m.)	^{1}H (p.p.m.)
B(4)		21.9	3.55
	B(4')	19.5	2.64
	B(2')	1.0	2.66
B(2)		0.0	2.70
B(5,7)	B(5',7')	-5.8	2.73
B(8,10)	B(8',10')	-14.5	2.39
B(1,3)		-30.1	1.21
	B(1',3')	-30.9	1.30
C(6)-$H_{(exo)}$		0.6	
	C(6')-$H_{(exo)}$		0.3
C(6)-$H_{(endo)}$		-0.5	
	C(6')-$H_{(endo)}$		-1.8
B(5,7)-H-B(8,10)			-2.4
	B(5',7')-H-B(8',10')		-2.9

Table 20*. Boron-11 and proton n.m.r. data for the cosmo auracarbaborane anion $[(CB_9H_{12})_2Au]^-$ of compounds (8) (10) and (13).

(* The atom numbering B(n) or B(n') in Table 15 distinguishes the syn and anti isomer resonances, but does not infer a particular isomer.)

auracarbaborane anion being present in approximately 1:0.8 ratio, as judged from the integration ratio of resonances (g) and (h) in Figure 108, these spectra are presented as subtractions of the ^{1}H n.m.r spectrum from the selectively ^{11}B decoupled ^{1}H n.m.r. spectra and therefore give only a qualitative assessment of relative integral.

As noted in Section 4.2, though the two overlapping 1:1:2:2:2 spectra can be distinguished, it is not possible to identify which arises from either the syn or anti auracarbaborane anion isomers. Neither was it possible to elucidate which of the bridging hydrogen resonances correlated to each isomer. By comparison of the two sets of $^{1}H\{^{11}B_{(selective)}\}$ n.m.r. spectra for the single isomer of auracarbaborane (8) (Figure 107) and the mixture of isomers (Figure 109), the correlation of the ^{1}H resonances to the observed ^{11}B n.m.r. resonances is confirmed (see Table 20) and the association of the bridging BHB, $CH_{(exo)}$ and $CH_{(endo)}$ resonances deduced.

The assignment of the resonances due to the bridging BHB, $CH_{(exo)}$ and $CH_{(endo)}$ hydrogens in each unspecified isomer was confirmed from the correlations found in the $^{1}H(^{11}B)$ COSY spectrum of auracarbaborane (13) (see Figure 110). As previously noted with respect to ^{11}B COSY spectra, two factors adversely affect the observed spectrum and hence its interpretation. Firstly, only resonances of sufficiently narrow linewidth in the normal spectrum produce a detectable response in the COSY spectrum and secondly the resonances must not overlap if a correlation is to be observed. The latter factor leads to problems in interpretation of the correlations to and between the $BH_{(terminal)}$ proton resonances observed in the ^{1}H COSY n.m.r. spectrum of auracarbaborane (13) since these resonances appear in the observed ^{1}H n.m.r. spectrum in two overlapping groups at 2.7 p.p.m.

and 1.2 p.p.m. as seen in Figure 109. Correlations between individual resonances of these groups are therefore mostly undetected. Only three of the expected correlations involving the terminal hydrogen resonances are observed with the origin of these correlations obscured by the closeness of the neighbouring resonances.

Fortunately the bridging hydrogen BHB and CH resonances are both sufficiently separated and narrow to give a meaningful response. Hence the significant peaks in ^{1}H COSY spectrum are the two CH(exo), two $CH_{(\underline{endo})}$ and two BHB resonances labelled, $C_{(\underline{exo}1)}$, $C_{(\underline{exo}2)}$, $C_{(\underline{endo}1)}$, $C_{(\underline{endo}2)}$, $BH_{(b1)}{}^{B}$ and $BH_{(b2)}{}^{B}$ respectively.

Considering the $CH_{(\underline{endo}1)}$ resonance on the normal spectrum (the diagonal on the COSY spectrum), two significant correlations are seen (off-diagonal peaks in the COSY spectrum). Firstly a strong correlation to the $CH_{(\underline{exo}1)}$ resonance and secondly a weaker coupling to the $BH_{(b1)}{}^{B}$ resonance. This indicates that the $CH_{(\underline{exo}1)}$ and $CH_{(\underline{endo}1)}$ hydrogens are bonded to the same skeletal carbon atom and being magnetically inequivalent give rise to a two bond coupling $^{2}J(H\text{-}C\text{-}H)$. The smaller coupling indicates that the $CH_{(\underline{endo}1)}$ hydrogen atom is associated with cluster containing the $BH_{(b1)}{}^{B}$ bridging hydogen atoms on the open face, giving rise to a three bond coupling, $^{3}J(H_{(b1)}\text{-}B\text{-}C\text{-}H_{(\underline{endo}1)})$. In addition to the couplings observed in the ^{1}H COSY spectrum additional coupling of the $CH_{(\underline{endo}1)}$ hydrogen atom to the two B-H terminal hydrogen atoms on B(5) and B(7) (not observed in the COSY spectrum) account for the observed multiplicity of the $CH_{(\underline{endo})}$ resonances in the ^{1}H n.m.r. spectrum.

The $CH_{(\underline{endo}1)}$, $CH_{(\underline{exo}1)}$ and $BH_{(b1)}{}^{B}$ hydrogens are therefore confirmed to be associated with either the *syn* or *anti* conformation of the $[(CB_{8}H_{12})Au(CB_{8}H_{12})]^{-}$ anion. Similar couplings observed for the

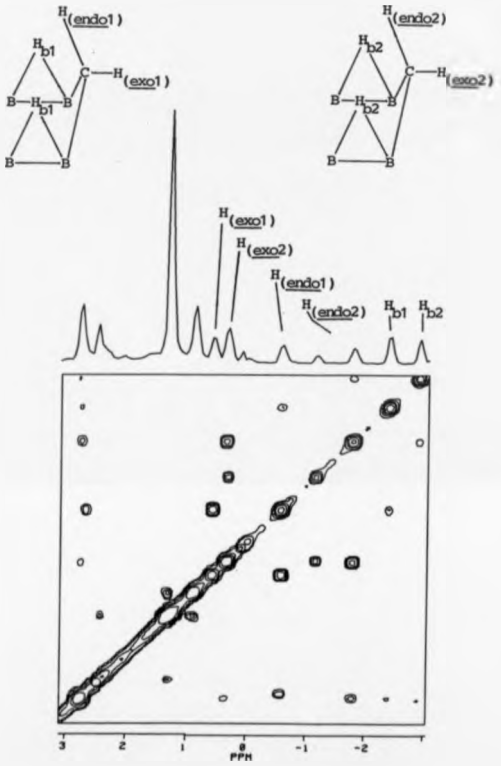

Figure 110. The $^{1}H\{^{11}B\}$ COSY n.m.r. spectrum of auracarbaborane (13).

$CH_{(endo2)}$ resonance, confirm that the $CH_{(endo2)}$, $CH_{(exo2)}$ and $BH_{(b2)}B$ hydrogens are associated with the alternative syn or anti $[(CB_8H_{12})Au(CB_8H_{12})]^-$ cluster anion.

Having unravelled the ^{11}B and ^1H n.m.r. resonances observed for the commo auracarbaborane anion $[(CB_8H_{12})_2Au]^-$ of compounds (8), (10) and (13) into two sets consistent with the presence of two isomeric conformations, the tentative assignment of the resonances to skeletal atoms (see Table 20) was made from the comparison of the ^1H-^{11}B n.m.r. shift correlation diagram of the auracarbaborane anion with those of the arachno ruthenacarbaborane (3) (see Figure 111). The assignment of the two sets of spectroscopic data to the specific syn or anti conformer of the $[(CB_8H_{12})Au(CB_8H_{12})]^-$ cluster anion is not possible from the data obtained. This could only be achieved by isolation of the anion as a single isomeric product as noted earlier, followed by n.m.r. identification using the above information, and finally structural characterisation by X-ray crystallography. Clearly, the first two steps of this has been accomplished as a result of the above work. Only the latter structural characterisation was unobtained due to the consistent twinning of crystalline product, though luckily the structural characterisation by X-ray crystallography of both isomers has, as described in Section 4.2, been accomplished in one study.

Though characterisation of the auracarbaborane component of compound (13) as the $[(CB_8H_{12})Au(CB_8H_{12})]^-$ cluster anion was achieved, the identification of the complex would be complete if the nature of the cationic counter ion were to be established. Note that for the analogous auracarbaboranes (8) and (10) the cation was the found to be $[PR_3AuPR_3]^+$ where R was C_6H_5 and cyclo-C_6H_{11} respectively.

As noted earlier, the auracarbaborane (13) was isolated under

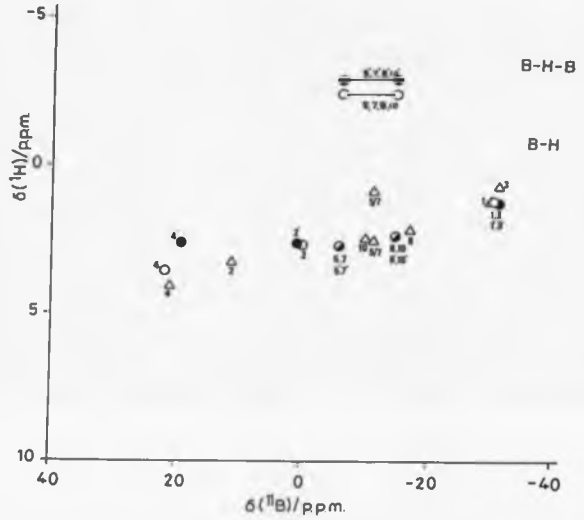

Figure 111. ^{1}H-^{11}B shift correlation map for the commo auracarbaborane anion $[(CB_8H_{12})Au(CB_8H_{12})]^-$ present in compounds (8), (10) and (13) (○,●= syn and anti isomers) and the arachno ruthenacarbaborane (3) (△).

two differing circumstances. Firstly, from the original reaction of $[CB_8H_{13}]^-$ and ClAu(dppe)AuCl and secondly by the room temperature degradation of the binuclear auracarbaborane (12) in dichloromethane solution. Whilst the two products could be identical, spectroscopic evidence indicated that the cationic components may be different.

The product isolated from the original reaction by preparative t.l.c. gave a ^1H n.m.r. spectrum in which the integration ratio of the resonances due to aromatic and BHB bridging hydrogens was approximately 80 : 4. This indicated a cation formulation containing four dppe ligands and at least four gold atoms. Since one dppe ligand can coordinate to either one or two gold atoms depending on whether it is chelating or bidentate, the cation could comprise between four and eight gold atoms if it has a univalent overall charge. If however, the cation were to be doubly charged, i.e. +2, then the 80 : 4 ratio of aromatic hydrogens to carbaborane bridging hydrogens would indicate a possible formulation of the cation as containing eight dppe ligands.

The possible formulation of the cationic component of auracarbaborane (13) as a gold-dppe cluster cation accounts for the excess gold reagent consumed in the reaction with the carbaborane precursor since the binuclear product only requires a half molar equivalent of gold reagent for complete reaction. The structural information obtainable from spectroscopic data would clearly be insufficient to structurally characterise the cluster cation, so an X-ray crystallographic study of the auracarbaborane (13) was therefore both necessary and desirable.

Crystals of the auracarbaborane (13) were grown from a number of solvents mixtures by the diffusion method. These were checked for suitability in an X-ray diffraction study and consistently found to

suffer from crystal twinning. Unfortunately insufficient time was available for further spectroscopic experimentation to assist in the identification of the unknown counter cation of auracarbaborane (13). Hence, the following discussion of the possible identity of the cation is purely speculative.

A range of gold cluster cations with eight coordinated phosphine ligands have been characterised, some examples of which are[213];

a) $[Au_6(dppp)_4](NO_3)_2$

b) $[Au_8(PR_3)_8](X)_2$ R;X = Ph;PF_6 and p-C_6H_4OMe;NO_3

c) $[Au_9(PR_3)_8](X)$ R;X = Ph;PF_6 and p-C_6H_4Me;PF_6

d) $[Au_9(PPh_3)_8](PF_6)_2$

e) $[Au_9(PR_3)_8](X)_3$ R;X = Ph;SCN p-C_6H_4Me;PF_6 and p-C_6H_4OMe;BF_4

f) $[Au_{11}(PPh_3)_8(Y)_2](X)$ R;X;Y = Ph;PF_6;Cl and Ph;PF_6;SCN

g) $[Au_{13}(PMePh_2)_8Br_4]Br$

These polygold phosphine clusters can be classified in terms of the nuclearity, nature of the phosphine, presence of other coordinated ligands, e.g. Cl, SCN, and the cluster cationic charge. Clearly, the major difference between these examples and the auracarbaborane (13) counter cation is the nature of the coordinated phosphine.

The hexanuclear gold-dppp cluster[217], $[Au_6(dppp)_4](NO_3)_2$, which has an edge bridged di-tetrahedral structure, is clearly the most similar to the auracarbaborane counter cation with respect to phosphine, since both dppp and dppe are bidentate ligands. The double cationic charge of the hexanuclear gold-dppp cluster does not however coincide with the uni-positive charge inferred for the possible analogous tetra-dppe hexanuclear gold cluster cation.

Several gold cluster complexes have been prepared from

ClAu(dppe)AuCl. Reduction of this complex with sodium borohydride yields the octahedral $Au_6(dppe)_2Cl_2$ cluster from which the green ionic $[Au_6(dppe)_3]Cl_2$ cluster has been prepared[218,219]. This cluster has not been structurally characterised and may be better formulated as $[Au_9(dppe)_4]^{3+}$, analogous to the well known $[Au_9(PR_3)_8]^{3+}$ cluster cations noted above. The structure of these cations has been found to be either a bicapped centered chair or a centred crown[213]. The triphenylphosphine analogue of this ennearuclear cluster can be reduced to give the monocharged $[Au_9(PPh_3)_8]^{+}$ cluster cation, the structure of which has been shown to be a distorted centred cube of gold atoms[220]. Both the charge and phosphine content of this ennearuclear cluster cation is as indicated for the counter cation of auracarbaborane (13).

Several obvious reservations about the identity of the cation exist. Firstly, there is a possibility that chlorine has been incorporated into the counter cation, either from the solvent CH_2Cl_2 (or from the initial gold reagent). No evidence to either prove or disprove this possibility has been obtained. Secondly, the dppe content of the complex inferred from the ^1H n.m.r. integration ratio has to be viewed in relation to the problems associated with comparing n.m.r. resonance integrations of such differing size, in particular integrations of resonances with differing linewidth. In these cases the accuracy of the ratio depends greatly on the correct measurement of the smaller integral, since any error in this estimate is amplified in the ratio to the larger integral.

Thus the identity of auracarbaborane (13) as isolated from the reaction of ClAu(dppe)AuCl with $[CB_8H_{13}]^-$ can only be described as consisting of the commo-auracarbaborane anion $[(CB_8H_{12})Au(CB_8H_{12})]^-$

with the counter ion postulated to be a poly-gold-dppe cluster cation.

As noted earlier, the auracarbaborane (13) was also observed to be formed when a dichloromethane solution of the auracarbaborane (12) was left to stand at room temperature for two days. The ^{11}B n.m.r. spectrum of auracarbaborane (13) prepared in this way showed only resonances due to the *commo*-auracarbaborane, there were no discernable resonances due to other carbaborane products. The reaction of $[(CB_8H_{12})_2Au_2(dppe)]$ to yield $[(CB_8H_{12})Au(CB_8H_{12})]^-$ is therefore indicated to proceed via the elimination of an $[Au(dppe)]$ fragment. The following disproportionation reactions are thus postulated for consideration.

$$n[(CB_8H_{12}Au)_2(dppe)] \longrightarrow n[(CB_8H_{12})_2Au]^- + n[Au(dppe)]^+ \quad (1)$$

$$n[(CB_8H_{12}Au)_2(dppe)] \longrightarrow n[(CB_8H_{12})_2Au]^- + [Au_{n-x}(dppe)_n]^{y+} + x[Au] \quad (2)$$

If the disproportionation reaction produces a stoichiometric equivalent of the ionic auracarbaborane complex, then the net result is the elimination of a single gold-phosphine fragment to yield the *commo* auracarbaborane anion and the $[Au(dppe)]^+$ cation (See equation 1). This formulation of the cation can be discounted immediately because of the cyclic nature of the coordinated phosphine ligand. The known bis-phosphine mononuclear gold cations have linear geometries, as typified by $[Au(PPh_3)_2]^+$ and $[Au(P(C_6H_{11})_3)_2]^+$. Whilst the coordination of two unidentate tricyclohexylphosphine ligands allows the adoption of a linear geometry, in the proposed $[Au(dppe)]^+$ cation a linear geometry would be prohibited because the size and angle of 'bite' of the chelating bidentate dppe ligand is insufficient to span the mutually trans coordination positions. One example of a chelating bidentate phosphine ligand that can achieve such coordination is

2,11-bis(diphenylphosphinomethyl)benzo-[C]-phenanthrene[221]. The gold complex of this ligand, [AuCl(P-P)], has a P-Au-P bond angle of 176° and is partially ionised in polar solvents to yield the linear $[Au(P-P)]^+$ cation.

Perhaps the most likely result of the disproportionation of $[(CB_8H_{12}Au)_2(dppe)]$ is the subsequent disproportionation of the eliminated $[Au(dppe)]^+$ fragments, to produce an $[Au_{n-x}(dppe)_n]^{y+}$ gold cation (See equation 2). Thus one possibility is the formation of the four coordinate Au(I) cation $[Au(dppe)_2]^+$, previously identified[222] from the reaction of dppe and ClAu(dppe)AuCl. Since this cation is uni-positive the disproportionation would have to result in complete degradation of half of the auracarbaborane (12) precursor to non-anionic carbaborane products in order to provide the required dppe. This does not appear to be the case as judged from n.m.r. evidence.

An additional factor in the disproportionation may be chlorine abstraction from the solvent, as noted from the synthesis of the chlorinated ruthenacarbaboranes(4) and (5) (see Chapter 3). The disproportionation of two molecules of the binuclear complex could thus yield the di-positive five coordinate mononuclear gold (III) cation $[Au(dppe)_2Cl]^{2+}$, analogous to the known cation[223] $[Au(diphos)_2Cl]^{2+}$. The product of the disproportionation of the binuclear auracarbaborane in dichloromethane may thus be $2[(CB_8H_{12})_2Au]^-\ [Au(dppe)_2Cl]^{2+}$.

Whilst discussion of the possible identity of the counter cation of auracarbaborane (13) has been made without the support of any definite chemical evidence, the most important aspect of its identity, namely the presence of the mononuclear arachno commo auracarbaborane anion $[(CB_8H_{12})_2Au]^-$, has been established.

CHAPTER 5. EXPERIMENTAL.

5.1. PREPARATIVE PROCEDURES.

5.1.1. GENERAL EXPERIMENTAL NOTES.

In view of the air sensitivity and toxicity of boron hydride derivatives, all reactions were carried out under a dry, oxygen-free nitrogen atmosphere, unless otherwise stated. Manipulations were facilitated using dry-box and Schlenk-tube techniques.

All transition metal reagents were prepared by literature methods as indicated in the text. Decaborane(14) was used as supplied commercially, as were all other standard reagents. Prior to use, solvents were purified, dried and deoxygenated by standard methods[224]. Unless otherwise specified, the light petroleum solvent used had a boiling point range of 60 - 80°C.

All preparative chromatography was carried out using dry silica gel (Merck, Kieselgel 60 (230 - 400 mesh on 20 x 20 cm glass plates), under the conditions stated. Qualitative chromatograpy (small scale t.l.c) was carried out using pre-coated aluminium plates,(Kieselgel, layer thickness 0.2 mm), and inspected visually before and after being developed with silver nitrate solution.

All n.m.r. spectra were recorded on spectrophotometers under the auspicies of the S.E.R.C., by Drs. O. W. Howarth, E. Curzon and A. Harrison (University of Warwick) and Drs. I. Sadler and D. Read (University of Edinburgh). The ^{11}B, ^{1}H and ^{31}P n.m.r. spectra were recorded on a Bruker WH-400 n.m.r. spectrometer, at 128.0, 400.1 and 162.0 MHz respectively. The $^{1}H\{^{11}B\}$ spectra were recorded at 360 MHz on a similar spectrometer. Unless otherwise stated, spectra were recorded as CD_2Cl_2 solutions under a nitrogen atmosphere in 5 mm or 10 mm quartz n.m.r. tubes. The ^{1}H, ^{11}B and ^{31}P spectra are referenced

(external) to $Si(CH_3)_4$, $BF_3.OEt_2$ and H_3PO_4 respectively, shifts to high frequency being positive. The selective decoupled $^1H\{^{11}B\}$ n.m.r. spectra obtained were recorded and presented as $^1H\{^{11}B_{(select)}\}-^1H$ subtraction plots thereby highlighting those protons coupling to the ^{11}B resonance of interest.

The ^{11}B COSY 2D spectra typically required a 128 x 128 point spectrum matrix, with 64 transients per 64 time-domain points, taking approximately 1 hour in total. The ^1H COSY and ^1H-^{11}B shift-correlated 2D spectra required a similar matrix, but overnight accumulation of typically 256 transients with inter-transient delays of 1 to 2 s. A double sine-bell window function was used for COSY, and a double Lorentz-to-Gaussian function for shift correlation, in which the interpulse spacings were a compromise between the optima for terminal H-B couplings and bridging H-B couplings.

Infrared spectra were recorded from KBr discs using a Perkin-Elmer 580B spectrophotometer.

All X-ray crystallographic studies were carried out by the author with expert assistance provided by Dr N. W. Alcock (University of Warwick). Diffraction data were collected with a Syntex $P2_1$ four circle diffractometer operating in the θ - 2θ mode, (precise experimental parameters are given in Section 5.2).

5.1.2. PREPARATION OF 6-TRIMETHYLAMINE-6-CARBA-NIDO-DECABORANE(11).

A mixture of $B_{10}H_{14}$ (20.0g, 0.16 mol), NaCN (25.0g, 0.5 mol), and water (300 mls) was stirred, under nitrogen, until all of the decaborane had dissolved, (~2hr). The solution, transferred to a dropping funnel, was run slowly with stirring, into 300 mls of a 2 : 1, concentrated HCl : H_2O solution, whilst being cooled in an ice bath.

Agitation and cooling was continued for 4 h, and then the solution stirred at room temperature for a further 2 h, after which time gas evolution had ceased. A solution of dioxane (107 mls, 1.26 mol) was added producing an immediate white precipitate. The filtered dioxane adduct was washed with water then redissolved in 350 mls of 15% aqueous KOH. Extreme care must be taken to ensure that excessively concentrated KOH is not used (i.e. not greater than 20%) as a degradation reaction has been observed to occur in such circumstances, resulting in a spectacular fire in which all the solid material undergoes rapid combustion. The addition of dimethyl sulphate (107 mls, 0.5 mol) with stirring produced another white precipitate, which was again filtered at the pump, washed with cold water and dried overnight under vacuum. The yield of product, a mixture of $6\text{-}NMe_3\text{-}6\text{-}CB_9H_{11}$ and $7\text{-}NMe_3\text{-}7\text{-}CB_{10}H_{12}$ varied from 21 to 22g (67 - 74% yield based on decaborane used).

5.1.3. CHROMATOGRAPHIC SEPARATION OF THE MONOCARBABORANES

The separation of the monocarbaborane product mixture from the above preparation was carried out on a 48 cm x 7 cm (dia.) column packed with silica to a height of 13 cm. The column was fitted with a nitrogen inlet valve[225] to control the pressurised solvent flow rate at a constant 100 mls/min.

The carbaborane mixture (10.6g) was adsorbed onto silica (4g) and the resultant free-flowing powder loaded onto the column under a top layer of sand. The column was eluted with 6.5 litres of a 70:30 mixture of CH_2Cl_2 : light petroleum (bp 40 - 60°C). Fractions collected were analysed qualitatively by small scale t.l.c. The Rf values obtained were 0.6 and 0.4 for $NMe_3CB_9H_{11}$ and $NMe_3CB_{10}H_{12}$

respectively. The recovered material consisted of 4.7g of $NMe_3CB_9H_{11}$, 4.85g of a mixture and 0.8g of $NMe_3CB_{10}H_{12}$.

N.M.R. SPECTRA OBTAINED FOR $NMe_3CB_9H_{11}$.

^{11}B - See Table 21 (p.249)

N.M.R. SPECTRA OBTAINED FOR $NMe_3CB_{10}H_{12}$.

^{11}B - See Table 21 (p.249)

^{11}B COSY - See Figure 33 p.72

5.1.4. PREPARATION OF DODECAHYDRO-6-CARBA-NIDO-DECABORANE(-1).

A three neck, 250 ml round bottom flask was fitted with a nitrogen inlet and a cold finger condenser fitted with a KOH drying tube. The flask was cooled in a solid CO_2/CCl_4 bath, the cold finger with a solid CO_2/acetone mixture and 80 ml of liquid ammonia condensed into the flask from a pressurised storage cylinder and the system was purged with nitrogen. The preparation was then continued in the following two ways.

a) Using pure $NMe_3CB_9H_{11}$ (see 5.1.3):

The $NMe_3CB_9H_{11}$ (3.5g, 0.02 mol) was added to the refluxing ammonia. Freshly cut sodium (1.4g, 0.06 mol) was then slowly added in small pieces with stirring. The mixture was stirred for a further half hour, after which methanol (40 mls) was added. All cooling was then removed and the ammonia was allowed to distill off through the drying tube. The last traces of ammonia were removed on a rotary evaporator under reduced pressure. Water (40 mls) was then added and the methanol removed on the rotary evaporator. To obtain a solid product, 10 mls of an aqueous solution of tetramethylammonium chloride (3g, 27 mmol) was

added, producing an immediate white precipitate. This was then filtered off, washed with cold water and dried under vacuum for 12 hours. The yield of $[CB_9H_{12}]^-[NMe_4]^+$ was 3.3 g, (86% based on $NMe_3CB_9H_{11}$ used).

b) Using a mixture of $NMe_3CB_9H_{11}$ and $NMe_3CB_{10}H_{12}$.

The preparation was carried out in a similar manner to that described in a) with the following differences. The composition of the mixture was calculated from the ^{11}B n.m.r. integration using the ratio of all the unique peaks for each species (see section 2.2.1, pages 63-4). The mixture (10.8g) containing 3.2g of the $[CB_9]$ component was added to the refluxing ammonia. After the ammonia/sodium work up the addition of methanol caused precipitation of the unreacted $[CB_{10}]$ component which was filtered off from the aqueous solution. The weight of recovered $NMe_3CB_{10}H_{12}$, (7.0g), was approximately that calculated prior to reaction, and gave a single spot on analysis by t.l.c. (Rf 0.6). The resultant aqueous $Na[CB_9H_{12}]$ solution was then used in the preparation of CB_8H_{14} as outlined in the following preparation. The solution of the anion was found to be stable over a number of days.

N.M.R. SPECTRA OBTAINED FOR $Na[CB_9H_{12}]$.

^{11}B - See Table 21 (p.249) and Figure 38 (p.76)

^{11}B COSY - See Figure 39 (p.77).

5.1.5. PREPARATION OF 3-CARBA ARACHNO NONABORANE(14).

The aqueous solution of $Na[CB_9H_{12}]$ from section 5.1.4(b) was diluted to 100 mls with water and 100 mls of light petroleum added (bp 30 - 40°C). A solution of $FeCl_3$ (23.4g, 0.085 mol) in water (70 mls) and concentrated HCl (32 mls) was then added dropwise to the solution over a period of 30 minutes, with stirring. After a further 30

minutes, gas evolution had ceased and the petroleum layer was removed. After two further extractions with petrol, the combined extracts were dried with anhydrous magnesium sulphate and the petroleum removed on a rotary evaporator. The white residue produced was then sublimed at 323 K and 0.01 mm Hg to give 0.63g of CB_8H_{14}, a yield of 31% based on $NMe_3CB_9H_{11}$.

N.M.R. SPECTRA OBTAINED FOR CB_8H_{14}.

^{11}B	- See Table 21 (p.249) and Figure 44 (p.81)
$^1H\{^{11}B_{(select)}\}$	- See Figure 45 (p.82)
^{11}B COSY	- See Figure 44 (p.81)
^1H-^{11}B Shift correlation	- See Figure 46 (p.84)

5.1.6. DEPROTONATION OF 3-CARBA-ARACHNO-NONABORANE(14).

In a dry-box with a nitrogen atmosphere, a 10 mm diameter n.m.r. tube, containing 0.82 cm^3 of a 0.16 mol dm^{-3} lithium butyl solution (0.13 mmol), was pumped under vacuum to remove the hexane solvent. The residue was dissolved in 1.0 cm^3 of tetrahydrofuran-d_8. To this solution was added 0.15g of CB_8H_{14} (0.13 mmol), dissolved in the same solvent, and the mixture agitated for 15 minutes, whereupon reaction to form the anionic derivative $Li[CB_8H_{13}]$ was complete.

N.M.R. SPECTRA OBTAINED FOR $Li[CB_8H_{13}]$.

^{11}B	- See Table 21 (p.249) and Figure 47 (p.87)
^{11}B COSY	- See Figure 47 p.87
^1H	- See Figure 50, p.92
$^1H\{^{11}B_{(select)}\}$	- See Figure 45 (p.82)
^1H-^{11}B Shift correlation	- See Figure 49 (p.90).
$^1H\{_{(select\ saturation)}\}$	- See Figure 52 p.94

TABLE 21. N.M.R. DATA OF PREPARED CARBABORANES.

$^{11}B-\{^1H\}$ N.M.R. SPECTRA

Compound	Solvent	Chemical Shift [B or H assignment*] (p.p.m.)
$NMe_3CB_9H_{11}$	CD_3COCD_3	1.7[1B], -1.4[2B], -5.6[2B], -11.7[2B], -29.6[1B], -37.7[1B].
$NMe_3CB_{10}H_{12}$	CD_3COCD_3	2.4[B(5)], -8.5[B(2,3)], -12.7[B(8,11)], -21.1[B(9,10)], -24.9[B(1)], -31.7[B(4,6)].
$Li[CB_9H_{12}]$	CD_3COCD_3	2.4[B(5,7)], -2.1[B(9)], -3.8[B(1,3)], -12.0[B(8,10)], -29.9[B(2)], -37.4[B(4)].
CB_8H_{14}	C_6D_6	17.0[B(7)], -3.7[B(1)], -6.3[B(5,9)], -34.9[B(6,8)], -41.1[B(2,3)].
$Li[CB_8H_{13}]$	D_8-thf	4.0[B(5,9)], -3.9[B(7)], -21.5[B(1)], -30.4[B(2,3)], -35.2[B(6,8)].

$^1B-\{^{11}B\}$ N.M.R. SPECTRA

Compound	Solvent	Chemical Shift [B or H assignment*] (p.p.m.)
CB_8H_{14}	C_6D_6	4.2[$H_{tB(7)}$], 3.17[$1H_{tB(1)}$], 2.83[$H_{tB(5,9)}$] 1.66[$H_{tB(6,8)}$], 1.0[$H_{tB(2,3)}$], -0.1[CH_{exo}] -0.6[$H_{bB(6,8-7)}$], -2.0[CH_{endo}], -3.7[$H_{bB(5,9-6,8)}$].
$Li[CB_8H_{13}]$	D_8-thf	3.93[$H_{tB(5,9)}$], 3.05[$H_{tB(7)}$], 2.52[$H_{tB(1)}$], 1.44[$H_{tB(2,3)}$], 1.29[$H_{tB(6,9)}$], 0.34[CH_{exo}] -0.36[CH_{endo}], -1.04[$H_{bB(5,9-6,8)}$], -2.0[$H_{bB(6,8-7)}$].

* Atom numbering corresponds to the structures shown in Chapter 2.

5.1.7. PREPARATION OF THE RUTHENACARBABORANES: [9,9,9-(CO)(PPh$_3$)$_2$-NIDO-9,6-RuCB$_8$H$_{10}$-5-(PPh$_3$)] (1), [9,9,9-(CO)(PPh$_3$)$_2$-NIDO-9,6-RuCB$_8$H$_9$-3-Cl-5-(PPh$_3$)] (4), [9,9,9-(CO)(PPh$_3$)$_2$-NIDO-9,6-RuCB$_8$H$_9$-7-Cl-5-(PPh$_3$)] (5) AND [2,2,2-(CO)(PPh$_3$)$_2$-CLOSO-2,1-RuCB$_8$H$_8$-10-(PPh$_3$)] (6).

Butyl lithium (0.5 cm^3 of a 1.5 mol dm^{-3} diethyl ether solution) was added to a solution of CB_8H_{14} (0.085g, 0.75 mmol) in benzene (40 cm^3) and left to stir under nitrogen. After 15 min $RuHCl(PPh_3)_3(CO)$ (0.7g, 0.73 mmol) was added and the solution refluxed for 30 min. The solvent was removed under vacuum from the resulting orange-red solution. Chromatography of the orange solid using CH_2Cl_2 - light petroleum yielded the compounds (1) and (6) (see Table 22). A further complex band was recovered and re-chromatographed in benzene with repeat dippings to isolate the two compounds (4) and (5).

Recystallisation from CH_2Cl_2 - petroleum ether afforded the pure compounds in the following yields; compound (1) 0.41g (0.4 mmol, 53%), compound(4) 0.02g (0.018 mmol, 3%), compound(5) 0.06g (0.054 mmol, 8%) and compound(6) 0.03g (0.03 mmol, 4%). Crystals of these compounds, suitable for X-ray diffraction analysis, were grown by slow diffusion of light petroleum into a CH_2Cl_2 or benzene solution.

Whilst the total yield of compounds (1) and (5) from repeat preparations was observed to be approximately constant, the individual yields were noted to be inversely related. Thus when the yield of compound (1) was low, the yield of compound (5) increased proportionately, and vice versa.

This was found to be due to the fact that compound (5) is the chlorinated derivative of compound (1), and results from chlorine

abstraction from the chlorinated solvent used in the t.l.c. work-up. Dichloromethane solutions of compound (1) were observed to be quantitatively transformed into compound (5) when left for either extended periods (several weeks) at ambient temperatures or more rapidly at elevated temperatures.

Note that compound (4), another chlorinated analogue, was not produced by such treatment, and must therefore have arisen from reaction with the chloride liberated from the $RuHCl(PPh_3)_3(CO)$ reagent during the initial preparation.

The reagent, $RuHCl(PPh_3)_3(CO)$, was prepared according to a literature method[226].

N.M.R. SPECTRA OBTAINED FOR

[9,9,9-(CO)$(PPh_3)_2$-NIDO-9,6-$RuCB_8H_{10}$-5-(PPh_3)] (1).

^{11}B - See Table 8 (p.106) and Figure 56 (p.104)

^1H and ^{31}P - See Table 8 (p.106)

$^1H(^{11}B_{(select)})$ - See Figure 57 (p.105)

N.M.R. SPECTRA OBTAINED FOR

[9,9,9-(CO)$(PPh_3)_2$-NIDO-9,6-$RuCB_8H_9$-3-Cl-5-(PPh_3)] (4) AND

[9,9,9-(CO)$(PPh_3)_2$-NIDO-9,6-$RuCB_8H_9$-7-Cl-5-(PPh_3)] (5).

^{11}B, ^1H, $^1H(^{11}B_{(select)})$ and ^{31}P - See Table 10 (p.135)

N.M.R. SPECTRA OBTAINED FOR

[2,2,2-(CO)$(PPh_3)_2$-CLOSO-2,1-$RuCB_9H_{10}$-10-(PPh_3)] (6).

^{11}B - See Table 11 (p.152) and Figure 77 (p.151)

^1H, $^1H(^{11}B_{(select)})$ and ^{31}P - See Table 11 (p.152)

5.1.8. PREPARATION OF THE OSMACARBABORANES

[9,9,9-(CO)$(PPh_3)_2$-NIDO-9,6-$OsCB_8H_{10}$-5-(PPh_3)] (2) AND

[2,2,2-(CO)$(PPh_3)_2$-CLOSO-2,1-$OsCB_8H_8$-3-(PPh_3)] (7).

The compounds (2) and (7) were prepared in an essentially identical procedure as that described for the ruthenium analogues. From CB_8H_{14} (0.05g, 0.44 mmol), reaction of $OsHCl(PPh_3)_3(CO)$ in refluxing benzene and subsequent chromatography (see Table 22) produced the compounds in the following yields; compound (2) 0.17g (0.15 mmol, 34%) and compound(7) 0.13g (0.12 mmol, 26%). Crystals of each compound were grown by the diffusion method described above.

A similar product distribution and yield was achieved from an ambient reaction left to stir under nitrogen over a period of 3 days.

The osmacarbaboranes were found to be more air sensitive than the ruthenium analogues and were thus best isolated by rapid chromatographic elution and extraction. Over exposure to the atmosphere resulted in degradation to a black amorphous material which was not characterised.

The reagent, $OsHCl(PPh_3)_3(CO)$, was prepared according to a literature method[227].

N.M.R. SPECTRA OBTAINED FOR

[9,9,9-(CO)$(PPh_3)_2$-NIDO-9,6-$OsCB_8H_{10}$-5-(PPh_3)] (2).

^{11}B - See Table 8 (p.106) and Figure 56 (p.104)

^1H, $^1H(^{11}B_{(select)})$ and ^{31}P - See Table 8 (p.106)

N.M.R. SPECTRA OBTAINED FOR

[2,2,2-(CO)$(PPh_3)_2$-CLOSO-2,1-$OsCB_8H_8$-3-(PPh_3)] (7).

^{11}B - See Table 11 (p.152) and Figure 80 (p.162)

^1H, $^1H(^{11}B_{(select)})$ and ^{31}P - See Table 11 (p.152)

SOLVENT SYSTEM CH_2Cl_2:PETROL (OTHER)	T.L.C. BAND Rf	COLOUR	INTEN-SITY	COMPOUND NUMBER	CRYSTAL COLOUR	DIFFUSION SOLVENT (EVAPORATION)
PRODUCTS FROM REACTION OF $Li[CB_9H_{12}]$ AND $RuHCl(PPh_3)_3(CO)$.						
50 : 50	0.63	orange	w			
	0.49	Yellow	w			
	0.44	Orange	m	6	Orange	Benzene
	0.28	Orange--red	s	4 + 5		
					(Bands below Rf = 0.3 - base line re-t.l.c.'d in 80 : 20 solvent)	
	0.2	Orange	s	1		
	0.1	Red	w			
	0.05	Green	w			
80 : 20	0.67	Green	w			
	0.63	Orange	m	6		
	0.56	Orange--yellow	s	4 + 5	(Re-t.l.c.'d in Benzene)	
	0.35	Yellow	w			
	0.27	Orange--red	s	1	Red	CH_2Cl_2
	0.18	Orange	w			
	0.09	Yellow	w			
(Benzene)	0.39	-	w			
	0.28	Orange--red	s	4	Orange--red	CH_2Cl_2
	0.15	Orange	s	5	Orange	CH_2Cl_2
PRODUCTS FROM REACTION OF $Li[CB_9H_{12}]$ AND $RuCl(\eta-C_5H_5)(PPh_3)_2$.						
75 : 25	0.85	Yellow	w			
	0.77	Yellow	w			
	0.68	Yellow	w			
	0.45	Orange	w			
	0.36	Orange	w			
	0.13	Yellow	s	3	Yellow	(CH_2Cl_2)
PRODUCTS FROM REACTION OF $Li[CB_9H_{13}]$ AND $OsHCl(PPh_3)_3(CO)$.						
(Benzene)	0.93	-	s			
	0.49	Yellow	s	7	Yellow	CH_2Cl_2
	0.40	Green	w			
	0.29	Orange	s	2	Orange	CH_2Cl_2

Table 22. Preparative t.l.c. and crystallisation data for the isolation of the prepared ruthena- and osmacarbaboranes.

(Band intensity denoted as; s = strong, m = medium, w = weak)

5.1.9. PREPARATION OF THE ARACHNO-RUTHENACARBABORANE, [9,9,9-(η-C_5H_5)(H)(PPh_3)-9,6-$RuCB_8H_{12}$] (3).

Butyl lithium (0.7 cm^3 of a 1.5 mol dm^{-3} diethyl ether solution, 0.91 mmol) was added to a solution of CB_8H_{14} (0.1g, 0.89 mmol) in benzene (30 cm^3), diethyl ether (20 cm^3) and left to stir under nitrogen. After 15 min $RuCl(\eta-C_5H_5)(PPh_3)_2$ (0.64g, 0.88 mmol) was added and the mixture refluxed for 48 h. A yellow turbid solution was produced, which gave a yellow precipitate on standing to cool. After removal of the solvent under vacuum, the solid was extracted with CH_2Cl_2 and recrystallised from CH_2Cl_2 - light petroleum to yield 0.32g (0.59 mmol, 67%) of product.

Slow evaporation of a CH_2Cl_2 solution gave yellow diamond block crystals, which were used for the X-ray structure determination.

Chromatography of the reaction mixture (see Table 22) showed that several minor products had also been formed in very small yield. None of these products were isolated or characterised. Compound (3) crystallised from dichloromethane was indicated to be pure from the single band produced on t.l.c. treatment.

The ruthenium reagent $RuCl(\eta-C_5H_5)(PPh_3)_2$ was prepared by standard methods[228].

N.M.R. SPECTRA OBTAINED FOR [9,9,9-(η-C_5H_5)(H)(PPh_3)-9,6-$RuCB_8H_{12}$] (3).

^{11}B - See Table 9 (p.119) and Figure 84 (p.176)

^1H and ^{31}P - See Table 9 (p.119)

$^1H\{^{11}B_{(select)}\}$ - See Figure 62 (p.118)

5.1.10. PREPARATION OF THE MONO AND HEPTANUCLEAR CONDO-AURA-CARBABORANES; [ARACHNO-9,6,6'-Au(CB_8H_{12})$_2$][Au(PPh_3)$_2$] (7) AND [(CB_8H_{11}Au)(AuPPh_3)$_5$(AuCB_8H_{12})$_2$] (11).

The addition of MeAu(PPh_3) (75 mg, 0.16 mmol) to an equimolar quantity of CB_8H_{14} (18 mg) in a 10 mm n.m.r. tube produced a vivid red colouration on agitation of the solids at room temperature. Dissolution in 2 cm^3 of CH_2Cl_2 produced a deep wine-red coloured solution. An ^{11}B n.m.r. spectrum of the resultant solution showed the carbaborane precursor to be the major component with a minor component identified from broad underlying resonances. Subsequent two and three-fold equivalent additions of the gold reagent were made, resulting in a further deepening in hue of the red solution. This was accompanied by depletion of the resonances in the ^{11}B n.m.r. spectrum due to the carborane precursor and growth of minor product resonances. After the six-fold addition of the gold reagent the carbaborane was found by n.m.r. to be exhausted.

A black glassy solid was obtained on removal of the solvent under vacuum, the components of which were separated by preparative t.l.c. using a 3:1 CH_2Cl_2 - light petroleum solvent system (See Table 23). An intense red band, auracarbaborane (8), and a faint yellow band, auracarbaborane (9), were removed from the t.l.c. plates and then extracted from the silica support with CH_2Cl_2.

Repeat preparations using 0.075g of CB_8H_{14} (0.44 mmol) and a similar six-fold ratio of the gold reagent, left to react at ambient temperature for 48 hours, yielded after t.l.c. work up and crystallisation from CH_2Cl_2 and light-petroleum, compound (8) 0.124g (0.14 mmol, 63%) and compound (9) 0.04g (uncharacterised).

SOLVENT SYSTEM CH_2Cl_2 : PETROL	Rf	T.L.C. BAND COLOUR	INTEN-SITY	COMPOUND NUMBER	CRYSTAL COLOUR	DIFFUSION SOLVENT (EVAPORATION)
PRODUCTS FROM REACTION OF $Li[CB_8H_{13}]$ AND $ClAu(PPh_3)$.						
75 : 25	0.89	Green	w			
	0.63	Yellow	m	9	Yellow	CH_2Cl_2
	0.42	Red	s	8	Dark red	CH_2Cl_2/Benzene
	0.29	Pink	w			
	0.18	Pink	w			
PRODUCTS FROM REACTION OF CB_8H_{14} AND $MeAu(P(cyclo\text{-}C_6H_{11})_3)$.						
50 : 50	0.66	Pink	w			
	0.66	Pink	w			
	0.36	Yellow	w			
	0.25	Pink	w			
	0.17	Yellow	s	10	Yellow	(CH_2Cl_2)
PRODUCTS FROM REACTION OF CB_8H_{14} AND $Cl_2Au_2(DPPE)$.						
75 : 25	0.85	-	w	CB_8H_{14}		
	0.67	Yellow	s	12	Yellow	CH_2Cl_2/Benzene
	0.50	Orange	m			
	0.35	Pink	w			
	0.26	Yellow	w			
	0.20	Green	w			
	0.09	Dark red	s	13	Dark red	CH_2Cl_2

Table 23. Preparative t.l.c. and crystallisation data for the isolation of the prepared auracarbaboranes (8) - (13).
(Band intensity denoted as; s = strong, m = medium, w = weak)

Dark red crystals of auracarbaborane (8) were grown by evaporation of a dichloromethane solution and slow diffusion of light petroleum into a number of solvent mixtures containing the compound(8). All crystals were found to be unsuitable for X-ray diffraction analysis due to crystal twinning. After repeated recrystallisations, one dark red crystal, suitable for X-ray diffraction analysis, was obtained from diffusion of light petroleum into a CH_2Cl_2 : C_6H_6 solvent mixture. This compound was characterised as the heptanuclear auracarbaborane (11), $(CB_8H_{11}Au)(AuPPh_3)_5(AuCB_8H_{12})_2$.

The origin of auracarbaborane (11) is thus unclear, other than it originated from the reaction of CB_8H_{14} and $MeAuPPh_3$. It may of course have been produced during the handling of auracarbaboranes (8) in various solvents, or have been produced in the initial reaction and present as a minor entrained product in the t.l.c. band isolated as auracarbaborane (8). Other pink coloured minor products were identified from the t.l.c. work-up (see Table 23). Investigation to ascertain the origin of this product was not undertaken because of time limitations.

The X-ray structure determination of auracarbaborane (11) was initiated under the mistaken belief that the compound was auracarbaborane (8), a mistake that became apparent, when the X-ray structure was established, by comparison of the symmetry suggested by the n.m.r. and X-ray data obtained (see Chapter 4).

Repeated attempts to crystallise auracarbaborane (9) from a range of solvents yielded only a single crystal, grown from diffusion of light-petroleum into a CH_2Cl_2 solution. This crystal was cleaved into two halves to obtain a suitable sample for a preliminary crystallographic examination. Both crystals were found to suffer from crystal twinning, thereby eluding X-ray characterisation.

Auracarbaborane (8) was also observed to be the major product of the similar reaction of the anionic $Li[CB_8H_{13}]$ with $ClAu(PPh_3)$ in diethyl ether. Auracarbaborane (9) was also observed to be a prominent minor product, but in this instance a further orange product at Rf 0.85 was observed. This changed to a deep red colour in toluene, yielding an ^{11}B n.m.r. spectrum suggesting the presence of three or more carbaborane residues. Further characterisation was not pursued.

The reagents $ClAuPPh_3$ and $MeAuPPh_3$ were prepared by standard literature methods[229,230].

N.M.R. SPECTRA OBTAINED FOR

[ARACHNO-9,6,6'-$Au(CB_8H_{12})_2$][$Au(PPh_3)_2$] (8)

^{11}B - See Table 20 (p.232) and Figures 84,85 (p.176,179)

^1H - See Table 20, p.232

$^1H\{^{11}B_{(select)}\}$ - See Figures 94,107 (p.194,229)

N.M.R. SPECTRA OBTAINED FOR AURACARBABORANE(9)

^{11}B - See Figure 84 (p.176)

5.1.11. PREPARATION OF THE CONDO-AURACARBABORANE: [ARACHNO-9,6,6'-$Au(CB_8H_{12})_2$] [$Au(P(cyclo\text{-}C_6H_{11})_3)_2$] (10).

$MeAu(P(cyclo\text{-}C_6H_{11})_3)$ was produced *in situ* by the addition of a slight excess of methyl lithium (0.30 cm^3 of a 1.6 mol dm^{-3} solution) to $ClAu(P(cyclo\text{-}C_6H_{11})_3)$ (0.21 g, 0.41 mmol) in diethyl ether (10 cm^3). After 10 minutes, the addition of an equimolar quantity of CB_8H_{14} (0.045g, 0.40 mmol) produced immediate gas evolution. After stirring for 60 minutes the ether was removed under vacuum, and the residue dissolved in CD_2Cl_2 to yield a pink solution. The ^{11}B n.m.r.

spectrum of this solution showed the carbaborane precursor to be the major component with a minor component giving broad underlying resonances.

A repeat reaction using a 2 : 1 ratio of gold : carbaborane reagents produced a similar pink solution in which the carbaborane precursor was absent. Preparative t.l.c. of this solution using a 1 : 1 CH_2Cl_2 - light-petroleum solvent system gave a strong yellow band (Rf 0.17) in addition to several very faint bands (see Table 23). A black insoluble residue present over the Rf range 0.1 - 0.45 caused contamination of the t.l.c. bands. Each of the observed product bands was removed from the t.l.c. plates, extracted with CH_2Cl_2 and purified by re-chromatography in an identical fashion. The yield of the main product, compound (10), was 0.138 g (0.15 mmol, 74%).

On prolonged exposure to the atmosphere all minor products were observed to darken to a deep red colouration, though compound (10) remained unaltered. This was confirmed by comparison of the ^{11}B n.m.r. spectra of the reaction mixture and isolated material.

Crystals of compound (10), suitable for X-ray diffraction analysis, were grown by slow evaporation of a CH_2Cl_2 solution.

The reagent $ClAuP(cyclo\text{-}C_6H_{11})_3$ was prepared by standard literature methods[231,232].

N.M.R. SPECTRA OBTAINED FOR

[ARACHNO-9,6,6'-Au(CB_9H_{12})$_2$][Au(P(cyclo-C_6H_{11})$_3$)$_2$] (10):-

^{11}B - See Table 20 (p.232) and Figure 86 (p.182)

^1H, $^1H(^{11}B_{(select)})$ - See Table 20, (p.232)

5.1.12. PREPARATION OF THE BINUCLEAR 'A' FRAME COMPLEX; [ARACHNO-4,5,6,7,8,9-$(CH_3)_2$]Au(dppm)Au(CB_8H_{12})] (12).

The carbaborane anion $[CB_8H_{13}]^-$ was prepared *in situ* from the reaction of a diethyl ether solution of CB_8H_{14} (0.05 g, 0.44 mmol) with an equimolar quantity of butyl lithium solution. After 15 minutes an equimolar quantity of Cl_2Au_2(dppm) (0.38 g, 0.44 mmol) was added to the stirred solution. An initial brown discolouration, observed after 1 hour, progressively darkened to give a red solution after mixing for 2 days.

A dark red solid was obtained on removal of the solvent under vacuum, the components of which were separated by preparative t.l.c using a 3:1 CH_2Cl_2 - light petroleum solvent system (see Table 23). A yellow band (Rf 0.67) corresponding to compound (12) 0.082 g (0.08 mmol, 37%) and a red band (Rf 0.09) compound (13) 0.038 g, accompanied a small amount of unreacted carbaborane (Rf 0.85). Other minor products, indicated to be present from the ^{11}B n.m.r. spectrum of the reaction mixture were also observed as noted in Table 23. None of these minor products was characterised.

Crystals of compound (12), suitable for X-ray diffraction analysis, were grown by slow diffusion of petrol into a CH_2Cl_2 : C_6H_6 solution. The crystals of compound (13) grown in a similar manner were found to suffer from crystal twinning.

Solutions of compound (12) left in dichloromethane for extended periods (~ week at ambient temperature) were observed to be transformed into compound (13). This transformation did not yield any other carbaborane or auracarbaborane products, as judged from absence of additional resonances in the ^{11}B n.m.r. spectra obtained. Compound

(13) was found to contain the cosmo auracarbaborane anion $[(CB_8H_{12})Au(CB_8H_{12})]^-$, identified as present in compounds (8) and (10) (see Chapter 4). The identity of the cation was not established.

The gold reagent Cl_2Au_2(dppa) was prepared using standard literature methods[218].

N.M.R. SPECTRA OBTAINED FOR

[ARACHNO-6,9,9',6'-$(CB_8H_{12})Au$(DPPE)$Au(CB_8H_{12})$] (12).

^{11}B	- See Table 18 (p.216) and Figure 100 (p.214)
^1H	- See Figure 18, p.216
$^1H\{^{11}B_{(select)}\}$	- See Figure 101 (p.215)

N.M.R. SPECTRA OBTAINED FOR $[(CB_8H_{12})_2Au][Au_2(DPPE)_3]$ (13).

^{11}B	- See Table 20 (p.232) and Figure 108 (p.230)
^1H COSY	- See Figure 110 (p.235)
^1H	- See Figure 20 (p.232)
$^1H\{^{11}B_{(select)}\}$	- See Figure 109 (p.231)

5.2. X-RAY CRYSTALLOGRAPHIC EXPERIMENTAL

All X-ray crystallographic studies were carried out by the author with expert guidance generously provided by Dr N. W. Alcock (University of Warwick).

The description of the X-ray crystallography work carried out has been organised into two sections. In the first section (5.2.1), the standard method used for data collection and structure solution is described and the experimental data collection and final refinement parameters provided in tabular format. Other features of each crystallographic study are then outlined. Additional information regarding the methods used in the X-ray crystallographic studies carried out at the University of Warwick is provided in Appendix I, which has been written to provide the reader with a brief over view of X-ray crystallographic theory and practice.

In the latter section (5.2.2), the final fractional coordinates, interatomic distances and interbond angles are provided for each compound studied. Discussion of the important features of this information can be found in the relevant sections of Chapters 3 and 4.

Space limitations do not permit the presentation in this thesis of the large volume of structure factor data obtained for the ten compounds characterised by X-ray crystallography. Complete sets of crystallographic data (including structure factor tables) for all of the compounds characterised in this thesis have been retained by Dr N. W. Alcock (University of Warwick, Coventry, CV4 7Al). This information will be deposited with the Cambridge Crystallographic Data Centre, (University Chemical Laboratory, Lensfield Road, Cambridge CB2 1EW), when all of the structures have been published.

5.2.1. DATA COLLECTION, REFINEMENT AND STRUCTURE SOLUTION.

The data collection, structure solution and refinement for all ten compounds studied was carried out as described below, with exceptions to the general procedure as noted. Discussion of the found structures are given in Chapters 4 and 5. To supplement the general description of the crystal structure analysis outlined below, information relevant to each individual X-ray study is then provided.

GENERAL METHOD

Crystals were mounted on quartz filaments and sealed in thin quartz glass Lindemann tubes under a nitrogen atmosphere, in order to protect the compounds from oxidative degradation or solvent losses.

Diffraction data was collected at ambient temperature with a Syntex $P2_1$ four circle diffractometer operating in the $\theta - 2\theta$ mode, with scan speed range of $2 - 29^{\circ}\ min^{-1}$, depending on the intensity of a 2 s pre-scan; backgrounds were measured at each end of the scan for 0.25 of the scan time. Three standard reflections were monitored every 200 reflections, and any slight changes were corrected by rescaling. Unit cell dimensions and standard deviations were obtained by least-squares fit to 15 high angle reflections.

Only observed reflections ($I / \sigma(I) > 3.0$) were used in refinement. Every reflection data set was corrected for Lorenz, polarisation and absorption effects using the Gaussian method[233], except in the case of compound (3) where ABSCOR [234] was used and compound (1) where no correction was made.

For each compound, the heavy atoms (Ru, Os, or Au) were located by the Patterson technique and the light atoms (P, Cl, B, C and cage bound H) then found on successive Fourier syntheses. The cluster and

ligand skeletal atoms of all compounds studied were found and refined. The carbon atom position within the carbaborane fragment of each cluster was deduced from the improved thermal parameter obtained when the atom was refined as a carbon atom when compared to refinement as a boron atom.

Non-cage hydrogen atoms were given fixed isotropic thermal parameters, U = 0.007 $Å^2$. Those hydrogens indicated by the molecular geometry (i.e. Non-cage bound hydrogens such as those present in the ligand PPh_3) were inserted at calculated positions and not refined.

Final refinement was on F by cascade least squares methods with anisotropic thermal parameters for all atoms other than hydrogen. Weighting schemes of the form $w = [1/[\sigma^2(F) + gF^2]$ were used, and shown to be satisfactory by weight analysis. Computing work was with the SHELXTL system[233] on a Data General DG30. Scattering factors in the analytical form and anomalous dispersion factors were taken from the literature[235].

The crystal data, collection and refinement parameters for compounds (1) - (7) and (10) - (12) are given in Tables 24 - 27.

SUPPLEMENTARY INFORMATION

[9,9,9-(CO)$(PPh_3)_2$-NIDO-9,6-$RuCB_8H_{10}$-8-(PPh_3)] (1)

The crystal used had an irregular complex tabular shape. Measurement of the crystal for absorption correction of the data was attempted but not completed. In view of the modest effect observed for the other compounds studied, this omission was not considered to be serious.

The $B-H_{(terminal)}$ and Ru-H-B bridging hydrogens were not located.

Table 24. Crystal data, collection and refinement parameters for compounds (1), (2) and (3).

Compound	(1)	(2)	(3)
Formula	$C_{56}H_{55}B_8P_3ORu$	$C_{56}H_{55}B_8P_3OOs$	$C_{24}H_{33}B_8PRu$
System	Monoclinic	Monoclinic	Monoclinic
Space group	$P2_1/n$	$P2_1/n$	$P2_1/n$
Absences	—— h0l; h + l = 2n + 1 and 0k0; k = 2n + 1 ——		
a/Å	17.023(7)	17.090(6)	12.642(2)
b/Å	13.628(7)	13.634(4)	14.832(5)
c/Å	22.353(7)	22.469(9)	14.327(4)
Beta/°	103.38(3)	103.65(3)	108.46(2)
U/Å^3	5045(4)	5087(3)	2548(1)
M	1024.5	1113.6	540.0
D_c/g cm^{-3}	1.35	1.45	1.41
D_m/g cm^{-3}	1.33	1.50	1.48
Z	4	4	4
μ(Mo-K_{alpha}/cm^{-1})	4.37	26.41	6.77
F(000)	2112	2240	1104
Total reflections	6733	6891	4806
Reflections with I/sigma(I) > 3.0	2670	3525	3523
2θ max/°	50	50	50
Range (2θ) about K_{alpha1} - $_{alpha2}$/ Position/°	+/-1.0	+/-1.0	+/-1.1
Transmission factors (max.-min.)	-	0.73-0.57	0.92-0.88
Crystal size / mm	-	0.52 x 0.24 x 0.47	0.7 x 0.3 x 0.55
g	0.0070	0.0014	0.00053
R	0.087	0.050	0.046
R'	0.089	0.050	0.047
Max.,min. on final delta F map/e Å^{-3}	1.2,-0.7	1.5,-1.0	0.9,-1.1
Final max. shift/error	0.27	0.5	0.03

Table 25. Crystal data, collection and refinement parameters for compounds (4) and (5).

Compound	(4)	(5)
Formula	$C_{56}H_{54}B_8P_3OClRu$	$C_{56}H_{54}B_8P_3OClRu$
System	Triclinic	Monoclinic
Space group	$P\bar{1}$	$P2_1/c$
Absences	None	h0l; l = 2n + 1 0k0; k = 2n + 1
a/Å	12.394(7)	17.408(6)
b/Å	12.971(7)	13.706(5)
c/Å	21.298(12)	24.696(9)
Alpha/°	96.16(4)	-
Beta/°	93.24(5)	115.38(3)
Gamma/°	120.75(3)	-
U/Å^3	2917(3)	5323(3)
M	1059.3	1059.3
D_c/g cm^{-3}	1.21	1.32
Z	2	4
μ(Mo-K_{alpha}/cm^{-1})	4.24	4.65
F(000)	1087	2176
Total reflections	5442	6227
Reflections with I/sigma(I) > 3.0	3281	3381
2θ max/°	40	45
Range (2θ) about K_{alpha1} - $_{alpha2}$/ Position/°	+/-1.2	+1.0/-1.2
Transmission factors (max.-min.)	0.93-0.89	0.96-0.89
Crystal size / mm	0.56 x 0.55 x 0.31	0.16 x 0.46 x 0.38
g	0.006	0.0000
R	0.097	0.0528
R'	0.101	0.0528
Max.,min. on final delta F map/e Å^{-3}	2.1,-0.9	0.5,-0.4
Final max. shift/error	0.2	-0.3

Table 26. Crystal data, collection and refinement parameters for compounds (6) and (7).

Compound	(6)	(7)
Formula	$C_{56}H_{53}B_8P_3ORu$	$C_{56}H_{53}B_8P_3OOs$
System	Monoclinic	Triclinic
Space group	$P2_1/c$	$P\bar{1}$
Absences	h0l; l = 2n + 1 0k0; k = 2n + 1	None
a/Å	12.401(2)	13.439(3)
b/Å	36.666(8)	25.360(7)
c/Å	11.684(2)	28.960(8)
Alpha/°	-	73.60(2)
Beta/°	103.35(1)	85.93(2)
Gamma/°	-	90.45(2)
U/Å^3	5169(3)	9441(4)
M	1022.8	1112.0
D_c/g cm^{-3}	1.31	1.17
Z	4	6
μ(Mo-K_{alpha}/cm^{-1})	4.62	21.93
F(000)	2104	3515
Total reflections	6740	20821
Reflections with I/sigma(I) > 3.0	4179	6466
2θ max/°	50	45
Range (2θ) about K_{alpha1} - $_{alpha2}$/ Position/°	+0.9/-1.0	+/-1.0
Transmission factors (max.-min.)	0.94-0.90	0.78-0.62
Crystal size / mm	0.41 x 0.24 x 0.33	0.30 x 0.25 x 0.27
g	0.0022	0.0426
R	0.0626	0.1151
R'	0.0638	0.1225
Max.,min. on final delta F map/e Å^{-3}	0.8,-0.01	0.6,-1.5
Final max. shift/error	-0.03	3.07

Table 27. Crystal data, collection and refinement parameters for compounds (10), (11) and (12).

Compound	(10)	(11)	(12)
Formula	$C_{38}H_{54}B_{16}P_2Au_2$	$C_{92}H_{98}B_{16}P_5Au_7$	$C_{28}H_{48}B_{16}P_2Au_2$
System	Triclinic	Triclinic	Monoclinic
Space group	$P\bar{1}$	$P\bar{1}$	$P2_1/n$
Absences	None	None	h0l; h + l = 2n + 1 0k0; k = 2n + 1
a/Å	12.310(4)	17.025(9)	12.782(3)
b/Å	12.747(4)	22.652(11)	18.609(3)
c/Å	18.167(9)	13.929(7)	19.543(5)
Alpha/°	85.51(3)	74.05(4)	-
Beta/°	73.40(3)	79.66(4)	102.36(2)
Gamma/°	77.36(3)	89.64(4)	-
U/Å^3	2665(2)	5076(4)	4541(2)
M	936.2	2910.9	1013.5
D_c/g cm^{-3}	2.33	1.90	1.48
D_m/g cm^{-3}	1.54	2.04	1.74
Z	4	2	4
μ(Mo-K$_{alpha}$/cm^{-1})	55.71	101.78	65.30
F(000)	1091	2715	1935
Total reflections	6987	13355	7641
Reflections with I/sigma(I) > 3.0	4361	5716	3751
2θ max/°	45	45	45
Range (2θ) about K$_{alpha1}$ - K$_{alpha2}$ Position/°	+/-1.1	+/-1.0	+/-1.0
Transmission factors (max.-min.)	0.50-0.40	0.40-0.31	0.38-0.30
Crystal size/mm	0.42x0.21x0.30	0.16x0.19x0.23	0.33x0.32x0.34
g	0.001	0.0003	0.002
R	0.063	0.055	0.068
R'	0.067	0.050	0.072
Max.,min. on final delta F map/e Å^{-3}	1.96,-2.3	1.45,-1.28	4.58,-2.7
Final max. shift/error	0.31	0.09	0.012

The poor R value is attributable to the weak diffracting power of the crystal, virtually no diffraction was observed above 40^{o}. The ratio of observed to unobserved reflections is only 0.4.

[9,9,9-(CO)$_3$(PPh$_3$)$_2$-*NIDO*-9,6-$OsCB_8H_{10}$-5-(PPh$_3$)] (2)

The $B\text{-}H_{(terminal)}$ and Os-H-B bridging hydrogens were not located.

[9,9,9-η-C_6H_5)(H)(PPh$_3$)-9,6-$RuCB_8H_{12}$] (3)

All $B\text{-}H_{(terminal)}$ hydrogens and B-H-B bridging hydrogen atoms were located and refined. The Ru-H hydride, indicated from n.m.r. spectroscopic evidence was not located.

[9,9,9-(CO)(PPh$_3$)$_2$-*NIDO*-9,6-$RuCB_8H_9$-3-Cl-5-(PPh$_3$)] (4)

The $B\text{-}H_{(terminal)}$ hydrogens and Ru-H-B bridging hydrogen atoms were not located. A single molecule of dichloromethane solvent was found to be present in the asymmetric unit.

[9,9,9-(CO)(PPh$_3$)$_2$-*NIDO*-9,6-$RuCB_8H_9$-7-Cl-5-(PPh$_3$)] (5)

All $B\text{-}H_{(terminal)}$ hydrogens and Ru-H-B bridging hydrogen atoms were found and refined.

[2,2,2-(CO)(PPh$_3$)$_2$-*CLOSO*-2,1-$RuCB_8H_9$-10-(PPh$_3$)] (6).

The $B\text{-}H_{(terminal)}$ hydrogens were not located.

[2,2,2-(CO)(PPh$_3$)$_2$-*CLOSO*-2,1-$OsCB_8H_9$-3-(PPh$_3$)] (7).

The crystal used was encapsulated in a light-petroleum solvent atmosphere in order to reduce solvent losses from the crystal, a problem experienced on previous attempts to obtain X-ray data.

Three isomeric osmacarbaborane clusters of the above formulae were identifed in the asymmetric unit. The SHELTXL[233] program has a limit on the number of atoms that it can refine. The limit is 200 atoms in the asymmetric unit and the number of isotropic atoms plus twice the number of anisotropic atoms may not exceed 320. This limitation restricted the refinement of the structure to the present R value of 0.1151, in which all of the carbon atoms in the position para- to the P-C bond of the phenyl rings on the PPh_3 ligands were omitted in order to not exceed the atom limit. Completion of this structure refinement is currently being pursued by Dr. N. W. Alcock (University of Warwick).

Two molecules of dichloromethane solvent were identified in the asymmetric unit but not refined. The $B\text{-}H_{(terminal)}$ hydrogens were not located.

[ARACHNO-9,6,6'-$Au(CH_2)_2$]$_2$[Au(P(cyclo-C_6H_{11})$_3$)$_2$] (10).

The possible gold positions generated by the computer from the Patterson map were found not to refine adequately. Alternative gold atom positions were therefore deduced from the cross-vector combinations calculated to produce the highest peaks in the observed Patterson map.

Three gold atom positions were located, two of which required the assignment of half occupancies in order to refine properly. This feature also manifests itself in the refinement of the carbaborane clusters attached to these gold atoms.

Two carbaborane clusters were identified as superimposed upon one another, the skeletal atoms of which were all assigned half

occupancies in order to refine the structure (see B(111) to B(220) in Table 49). These half occupancy carbaborane fragments are the *syn* and *anti* carbaborane clusters of the *commo* auracarbaborane anion $[(CB_8H_{12})Au(CB_8H_{12})]^-$, (see Chapter 5.1). The cation was identified as $[Au(P(cyclo\text{-}C_6H_{11})_3)_2]^+$, the atoms of which refined normally.

This effect is presumably due to dominance of the gold atom in the diffraction of X-rays compared to the associated lighter atoms of the carbaborane cluster. Ideally, one might expect that the *syn* and *anti* conformations of the $[(CB_8H_{12})Au(CB_8H_{12})]^-$ anion would be distinguishable because of the differences in orientation of the carbaborane fragments around the central gold atom. Because the two sub-cluster carbaborane fragments of each isomer are related by a mirror plane symmetry, for both *syn* and *anti* conformations, one might also not be surprised if only half of the molecule was revealed if the gold atom were positioned on an inversion centre, i.e. the $[(CB_8H_{12})Au]$ component. In this instance, both halves of the molecule were detected, albeit with one half consisting of the superimposition of two oppositely orientated carbaborane fragments (see Figure 89, p.187). For both the *syn* and *anti* isomer one half of the molecule is identical. The superition of these two fragments gives perfect overlap, and the resultant auracarbaborane cage is easily resolved. This half of the anion is referred to in the text (Chapter 4, Section 1) as the ordered sub-unit. For the remaining halves of the *syn* and *anti* isomers, their superimposition produces an array of eighteen atoms that required disentanglement into two CB_8 cages, the disordered sub-units. This of course became apparent only after numerous unsuccessful attempts to refine the single *anti* conformation of the anion from this array of possible atom positions.

The dominance of the diffraction of X-rays by the gold atom has thus resulted in both the *syn* and *anti* conformations of the auraborane anion being located in crystallographically similar positions, with the two half occupancy gold positions found to be only 102 pm apart.

The superposition of two borane ligands resulting from the location of a central gold atom on an inversion centre has been found by Welch *et al*[205] for the *commo* auraboranes $[(B_{10}H_{12})Au(B_{10}H_{12})]^-$ and $[(B_{10}H_{12})Au(B_{10}H_{13})]^{2-}$.

The problems encountered in the X-ray crystallograpic study of gold phosphine cluster compounds has been noted in the literature[236], wherein the value of even partial structure elucidation is seen to be of benefit. The $B\text{-}H_{(terminal)}$ and B-H-B bridging hydrogens were not located.

$[(CB_9H_{11}Au)(AuPPh_3)_2(AuCB_9H_{12})_2]$ (11).

The $B\text{-}H_{(terminal)}$ and B-H-B bridging hydrogens were not located. One molecule of an organic solvent (linear - C_5 or C_6) was partially located but not refined.

[ARACHNO-6,9,9',6'-$(CB_9H_{12})Au(DPPE)Au(CB_9H_{12})$] (12).

The possible gold positions generated by the computer from the Patterson map were found to be inconsistent. An alternative gold atom position was therefore deduced from the cross-vector combinations calculated to produce the highest peaks in the observed Patterson map. A re-run Patterson map with this gold position included generated the required second gold atom position.

The $B\text{-}H_{(terminal)}$ and B-H-B bridging hydrogens were not located.

5.2.2. INTERATOMIC DISTANCES, INTERBOND ANGLES AND ATOMIC CO-ORDINATES.

The interatomic distances, interbond angles and atomic coordinates found from the X-ray crystallographic studies of compunds (1) to (6) and (10) to (12) are given in Tables 28 - 52. The data for compound (7), the closo osmacarbaborane have not been included because the refinement of this structure is not yet complete. The data for this compound will be published on completion.

The Tables 28 - 34 are those provided for publication (see Conference Papers and Publications, p. III) and consist of selected interatomic distances and bond angles. The Tables 35 to 52 inclusive are reproductions of the original X-ray publication tables generated from computer files of these individual X-ray studies. These have been used in preference to the previous format, in order to eliminate the possibility of typographical errors.

The atomic numbering scheme used for description of all of the structures of the prepared metallacarbaboranes in Chapters 4 and 5 of this thesis has been based on the atomic numbering system used for ruthenacarbaborane(1) (see Figure 59, p. 112). This consistent numbering enabled easy comparison of the carbaborane fragments of each cluster structure. During the crystallographic refinement procedure however, compounds (4) and (5) were assigned skeletal boron atom numbers that differ from this standard system. Thus when inspecting the Tables 35-40 the following atom numbering variation must be noted. The atoms identified as B(3),(1),(7),(5),(10),(8) and P(2),(1) in the Tables correspond to the atoms B(1),(3),(5),(7),(8),(10) and P(1),(2) respectively, used in the text (see Figures 72-73, p.140-141).

For the osmacarbaborane(2), the similar interchange of B(1,3)

and P(1,2) have been made from the original crystallographic numbering, but in this instance, the Tables 28-29 and 31 are those provided for publication, as noted earlier, and have been altered to conform to the standard numbering scheme.

The crystallographic numbering scheme used for the remaining compounds are as given in the text. Note that the numbering schemes used for the auracarbaboranes (10), (11) and (12) are the same as that used in the text, (Chapter 5) and conform to the standard scheme, albeit with the first and second carbaborane fragments being numbered as B(10x) and B(20x) respectively. In the case of compound (10), where three carbaborane fragments exist, these are denoted by B(10x), B(11x) and B(21x)

Discussion of the important interatomic distances and interbond angles can be found at the relevant parts of Chapters 3 and 4.

The units for the Isotropic Thermal Parameter, U, presented in Tables 37, 40, 43, 46, 49 and 52 are $Å^2 \times 10^3$.

Table 28. Selected interatomic distances (pm) with standard deviations in parenthesis, for [9,9,9-(CO)(PPh$_3$)$_2$-Nido-9,6-RuCB$_8$H$_{10}$-5-(PPh$_3$)] (1) and [9,9,9-(CO)(PPh$_3$)$_2$-Nido-9,6-OsCB$_8$H$_{10}$-5-(PPh$_3$)] (2).

Compound	(1)	(2)		(1)	(2)
a) From the Metal atom, (M = Ru, Os).					
M(9)-P(1)	233.9(5)	234.9(4)	M(9)-B(8)	227(2)	226(2)
M(9)-P(2)	239.8(5)	238.1(4)	M(9)-B(10)	236(2)	234(2)
M(9)-B(4)	227(2)	230(2)	M(9)-C(1)	190(2)	175(2)
b) Boron-boron					
B(1)-B(2)	178(3)	180(3)	B(3)-B(4)	190(3)	182(3)
B(1)-B(3)	179(3)	183(2)	B(3)-B(7)	169(3)	178(2)
B(1)-B(4)	178(3)	182(2)	B(3)-B(8)	175(3)	172(2)
B(1)-B(5)	174(3)	178(2)	B(4)-B(8)	186(3)	182(2)
B(1)-B(10)	170(3)	183(2)	B(4)-B(10)	185(3)	187(2)
B(2)-B(3)	172(3)	182(2)	B(5)-B(10)	185(3)	191(3)
B(2)-B(5)	182(3)	175(2)	B(7)-B(8)	194(3)	207(3)
B(2)-B(7)	186(3)	183(2)			
c) Boron-carbon					
C(6)-B(2)	175(3)	173(2)	C(6)-B(5)	154(3)	152(2)
C(6)-B(7)	157(3)	152(2)			
d) Phosporus-carbon					
P(1)-C(111)	183(2)	184(1)	P(1)-C(121)	183(2)	187(1)
P(1)-C(131)	187(2)	184(1)	P(2)-C(211)	185(2)	188(1)
P(2)-C(221)	178(2)	187(1)	P(2)-C(231)	188(2)	186(1)
P(3)-C(311)	182(2)	181(1)	P(3)-C(321)	182(2)	182(1)
P(3)-C(331)	180(2)	181(1)			
e) Others					
B(5)-P(3)	192(2)	197(1)	C(1)-O(1)	110(2)	122(2)

Table 29. Selected inter-bond angles (°), with standard deviations in parenthesis, for [9,9,9-(CO)(PPh$_3$)$_2$-Nido-9,6-RuCB$_8$H$_{10}$-5-(PPh$_3$)] (1) and [9,9,9-(CO)(PPh$_3$)$_2$-Nido-9,6-OsCB$_8$H$_{10}$-5-(PPh$_3$)] (2).

Compound	(1)	(2)		(1)	(2)
a) At the Metal atom, (M = Ru, Os).					
P(1)-M(9)-P(2)	99.8(2)	99.4(1)	B(4)-M(9)-B(8)	48.4(7)	47.0(6)
P(1)-M(9)-C(1)	89.5(6)	90.0(6)	B(4)-M(9)-B(10)	47.1(7)	47.5(5)
P(2)-M(9)-C(1)	97.3(5)	96.7(6)	B(8)-M(9)-B(10)	78.1(7)	78.8(6)
P(1)-M(9)-B(4)	100.0(5)	100.8(4)	P(2)-M(9)-B(4)	159.3(6)	158.5(5)
P(1)-M(9)-B(8)	86.6(6)	85.7(4)	P(2)-M(9)-B(8)	127.2(6)	128.1(5)
P(1)-M(9)-B(10)	145.2(5)	146.3(4)	P(2)-M(9)-B(10)	114.4(5)	113.8(4)
C(1)-RU(9)-B(4)	88.9(7)	90.6(8)	C(1)-RU(9)-B(8)	135.4(8)	135.1(7)
C(1)-RU(9)-B(10)	80.3(8)	80.7(7)			
b) About open face					
B(5)-C(6)-B(7)	114.6(19)	114.2(13)	C(6)-B(7)-B(8)	118.2(17)	117.8(12)
B(7)-B(8)-M(9)	120.2(11)	118.0(10)	B(8)-M(9)-B(10)	78.1(7)	78.8(6)
RU(9)-B(10)-B(5)	122.8(12)	122.3(10)	B(10)-B(5)-C(6)	117.4(16)	117.8(12)
c) Open face to cluster base					
M(9)-B(4)-B(1)	119.5(11)	122.2(10)	C(6)-B(2)-B(1)	98.4(14)	102.4(11)
M(9)-B(4)-B(3)	115.7(11)	116.2(10)	C(6)-B(2)-B(3)	98.3(15)	98.5(12)
B(5)-B(1)-B(10)	65.0(13)	63.8(9)	B(7)-B(3)-B(8)	68.5(13)	72.4(11)
d) Ligand to cluster					
P(3)-B(5)-B(1)	121.8(13)	118.9(10)	P(3)-B(5)-B(2)	118.6(13)	120.5(11)
P(3)-B(5)-C(6)	120.2(16)	120.8(11)	P(3)-B(5)-B(10)	116.2(12)	112.4(10)

Table 30. Final fractional coordinates (x 10^4), with standard deviations in parenthesis, for [9,9,9-(CO)(PPh_3)$_2$-*Nido*-9,6-$RuCB_8H_{10}$-5-(PPh_3)] (1).

Atom	X	Y	Z
Ru(9)	3276(1)	6436(1)	6091(1)
B(1)	4053(13)	8704(15)	5764(9)
B(2)	4651(13)	8547(16)	5215(8)
B(3)	3656(14)	8179(14)	5020(9)
B(4)	3169(13)	7977(13)	5695(8)
B(5)	4968(13)	8093(14)	5998(9)
C(6)	5087(14)	7418(12)	5471(8)
B(7)	4319(15)	7296(16)	4933(10)
B(8)	3297(14)	7005(14)	5140(9)
B(10)	4085(14)	7855(15)	6327(9)
P(1)	1982(3)	5841(3)	5650(2)
P(2)	3891(3)	4964(3)	6571(2)
P(3)	5886(3)	8693(3)	6540(2)
C(1)	2890(12)	6916(13)	6769(8)
O(1)	2671(9)	7284(10)	7137(6)
C(111)	1538(13)	4996(13)	6115(8)
C(112)	995(11)	4216(15)	5865(9)
C(113)	725(12)	3621(15)	6238(9)
C(114)	857(11)	3706(14)	6831(9)
C(115)	1338(12)	4471(13)	7115(8)
C(116)	1655(15)	5106(14)	6750(8)
C(121)	1876(11)	5147(11)	4935(7)
C(122)	2344(12)	4409(13)	4894(8)
C(123)	2297(15)	3808(14)	4375(9)
C(124)	1641(15)	3986(14)	3880(10)
C(125)	1090(15)	4738(16)	3921(9)
C(126)	1181(14)	5309(13)	4428(8)
C(131)	1165(11)	6784(12)	5462(7)
C(132)	1281(12)	7536(11)	5066(8)
C(133)	690(12)	8216(16)	4907(8)
C(134)	-13(17)	8187(15)	5096(10)
C(135)	-108(14)	7432(15)	5473(10)
C(136)	504(12)	6745(13)	5658(8)

Table 30 continued,

C(211)	4018(13)	4940(12)	7416(8)
C(212)	3893(15)	4123(15)	7730(9)
C(213)	4003(19)	4146(19)	8378(11)
C(214)	4224(23)	5045(19)	8680(10)
C(215)	4464(20)	5878(17)	8343(10)
C(216)	4316(14)	5770(12)	7730(8)
C(221)	4908(14)	4939(11)	6488(9)
C(222)	5159(12)	5220(12)	5964(9)
C(223)	5896(12)	5137(14)	5834(10)
C(224)	6534(19)	4722(14)	6329(11)
C(225)	6268(12)	4398(13)	6873(8)
C(226)	5575(12)	4524(14)	6928(9)
C(231)	3551(11)	3681(13)	6341(7)
C(232)	2933(14)	3264(13)	6497(8)
C(233)	2748(14)	2311(13)	6316(10)
C(234)	3113(12)	1789(14)	6024(8)
C(235)	3768(17)	2180(18)	5829(9)
C(236)	3990(15)	3153(14)	6001(8)
C(311)	6796(11)	8762(11)	6249(7)
C(312)	7524(15)	8450(15)	6592(9)
C(313)	8233(15)	8609(19)	6370(11)
C(314)	8219(13)	9133(15)	5813(10)
C(315)	7450(18)	9412(16)	5505(11)
C(316)	6771(13)	9241(13)	5722(9)
C(321)	6193(13)	8020(13)	7261(7)
C(322)	6535(14)	8517(15)	7821(8)
C(323)	6772(15)	7963(17)	8349(10)
C(324)	6696(14)	6993(16)	8382(11)
C(325)	6378(18)	6527(15)	7811(11)
C(326)	6095(19)	7023(16)	7280(10)
C(331)	5693(12)	9927(13)	6760(8)
C(332)	6175(16)	10699(14)	6669(10)
C(333)	6009(17)	11655(19)	6862(11)
C(334)	5393(14)	11788(12)	7169(9)
C(335)	4997(15)	11053(17)	7240(9)
C(336)	5125(14)	10090(14)	7038(9)

Table 31. Final fractional coordinates (x 10^4), with standard deviations in parenthesis, for [9,9,9-(CO)$(PPh_3)_2$-Nido-9,6-$OsCB_8H_{10}$-5-(PPh_3)] (2).

Atom	X	Y	Z
Os(9)	3273(1)	6453(1)	6090(1)
B(1)	4051(10)	8796(12)	5749(8)
B(2)	4667(10)	8546(14)	5217(7)
B(3)	3614(10)	8181(13)	5025(7)
B(4)	3179(11)	8007(12)	5681(8)
B(5)	4961(9)	8115(12)	5967(8)
C(6)	5087(9)	7425(10)	5467(6)
B(7)	4354(10)	7312(12)	4936(7)
B(8)	3261(10)	7035(12)	5146(8)
B(10)	4083(9)	7852(13)	6330(7)
P(1)	1983(2)	5839(3)	5644(2)
P(2)	3888(2)	4994(3)	6563(2)
P(3)	5889(2)	8704(3)	6550(2)
C(1)	2925(10)	6881(13)	6717(9)
O(1)	2695(7)	7267(9)	7134(5)
C(111)	1533(7)	4987(10)	6107(5)
C(112)	1045(8)	4219(10)	5846(6)
C(113)	726(9)	3584(12)	6197(6)
C(114)	856(9)	3698(11)	6802(7)
C(115)	1335(9)	4491(12)	7074(7)
C(116)	1683(9)	5131(12)	6724(7)
C(121)	1179(8)	6791(10)	5440(6)
C(122)	494(9)	6758(10)	5657(7)
C(123)	-108(10)	7456(12)	5490(8)
C(124)	-28(10)	8182(11)	5103(7)
C(125)	662(10)	8243(11)	4886(7)
C(126)	1262(9)	7544(11)	5053(6)
C(131)	1833(8)	5156(10)	4918(6)
C(132)	2388(9)	4430(11)	4886(6)
C(133)	2253(10)	3856(12)	4355(7)
C(134)	1595(9)	4018(11)	3865(6)
C(135)	1095(8)	4732(11)	3922(6)
C(136)	1199(8)	5303(10)	4431(6)

Table 31 continued,

C(211)	4954(8)	4926(10)	6476(7)
C(212)	5156(9)	5250(10)	5952(7)
C(213)	5922(9)	5118(12)	5864(8)
C(214)	6496(11)	4702(12)	6311(8)
C(215)	6334(10)	4402(12)	6852(10)
C(216)	5575(9)	4505(11)	6953(7)
C(221)	3565(9)	3719(10)	6317(7)
C(222)	3992(10)	3192(10)	5974(7)
C(223)	3756(10)	2245(11)	5811(7)
C(224)	3141(11)	1825(11)	5988(7)
C(225)	2703(11)	2322(12)	6316(8)
C(226)	2926(8)	3301(11)	6475(7)
C(231)	4029(9)	4963(11)	7411(6)
C(232)	32891(11)	4108(12)	7731(7)
C(233)	4024(15)	4161(16)	8363(8)
C(234)	4260(15)	5034(14)	8674(8)
C(235)	4412(13)	5843(14)	8360(8)
C(236)	4289(11)	5796(11)	7724(7)
C(311)	6782(8)	8782(9)	6247(6)
C(312)	6757(9)	9253(11)	5700(7)
C(313)	7434(9)	9403(13)	5483(7)
C(314)	8185(11)	9130(13)	5857(7)
C(315)	8242(9)	8635(13)	6376(7)
C(316)	7540(9)	8437(11)	6583(7)
C(321)	5728(9)	9960(10)	6768(6)
C(322)	5110(10)	10113(12)	7047(7)
C(323)	4977(10)	11073(12)	7247(8)
C(324)	5442(11)	11807(11)	7162(7)
C(325)	6046(14)	11646(12)	6863(9)
C(326)	6172(10)	10761(11)	6677(8)
C(331)	6196(8)	8050(11)	7266(6)
C(332)	6139(11)	7038(12)	7274(7)
C(333)	6418(11)	6522(13)	7822(7)
C(334)	6712(9)	6990(13)	8352(7)
C(335)	6770(11)	7975(14)	8359(8)
C(336)	6509(9)	8502(12)	7815(6)

Table 32. Selected interatomic distances (pm), with standard deviations in parenthesis, for [9,9,9-(η-C_5H_5)(H)(PPh_3)-*arachno*-9,6-$RuCB_8H_{12}$] (3).

a) From the ruthenium atom

Ru(9)-P(1)	231.1(1)	Ru(9)-C(55)	219.3(5)
Ru(9)-C(51)	222.2(5)	Ru(9)-B(4)	225.2(5)
Ru(9)-C(52)	229.8(5)	Ru(9)-B(8)	231.6(5)
Ru(9)-C(53)	228.5(5)	Ru(9)-B(10)	230.3(6)
Ru(9)-C(54)	222.4(5)		

b) Boron-boron

B(1)-B(2)	172.0(10)	B(3)-B(4)	176.6(9)
B(1)-B(3)	178.0(10)	B(3)-B(7)	177.4(9)
B(1)-B(4)	178.0(10)	B(3)-B(8)	178.8(9)
B(1)-B(5)	180.7(9)	B(4)-B(8)	176.1(7)
B(1)-B(10)	178.6(9)	B(4)-B(10)	178.2(8)
B(2)-B(3)	172.3(11)	B(5)-B(10)	190.4(10)
B(2)-B(5)	176.9(10)	B(7)-B(8)	186.3(11)
B(2)-B(7)	177.4(10)		

c) Boron-carbon

C(6)-B(2)	166.0(7)	C(6)-B(5)	171.2(9)
C(6)-B(7)	173.6(10)		

d) Phosphorus-carbon

P(1)-C(111)	183.6(5)	P(1)-C(121)	183.1(4)
P(1)-C(131)	184.5(4)		

Table 33. Selected inter-bond angles (°), with standard deviations in parenthesis, for [9,9,9-(η-C_5H_5)(H)(PPh$_3$)-*arachno*-9,6-$RuCB_8H_{12}$] (3).

a) At the ruthenium atom

P(1)-Ru(9)-C(51)	96.2(2)	B(4)-Ru(9)-B(8)	45.3(2)
P(1)-Ru(9)-C(52)	127.4(2)	B(4)-Ru(9)-B(10)	46.1(2)
P(1)-Ru(9)-C(53)	155.0(2)	B(8)-Ru(9)-B(10)	78.9(2)
P(1)-Ru(9)-C(54)	127.4(2)	B(4)-Ru(9)-C(51)	149.1(2)
P(1)-Ru(9)-C(55)	95.8(1)	B(4)-Ru(9)-C(52)	126.8(2)
P(1)-Ru(9)-B(4)	79.7(2)	B(4)-Ru(9)-C(53)	124.6(2)
P(1)-Ru(9)-B(8)	89.8(2)	B(4)-Ru(9)-C(54)	143.5(3)
P(1)-Ru(9)-B(10)	111.9(1)	B(4)-Ru(9)-C(55)	172.5(2)

b) About open face

B(5)-C(6)-B(7)	110.7(4)	C(6)-B(7)-B(8)	115.9(5)
B(7)-B(8)-Ru(9)	122.1(3)	B(8)-Ru(9)-B(10)	78.9(2)
Ru(9)-B(10)-B(5)	121.3(*)	B(10)-B(5)-C(6)	115.6(*)
B(5)-H(510)-B(10)	89.3(29)	B(7)-B(78)-B(8)	87.9(22)
C(6)-B(5)-H(510)	93.0(23)	C(6)-B(7)-H(78)	94.7(19)
Ru(9)-B(10)-H(510)	88.2(25)	Ru(9)-B(8)-H(78)	87.4(20)
B(2)-C(6)-H(61)	108.7(25)	B(5)-C(6)-H(61)	118.6(29)
B(7)-C(6)-H(61)	117.6(29)	B(2)-C(6)-H(62)	143.3(50)
B(5)-C(6)-H(62)	93.2(41)	B(7)-C(6)-H(62)	105.5(50)
H(61)-C(6)-H(62)	107.2(57)		

c) Open face to cluster base

Ru(9)-B(4)-B(1)	124.0(3)	C(6)-B(2)-B(1)	111.3(5)
Ru(9)-B(4)-B(3)	125.1(3)	C(6)-B(2)-B(3)	112.9(5)
B(5)-B(1)-B(10)	64.0(4)	B(7)-B(3)-B(8)	63.1(4)

Table 34. Final fractional coordinates (x 10^4), with standard deviations in parenthesis, for [9,9,9-(η-C_5H_5)(H)(PPh_3)-*arachno*-9,6-$RuCB_8H_{12}$] (3).

Atom	X	Y	Z
Ru(9)	2226(1)	7212(1)	7709(1)
B(1)	5178(5)	7461(5)	8387(4)
B(2)	5262(5)	8288(5)	7572(4)
B(3)	4683(5)	8572(4)	8471(4)
B(4)	3928(5)	7635(4)	8683(4)
B(5)	4834(6)	7201(5)	7093(4)
C(6)	4318(5)	8173(4)	6469(4)
B(7)	4043(6)	8966(4)	7253(5)
B(8)	3192(5)	8563(4)	8021(4)
B(10)	4012(5)	6730(4)	7891(4)
P(1)	1901(1)	7325(1)	9204(1)
C(51)	513(4)	7591(4)	6786(4)
C(52)	1210(5)	7857(4)	6241(4)
C(53)	1723(5)	7076(4)	6037(3)
C(54)	1340(5)	6338(4)	6441(4)
C(55)	584(4)	6657(4)	6900(3)
C(111)	481(4)	6968(3)	9112(3)
C(112)	-421(4)	7544(4)	9001(4)
C(113)	-1474(4)	7221(4)	8844(4)
C(114)	-1677(4)	6318(4)	8811(4)
C(115)	-801(4)	5727(3)	8945(4)
C(116)	257(4)	6047(3)	9100(3)
C(121)	2009(4)	8449(3)	9754(3)

Table 34 continued.

C(122)	2745(4)	8664(3)	10660(4)
C(123)	2805(4)	9541(4)	11019(4)
C(124)	2136(6)	10198(4)	10482(4)
C(125)	1385(5)	9998(3)	9565(4)
C(126)	1336(4)	9138(3)	9199(4)
C(131)	2678(4)	6578(3)	10220(3)
C(132)	2445(4)	6597(3)	11106(3)
C(133)	2988(4)	6003(3)	11857(3)
C(134)	3740(4)	5386(3)	11737(3)
C(135)	3958(4)	5355(3)	10846(4)
C(136)	3448(4)	5949(3)	10107(3)
H(01)	5919(46)	7255(33)	8886(41)
H(02)	5993(41)	8536(31)	7536(34)
H(03)	5112(44)	9007(37)	9065(40)
H(04)	4008(38)	7517(30)	9412(33)
H(05)	5363(44)	6720(37)	6812(38)
H(61)	4640(39)	8390(32)	5969(34)
H(62)	3609(63)	7903(48)	6125(58)
H(07)	4051(42)	9653(32)	7118(37)
H(08)	2831(35)	9102(29)	8341(29)
H(10)	4199(36)	6001(30)	8058(31)
H(78)	2933(34)	8664(29)	7107(31)
H(510)	3789(45)	6836(39)	6922(40)

Table 35. Interatomic distances (pm), with standard deviations in parenthesis, for [9,9,9-(CO)(PPh$_3$)$_2$-*nido*-9,6-RuCB$_8$H$_9$-3-Cl-5-(PPh$_3$)] (4).

Ru(9)-P(1)	2.366(4)	Ru(9)-P(2)	2.368(6)
Ru(9)-C(1)	1.806(25)	Ru(9)-B(4)	2.268(17)
Ru(9)-B(8)	2.293(23)	Ru(9)-B(10)	2.316(22)
P(1)-C(111)	1.842(24)	P(1)-C(121)	1.879(20)
P(1)-C(131)	1.898(24)	P(2)-C(211)	1.873(23)
P(2)-C(221)	1.791(19)	P(2)-C(231)	1.803(16)
P(3)-B(7)	1.965(26)	P(3)-C(311)	1.794(25)
P(3)-C(321)	1.784(16)	P(3)-C(331)	1.826(21)
Cl(1)-B(1)	1.883(19)	Cl(11)-C(10)	1.932(45)
Cl(12)-C(10)	1.651(55)	C(1)-O(1)	1.177(31)
B(1)-B(2)	1.748(41)	B(1)-B(3)	1.748(33)
B(1)-B(4)	1.852(37)	B(1)-B(5)	1.774(32)
B(1)-B(10)	1.774(38)	B(2)-B(3)	1.811(44)
B(2)-B(5)	1.878(32)	B(2)-C(6)	1.668(23)
B(2)-B(7)	1.788(33)	B(3)-B(4)	1.833(39)
B(3)-B(7)	1.776(33)	B(3)-B(8)	1.795(33)
B(4)-B(8)	1.816(27)	B(4)-B(10)	1.862(28)
B(5)-C(6)	1.548(38)	C(6)-B(7)	1.558(31)
B(7)-B(8)	1.896(44)	C(111)-C(112)	1.427(35)
C(111)-C(116)	1.336(48)	C(112)-C(113)	1.419(52)
C(113)-C(114)	1.432(63)	C(114)-C(115)	1.333(83)
C(115)-C(116)	1.389(54)	C(121)-C(122)	1.334(23)
C(121)-C(126)	1.294(26)	C(122)-C(123)	1.446(34)
C(123)-C(124)	1.432(35)	C(124)-C(125)	1.318(29)
C(125)-C(126)	1.368(34)	C(131)-C(132)	1.486(37)
C(131)-C(136)	1.331(21)	C(132)-C(133)	1.383(39)
C(133)-C(134)	1.458(25)	C(134)-C(135)	1.385(41)
C(135)-C(136)	1.488(37)	C(211)-C(212)	1.378(31)
C(211)-C(216)	1.332(26)	C(212)-C(213)	1.451(39)
C(213)-C(214)	1.295(34)	C(214)-C(215)	1.343(37)
C(215)-C(216)	1.445(36)	C(221)-C(222)	1.344(30)
C(221)-C(226)	1.431(29)	C(222)-C(223)	1.443(32)
C(223)-C(224)	1.376(39)	C(224)-C(225)	1.386(33)
C(225)-C(226)	1.357(28)	C(231)-C(232)	1.392(36)
C(231)-C(236)	1.278(33)	C(232)-C(233)	1.278(29)
C(233)-C(234)	1.297(48)	C(234)-C(235)	1.376(47)
C(235)-C(236)	1.525(27)	C(311)-C(312)	1.356(36)
C(311)-C(316)	1.314(28)	C(312)-C(313)	1.353(49)
C(313)-C(314)	1.292(37)	C(314)-C(315)	1.351(49)
C(315)-C(316)	1.483(45)	C(321)-C(322)	1.317(31)
C(321)-C(325)	1.583(39)	C(322)-C(323)	1.417(24)
C(323)-C(324)	1.376(40)	C(324)-C(326)	1.396(36)
C(325)-C(326)	1.388(26)	C(331)-C(332)	1.416(27)
C(331)-C(336)	1.321(27)	C(332)-C(333)	1.332(35)
C(333)-C(334)	1.310(31)	C(334)-C(335)	1.462(32)
C(335)-C(336)	1.336(37)		

Table 36. Interbond angles (°), with standard deviations in parenthesis, for [9,9,9-(CO)$(PPh_3)_2$-nido-9,6-$RuCB_8H_9$-3-Cl-5-(PPh_3)] (4).

P(1)-Ru(9)-P(2)	100.6(2)	P(1)-Ru(9)-C(1)	91.6(5)
P(2)-Ru(9)-C(1)	92.4(8)	P(1)-Ru(9)-B(4)	159.6(6)
P(2)-Ru(9)-B(4)	98.9(5)	C(1)-Ru(9)-B(4)	93.8(8)
P(1)-Ru(9)-B(8)	114.6(5)	P(2)-Ru(9)-B(8)	144.6(5)
C(1)-Ru(9)-B(8)	82.8(10)	B(4)-Ru(9)-B(8)	46.9(7)
P(1)-Ru(9)-B(10)	128.9(5)	P(2)-Ru(9)-B(10)	83.8(6)
C(1)-Ru(9)-B(10)	139.4(7)	B(4)-Ru(9)-B(10)	47.9(7)
B(8)-Ru(9)-B(10)	78.5(8)	Ru(9)-P(1)-C(111)	120.6(6)
Ru(9)-P(1)-C(121)	114.6(5)	C(111)-P(1)-C(121)	102.6(10)
Ru(9)-P(1)-C(131)	115.1(7)	C(111)-P(1)-C(131)	101.8(10)
C(121)-P(1)-C(131)	100.0(9)	Ru(9)-P(2)-C(211)	119.8(6)
Ru(9)-P(2)-C(221)	116.7(8)	C(211)-P(2)-C(221)	102.8(9)
Ru(9)-P(2)-C(231)	111.7(7)	C(211)-P(2)-C(231)	101.2(10)
C(221)-P(2)-C(231)	103.2(8)	B(7)-P(3)-C(311)	111.9(10)
B(7)-P(3)-C(321)	109.3(9)	C(311)-P(3)-C(321)	106.8(11)
B(7)-P(3)-C(331)	114.8(12)	C(311)-P(3)-C(331)	108.4(9)
C(321)-P(3)-C(331)	106.8(9)	C1(11)-C(10)-C1(12)	105.8(22)
Ru(9)-C(1)-O(1)	172.5(17)	C1(1)-B(1)-B(2)	114.7(15)
C1(1)-B(1)-B(3)	121.3(12)	B(2)-B(1)-B(3)	62.4(16)
C1(1)-B(1)-B(4)	114.7(15)	B(2)-B(1)-B(4)	118.1(16)
B(3)-B(1)-B(4)	61.1(15)	C1(1)-B(1)-B(5)	119.5(15)
B(2)-B(1)-B(5)	64.1(14)	B(3)-B(1)-B(5)	110.5(16)
B(4)-B(1)-B(5)	116.4(14)	C1(1)-B(1)-B(10)	113.8(14)
B(2)-B(1)-B(10)	123.4(14)	B(3)-B(1)-B(10)	112.0(16)
B(4)-B(1)-B(10)	61.8(13)	B(5)-B(1)-B(10)	67.6(14)
B(1)-B(2)-B(3)	58.8(15)	B(1)-B(2)-B(5)	58.6(13)
B(3)-B(2)-B(5)	103.6(20)	B(1)-B(2)-C(6)	98.1(17)
B(3)-B(2)-C(6)	102.3(18)	B(5)-B(2)-C(6)	51.2(11)
B(1)-B(2)-B(7)	99.2(20)	B(3)-B(2)-B(7)	59.3(15)
B(5)-B(2)-B(7)	53.4(14)	C(6)-B(2)-B(7)	53.6(12)
B(1)-B(3)-B(2)	58.8(15)	B(1)-B(3)-B(4)	62.2(14)
B(2)-B(3)-B(4)	115.9(16)	B(1)-B(3)-B(7)	99.3(16)
B(2)-B(3)-B(7)	53.5(14)	B(4)-B(3)-B(7)	110.3(15)
B(1)-B(3)-B(8)	106.0(16)	B(2)-B(3)-B(8)	116.8(15)
B(4)-B(3)-B(8)	60.1(13)	B(7)-B(3)-B(8)	64.1(14)
Ru(9)-B(4)-B(1)	117.8(10)	Ru(9)-B(4)-B(3)	121.2(11)
B(1)-B(4)-B(3)	56.6(14)	Ru(9)-B(4)-B(8)	67.3(8)
B(1)-B(4)-B(8)	101.0(17)	B(3)-B(4)-B(8)	58.9(12)
Ru(9)-B(4)-B(10)	67.4(8)	B(1)-B(4)-B(10)	57.1(12)
B(3)-B(4)-B(10)	104.4(17)	B(8)-B(4)-B(10)	104.8(13)
B(1)-B(5)-B(2)	57.3(14)	B(1)-B(5)-C(6)	102.8(17)
B(2)-B(5)-C(6)	57.6(12)	B(2)-C(6)-B(5)	71.2(13)
B(2)-C(6)-B(7)	66.9(13)	B(5)-C(6)-B(7)	118.2(19)
P(3)-B(7)-B(2)	121.2(19)	P(3)-B(7)-B(3)	124.1(13)
B(2)-B(7)-B(3)	61.2(15)	P(3)-B(7)-C(6)	118.6(19)
B(2)-B(7)-C(6)	59.5(12)	B(3)-B(7)-C(6)	108.7(16)
P(3)-B(7)-B(8)	115.9(14)	B(2)-B(7)-B(8)	112.6(18)

Table 36 continued

B(3)-B(7)-B(8)	58.4(15)	C(6)-B(7)-B(8)	117.3(19)
Ru(9)-B(8)-B(3)	121.7(13)	Ru(9)-B(8)-B(4)	65.8(9)
B(3)-B(8)-B(4)	61.8(13)	Ru(9)-B(8)-B(7)	121.7(12)
B(3)-B(8)-B(7)	57.4(14)	B(4)-B(8)-B(7)	105.8(16)
Ru(9)-B(10)-B(1)	119.8(12)	Ru(9)-B(10)-B(4)	64.7(9)
B(1)-B(10)-B(4)	61.2(12)	P(1)-C(111)-C(112)	119.7(21)
P(1)-C(111)-C(116)	119.2(20)	C(112)-C(111)-C(116)	121.1(25)
C(111)-C(112)-C(113)	113.3(28)	C(112)-C(113)-C(114)	116.7(38)
C(113)-C(114)-C(115)	124.3(44)	C(114)-C(115)-C(116)	125.5(48)
C(111)-C(116)-C(115)	118.5(34)	P(1)-C(121)-C(122)	117.1(15)
P(1)-C(121)-C(126)	118.9(12)	C(122)-C(121)-C(126)	123.7(19)
C(121)-C(122)-C(123)	118.4(20)	C(122)-C(123)-C(124)	113.4(18)
C(123)-C(124)-C(125)	126.1(25)	C(124)-C(125)-C(126)	114.9(23)
C(121)-C(126)-C(125)	123.3(17)	P(1)-C(131)-C(132)	117.5(12)
P(1)-C(131)-C(136)	122.1(20)	C(132)-C(131)-C(136)	120.4(22)
C(131)-C(132)-C(133)	119.5(16)	C(132)-C(133)-C(134)	120.4(25)
C(133)-C(134)-C(135)	117.1(25)	C(134)-C(135)-C(136)	121.1(17)
C(131)-C(136)-C(135)	121.3(23)	P(2)-C(211)-C(212)	117.8(15)
P(2)-C(211)-C(216)	122.1(17)	C(212)-C(211)-C(216)	119.9(22)
C(211)-C(212)-C(213)	116.4(19)	C(212)-C(213)-C(214)	123.5(24)
C(213)-C(214)-C(215)	120.2(25)	C(214)-C(215)-C(216)	118.3(20)
C(211)-C(216)-C(215)	121.5(20)	P(2)-C(221)-C(222)	121.6(17)
P(2)-C(221)-C(226)	120.7(14)	C(222)-C(221)-C(226)	117.5(18)
C(221)-C(222)-C(223)	121.0(23)	C(222)-C(223)-C(224)	119.7(22)
C(223)-C(224)-C(225)	119.5(21)	C(224)-C(225)-C(226)	120.1(23)
C(221)-C(226)-C(225)	122.2(19)	P(2)-C(231)-C(232)	124.4(15)
P(2)-C(231)-C(236)	121.2(19)	C(232)-C(231)-C(236)	114.3(18)
C(231)-C(232)-C(233)	126.7(27)	C(232)-C(233)-C(234)	119.3(33)
C(233)-C(234)-C(235)	124.5(21)	C(234)-C(235)-C(236)	111.2(22)
C(231)-C(236)-C(235)	124.0(26)	P(3)-C(311)-C(312)	123.5(15)
P(3)-C(311)-C(316)	123.2(20)	C(312)-C(311)-C(316)	113.2(25)
C(311)-C(312)-C(313)	124.3(20)	C(312)-C(313)-C(314)	118.7(30)
C(313)-C(314)-C(315)	123.2(34)	C(314)-C(315)-C(316)	114.1(27)
C(311)-C(316)-C(315)	126.3(28)	P(3)-C(321)-C(322)	121.3(19)
P(3)-C(321)-C(325)	121.4(15)	C(322)-C(321)-C(325)	117.3(16)
C(321)-C(322)-C(323)	124.6(24)	C(322)-C(323)-C(324)	116.3(22)
C(323)-C(324)-C(326)	120.4(18)	C(321)-C(325)-C(326)	117.7(24)
C(324)-C(326)-C(325)	123.7(28)	P(3)-C(331)-C(332)	120.9(15)
P(3)-C(331)-C(336)	121.8(17)	C(332)-C(331)-C(336)	117.3(21)
C(331)-C(332)-C(333)	123.5(19)	C(332)-C(333)-C(334)	118.2(22)
C(333)-C(334)-C(335)	120.2(23)	C(334)-C(335)-C(336)	118.3(20)
C(331)-C(336)-C(335)	122.8(20)		

Table 37. Final fractional coordinates ($\times 10^4$), with standard deviations in parenthesis, for [9,9,9-(CO)(PPh_3)$_2$-*nido*-9,6-$RuCB_8H_9$-3-Cl-5-(PPh_3)] (4).

	x	y	z	U
Ru(9)	1673(1)	2019(1)	2698(1)	40(1)*
P(1)	3619(4)	3873(5)	2928(2)	54(3)*
P(2)	491(4)	2292(4)	3457(2)	46(3)*
P(3)	3368(5)	-52(5)	1174(2)	55(3)*
Cl(1)	-963(5)	-2470(5)	2822(3)	73(3)*
Cl(11)	1397(16)	3476(12)	9713(8)	155(10)*
Cl(12)	114(13)	4447(17)	9058(8)	158(11)*
C(10)	1196(34)	4091(33)	8943(17)	62(11)
C(1)	1122(20)	2614(18)	2101(10)	61(13)*
O(1)	691(15)	2872(14)	1677(7)	88(11)*
B(1)	510(20)	-1112(18)	2614(10)	51(12)*
B(2)	1551(21)	-1439(22)	2255(11)	62(14)*
B(3)	739(20)	-829(22)	1828(11)	63(14)*
B(4)	266(16)	67(17)	2315(8)	48(8)*
B(5)	1975(19)	-600(20)	3068(11)	68(13)*
C(6)	2899(17)	-195(16)	2558(9)	58(11)*
B(7)	2411(22)	-99(21)	1888(10)	68(14)*
B(8)	1578(19)	784(19)	1843(10)	48(6)
B(10)	1012(19)	227(18)	3128(9)	46(5)
C(111)	3726(16)	5158(17)	3412(12)	83(12)*
C(112)	4078(19)	5331(23)	4077(12)	128(16)*
C(113)	4055(21)	6316(34)	4398(16)	195(24)*
C(114)	3645(24)	6979(25)	4086(27)	323(40)*
C(115)	3493(36)	6841(26)	3517(29)	334(42)*
C(116)	3464(21)	5989(19)	3137(15)	110(16)*
C(121)	4378(14)	4570(16)	2282(10)	68(8)*
C(122)	5388(19)	5682(21)	2298(11)	89(14)*
C(123)	6892(20)	6177(25)	1768(13)	123(18)*
C(124)	5531(24)	5403(25)	1183(12)	118(21)*
C(125)	4584(21)	4318(21)	1186(13)	101(15)*
C(126)	3951(18)	3920(18)	1656(9)	67(12)*
C(131)	4945(17)	3772(19)	3336(8)	58(12)*
C(132)	4759(18)	2613(20)	3368(10)	78(13)*
C(133)	5744(20)	2497(20)	3614(12)	99(15)*
C(134)	6946(19)	3565(22)	3871(12)	101(15)*
C(135)	7057(20)	4678(20)	3842(11)	94(14)*
C(136)	6047(16)	4766(18)	3584(10)	74(11)*
C(211)	485(16)	3735(16)	3554(8)	51(10)*
C(212)	257(19)	4150(19)	3818(9)	76(14)*
C(213)	207(21)	5244(18)	3111(11)	84(15)*
C(214)	349(18)	5813(17)	3664(13)	81(13)*
C(215)	584(19)	5416(18)	4189(10)	70(13)*
C(216)	612(16)	4313(16)	4121(9)	60(11)*
C(221)	836(16)	2128(15)	4259(8)	54(10)*
C(222)	2(20)	1884(18)	4685(10)	74(13)*
C(223)	328(23)	1819(20)	5338(11)	95(16)*
C(224)	1509(21)	2049(19)	5532(10)	87(15)*

Table 37 continued

C(225)	2372(21)	2299(19)	5093(18)	83(13)*
C(226)	2858(16)	2331(17)	4478(8)	59(11)*
C(231)	-1174(17)	1198(16)	3286(8)	58(10)*
C(232)	-2019(20)	1368(22)	2915(11)	104(15)*
C(233)	-3195(22)	607(26)	2763(17)	197(23)*
C(234)	-3693(20)	-458(31)	2958(11)	141(22)*
C(235)	-3058(20)	-838(21)	3329(13)	99(15)*
C(236)	-1659(20)	150(22)	3472(135)	96(16)*
C(311)	3322(17)	-1448(17)	998(7)	56(11)*
C(312)	3586(22)	-2818(23)	1442(9)	108(20)*
C(313)	3615(26)	-3032(25)	1313(11)	118(22)*
C(314)	3323(25)	-3547(24)	736(14)	117(20)*
C(315)	2995(28)	-3110(22)	251(16)	126(21)*
C(316)	3055(22)	-2015(22)	423(11)	101(17)*
C(321)	4987(17)	1094(18)	1376(8)	53(11)*
C(322)	5317(18)	2107(19)	1738(10)	67(12)*
C(323)	6578(20)	3071(21)	1895(10)	85(14)*
C(324)	7503(19)	2912(21)	1663(11)	101(14)*
C(325)	6829(21)	950(22)	1143(11)	83(15)*
C(326)	7185(21)	1831(21)	1305(10)	86(15)*
C(331)	2854(19)	318(18)	447(8)	62(12)*
C(332)	1572(18)	-350(21)	186(10)	86(13)*
C(333)	1154(22)	-158(23)	-357(9)	97(17)*
C(334)	1983(25)	636(24)	-687(10)	110(21)*
C(335)	3305(22)	1397(23)	-423(11)	99(18)*
C(336)	3658(22)	1188(21)	135(10)	86(16)*

* Equivalent isotropic U defined as one third of the trace of the orthogonalised U_{ij} tensor

Table 38. Interatomic distances (pm), with standard deviations in parenthesis, for [9,9,9-(CO)(PPh$_3$)$_2$-nido-9,6-RuCB$_8$H$_9$-7-Cl-5-(PPh$_3$)] (5).

Ru-P(1)	2.337(4)	Ru-P(2)	2.398(4)
Ru-C(1)	1.840(11)	Ru-B(4)	2.287(13)
Ru-B(8)	2.337(15)	Ru-B(10)	2.230(12)
Ru-H(001)	1.603(96)	Ru-H(002)	1.534(148)
P(1)-C(111)	1.835(11)	P(1)-C(121)	1.832(14)
P(1)-C(131)	1.834(11)	P(2)-C(211)	1.855(12)
P(2)-C(221)	1.831(12)	P(2)-C(231)	1.826(15)
P(3)-B(7)	1.921(18)	P(3)-C(311)	1.809(13)
P(3)-C(321)	1.801(13)	P(3)-C(331)	1.801(12)
Cl(1)-B(5)	1.798(13)	C(1)-O(1)	1.174(14)
B(1)-B(2)	1.753(27)	B(1)-B(3)	1.821(24)
B(1)-B(4)	1.794(17)	B(1)-B(5)	1.738(24)
B(1)-B(10)	1.750(22)	B(1)-H(01)	1.078(123)
B(2)-B(3)	1.761(20)	B(2)-B(5)	1.783(21)
B(2)-C(6)	1.675(20)	B(2)-B(7)	1.810(21)
B(2)-H(02)	1.214(117)	B(3)-B(4)	1.795(25)
B(3)-B(7)	1.754(27)	B(3)-B(8)	1.794(20)
B(3)-H(03)	1.144(111)	B(4)-B(8)	1.825(23)
B(4)-B(10)	1.821(18)	B(4)-H(04)	1.313(129)
B(5)-C(6)	1.582(25)	B(5)-B(10)	1.978(23)
C(6)-B(7)	1.556(17)	C(6)-H(06)	0.758(134)
B(7)-B(8)	1.872(21)	B(8)-H(08)	1.143(106)
B(8)-H(002)	1.458(120)	B(10)-H(010)	1.101(138)
B(10)-H(001)	1.278(131)	C(111)-C(112)	1.392(15)
C(111)-C(116)	1.407(20)	C(112)-C(113)	1.367(17)
C(113)-C(114)	1.397(20)	C(114)-C(115)	1.378(15)
C(115)-C(116)	1.356(17)	C(121)-C(122)	1.396(18)
C(121)-C(126)	1.361(17)	C(122)-C(123)	1.370(23)
C(123)-C(124)	1.343(20)	C(124)-C(125)	1.391(21)
C(125)-C(126)	1.372(21)	C(131)-C(132)	1.396(20)
C(131)-C(136)	1.374(15)	C(132)-C(133)	1.362(17)
C(133)-C(134)	1.338(22)	C(134)-C(135)	1.388(25)
C(135)-C(136)	1.379(18)	C(211)-C(212)	1.364(20)
C(211)-C(216)	1.376(16)	C(212)-C(213)	1.402(21)
C(213)-C(214)	1.343(22)	C(214)-C(215)	1.399(26)
C(215)-C(216)	1.375(21)	C(221)-C(222)	1.369(21)
C(221)-C(226)	1.385(18)	C(222)-C(223)	1.380(19)
C(223)-C(224)	1.345(27)	C(224)-C(225)	1.347(29)
C(225)-C(226)	1.372(18)	C(231)-C(232)	1.383(15)
C(231)-C(236)	1.370(24)	C(232)-C(233)	1.398(22)
C(233)-C(234)	1.383(34)	C(234)-C(235)	1.333(25)
C(235)-C(236)	1.347(29)	C(311)-C(312)	1.406(17)
C(311)-C(316)	1.371(22)	C(312)-C(313)	1.396(21)
C(313)-C(314)	1.347(29)	C(314)-C(315)	1.356(21)
C(315)-C(316)	1.385(22)	C(321)-C(322)	1.374(21)
C(321)-C(326)	1.395(21)	C(322)-C(323)	1.379(20)
C(323)-C(324)	1.363(24)	C(324)-C(325)	1.370(23)
C(325)-C(326)	1.361(21)	C(331)-C(332)	1.385(19)
C(331)-C(336)	1.379(19)	C(332)-C(333)	1.354(19)
C(333)-C(334)	1.382(22)	C(334)-C(335)	1.356(26)
C(335)-C(336)	1.413(23)		

Table 39. Interbond angles (°), with standard deviations in parenthesis, for [9,9,9-(CO)(PPh_3)$_2$-nido-9,6-$RuCB_8H_9$-7-Cl-5-(PPh_3)] (5).

P(1)-Ru-P(2)	99.6(1)	P(1)-Ru-C(1)	98.9(5)
P(2)-Ru-C(1)	97.0(4)	P(1)-Ru-B(4)	101.4(5)
P(2)-Ru-B(4)	158.0(5)	C(1)-Ru-B(4)	89.0(5)
P(1)-Ru-B(8)	146.2(4)	P(2)-Ru-B(8)	113.7(4)
C(1)-Ru-B(8)	79.9(5)	B(4)-Ru-B(8)	46.5(6)
P(1)-Ru-B(10)	85.2(5)	P(2)-Ru-B(10)	128.9(4)
C(1)-Ru-B(10)	133.9(6)	B(4)-Ru-B(10)	47.5(5)
B(8)-Ru-B(10)	78.5(5)	P(1)-Ru-H(001)	94.8(49)
P(2)-Ru-H(001)	94.9(45)	C(1)-Ru-H(001)	165.8(44)
B(4)-Ru-H(001)	77.1(44)	B(8)-Ru-H(001)	88.2(46)
B(10)-Ru-H(001)	34.3(46)	P(1)-Ru-H(002)	166.9(48)
P(2)-Ru-H(002)	81.2(47)	C(1)-Ru-H(002)	102.8(37)
B(4)-Ru-H(002)	76.9(47)	B(8)-Ru-H(002)	37.5(45)
B(10)-Ru-H(002)	84.3(41)	H(001)-Ru-H(002)	72.1(61)
Ru-P(1)-C(111)	116.3(5)	Ru-P(1)-C(121)	114.7(5)
C(111)-P(1)-C(121)	101.5(6)	Ru-P(1)-C(131)	116.5(5)
C(111)-P(1)-C(131)	102.5(5)	C(121)-P(1)-C(131)	103.2(6)
Ru-P(2)-C(211)	126.4(5)	Ru-P(2)-C(221)	113.2(5)
C(211)-P(2)-C(221)	104.8(5)	Ru-P(2)-C(231)	108.2(4)
C(211)-P(2)-C(231)	99.7(6)	C(221)-P(2)-C(231)	102.2(7)
B(7)-P(3)-C(311)	111.8(6)	B(7)-P(3)-C(321)	114.1(7)
C(311)-P(3)-C(321)	105.9(6)	B(7)-P(3)-C(331)	113.7(6)
C(311)-P(3)-C(331)	105.4(6)	C(321)-P(3)-C(331)	105.3(6)
Ru-C(1)-O(1)	173.8(13)	B(2)-B(1)-B(3)	59.0(9)
B(2)-B(1)-B(4)	113.7(12)	B(3)-B(1)-B(4)	59.5(9)
B(2)-B(1)-B(5)	61.4(10)	B(3)-B(1)-B(5)	103.9(13)
B(4)-B(1)-B(5)	114.1(11)	B(2)-B(1)-B(10)	121.9(13)
B(3)-B(1)-B(10)	109.7(10)	B(4)-B(1)-B(10)	61.8(8)
B(5)-B(1)-B(10)	69.1(10)	B(2)-B(1)-H(01)	117.3(67)
B(3)-B(1)-H(01)	137.2(66)	B(4)-B(1)-H(01)	123.7(64)
B(5)-B(1)-H(01)	110.8(61)	B(10)-B(1)-H(01)	106.4(70)
B(1)-B(2)-B(3)	62.4(10)	B(1)-B(2)-B(5)	58.9(10)
B(3)-B(2)-B(5)	104.5(11)	B(1)-B(2)-C(6)	100.2(11)
B(3)-B(2)-C(6)	102.1(10)	B(5)-B(2)-C(6)	51.4(9)
B(1)-B(2)-B(7)	102.4(10)	B(3)-B(2)-B(7)	58.8(9)
B(5)-B(2)-B(7)	92.8(9)	C(6)-B(2)-B(7)	52.8(7)
B(1)-B(2)-H(02)	126.1(69)	B(3)-B(2)-H(02)	118.1(51)
B(5)-B(2)-H(02)	133.6(53)	C(6)-B(2)-H(02)	128.2(64)
B(7)-B(2)-H(02)	124.1(64)	B(1)-B(3)-B(2)	58.6(9)
B(1)-B(3)-B(4)	59.5(9)	B(2)-B(3)-B(4)	113.2(11)
B(1)-B(3)-B(7)	101.9(10)	B(2)-B(3)-B(7)	62.8(9)
B(4)-B(3)-B(7)	111.8(11)	B(1)-B(3)-B(8)	105.5(11)
B(2)-B(3)-B(8)	116.5(11)	B(4)-B(3)-B(8)	61.1(9)
B(7)-B(3)-B(8)	63.7(9)	B(1)-B(3)-H(03)	121.4(71)
B(2)-B(3)-H(03)	127.2(58)	B(4)-B(3)-H(03)	104.6(73)
B(7)-B(3)-H(03)	133.8(78)	B(8)-B(3)-H(03)	113.6(52)
Ru-B(4)-B(1)	117.9(8)	Ru-B(4)-B(3)	122.9(11)
B(1)-B(4)-B(3)	61.0(9)	Ru-B(4)-B(8)	68.2(6)

Table 39 continued

B(1)-B(4)-B(8)	105	3(11)	B(3)-B(4)-B(8)	59	4(9)
Ru-B(4)-B(10)	64	6(6)	B(1)-B(4)-B(10)	57	9(8)
B(3)-B(4)-B(10)	107	7(10)	B(8)-B(4)-B(10)	105	8(10)
Ru-B(4)-H(04)	112	9(55)	B(1)-B(4)-H(04)	115	7(46)
B(3)-B(4)-H(04)	116	9(68)	B(8)-B(4)-H(04)	129	8(47)
B(10)-B(4)-H(04)	121	8(56)	C1(1)-B(5)-B(1)	124	3(12)
C1(1)-B(5)-B(2)	127	5(9)	B(1)-B(5)-B(2)	59	7(10)
C1(1)-B(5)-C(6)	122	8(12)	B(1)-B(5)-C(6)	106	4(11)
B(2)-B(5)-C(6)	60	6(10)	C1(1)-B(5)-B(10)	111	7(10)
B(1)-B(5)-B(10)	55	7(9)	B(2)-B(5)-B(10)	108	9(10)
C(6)-B(5)-B(10)	117	3(9)	B(2)-C(6)-B(5)	68	8(10)
B(2)-C(6)-B(7)	68	1(9)	B(5)-C(6)-B(7)	116	6(13)
B(2)-C(6)-H(06)	112	1(91)	B(5)-C(6)-H(06)	122	8(98)
B(7)-C(6)-H(06)	115	8(94)	P(3)-B(7)-B(2)	119	2(9)
P(3)-B(7)-B(3)	121	3(9)	B(2)-B(7)-B(3)	59	2(9)
P(3)-B(7)-C(6)	119	4(12)	B(2)-B(7)-C(6)	59	1(8)
B(3)-B(7)-C(6)	107	6(12)	P(3)-B(7)-B(8)	118	5(8)
B(2)-B(7)-B(8)	110	4(12)	B(3)-B(7)-B(8)	59	2(9)
C(6)-B(7)-B(8)	116	2(12)	Ru-B(8)-B(3)	120	2(9)
Ru-B(8)-B(4)	65	3(6)	B(3)-B(8)-B(4)	59	4(9)
Ru-B(8)-B(7)	122	8(7)	B(3)-B(8)-B(7)	57	1(9)
B(4)-B(8)-B(7)	104	6(9)	Ru-B(8)-H(08)	118	5(61)
B(3)-B(8)-H(08)	111	8(61)	B(4)-B(8)-H(08)	126	6(72)
B(7)-B(8)-H(08)	111	7(67)	Ru-B(8)-H(002)	39	8(55)
B(3)-B(8)-H(002)	126	8(40)	B(4)-B(8)-H(002)	95	7(56)
B(7)-B(8)-H(002)	91	8(45)	H(08)-B(8)-H(002)	120	8(75)
Ru-B(10)-B(1)	123	8(9)	Ru-B(10)-B(4)	67	9(5)
B(1)-B(10)-B(4)	60	3(7)	Ru-B(10)-B(5)	120	9(10)
B(1)-B(10)-B(5)	55	2(8)	B(4)-B(10)-B(5)	102	5(10)
Ru-B(10)-H(010)	124	5(58)	B(1)-B(10)-H(010)	106	8(59)
B(4)-B(10)-H(010)	128	4(64)	B(5)-B(10)-H(010)	107	2(61)
Ru-B(10)-H(001)	44	9(43)	B(1)-B(10)-H(001)	131	7(62)
B(4)-B(10)-H(001)	105	1(49)	B(5)-B(10)-H(001)	89	5(53)
H(010)-B(10)-H(001)	116	2(85)	Ru-H(001)-B(10)	100	9(73)
Ru-H(002)-B(8)	103	7(79)	P(1)-C(111)-C(112)	120	8(10)
P(1)-C(111)-C(116)	121	6(8)	C(112)-C(111)-C(116)	117	6(10)
C(111)-C(112)-C(113)	121	6(13)	C(112)-C(113)-C(114)	119	7(11)
C(113)-C(114)-C(115)	118	9(11)	C(114)-C(115)-C(116)	121	5(13)
C(111)-C(116)-C(115)	120	5(11)	P(1)-C(121)-C(122)	122	5(9)
P(1)-C(121)-C(126)	121	9(10)	C(122)-C(121)-C(126)	115	6(13)
C(121)-C(122)-C(123)	121	2(11)	C(122)-C(123)-C(124)	121	6(14)
C(123)-C(124)-C(125)	119	2(16)	C(124)-C(125)-C(126)	118	1(12)
C(121)-C(126)-C(125)	124	3(13)	P(1)-C(131)-C(132)	122	7(9)
P(1)-C(131)-C(136)	120	5(10)	C(132)-C(131)-C(136)	116	7(10)
C(131)-C(132)-C(133)	121	4(13)	C(132)-C(133)-C(134)	120	9(15)
C(133)-C(134)-C(135)	120	8(13)	C(134)-C(135)-C(136)	119	2(14)
C(131)-C(136)-C(135)	121	7(14)	P(2)-C(211)-C(212)	120	2(9)
P(2)-C(211)-C(216)	121	2(10)	C(212)-C(211)-C(216)	118	4(11)
C(211)-C(212)-C(213)	119	9(12)	C(212)-C(213)-C(214)	121	9(16)
C(213)-C(214)-C(215)	118	2(16)	C(214)-C(215)-C(216)	119	9(14)
C(211)-C(216)-C(215)	121	6(13)	P(2)-C(221)-C(222)	117	4(10)
P(2)-C(221)-C(226)	125	9(10)	C(222)-C(221)-C(226)	116	6(12)

Table 39 continued

C(221)-C(222)-C(223)	119.3(14)	C(222)-C(223)-C(224)	122.3(16)
C(223)-C(224)-C(225)	120.0(15)	C(224)-C(225)-C(226)	118.1(16)
C(221)-C(226)-C(225)	123.3(14)	P(2)-C(231)-C(232)	120.2(12)
P(2)-C(231)-C(236)	122.7(9)	C(232)-C(231)-C(236)	116.9(14)
C(231)-C(232)-C(233)	120.9(16)	C(232)-C(233)-C(234)	118.6(14)
C(233)-C(234)-C(235)	119.9(22)	C(234)-C(235)-C(236)	121.3(22)
C(231)-C(236)-C(235)	122.3(13)	P(3)-C(311)-C(312)	119.3(11)
P(3)-C(311)-C(316)	122.5(8)	C(312)-C(311)-C(316)	118.2(12)
C(311)-C(312)-C(313)	120.1(15)	C(312)-C(313)-C(314)	119.6(14)
C(313)-C(314)-C(315)	121.2(17)	C(314)-C(315)-C(316)	120.3(18)
C(311)-C(316)-C(315)	120.5(12)	P(3)-C(321)-C(322)	127.6(11)
P(3)-C(321)-C(326)	115.3(10)	C(322)-C(321)-C(326)	117.0(12)
C(321)-C(322)-C(323)	120.0(15)	C(322)-C(323)-C(324)	121.6(15)
C(323)-C(324)-C(325)	119.5(13)	C(324)-C(325)-C(326)	118.8(15)
C(321)-C(326)-C(325)	123.0(15)	P(3)-C(331)-C(332)	119.7(9)
P(3)-C(331)-C(336)	121.2(11)	C(332)-C(331)-C(336)	119.0(12)
C(331)-C(332)-C(333)	121.3(13)	C(332)-C(333)-C(334)	120.1(15)
C(333)-C(334)-C(335)	120.1(15)	C(334)-C(335)-C(336)	120.0(16)
C(331)-C(336)-C(335)	119.3(15)		

Table 40. Final fractional coordinates (x 10^4), with standard deviations in parenthesis, for [9,9,9-(CO)$(PPh_3)_2$-nido-9,6-$RuCB_8H_9$-7-Cl-5-(PPh_3)] (5).

	x	y	z	U
Ru	2395(1)	6583(1)	6283(1)	25(1)Å
P(1)	3781(2)	5891(2)	5714(1)	31(1)Å
P(2)	2800(2)	5038(2)	6655(1)	31(1)Å
P(3)	911(2)	8772(2)	6716(1)	34(1)Å
Cl(1)	243(2)	7060(4)	4480(2)	82(2)Å
C(1)	3975(8)	6915(9)	6838(6)	41(6)Å
O(1)	4682(6)	7245(8)	7210(4)	76(5)Å
B(1)	1777(10)	8352(13)	5238(7)	48(7)Å
B(2)	362(10)	8695(10)	5429(7)	42(7)Å
B(3)	2019(11)	8876(12)	5963(7)	51(8)Å
B(4)	2764(9)	8080(10)	5859(6)	32(6)Å
B(5)	970(10)	7521(11)	5128(6)	42(7)Å
C(6)	728(6)	7611(9)	5633(5)	41(6)Å
B(7)	1336(10)	8218(10)	6183(6)	41(7)Å
B(8)	2493(8)	7985(10)	6489(5)	31(6)Å
B(10)	2159(9)	7154(11)	5315(6)	34(6)Å
C(111)	4604(7)	4992(9)	6130(5)	31(5)Å
C(112)	5085(7)	5082(10)	6746(5)	43(6)Å
C(113)	5685(8)	4405(10)	7066(6)	48(6)Å
C(114)	5869(8)	3639(9)	6768(5)	43(6)Å
C(115)	5398(8)	3547(11)	6157(5)	47(6)Å
C(116)	4783(8)	4199(10)	5840(6)	49(6)Å
C(121)	4399(7)	6805(9)	5528(5)	34(5)Å
C(122)	5275(8)	6725(9)	5717(6)	48(7)Å
C(123)	5708(9)	7374(11)	5528(7)	61(8)Å
C(124)	5317(10)	8141(11)	5188(7)	64(8)Å
C(125)	4447(8)	8259(9)	4989(5)	49(5)Å
C(126)	4032(9)	7580(10)	5167(5)	43(6)Å
C(131)	3178(7)	5273(9)	4997(5)	34(5)Å
C(132)	3355(7)	5399(9)	4508(5)	36(6)Å
C(133)	2917(8)	4961(11)	3980(6)	57(7)Å
C(134)	2310(10)	4262(12)	3932(6)	63(7)Å
C(135)	2126(9)	4093(11)	4415(6)	55(7)Å
C(136)	2545(8)	4622(9)	4934(5)	46(6)Å
C(211)	2795(8)	3777(8)	6381(5)	36(6)Å
C(212)	3540(8)	3338(10)	6470(6)	48(6)Å
C(213)	3531(10)	2375(11)	6263(7)	61(8)Å
C(214)	2801(11)	1895(12)	5949(7)	71(10)Å
C(215)	2035(11)	2368(12)	5835(7)	76(9)Å
C(216)	2044(8)	3297(9)	6047(5)	43(6)Å
C(221)	3491(9)	4963(9)	7459(6)	49(7)Å
C(222)	3562(12)	5768(11)	7793(7)	88(10)Å
C(223)	4110(13)	5768(12)	8399(6)	114(12)Å
C(224)	4548(15)	4966(17)	8675(8)	127(13)Å
C(225)	4451(14)	4131(14)	8365(6)	120(11)Å
C(226)	3904(10)	4133(10)	7767(6)	78(8)Å

Table 40 continued

C(231)	1742(8)	5072(8)	6639(6)	35(6)*
C(232)	1054(8)	5399(10)	6133(6)	50(7)*
C(233)	237(8)	5406(10)	6108(8)	73(8)*
C(234)	125(13)	5054(13)	6594(10)	98(13)*
C(235)	788(12)	4710(12)	7071(9)	84(11)*
C(236)	1576(10)	4711(9)	7095(7)	53(7)*
C(311)	-237(7)	8733(8)	6399(5)	35(5)*
C(312)	-714(9)	9226(11)	5858(6)	57(7)*
C(313)	-1681(10)	9219(11)	5613(7)	62(8)*
C(314)	-1996(11)	8748(11)	5981(7)	83(9)*
C(315)	-1549(11)	8244(12)	6413(7)	83(10)*
C(316)	-668(9)	8252(9)	6671(6)	48(7)*
C(321)	1199(9)	10838(9)	6304(6)	48(6)*
C(322)	665(10)	10886(11)	6829(7)	68(8)*
C(323)	996(12)	11732(9)	6998(7)	88(10)*
C(324)	1851(10)	11895(11)	7262(6)	70(8)*
C(325)	2398(11)	11127(12)	7358(7)	65(8)*
C(326)	2071(11)	10218(10)	7182(6)	60(8)*
C(331)	1270(7)	8147(8)	7424(5)	36(6)*
C(332)	1274(8)	8638(10)	7917(5)	46(6)*
C(333)	1485(9)	8165(11)	8446(6)	62(7)*
C(334)	1721(11)	7194(12)	8506(7)	81(9)*
C(335)	1728(13)	6698(13)	8032(7)	103(12)*
C(336)	1502(11)	7177(10)	7478(7)	79(10)*
H(01)	1732(69)	8684(90)	4804(48)	70
H(02)	507(72)	9485(87)	5247(50)	70
H(03)	2379(73)	9603(86)	6109(50)	70
H(04)	3443(68)	8488(93)	5853(48)	70
H(06)	276(74)	7586(87)	5593(51)	70
H(08)	2661(78)	8193(86)	6966(49)	70
H(010)	2186(73)	6965(86)	4890(51)	70
H(081)	2838(68)	6439(90)	5626(49)	70
H(083)	2306(72)	6867(86)	6366(49)	70

* Equivalent isotropic U defined as one third of the trace of the orthogonalised U_{ij} tensor

Table 41. Interatomic distances (pm), with standard deviations in parenthesis, for [2,2,2-(CO)(PPh$_3$)$_2$-*closo*-2,1-RuCB$_8$H$_8$-10-(PPh$_3$)] (6).

Ru(2)-P(1)	2	384(3)	Ru(2)-P(2)	2	387(2)
Ru(2)-C(1)	2	115(10)	Ru(2)-C(21)	1	865(10)
Ru(2)-B(3)	2	310(12)	Ru(2)-B(5)	2	323(11)
Ru(2)-B(7)	2	302(11)	Ru(2)-B(6)	2	325(9)
P(1)-C(111)	1	846(11)	P(1)-C(121)	1	819(8)
P(1)-C(131)	1	830(11)	P(2)-C(211)	1	851(12)
P(2)-C(221)	1	821(10)	P(2)-C(231)	1	847(10)
P(3)-B(10)	1	886(10)	P(3)-C(311)	1	807(11)
P(3)-C(321)	1	796(10)	P(3)-C(331)	1	802(9)
C(1)-B(3)	1	572(17)	C(1)-B(4)	1	618(13)
C(1)-B(5)	1	638(14)	C(1)-H(01)	0	911(9)
C(21)-O(21)	1	146(13)	B(3)-B(4)	1	845(17)
B(3)-B(7)	1	853(15)	B(3)-B(8)	1	858(13)
B(3)-H(03)	1	160(12)	B(4)-B(5)	1	872(18)
B(4)-B(8)	1	755(18)	B(4)-B(9)	1	761(16)
B(4)-H(04)	1	206(13)	B(5)-B(9)	1	852(15)
B(5)-B(6)	1	835(16)	B(5)-H(05)	1	457(13)
B(7)-B(8)	1	871(16)	B(7)-B(10)	1	698(13)
B(7)-H(07)	1	115(13)	B(8)-B(9)	1	854(18)
B(8)-B(10)	1	673(15)	B(8)-H(08)	1	143(12)
B(9)-B(6)	1	825(16)	B(9)-B(10)	1	679(18)
B(9)-H(09)	1	092(11)	B(6)-B(10)	1	688(15)
B(6)-H(06)	1	157(10)	C(111)-C(112)	1	373(12)
C(111)-C(116)	1	386(17)	C(112)-C(113)	1	385(16)
C(113)-C(114)	1	339(17)	C(114)-C(115)	1	357(14)
C(115)-C(116)	1	398(18)	C(121)-C(122)	1	411(15)
C(121)-C(126)	1	378(14)	C(122)-C(123)	1	383(13)
C(123)-C(124)	1	311(15)	C(124)-C(125)	1	446(17)
C(125)-C(126)	1	398(13)	C(131)-C(132)	1	408(14)
C(131)-C(136)	1	388(16)	C(132)-C(133)	1	371(18)
C(133)-C(134)	1	336(19)	C(134)-C(135)	1	362(18)
C(135)-C(136)	1	363(19)	C(211)-C(212)	1	349(15)
C(211)-C(216)	1	356(15)	C(212)-C(213)	1	402(19)
C(213)-C(214)	1	368(22)	C(214)-C(215)	1	388(22)
C(215)-C(216)	1	358(22)	C(221)-C(222)	1	395(16)
C(221)-C(226)	1	399(14)	C(222)-C(223)	1	391(17)
C(223)-C(224)	1	352(20)	C(224)-C(225)	1	368(20)
C(225)-C(226)	1	383(16)	C(231)-C(232)	1	373(15)
C(231)-C(236)	1	369(14)	C(232)-C(233)	1	411(18)
C(233)-C(234)	1	346(18)	C(234)-C(235)	1	347(22)
C(235)-C(236)	1	393(19)	C(311)-C(312)	1	381(13)
C(311)-C(316)	1	386(16)	C(312)-C(313)	1	390(18)
C(313)-C(314)	1	388(26)	C(314)-C(315)	1	404(20)
C(315)-C(316)	1	368(19)	C(321)-C(322)	1	361(17)
C(321)-C(326)	1	372(17)	C(322)-C(323)	1	476(20)
C(323)-C(324)	1	279(21)	C(324)-C(325)	1	348(22)
C(325)-C(326)	1	379(23)	C(331)-C(332)	1	345(17)
C(331)-C(336)	1	373(17)	C(332)-C(333)	1	384(15)
C(333)-C(334)	1	357(21)	C(334)-C(335)	1	382(24)
C(335)-C(336)	1	372(17)			

Table 42. Interbond angles (°), with standard deviations in parenthesis, for [2,2,2-(CO)$(PPh_3)_2$-*closo*-2,1-$RuCB_8H_8$-10-(PPh_3)] (6).

P(1)-Ru(2)-P(2)	96.9(1)	P(1)-Ru(2)-C(1)	96.0(3)
P(2)-Ru(2)-C(1)	99.2(2)	P(1)-Ru(2)-C(21)	91.0(3)
P(2)-Ru(2)-C(21)	98.0(3)	C(1)-Ru(2)-C(21)	160.5(3)
P(1)-Ru(2)-B(3)	136.5(3)	P(2)-Ru(2)-B(3)	85.3(3)
C(1)-Ru(2)-B(3)	41.3(4)	C(21)-Ru(2)-B(3)	131.9(4)
P(1)-Ru(2)-B(5)	85.9(3)	P(2)-Ru(2)-B(5)	142.0(3)
C(1)-Ru(2)-B(5)	43.0(4)	C(21)-Ru(2)-B(5)	119.9(4)
B(3)-Ru(2)-B(5)	67.9(4)	P(1)-Ru(2)-B(7)	159.3(3)
P(2)-Ru(2)-B(7)	103.8(3)	C(1)-Ru(2)-B(7)	81.1(4)
C(21)-Ru(2)-B(7)	85.9(4)	B(3)-Ru(2)-B(7)	47.4(4)
B(5)-Ru(2)-B(7)	78.0(4)	P(1)-Ru(2)-B(6)	109.7(3)
P(2)-Ru(2)-B(6)	153.3(3)	C(1)-Ru(2)-B(6)	81.0(3)
C(21)-Ru(2)-B(6)	79.5(4)	B(3)-Ru(2)-B(6)	77.2(4)
B(5)-Ru(2)-B(6)	46.5(4)	B(7)-Ru(2)-B(6)	49.6(4)
Ru(2)-P(1)-C(111)	116.3(3)	Ru(2)-P(1)-C(121)	121.5(4)
C(111)-P(1)-C(121)	98.2(4)	Ru(2)-P(1)-C(131)	114.3(3)
C(111)-P(1)-C(131)	102.1(5)	C(121)-P(1)-C(131)	101.3(4)
Ru(2)-P(2)-C(211)	118.3(3)	Ru(2)-P(2)-C(221)	113.1(3)
C(211)-P(2)-C(221)	102.4(5)	Ru(2)-P(2)-C(231)	123.4(3)
C(211)-P(2)-C(231)	91.8(5)	C(221)-P(2)-C(231)	104.2(4)
B(10)-P(3)-C(311)	113.1(5)	B(10)-P(3)-C(321)	110.7(4)
C(311)-P(3)-C(321)	105.1(5)	B(10)-P(3)-C(331)	115.3(5)
C(311)-P(3)-C(331)	106.0(5)	C(321)-P(3)-C(331)	105.9(5)
Ru(2)-C(1)-B(3)	76.0(6)	Ru(2)-C(1)-B(4)	120.8(7)
B(3)-C(1)-B(4)	70.6(7)	Ru(2)-C(1)-B(5)	75.3(6)
B(3)-C(1)-B(5)	107.4(7)	B(4)-C(1)-B(5)	70.2(7)
Ru(2)-C(1)-H(01)	126.9(7)	B(3)-C(1)-H(01)	106.8(9)
B(4)-C(1)-H(01)	108.9(9)	B(5)-C(1)-H(01)	143.8(11)
Ru(2)-C(21)-O(21)	171.4(7)	Ru(2)-B(3)-C(1)	62.7(5)
Ru(2)-B(3)-B(4)	102.5(7)	C(1)-B(3)-B(4)	55.8(6)
Ru(2)-B(3)-B(7)	66.1(5)	C(1)-B(3)-B(7)	114.0(8)
B(4)-B(3)-B(7)	108.9(7)	Ru(2)-B(3)-B(8)	114.3(6)
C(1)-B(3)-B(8)	108.5(8)	B(4)-B(3)-B(8)	56.6(6)
B(7)-B(3)-B(8)	60.6(6)	Ru(2)-B(3)-H(03)	132.9(7)
C(1)-B(3)-H(03)	125.3(9)	B(4)-B(3)-H(03)	119.8(9)
B(7)-B(3)-H(03)	119.7(10)	B(8)-B(3)-H(03)	106.1(8)
C(1)-B(4)-B(3)	53.5(6)	C(1)-B(4)-B(5)	55.4(6)
B(3)-B(4)-B(5)	88.2(7)	C(1)-B(4)-B(8)	111.5(9)
B(3)-B(4)-B(8)	62.1(6)	B(5)-B(4)-B(8)	105.1(8)
C(1)-B(4)-B(9)	111.9(9)	B(3)-B(4)-B(9)	104.9(8)
B(5)-B(4)-B(9)	61.2(6)	B(8)-B(4)-B(9)	63.7(7)
C(1)-B(4)-H(04)	115.2(9)	B(3)-B(4)-H(04)	126.4(9)
B(5)-B(4)-H(04)	131.6(10)	B(8)-B(4)-H(04)	128.2(9)
B(9)-B(4)-H(04)	124.4(8)	Ru(2)-B(5)-C(1)	61.7(5)
Ru(2)-B(5)-B(4)	101.2(6)	C(1)-B(5)-B(4)	54.4(6)
Ru(2)-B(5)-B(9)	113.6(7)	C(1)-B(5)-B(9)	106.6(8)
B(4)-B(5)-B(9)	56.5(6)	Ru(2)-B(5)-B(6)	66.8(5)
C(1)-B(5)-B(6)	112.3(9)	B(4)-B(5)-B(6)	99.6(8)
B(9)-B(5)-B(6)	59.3(6)	Ru(2)-B(5)-H(05)	124.9(6)

Table 42 continued

C(1)-B(5)-H(05)	110.8(8)	B(4)-B(5)-H(05)	117.5(8)
B(9)-B(5)-H(05)	120.1(8)	B(6)-B(5)-H(05)	134.3(8)
Ru(2)-B(7)-B(3)	66.5(5)	Ru(2)-B(7)-B(8)	114.1(7)
B(3)-B(7)-B(8)	59.9(6)	Ru(2)-B(7)-B(10)	119.2(7)
B(3)-B(7)-B(10)	109.6(8)	B(8)-B(7)-B(10)	55.7(6)
Ru(2)-B(7)-H(07)	109.2(7)	B(3)-B(7)-H(07)	117.3(8)
B(8)-B(7)-H(07)	127.6(10)	B(10)-B(7)-H(07)	122.5(9)
B(3)-B(8)-B(4)	61.3(6)	B(3)-B(8)-B(7)	59.6(6)
B(4)-B(8)-B(7)	103.6(8)	B(3)-B(8)-B(9)	100.8(8)
B(4)-B(8)-B(9)	58.3(7)	B(7)-B(8)-B(9)	91.0(7)
B(3)-B(8)-B(10)	110.4(7)	B(4)-B(8)-B(10)	110.4(9)
B(7)-B(8)-B(10)	56.9(6)	B(9)-B(8)-B(10)	56.6(7)
B(3)-B(8)-H(08)	121.9(9)	B(4)-B(8)-H(08)	130.8(10)
B(7)-B(8)-H(08)	119.8(10)	B(9)-B(8)-H(08)	135.5(8)
B(10)-B(8)-H(08)	112.1(8)	B(4)-B(9)-B(5)	62.3(6)
B(4)-B(9)-B(8)	58.0(7)	B(5)-B(9)-B(8)	102.0(7)
B(4)-B(9)-B(6)	104.2(7)	B(5)-B(9)-B(6)	59.9(6)
B(8)-B(9)-B(6)	91.7(7)	B(4)-B(9)-B(10)	109.8(9)
B(5)-B(9)-B(10)	111.2(8)	B(8)-B(9)-B(10)	56.3(7)
B(6)-B(9)-B(10)	57.4(6)	B(4)-B(9)-H(09)	117.0(10)
B(5)-B(9)-H(09)	128.6(11)	B(8)-B(9)-H(09)	128.7(10)
B(6)-B(9)-H(09)	132.9(10)	B(10)-B(9)-H(09)	121.5(9)
Ru(2)-B(6)-B(5)	66.7(4)	Ru(2)-B(6)-B(9)	114.6(6)
B(5)-B(6)-B(9)	60.8(6)	Ru(2)-B(6)-B(10)	118.5(6)
B(5)-B(6)-B(10)	111.6(8)	B(9)-B(6)-B(10)	57.0(7)
Ru(2)-B(6)-H(06)	119.9(7)	B(5)-B(6)-H(06)	137.6(10)
B(9)-B(6)-H(06)	124.9(7)	B(10)-B(6)-H(06)	101.1(7)
P(3)-B(10)-B(7)	122.5(8)	P(3)-B(10)-B(8)	128.3(8)
B(7)-B(10)-B(8)	67.4(6)	P(3)-B(10)-B(9)	133.8(6)
B(7)-B(10)-B(9)	103.7(7)	B(8)-B(10)-B(9)	67.2(7)
P(3)-B(10)-B(6)	127.9(7)	B(7)-B(10)-B(6)	70.8(6)
B(8)-B(10)-B(6)	103.6(7)	B(9)-B(10)-B(6)	65.6(7)
P(1)-C(111)-C(112)	120.6(8)	P(1)-C(111)-C(116)	120.9(7)
C(112)-C(111)-C(116)	118.3(10)	C(111)-C(112)-C(113)	120.2(10)
C(112)-C(113)-C(114)	121.5(9)	C(113)-C(114)-C(115)	119.6(11)
C(114)-C(115)-C(116)	120.2(11)	C(111)-C(116)-C(115)	120.0(9)
P(1)-C(121)-C(122)	118.0(7)	P(1)-C(121)-C(126)	124.9(8)
C(122)-C(121)-C(126)	117.1(8)	C(121)-C(122)-C(123)	120.3(9)
C(122)-C(123)-C(124)	122.3(11)	C(123)-C(124)-C(125)	120.4(9)
C(124)-C(125)-C(126)	116.3(10)	C(121)-C(126)-C(125)	123.2(10)
P(1)-C(131)-C(132)	118.2(8)	P(1)-C(131)-C(136)	124.7(8)
C(132)-C(131)-C(136)	117.1(10)	C(131)-C(132)-C(133)	120.5(10)
C(132)-C(133)-C(134)	121.7(11)	C(133)-C(134)-C(135)	118.3(12)
C(134)-C(135)-C(136)	122.3(12)	C(131)-C(136)-C(135)	120.1(11)
P(2)-C(211)-C(212)	118.1(8)	P(2)-C(211)-C(216)	124.4(9)
C(212)-C(211)-C(216)	116.7(11)	C(211)-C(212)-C(213)	122.3(11)
C(212)-C(213)-C(214)	119.9(13)	C(213)-C(214)-C(215)	117.5(15)
C(214)-C(215)-C(216)	120.4(14)	C(211)-C(216)-C(215)	123.2(12)
P(2)-C(221)-C(222)	119.6(7)	P(2)-C(221)-C(226)	122.3(8)
C(222)-C(221)-C(226)	117.5(10)	C(221)-C(222)-C(223)	121.5(11)
C(222)-C(223)-C(224)	119.7(12)	C(223)-C(224)-C(225)	120.2(13)
C(224)-C(225)-C(226)	121.4(12)	C(221)-C(226)-C(225)	119.6(11)
P(2)-C(231)-C(232)	120.6(7)	P(2)-C(231)-C(236)	121.1(9)

Table 42 continued

C(232)-C(231)-C(236)	117.9(10)	C(231)-C(232)-C(233)	120.3(10)
C(232)-C(233)-C(234)	120.2(13)	C(233)-C(234)-C(235)	120.1(13)
C(234)-C(235)-C(236)	120.3(11)	C(231)-C(236)-C(235)	121.2(12)
P(3)-C(311)-C(312)	122.4(9)	P(3)-C(311)-C(316)	117.6(7)
C(312)-C(311)-C(316)	119.8(10)	C(311)-C(312)-C(313)	119.5(12)
C(312)-C(313)-C(314)	119.8(12)	C(313)-C(314)-C(315)	121.0(14)
C(314)-C(315)-C(316)	117.9(15)	C(311)-C(316)-C(315)	121.6(10)
P(3)-C(321)-C(322)	121.2(8)	P(3)-C(321)-C(326)	120.3(9)
C(322)-C(321)-C(326)	118.5(11)	C(321)-C(322)-C(323)	120.0(12)
C(322)-C(323)-C(324)	117.4(14)	C(323)-C(324)-C(325)	123.0(15)
C(324)-C(325)-C(326)	121.1(14)	C(321)-C(326)-C(325)	119.5(12)
P(3)-C(331)-C(332)	122.3(9)	P(3)-C(331)-C(336)	120.3(9)
C(332)-C(331)-C(336)	117.3(10)	C(331)-C(332)-C(333)	122.9(12)
C(332)-C(333)-C(334)	117.6(14)	C(333)-C(334)-C(335)	122.4(12)
C(334)-C(335)-C(336)	116.8(15)	C(331)-C(336)-C(335)	123.0(14)

Table 43. Final fractional coordinates (x 10^4), with standard deviations in parenthesis, for [2,2,2-(CO)$(PPh_3)_2$-*closo*-2,1-$RuCB_8H_8$-10-(PPh_3)] (6).

	x	y	z	U
Ru(2)	6432(1)	6124(1)	6817(1)	24(1)*
P(1)	7501(2)	5580(1)	6892(2)	31(1)*
P(2)	7726(2)	6453(1)	8281(2)	32(1)*
P(3)	2987(2)	6646(1)	4057(2)	34(1)*
C(1)	5381(7)	5926(3)	7869(8)	34(3)*
C(21)	6910(7)	6286(3)	5503(8)	37(4)*
O(21)	7071(6)	6376(3)	4619(6)	62(3)*
B(3)	5110(8)	6345(4)	7743(9)	35(4)*
B(4)	4053(9)	5981(4)	7468(11)	41(4)*
B(5)	4907(8)	5739(4)	6577(10)	35(4)*
B(7)	4988(9)	6525(4)	6235(9)	34(4)*
B(8)	3711(8)	6402(4)	6760(9)	36(4)*
B(9)	3574(8)	5967(4)	5927(10)	39(4)*
B(6)	4801(8)	6068(3)	5371(8)	31(4)*
B(10)	3780(8)	6374(3)	5349(9)	28(4)*
C(111)	7588(8)	5364(3)	5466(8)	41(4)*
C(112)	6609(8)	5397(4)	4532(8)	51(4)*
C(113)	6599(9)	5219(4)	3484(9)	51(4)*
C(114)	7466(9)	5021(3)	3340(9)	50(4)*
C(115)	8342(9)	4969(4)	4264(11)	62(5)*
C(116)	8375(9)	5142(4)	5340(10)	68(6)*
C(121)	8989(7)	5579(3)	7511(8)	33(3)*
C(122)	9641(8)	5840(3)	7895(8)	44(4)*
C(123)	10777(7)	5847(3)	7526(9)	43(4)*
C(124)	11286(8)	5628(4)	8364(9)	53(5)*
C(125)	10684(8)	5339(3)	8786(10)	50(4)*
C(126)	9536(7)	5336(3)	8345(9)	43(4)*
C(131)	7848(7)	5205(3)	7701(8)	32(3)*
C(132)	7834(7)	5262(3)	8882(8)	38(4)*
C(133)	6639(9)	4997(4)	9507(10)	62(5)*
C(134)	6271(9)	4677(4)	9023(10)	54(5)*
C(135)	6313(10)	4615(4)	7885(11)	65(5)*
C(136)	6683(8)	4871(4)	7221(10)	58(4)*
C(211)	7304(7)	6903(3)	8749(8)	39(4)*
C(212)	6876(8)	7149(3)	7988(10)	44(4)*
C(213)	6781(10)	7514(4)	8170(13)	72(6)*
C(214)	6969(12)	7631(4)	9313(14)	86(7)*
C(215)	7379(15)	7374(5)	10175(14)	108(8)*
C(216)	7545(11)	7025(4)	9876(10)	64(5)*
C(221)	8132(7)	6209(3)	9671(8)	43(4)*
C(222)	7368(9)	6157(4)	10356(8)	55(4)*
C(223)	7583(10)	5931(4)	11338(9)	65(5)*
C(224)	8575(12)	5762(5)	11656(10)	94(7)*
C(225)	9356(10)	5812(4)	11013(9)	67(5)*
C(226)	9140(9)	6022(3)	10004(9)	49(4)*
C(231)	9038(7)	6641(3)	8843(8)	41(4)*

Table 43 continued

C(232)	9160(8)	6714(3)	6927(9)	50(4)#
C(233)	10103(10)	6902(4)	6758(13)	79(7)#
C(234)	10911(10)	6999(4)	7688(13)	75(6)#
C(235)	10799(9)	6932(4)	8788(13)	80(6)#
C(236)	9867(9)	6750(4)	8969(10)	72(6)#
C(311)	3270(8)	6505(3)	2673(8)	42(4)#
C(312)	2441(10)	6402(4)	1722(9)	57(5)#
C(313)	2718(14)	6284(4)	697(10)	84(6)#
C(314)	3813(15)	6282(6)	626(12)	116(10)#
C(315)	4662(13)	6381(4)	1595(11)	77(6)#
C(316)	4370(10)	6475(4)	2616(9)	57(5)#
C(321)	3376(7)	7119(3)	4207(8)	33(3)#
C(322)	3848(10)	7287(4)	3486(10)	60(5)#
C(323)	4850(10)	7684(4)	3480(12)	67(6)#
C(324)	3892(11)	7849(4)	4391(12)	72(6)#
C(325)	3444(13)	7686(5)	5205(12)	83(7)#
C(326)	3200(11)	7318(4)	5140(10)	74(6)#
C(331)	1501(7)	6637(4)	3847(8)	48(4)#
C(332)	965(8)	6354(4)	4196(9)	54(5)#
C(333)	-178(9)	6339(5)	4007(11)	74(6)#
C(334)	-766(10)	6627(5)	3461(11)	71(6)#
C(335)	-263(10)	6932(5)	3127(13)	95(8)#
C(336)	871(9)	6924(4)	3316(11)	69(5)#

Equivalent isotropic U defined as one third of the trace of the orthogonalised U_{ij} tensor

Table 44. Interatomic distances (pm), with standard deviations in parenthesis, for [arachno-9,6,6'-Au(CB_8H_{12})$_2$] [Au(P(cyclo-C_6H_{11})$_3$)$_2$] (10).

Au(3)-P(1)	2.320(4)	Au(3)-P(2)	2.312(4)
Au(9)-Au(9a)	1.822(3)	Au(9)-B(104)	2.499(26)
Au(9)-B(108)	2.303(24)	Au(9)-B(110)	2.348(25)
Au(9)-B(114)	2.237(49)	Au(9)-B(118)	2.195(40)
Au(9)-B(120)	2.275(42)	Au(9)-B(214)	2.648(42)
Au(9)-B(215)	2.624(57)	Au(9)-C(216)	2.679(41)
Au(9)-B(217)	2.984(48)	Au(9)-B(218)	2.394(38)
Au(9)-B(220)	2.193(50)	Au(9a)-B(104)	2.063(23)
Au(9a)-B(108)	2.379(21)	Au(9a)-B(110)	2.274(26)
Au(9a)-B(114)	2.911(54)	Au(9a)-C(116)	2.999(29)
Au(9a)-B(118)	2.527(41)	Au(9a)-B(120)	2.605(48)
Au(9a)-B(214)	2.203(38)	Au(9a)-B(218)	2.290(41)
Au(9a)-B(220)	2.146(46)	P(1)-C(311)	1.818(18)
P(1)-C(321)	1.816(19)	P(1)-C(331)	1.856(24)
P(2)-C(411)	1.811(24)	P(2)-C(421)	1.902(17)
P(2)-C(431)	1.817(20)	B(101)-B(102)	1.752(37)
B(101)-B(103)	1.813(38)	B(101)-B(104)	1.803(37)
B(101)-B(105)	1.828(41)	B(101)-B(110)	1.785(34)
B(102)-B(103)	1.801(46)	B(102)-B(105)	1.834(38)
B(102)-C(106)	1.755(32)	B(102)-B(107)	1.842(36)
B(103)-B(104)	1.809(34)	B(103)-B(107)	1.793(39)
B(103)-B(108)	1.758(33)	B(104)-B(108)	1.892(36)
B(104)-B(110)	1.785(44)	B(105)-C(106)	1.807(31)
B(105)-B(110)	1.834(39)	C(106)-B(107)	1.771(42)
B(107)-B(108)	1.726(41)	B(111)-B(112)	1.893(74)
B(111)-B(113)	1.904(75)	B(111)-B(114)	1.758(65)
B(111)-B(115)	1.831(64)	B(111)-B(120)	1.785(58)
B(111)-B(211)	2.126(86)	B(111)-B(212)	0.884(73)
B(111)-B(213)	1.121(82)	B(111)-C(216)	1.987(59)
B(111)-B(217)	1.102(66)	B(111)-B(218)	2.172(62)
B(112)-B(113)	1.727(63)	B(112)-B(115)	1.911(52)
B(112)-C(116)	1.702(53)	B(112)-B(117)	1.817(62)
B(112)-B(211)	1.811(63)	B(112)-B(212)	1.760(77)
B(112)-B(213)	1.197(69)	B(112)-B(214)	1.927(52)
B(113)-B(114)	1.768(72)	B(113)-B(117)	1.785(80)
B(113)-B(118)	1.906(59)	B(113)-B(211)	1.029(83)
B(113)-B(212)	1.132(85)	B(113)-B(213)	2.124(69)
B(113)-B(215)	1.192(72)	B(113)-C(216)	2.281(70)
B(113)-B(220)	2.027(70)	B(114)-B(118)	1.869(78)
B(114)-B(120)	1.878(66)	B(114)-B(212)	1.558(66)
B(114)-B(215)	1.227(92)	B(114)-C(216)	0.762(80)
B(114)-B(217)	1.707(72)	B(114)-B(220)	2.243(88)
B(115)-C(116)	1.913(58)	B(115)-B(120)	1.793(60)
B(115)-B(213)	0.953(60)	B(115)-B(214)	1.644(62)
B(115)-B(217)	1.999(70)	B(115)-B(218)	1.172(50)
C(116)-B(117)	1.716(53)	C(116)-B(211)	1.842(66)
C(116)-B(213)	2.001(73)	C(116)-B(214)	0.872(55)
C(116)-B(220)	2.255(57)	B(117)-B(118)	1.951(62)
B(117)-B(211)	1.038(81)	B(117)-B(214)	1.810(60)

Table 44 continued

B(117)-B(215)	2	172(91)	B(117)-B(220)	1	355(62)
B(118)-B(211)	2	137(60)	B(118)-B(215)	1	016(83)
B(118)-B(220)	0	915(71)	B(120)-B(213)	1	978(65)
B(120)-C(216)	2	126(68)	B(120)-B(217)	0	978(66)
B(120)-B(218)	1	027(73)	B(211)-B(212)	1	671(94)
B(211)-B(213)	1	765(77)	B(211)-B(214)	1	850(65)
B(211)-B(215)	1	868(84)	B(211)-B(220)	1	788(65)
B(212)-B(213)	1	574(76)	B(212)-B(215)	1	822(83)
B(212)-C(216)	1	855(65)	B(212)-B(217)	1	800(72)
B(213)-B(214)	1	821(72)	B(213)-B(217)	1	788(80)
B(213)-B(218)	1	772(59)	B(214)-B(218)	1	747(70)
B(214)-B(220)	1	778(63)	B(215)-C(216)	1	768(91)
B(215)-B(220)	1	614(93)	C(216)-B(217)	1	751(60)
B(217)-B(218)	1	780(72)	C(311)-C(312)	1	429(29)
C(311)-C(316)	1	476(24)	C(312)-C(313)	1	542(32)
C(313)-C(314)	1	431(30)	C(314)-C(315)	1	364(36)
C(314)-C(316)	2	388(30)	C(315)-C(316)	1	458(32)
C(321)-C(322)	1	530(21)	C(321)-C(326)	1	493(26)
C(322)-C(323)	1	504(30)	C(323)-C(324)	1	473(33)
C(324)-C(325)	1	517(28)	C(325)-C(326)	1	500(30)
C(331)-C(332)	1	462(25)	C(331)-C(336)	1	333(37)
C(332)-C(333)	1	497(32)	C(333)-C(334)	1	298(45)
C(333)-C(335)	2	327(31)	C(334)-C(335)	1	356(33)
C(335)-C(336)	1	442(35)	C(411)-C(412)	1	472(38)
C(411)-C(416)	1	530(27)	C(412)-C(413)	1	586(48)
C(413)-C(414)	1	531(38)	C(414)-C(415)	1	509(45)
C(415)-C(416)	1	451(38)	C(421)-C(422)	1	552(24)
C(421)-C(426)	1	486(29)	C(422)-C(423)	1	573(28)
C(423)-C(424)	1	397(37)	C(423)-C(425)	2	379(32)
C(424)-C(425)	1	479(28)	C(425)-C(426)	1	495(27)
C(431)-C(432)	1	549(22)	C(431)-C(436)	1	556(28)
C(432)-C(433)	1	500(31)	C(433)-C(434)	1	529(34)
C(434)-C(435)	1	471(28)	C(435)-C(436)	1	491(30)

Table 45. Interbond angles (°), with standard deviations in parenthesis, for [arachno-9,6,6'-Au(CB_8H_{12})$_2$] [Au(P(cyclo-C_6H_{11})$_3$)$_2$] (10).

P(1)-Au(3)-P(2)	176.3(2)	Au(9a)-Au(9)-B(104)	53.5(6)
Au(9a)-Au(9)-B(108)	81.6(8)	B(104)-Au(9)-B(108)	46.2(9)
Au(9a)-Au(9)-B(110)	73.2(8)	B(104)-Au(9)-B(110)	43.1(10)
B(108)-Au(9)-B(110)	81.8(9)	Au(9a)-Au(9)-B(114)	122.1(15)
B(104)-Au(9)-B(114)	174.9(17)	B(108)-Au(9)-B(114)	133.3(15)
B(110)-Au(9)-B(114)	140.5(17)	Au(9a)-Au(9)-B(118)	96.7(13)
B(104)-Au(9)-B(118)	126.2(14)	B(108)-Au(9)-B(118)	91.2(12)
B(110)-Au(9)-B(118)	168.4(16)	B(114)-Au(9)-B(118)	49.9(20)
Au(9a)-Au(9)-B(120)	97.0(13)	B(104)-Au(9)-B(120)	131.4(13)
B(108)-Au(9)-B(120)	177.6(13)	B(110)-Au(9)-B(120)	95.9(13)
B(114)-Au(9)-B(120)	49.2(17)	B(118)-Au(9)-B(120)	90.9(15)
Au(9a)-Au(9)-B(214)	53.7(10)	B(104)-Au(9)-B(214)	107.3(12)
B(108)-Au(9)-B(214)	121.1(13)	B(110)-Au(9)-B(214)	113.1(11)
B(114)-Au(9)-B(214)	68.4(17)	B(118)-Au(9)-B(214)	62.8(14)
B(120)-Au(9)-B(214)	59.0(17)	Au(9a)-Au(9)-B(215)	110.2(16)
B(104)-Au(9)-B(215)	148.3(18)	B(108)-Au(9)-B(215)	110.8(16)
B(110)-Au(9)-B(215)	167.9(17)	B(114)-Au(9)-B(215)	27.8(22)
B(118)-Au(9)-B(215)	22.1(21)	B(120)-Au(9)-B(215)	72.3(18)
B(214)-Au(9)-B(215)	63.6(17)	Au(9a)-Au(9)-C(216)	135.1(9)
B(104)-Au(9)-C(216)	170.5(11)	B(108)-Au(9)-C(216)	132.3(11)
B(110)-Au(9)-C(216)	130.6(12)	B(114)-Au(9)-C(216)	14.6(18)
B(118)-Au(9)-C(216)	68.7(16)	B(120)-Au(9)-C(216)	50.0(15)
B(214)-Au(9)-C(216)	81.6(13)	B(215)-Au(9)-C(216)	38.9(20)
Au(9a)-Au(9)-B(217)	107.4(10)	B(104)-Au(9)-B(217)	146.2(11)
B(108)-Au(9)-B(217)	167.6(11)	B(110)-Au(9)-B(217)	108.8(12)
B(114)-Au(9)-B(217)	34.6(16)	B(118)-Au(9)-B(217)	79.4(14)
B(120)-Au(9)-B(217)	14.8(15)	B(214)-Au(9)-B(217)	61.6(15)
B(215)-Au(9)-B(217)	59.2(17)	C(216)-Au(9)-B(217)	35.5(12)
Au(9a)-Au(9)-B(218)	71.8(12)	B(104)-Au(9)-B(218)	113.3(12)
B(108)-Au(9)-B(218)	153.4(15)	B(110)-Au(9)-B(218)	90.3(11)
B(114)-Au(9)-B(218)	65.3(16)	B(118)-Au(9)-B(218)	91.9(14)
B(120)-Au(9)-B(218)	25.2(18)	B(214)-Au(9)-B(218)	48.2(16)
B(215)-Au(9)-B(218)	80.1(16)	C(216)-Au(9)-B(218)	71.8(14)
B(217)-Au(9)-B(218)	36.6(15)	Au(9a)-Au(9)-B(220)	73.8(14)
B(104)-Au(9)-B(220)	114.2(16)	B(108)-Au(9)-B(220)	95.8(15)
B(110)-Au(9)-B(220)	147.8(16)	B(114)-Au(9)-B(220)	68.8(21)
B(118)-Au(9)-B(220)	24.1(18)	B(120)-Au(9)-B(220)	86.4(17)
B(214)-Au(9)-B(220)	41.8(15)	B(215)-Au(9)-B(220)	37.8(23)
C(216)-Au(9)-B(220)	74.6(17)	B(217)-Au(9)-B(220)	79.7(17)
B(218)-Au(9)-B(220)	77.8(16)	Au(9)-Au(9a)-B(104)	103.8(8)
Au(9)-Au(9a)-B(108)	73.3(8)	B(104)-Au(9a)-B(108)	49.8(9)
Au(9)-Au(9a)-B(110)	81.3(8)	B(104)-Au(9a)-B(110)	48.3(11)
B(108)-Au(9a)-B(110)	81.8(9)	Au(9)-Au(9a)-B(114)	48.6(10)
B(104)-Au(9a)-B(114)	143.5(13)	B(108)-Au(9a)-B(114)	103.5(12)
B(110)-Au(9a)-B(114)	112.1(14)	Au(9)-Au(9a)-C(116)	111.1(7)
B(104)-Au(9a)-C(116)	145.6(11)	B(108)-Au(9a)-C(116)	137.2(9)
B(110)-Au(9a)-C(116)	140.6(9)	B(114)-Au(9a)-C(116)	70.5(12)

Table 45 continued

Au(9)-Au(9a)-B(118)	59.6(11)		B(104)-Au(9a)-B(118)	131.4(11)	
B(108)-Au(9a)-B(118)	81.8(10)		B(110)-Au(9a)-B(118)	140.5(13)	
B(114)-Au(9a)-B(118)	39.4(16)		C(116)-Au(9a)-B(118)	67.0(11)	
Au(9)-Au(9a)-B(120)	60.1(10)		B(104)-Au(9a)-B(120)	137.3(13)	
B(108)-Au(9a)-B(120)	133.3(13)		B(110)-Au(9a)-B(120)	89.2(12)	
B(114)-Au(9a)-B(120)	39.3(14)		C(116)-Au(9a)-B(120)	68.2(12)	
B(118)-Au(9a)-B(120)	76.8(14)		Au(9)-Au(9a)-B(214)	104.3(13)	
B(104)-Au(9a)-B(214)	152.7(15)		B(108)-Au(9a)-B(214)	140.7(13)	
B(110)-Au(9a)-B(214)	137.4(13)		B(114)-Au(9a)-B(214)	63.8(16)	
C(116)-Au(9a)-B(214)	7.9(15)		B(118)-Au(9a)-B(214)	64.9(14)	
B(120)-Au(9a)-B(214)	60.5(17)		Au(9)-Au(9a)-B(218)	83.1(12)	
B(104)-Au(9a)-B(218)	139.7(13)		B(108)-Au(9a)-B(218)	156.4(15)	
B(110)-Au(9a)-B(218)	94.9(13)		B(114)-Au(9a)-B(218)	56.0(15)	
C(116)-Au(9a)-B(218)	52.4(14)		B(118)-Au(9a)-B(218)	86.3(14)	
B(120)-Au(9a)-B(218)	23.1(16)		B(214)-Au(9a)-B(218)	45.7(17)	
Au(9)-Au(9a)-B(220)	79.0(16)		B(104)-Au(9a)-B(220)	139.1(15)	
B(108)-Au(9a)-B(220)	94.1(14)		B(110)-Au(9a)-B(220)	160.2(18)	
B(114)-Au(9a)-B(220)	49.9(20)		C(116)-Au(9a)-B(220)	48.6(14)	
B(118)-Au(9a)-B(220)	20.6(18)		B(120)-Au(9a)-B(220)	79.6(18)	
B(214)-Au(9a)-B(220)	48.2(16)		B(218)-Au(9a)-B(220)	81.1(17)	
Au(3)-P(1)-C(311)	111.4(6)		Au(3)-P(1)-C(321)	110.6(5)	
C(311)-P(1)-C(321)	108.7(9)		Au(3)-P(1)-C(331)	110.9(7)	
C(311)-P(1)-C(331)	105.5(10)		C(321)-P(1)-C(331)	109.6(10)	
Au(3)-P(2)-C(411)	113.9(8)		Au(3)-P(2)-C(421)	109.5(5)	
C(411)-P(2)-C(421)	107.6(11)		Au(3)-P(2)-C(431)	110.0(5)	
C(411)-P(2)-C(431)	108.4(9)		C(421)-P(2)-C(431)	107.2(9)	
B(102)-B(101)-B(103)	60.7(16)		B(102)-B(101)-B(104)	109.7(18)	
B(103)-B(101)-B(104)	60.0(14)		B(102)-B(101)-B(105)	61.6(15)	
B(103)-B(101)-B(105)	108.2(17)		B(104)-B(101)-B(105)	107.2(16)	
B(102)-B(101)-B(110)	112.4(18)		B(103)-B(101)-B(110)	109.3(16)	
B(104)-B(101)-B(110)	59.7(15)		B(105)-B(101)-B(110)	61.0(15)	
B(101)-B(102)-B(103)	61.3(16)		B(101)-B(102)-B(105)	61.2(15)	
B(103)-B(102)-B(105)	108.4(18)		B(101)-B(102)-C(106)	111.7(17)	
B(103)-B(102)-C(106)	109.3(18)		B(105)-B(102)-C(106)	60.4(13)	
B(101)-B(102)-B(107)	107.4(19)		B(103)-B(102)-B(107)	58.9(16)	
B(105)-B(102)-B(107)	104.4(15)		C(106)-B(102)-B(107)	58.9(15)	
B(101)-B(103)-B(102)	58.0(15)		B(101)-B(103)-B(104)	59.7(14)	
B(102)-B(103)-B(104)	107.3(20)		B(101)-B(103)-B(107)	106.9(20)	
B(102)-B(103)-B(107)	61.7(15)		B(104)-B(103)-B(107)	107.9(17)	
B(101)-B(103)-B(108)	111.4(17)		B(102)-B(103)-B(108)	110.1(20)	
B(104)-B(103)-B(108)	64.1(13)		B(107)-B(103)-B(108)	58.2(15)	
Au(9)-B(104)-Au(9a)	23.5(3)		Au(9)-B(104)-B(101)	109.6(17)	
Au(9a)-B(104)-B(101)	127.9(19)		Au(9)-B(104)-B(103)	107.6(15)	
Au(9a)-B(104)-B(103)	127.6(16)		B(101)-B(104)-B(103)	60.3(14)	
Au(9)-B(104)-B(108)	61.4(10)		Au(9a)-B(104)-B(108)	73.8(11)	
B(101)-B(104)-B(108)	105.9(18)		B(103)-B(104)-B(108)	56.7(12)	
Au(9)-B(104)-B(110)	64.0(12)		Au(9a)-B(104)-B(110)	72.1(12)	
B(101)-B(104)-B(110)	59.6(15)		B(103)-B(104)-B(110)	109.5(20)	
B(108)-B(104)-B(110)	111.9(21)		B(101)-B(105)-B(102)	57.2(14)	
B(101)-B(105)-C(106)	106.0(18)		B(102)-B(105)-C(106)	57.6(13)	
B(101)-B(105)-B(110)	58.3(15)		B(102)-B(105)-B(110)	106.5(21)	
C(106)-B(105)-B(110)	115.7(18)		B(102)-C(106)-B(105)	61.9(13)	
B(102)-C(106)-B(107)	63.0(16)		B(105)-C(106)-B(107)	108.5(18)	

Table 45 continued

B(102)-B(107)-B(103)	59	4(16)	
B(103)-B(107)-C(106)	109	0(17)	
B(103)-B(107)-B(108)	59.9	(15)	
Au(9)-B(108)-Au(9a)	25	1(2)	
Au(9a)-B(108)-B(103)	113	4(14)	
Au(9a)-B(108)-B(104)	56	4(9)	
Au(9)-B(108)-B(107)	103	7(17)	
B(103)-B(108)-B(107)	61	9(15)	
Au(9)-B(110)-Au(9a)	25	5(3)	
Au(9a)-B(110)-B(101)	117	3(17)	
Au(9a)-B(110)-B(104)	59	6(11)	
Au(9)-B(110)-B(105)	100	7(14)	
B(101)-B(110)-B(105)	60	7(15)	
B(112)-B(111)-B(113)	54	1(25)	
B(113)-B(111)-B(114)	57	7(27)	
B(113)-B(111)-B(115)	103	5(35)	
B(112)-B(111)-B(120)	110	7(35)	
B(114)-B(111)-B(120)	64	2(25)	
B(112)-B(111)-B(211)	28	4(19)	
B(114)-B(111)-B(211)	74	2(31)	
B(120)-B(111)-B(211)	103	5(32)	
B(113)-B(111)-B(212)	21	7(48)	
B(115)-B(111)-B(212)	124	1(67)	
B(211)-B(111)-B(212)	48	1(54)	
B(113)-B(111)-B(213)	85	0(45)	
B(115)-B(111)-B(213)	25	6(30)	
B(211)-B(111)-B(213)	56	1(39)	
B(112)-B(111)-C(216)	123	2(32)	
B(114)-B(111)-C(216)	22	4(26)	
B(120)-B(111)-C(216)	68	4(23)	
B(212)-B(111)-C(216)	68	5(45)	
B(112)-B(111)-B(217)	139	3(50)	
B(114)-B(111)-B(217)	69	3(37)	
B(120)-B(111)-B(217)	28	9(36)	
B(212)-B(111)-B(217)	139	8(63)	
C(216)-B(111)-B(217)	61	4(34)	
B(113)-B(111)-B(218)	103	7(30)	
B(115)-B(111)-B(218)	32	6(17)	
B(211)-B(111)-B(218)	85	4(28)	
B(213)-B(111)-B(218)	54	4(32)	
B(217)-B(111)-B(218)	54	8(37)	
B(111)-B(112)-B(115)	57	5(23)	
B(111)-B(112)-C(116)	111	9(26)	
B(115)-B(112)-C(116)	63	6(21)	
B(113)-B(112)-B(117)	60	4(28)	
C(116)-B(112)-B(117)	58	3(22)	
B(113)-B(112)-B(211)	32	5(45)	
C(116)-B(112)-B(211)	81	2(42)	
B(111)-B(112)-B(212)	27	7(24)	
B(115)-B(112)-B(212)	83	2(28)	
B(117)-B(112)-B(212)	95	0(30)	
B(111)-B(112)-B(213)	34	0(33)	
B(115)-B(112)-B(213)	24	1(32)	
B(102)-B(107)-C(106)	58	1(14)	
B(102)-B(107)-B(108)	109	7(19)	
C(106)-B(107)-B(108)	117	3(17)	
Au(9)-B(108)-B(103)	118	4(16)	
Au(9)-B(108)-B(104)	72	4(11)	
B(103)-B(108)-B(104)	59	3(13)	
Au(9a)-B(108)-B(107)	125	0(18)	
B(104)-B(108)-B(107)	107	0(18)	
Au(9)-B(110)-B(101)	117	0(16)	
Au(9)-B(110)-B(104)	73	0(12)	
B(101)-B(110)-B(104)	60	7(15)	
Au(9a)-B(110)-B(105)	124	3(15)	
B(104)-B(110)-B(105)	107	7(18)	
B(112)-B(111)-B(114)	101	9(36)	
B(112)-B(111)-B(115)	61	7(25)	
B(114)-B(111)-B(115)	105	6(32)	
B(113)-B(111)-B(120)	110	5(31)	
B(115)-B(111)-B(120)	59	4(24)	
B(113)-B(111)-B(211)	28	9(24)	
B(115)-B(111)-B(211)	76	0(29)	
B(112)-B(111)-B(212)	67	7(54)	
B(114)-B(111)-B(212)	62	8(43)	
B(120)-B(111)-B(212)	124	8(52)	
B(112)-B(111)-B(213)	36	6(33)	
B(114)-B(111)-B(213)	110	4(48)	
B(120)-B(111)-B(213)	82	4(39)	
B(212)-B(111)-B(213)	102	8(72)	
B(113)-B(111)-C(216)	71	7(26)	
B(115)-B(111)-C(216)	121	9(27)	
B(211)-B(111)-C(216)	93	9(28)	
B(213)-B(111)-C(216)	132	0(44)	
B(113)-B(111)-B(217)	126	3(43)	
B(115)-B(111)-B(217)	81	9(40)	
B(211)-B(111)-B(217)	129	8(46)	
B(213)-B(111)-B(217)	107	1(53)	
B(112)-B(111)-B(218)	84	7(27)	
B(114)-B(111)-B(218)	78	5(25)	
B(120)-B(111)-B(218)	27	9(22)	
B(212)-B(111)-B(218)	124	5(58)	
C(216)-B(111)-B(218)	90	5(22)	
B(111)-B(112)-B(113)	63	3(28)	
B(113)-B(112)-B(115)	107	3(28)	
B(113)-B(112)-C(116)	109	1(27)	
B(111)-B(112)-B(117)	111	3(28)	
B(115)-B(112)-B(117)	107	5(24)	
B(111)-B(112)-B(211)	88	7(48)	
B(115)-B(112)-B(211)	109	9(39)	
B(117)-B(112)-B(211)	28	8(42)	
B(113)-B(112)-B(212)	37	9(29)	
C(116)-B(112)-B(212)	123	3(28)	
B(211)-B(112)-B(212)	68	1(48)	
B(113)-B(112)-B(213)	91	3(39)	
C(116)-B(112)-B(213)	85	4(35)	

Table 45 continued

B(117)-B(112)-B(213)	115	6(35)	B(211)-B(112)-B(213)	105	9(50)
B(212)-B(112)-B(213)	60	8(37)	B(111)-B(112)-B(214)	86	7(25)
B(113)-B(112)-B(214)	89	7(25)	B(115)-B(112)-B(214)	50	7(20)
C(116)-B(112)-B(214)	26	9(19)	B(117)-B(112)-B(214)	57	7(21)
B(211)-B(112)-B(214)	70	3(37)	B(212)-B(112)-B(214)	96	6(27)
B(213)-B(112)-B(214)	66	6(33)	B(111)-B(113)-B(112)	62	6(27)
B(111)-B(113)-B(114)	56	8(27)	B(112)-B(113)-B(114)	108	2(33)
B(111)-B(113)-B(117)	112	2(33)	B(112)-B(113)-B(117)	62	3(28)
B(114)-B(113)-B(117)	110	2(33)	B(111)-B(113)-B(118)	109	9(28)
B(112)-B(113)-B(118)	114	4(33)	B(114)-B(113)-B(118)	61	8(27)
B(117)-B(113)-B(118)	63	7(26)	B(111)-B(113)-B(211)	87	6(47)
B(112)-B(113)-B(211)	31	9(38)	B(114)-B(113)-B(211)	112	2(47)
B(117)-B(113)-B(211)	38	4(38)	B(118)-B(113)-B(211)	88	2(44)
B(111)-B(113)-B(212)	16	8(34)	B(112)-B(113)-B(212)	72	6(41)
B(114)-B(113)-B(212)	60	4(38)	B(117)-B(113)-B(212)	128	1(49)
B(118)-B(113)-B(212)	119	7(42)	B(211)-B(113)-B(212)	101	2(59)
B(111)-B(113)-B(213)	31	7(25)	B(112)-B(113)-B(213)	34	3(23)
B(114)-B(113)-B(213)	75	8(28)	B(117)-B(113)-B(213)	81	8(29)
B(118)-B(113)-B(213)	105	8(27)	B(211)-B(113)-B(213)	55	9(43)
B(212)-B(113)-B(213)	46	4(38)	B(111)-B(113)-B(215)	100	4(48)
B(112)-B(113)-B(215)	134	4(47)	B(114)-B(113)-B(215)	43	8(42)
B(117)-B(113)-B(215)	91	5(50)	B(118)-B(113)-B(215)	27	8(42)
B(211)-B(113)-B(215)	114	3(60)	B(212)-B(113)-B(215)	103	2(60)
B(213)-B(113)-B(215)	111	1(43)	B(111)-B(113)-C(216)	55	8(23)
B(112)-B(113)-C(216)	115	2(31)	B(114)-B(113)-C(216)	16	1(22)
B(117)-B(113)-C(216)	126	3(27)	B(118)-B(113)-C(216)	72	6(23)
B(211)-B(113)-C(216)	126	3(45)	B(212)-B(113)-C(216)	53	9(36)
B(213)-B(113)-C(216)	80	9(25)	B(215)-B(113)-C(216)	50	8(44)
B(111)-B(113)-B(220)	102	8(29)	B(112)-B(113)-B(220)	88	1(29)
B(114)-B(113)-B(220)	72	1(29)	B(117)-B(113)-B(220)	41	8(23)
B(118)-B(113)-B(220)	26	7(21)	B(211)-B(113)-B(220)	61	8(39)
B(212)-B(113)-B(220)	117	9(42)	B(213)-B(113)-B(220)	85	9(26)
B(215)-B(113)-B(220)	52	8(43)	C(216)-B(113)-B(220)	87	3(25)
Au(9)-B(114)-Au(9a)	17	3(5)	Au(9)-B(114)-B(111)	118	4(31)
Au(9a)-B(114)-B(111)	104	8(29)	Au(9)-B(114)-B(113)	117	4(36)
Au(9a)-B(114)-B(113)	102	8(32)	B(111)-B(114)-B(113)	65	5(29)
Au(9)-B(114)-B(118)	63	9(21)	Au(9a)-B(114)-B(118)	59	1(20)
B(111)-B(114)-B(118)	119	0(39)	B(113)-B(114)-B(118)	63	1(29)
Au(9)-B(114)-B(120)	66	5(20)	Au(9a)-B(114)-B(120)	61	5(21)
B(111)-B(114)-B(120)	58	8(24)	B(113)-B(114)-B(120)	112	5(34)
B(118)-B(114)-B(120)	116	5(37)	Au(9)-B(114)-B(212)	135	8(40)
Au(9a)-B(114)-B(212)	118	6(37)	B(111)-B(114)-B(212)	30	3(27)
B(113)-B(114)-B(212)	39	1(31)	B(118)-B(114)-B(212)	101	2(41)
B(120)-B(114)-B(212)	88	2(32)	Au(9)-B(114)-B(215)	93	9(43)
Au(9a)-B(114)-B(215)	88	4(43)	B(111)-B(114)-B(215)	107	6(45)
B(113)-B(114)-B(215)	42	3(35)	B(118)-B(114)-B(215)	30	1(35)
B(120)-B(114)-B(215)	137	7(57)	B(212)-B(114)-B(215)	80	8(44)
Au(9)-B(114)-C(216)	117	9(48)	Au(9a)-B(114)-C(216)	133	5(48)
B(111)-B(114)-C(216)	96	5(56)	B(113)-B(114)-C(216)	123	7(55)
B(118)-B(114)-C(216)	139	2(60)	B(120)-B(114)-C(216)	98	3(57)
B(212)-B(114)-C(216)	100	5(57)	B(215)-B(114)-C(216)	123	8(69)
Au(9)-B(114)-B(217)	97	5(27)	Au(9a)-B(114)-B(217)	92	2(26)
B(111)-B(114)-B(217)	37	1(24)	B(113)-B(114)-B(217)	102	3(33)

Table 45 continued

B(118)-B(114)-B(217)	140	1(42)	B(120)-B(114)-B(217)	31	2(23)
B(212)-B(114)-B(217)	66	7(32)	B(215)-B(114)-B(217)	143	2(51)
C(216)-B(114)-B(217)	80	5(55)	Au(9)-B(114)-B(220)	58	6(18)
Au(9a)-B(114)-B(220)	47	0(16)	B(111)-B(114)-B(220)	99	9(35)
B(113)-B(114)-B(220)	59	3(28)	B(118)-B(114)-B(220)	23	5(20)
B(120)-B(114)-B(220)	95	5(32)	B(212)-B(114)-B(220)	98	6(38)
B(215)-B(114)-B(220)	44	4(40)	C(216)-B(114)-B(220)	162	5(59)
B(217)-B(114)-B(220)	116	6(36)	B(111)-B(115)-B(112)	60	7(24)
B(111)-B(115)-C(116)	105	5(26)	B(112)-B(115)-C(116)	52	8(20)
B(111)-B(115)-B(120)	59	0(24)	B(112)-B(115)-B(120)	109	5(26)
C(116)-B(115)-B(120)	117	0(25)	B(111)-B(115)-B(213)	30	6(42)
B(112)-B(115)-B(213)	30	8(42)	C(116)-B(115)-B(213)	81	1(46)
B(120)-B(115)-B(213)	86	5(43)	B(111)-B(115)-B(214)	97	9(29)
B(112)-B(115)-B(214)	65	1(23)	C(116)-B(115)-B(214)	27	0(18)
B(120)-B(115)-B(214)	90	6(27)	B(213)-B(115)-B(214)	84	6(44)
B(111)-B(115)-B(217)	33	1(21)	B(112)-B(115)-B(217)	92	3(24)
C(116)-B(115)-B(217)	125	1(25)	B(120)-B(115)-B(217)	29	3(21)
B(213)-B(115)-B(217)	63	4(44)	B(214)-B(115)-B(217)	105	0(28)
B(111)-B(115)-B(218)	89	9(35)	B(112)-B(115)-B(218)	124	1(34)
C(116)-B(115)-B(218)	100	6(35)	B(120)-B(115)-B(218)	32	7(31)
B(213)-B(115)-B(218)	112	7(48)	B(214)-B(115)-B(218)	74	6(33)
B(217)-B(115)-B(218)	62	0(33)	Au(9a)-C(116)-B(112)	109	3(21)
Au(9a)-C(116)-B(115)	76	8(14)	B(112)-C(116)-B(115)	63	5(22)
Au(9a)-C(116)-B(117)	82	3(17)	B(112)-C(116)-B(117)	64	2(24)
B(115)-C(116)-B(117)	111	8(29)	Au(9a)-C(116)-B(211)	88	6(19)
B(112)-C(116)-B(211)	32	8(21)	B(115)-C(116)-B(211)	81	3(27)
B(117)-C(116)-B(211)	33	7(26)	Au(9a)-C(116)-B(213)	85	8(18)
B(112)-C(116)-B(213)	36	6(22)	B(115)-C(116)-B(213)	28	1(19)
B(117)-C(116)-B(213)	87	2(28)	B(211)-C(116)-B(213)	54	5(26)
Au(9a)-C(116)-B(214)	28	4(34)	B(112)-C(116)-B(214)	91	1(43)
B(115)-C(116)-B(214)	59	0(39)	B(117)-C(116)-B(214)	81	8(38)
B(211)-C(116)-B(214)	76	8(39)	B(213)-C(116)-B(214)	65	4(41)
Au(9a)-C(116)-B(220)	45	5(13)	B(112)-C(116)-B(220)	81	6(22)
B(115)-C(116)-B(220)	95	4(24)	B(117)-C(116)-B(220)	36	9(19)
B(211)-C(116)-B(220)	50	5(21)	B(213)-C(116)-B(220)	83	1(24)
B(214)-C(116)-B(220)	46	9(34)	B(112)-B(117)-B(113)	57	3(26)
B(112)-B(117)-C(116)	57	5(22)	B(113)-B(117)-C(116)	105	8(34)
B(112)-B(117)-B(118)	108	3(34)	B(113)-B(117)-B(118)	61	2(26)
C(116)-B(117)-B(118)	113	9(29)	B(112)-B(117)-B(211)	27	2(36)
B(113)-B(117)-B(211)	30	1(39)	C(116)-B(117)-B(211)	79	8(42)
B(118)-B(117)-B(211)	85	5(45)	B(112)-B(117)-B(214)	64	2(23)
B(113)-B(117)-B(214)	91	8(33)	C(116)-B(117)-B(214)	28	5(19)
B(118)-B(117)-B(214)	85	4(26)	B(211)-B(117)-B(214)	75	6(42)
B(112)-B(117)-B(215)	84	7(31)	B(113)-B(117)-B(215)	33	3(24)
C(116)-B(117)-B(215)	113	4(33)	B(118)-B(117)-B(215)	27	9(22)
B(211)-B(117)-B(215)	59	3(43)	B(214)-B(117)-B(215)	88	0(31)
B(112)-B(117)-B(220)	110	5(42)	B(113)-B(117)-B(220)	79	1(38)
C(116)-B(117)-B(220)	93	7(33)	B(118)-B(117)-B(220)	24	6(27)
B(211)-B(117)-B(220)	95	8(54)	B(214)-B(117)-B(220)	66	5(30)
B(215)-B(117)-B(220)	47	8(33)	Au(9)-B(118)-Au(9a)	23	7(4)
Au(9)-B(118)-B(113)	113	3(25)	Au(9a)-B(118)-B(113)	113	7(23)

Table 45 continued

Au(9)-B(118)-B(114)	66	2(20)	Au(9a)-B(118)-B(114)	81	4(21)
B(113)-B(118)-B(114)	55	9(26)	Au(9)-B(118)-B(117)	111	7(23)
Au(9a)-B(118)-B(117)	92	1(21)	B(113)-B(118)-B(117)	55	1(25)
B(114)-B(118)-B(117)	99	4(28)	Au(9)-B(118)-B(211)	106	7(22)
Au(9a)-B(118)-B(211)	96	2(20)	B(113)-B(118)-B(211)	28	8(24)
B(114)-B(118)-B(211)	71	8(27)	B(117)-B(118)-B(211)	29	0(24)
Au(9)-B(118)-B(215)	103	4(48)	Au(9a)-B(118)-B(215)	117	4(47)
B(113)-B(118)-B(215)	33	1(43)	B(114)-B(118)-B(215)	37	3(44)
B(117)-B(118)-B(215)	88	2(47)	B(211)-B(118)-B(215)	68	9(45)
Au(9)-B(118)-B(220)	77	9(39)	Au(9a)-B(118)-B(220)	55	5(35)
B(113)-B(118)-B(220)	84	0(41)	B(114)-B(118)-B(220)	101	8(58)
B(117)-B(118)-B(220)	38	1(34)	B(211)-B(118)-B(220)	55	6(37)
B(215)-B(118)-B(220)	113	3(61)	Au(9)-B(120)-Au(9a)	22	9(5)
Au(9)-B(120)-B(111)	115	0(27)	Au(9a)-B(120)-B(111)	116	7(29)
Au(9)-B(120)-B(114)	64	3(20)	Au(9a)-B(120)-B(114)	79	2(23)
B(111)-B(120)-B(114)	57	0(24)	Au(9)-B(120)-B(115)	109	8(28)
Au(9a)-B(120)-B(115)	90	2(25)	B(111)-B(120)-B(115)	61	6(24)
B(114)-B(120)-B(115)	102	0(29)	Au(9)-B(120)-B(213)	109	2(27)
Au(9a)-B(120)-B(213)	98	0(27)	B(111)-B(120)-B(213)	34	2(25)
B(114)-B(120)-B(213)	76	4(26)	B(115)-B(120)-B(213)	28	7(28)
Au(9)-B(120)-C(216)	74	9(17)	Au(9a)-B(120)-C(216)	94	1(19)
B(111)-B(120)-C(216)	60	3(22)	B(114)-B(120)-C(216)	20	8(24)
B(115)-B(120)-C(216)	116	5(26)	B(213)-B(120)-C(216)	88	3(24)
Au(9)-B(120)-B(217)	128	6(43)	Au(9a)-B(120)-B(217)	142	3(45)
B(111)-B(120)-B(217)	32	9(40)	B(114)-B(120)-B(217)	64	7(40)
B(115)-B(120)-B(217)	87	1(41)	B(213)-B(120)-B(217)	64	4(42)
C(216)-B(120)-B(217)	54	6(36)	Au(9)-B(120)-B(218)	83	9(36)
Au(9a)-B(120)-B(218)	61	0(32)	B(111)-B(120)-B(218)	97	4(40)
B(114)-B(120)-B(218)	115	8(47)	B(115)-B(120)-B(218)	38	1(28)
B(213)-B(120)-B(218)	63	3(34)	C(216)-B(120)-B(218)	136	5(45)
B(217)-B(120)-B(218)	125	2(55)	B(111)-B(211)-B(112)	62	9(44)
B(111)-B(211)-B(113)	63	5(46)	B(112)-B(211)-B(113)	115	7(72)
B(111)-B(211)-C(116)	97	1(29)	B(112)-B(211)-C(116)	65	9(38)
B(113)-B(211)-C(116)	151	9(52)	B(111)-B(211)-B(117)	148	9(46)
B(112)-B(211)-B(117)	124	9(70)	B(113)-B(211)-B(117)	119	4(63)
C(116)-B(211)-B(117)	66	5(41)	B(111)-B(211)-B(118)	94	0(29)
B(112)-B(211)-B(118)	150	0(49)	B(113)-B(211)-B(118)	63	0(37)
C(116)-B(211)-B(118)	101	0(27)	B(117)-B(211)-B(118)	65	5(37)
B(111)-B(211)-B(212)	23	2(24)	B(112)-B(211)-B(212)	77	7(58)
B(113)-B(211)-B(212)	41	6(44)	C(116)-B(211)-B(212)	128	2(38)
B(117)-B(211)-B(212)	153	0(52)	B(118)-B(211)-B(212)	87	5(32)
B(111)-B(211)-B(213)	31	8(26)	B(112)-B(211)-B(213)	48	7(36)
B(113)-B(211)-B(213)	95	3(56)	C(116)-B(211)-B(213)	67	3(29)
B(117)-B(211)-B(213)	131	3(52)	B(118)-B(211)-B(213)	109	8(32)
B(212)-B(211)-B(213)	94	4(33)	B(111)-B(211)-B(214)	82	2(29)
B(112)-B(211)-B(214)	78	7(39)	B(113)-B(211)-B(214)	125	0(49)
C(116)-B(211)-B(214)	27	3(19)	B(117)-B(211)-B(214)	71	5(41)
B(118)-B(211)-B(214)	79	3(24)	B(212)-B(211)-B(214)	102	8(37)
B(213)-B(211)-B(214)	60	4(28)	B(111)-B(211)-B(215)	74	3(34)
B(112)-B(211)-B(215)	137	2(64)	B(113)-B(211)-B(215)	35	6(36)
C(116)-B(211)-B(215)	122	9(33)	B(117)-B(211)-B(215)	92	2(46)
B(118)-B(211)-B(215)	28	4(26)	B(212)-B(211)-B(215)	61	7(36)
B(213)-B(211)-B(215)	100	8(40)	B(214)-B(211)-B(215)	96	7(31)

Table 45 continued

B(111)-B(211)-B(220)	103.1(33)	B(112)-B(211)-B(220)	136.9(49)
B(113)-B(211)-B(220)	87.7(43)	C(116)-B(211)-B(220)	76.8(28)
B(117)-B(211)-B(220)	48.9(36)	B(118)-B(211)-B(220)	25.0(23)
B(212)-B(211)-B(220)	105.0(38)	B(213)-B(211)-B(220)	105.6(33)
B(214)-B(211)-B(220)	58.5(25)	B(215)-B(211)-B(220)	52.3(31)
B(111)-B(212)-B(112)	84.6(56)	B(111)-B(212)-B(113)	141.4(78)
B(112)-B(212)-B(113)	69.5(44)	B(111)-B(212)-B(114)	87.0(48)
B(112)-B(212)-B(114)	117.0(43)	B(113)-B(212)-B(114)	80.5(44)
B(111)-B(212)-B(211)	108.7(65)	B(112)-B(212)-B(211)	34.2(25)
B(113)-B(212)-B(211)	37.2(38)	B(114)-B(212)-B(211)	93.8(41)
B(111)-B(212)-B(213)	44.0(51)	B(112)-B(212)-B(213)	41.6(28)
B(113)-B(212)-B(213)	102.2(56)	B(114)-B(212)-B(213)	99.2(38)
B(211)-B(212)-B(213)	65.9(37)	B(111)-B(212)-B(215)	123.2(53)
B(112)-B(212)-B(215)	97.8(42)	B(113)-B(212)-B(215)	39.6(36)
B(114)-B(212)-B(215)	41.6(32)	B(211)-B(212)-B(215)	64.5(36)
B(213)-B(212)-B(215)	110.0(43)	B(111)-B(212)-C(216)	85.1(49)
B(112)-B(212)-C(216)	140.0(36)	B(113)-B(212)-C(216)	96.6(42)
B(114)-B(212)-C(216)	23.8(29)	B(211)-B(212)-C(216)	116.9(36)
B(213)-B(212)-C(216)	112.8(34)	B(215)-B(212)-C(216)	57.5(31)
B(111)-B(212)-B(217)	28.1(39)	B(112)-B(212)-B(217)	104.8(35)
B(113)-B(212)-B(217)	133.5(46)	B(114)-B(212)-B(217)	60.6(30)
B(211)-B(212)-B(217)	116.7(39)	B(213)-B(212)-B(217)	63.6(32)
B(215)-B(212)-B(217)	100.6(33)	C(216)-B(212)-B(217)	57.2(25)
B(111)-B(213)-B(112)	109.4(50)	B(111)-B(213)-B(113)	63.3(38)
B(112)-B(213)-B(113)	54.4(30)	B(111)-B(213)-B(115)	123.8(64)
B(112)-B(213)-B(115)	125.1(69)	B(113)-B(213)-B(115)	141.9(46)
B(111)-B(213)-C(116)	143.7(45)	B(112)-B(213)-C(116)	58.8(33)
B(113)-B(213)-C(116)	85.1(28)	B(115)-B(213)-C(116)	70.8(45)
B(111)-B(213)-B(120)	63.4(35)	B(112)-B(213)-B(120)	143.7(40)
B(113)-B(213)-B(120)	95.3(27)	B(115)-B(213)-B(120)	64.8(38)
C(116)-B(213)-B(120)	105.1(28)	B(111)-B(213)-B(211)	92.1(45)
B(112)-B(213)-B(211)	33.4(27)	B(113)-B(213)-B(211)	28.8(27)
B(115)-B(213)-B(211)	125.7(57)	C(116)-B(213)-B(211)	58.2(28)
B(120)-B(213)-B(211)	110.5(30)	B(111)-B(213)-B(212)	33.2(38)
B(112)-B(213)-B(212)	77.5(39)	B(113)-B(213)-B(212)	31.4(30)
B(115)-B(213)-B(212)	148.8(54)	C(116)-B(213)-B(212)	116.4(39)
B(120)-B(213)-B(212)	84.3(33)	B(211)-B(213)-B(212)	59.7(36)
B(111)-B(213)-B(214)	124.4(43)	B(112)-B(213)-B(214)	76.3(38)
B(113)-B(213)-B(214)	81.4(28)	B(115)-B(213)-B(214)	64.8(41)
C(116)-B(213)-B(214)	25.8(18)	B(120)-B(213)-B(214)	80.8(27)
B(211)-B(213)-B(214)	62.1(29)	B(212)-B(213)-B(214)	108.3(37)
B(111)-B(213)-B(217)	36.1(32)	B(112)-B(213)-B(217)	140.9(45)
B(113)-B(213)-B(217)	87.1(30)	B(115)-B(213)-B(217)	88.1(46)
C(116)-B(213)-B(217)	132.6(30)	B(120)-B(213)-B(217)	29.5(23)
B(211)-B(213)-B(217)	112.5(36)	B(212)-B(213)-B(217)	64.4(34)
B(214)-B(213)-B(217)	106.8(30)	B(111)-B(213)-B(218)	94.6(41)
B(112)-B(213)-B(218)	134.3(48)	B(113)-B(213)-B(218)	110.7(28)
B(115)-B(213)-B(218)	37.6(31)	C(116)-B(213)-B(218)	79.5(28)
B(120)-B(213)-B(218)	31.2(24)	B(211)-B(213)-B(218)	111.8(33)
B(212)-B(213)-B(218)	111.6(36)	B(214)-B(213)-B(218)	58.2(26)
B(217)-B(213)-B(218)	60.8(27)	Au(9)-B(214)-Au(9a)	22.8(5)
Au(9)-B(214)-B(112)	120.3(25)	Au(9a)-B(214)-B(112)	142.1(28)

Table 45 continued

Au(9)-B(214)-B(115)	99 5(26)	Au(9a)-B(214)-B(115)	110 1(27)
B(112)-B(214)-B(115)	64 2(22)	Au(9)-B(214)-C(116)	165 7(45)
Au(9a)-B(214)-C(116)	151 7(48)	B(112)-B(214)-C(116)	62 0(35)
B(115)-B(214)-C(116)	93 9(40)	Au(9)-B(214)-B(117)	99 0(22)
Au(9a)-B(214)-B(117)	107 7(23)	B(112)-B(214)-B(117)	58 1(22)
B(115)-B(214)-B(117)	121 0(30)	C(116)-B(214)-B(117)	69 7(36)
Au(9)-B(214)-B(211)	99 7(25)	Au(9a)-B(214)-B(211)	118 1(26)
B(112)-B(214)-B(211)	31 0(20)	B(115)-B(214)-B(211)	88 7(30)
C(116)-B(214)-B(211)	75 9(37)	B(117)-B(214)-B(211)	32 9(26)
Au(9)-B(214)-B(213)	100 3(27)	Au(9a)-B(214)-B(213)	119 6(30)
B(112)-B(214)-B(213)	37 1(23)	B(115)-B(214)-B(213)	31 4(22)
C(116)-B(214)-B(213)	88 8(41)	B(117)-B(214)-B(213)	90 2(28)
B(211)-B(214)-B(213)	57 5(27)	Au(9)-B(214)-B(218)	62 1(18)
Au(9a)-B(214)-B(218)	69 8(19)	B(112)-B(214)-B(218)	96 6(30)
B(115)-B(214)-B(218)	40 3(21)	C(116)-B(214)-B(218)	132 1(46)
B(117)-B(214)-B(218)	137 1(37)	B(211)-B(214)-B(218)	108 2(36)
B(213)-B(214)-B(218)	59 5(26)	Au(9)-B(214)-B(220)	55 3(20)
Au(9a)-B(214)-B(220)	64 2(19)	B(112)-B(214)-B(220)	89 9(25)
B(115)-B(214)-B(220)	129 1(38)	C(116)-B(214)-B(220)	112 1(45)
B(117)-B(214)-B(220)	44 4(22)	B(211)-B(214)-B(220)	59 0(24)
B(213)-B(214)-B(220)	103 7(33)	B(218)-B(214)-B(220)	109 9(34)
Au(9)-B(215)-B(113)	123 5(45)	Au(9)-B(215)-B(114)	58 2(33)
B(113)-B(215)-B(114)	93 9(56)	Au(9)-B(215)-B(117)	91 0(26)
B(113)-B(215)-B(117)	55 2(42)	B(114)-B(215)-B(117)	115 2(49)
Au(9)-B(215)-B(118)	54 4(37)	B(113)-B(215)-B(118)	119 1(77)
B(114)-B(215)-B(118)	112 6(61)	B(117)-B(215)-B(118)	63 9(47)
Au(9)-B(215)-B(211)	100 0(30)	B(113)-B(215)-B(211)	30 1(36)
B(114)-B(215)-B(211)	97 1(46)	B(117)-B(215)-B(211)	28 5(25)
B(118)-B(215)-B(211)	90 7(57)	Au(9)-B(215)-B(212)	103 4(31)
B(113)-B(215)-B(212)	37 2(39)	B(114)-B(215)-B(212)	57 6(38)
B(117)-B(215)-B(212)	82 2(33)	B(118)-B(215)-B(212)	136 7(61)
B(211)-B(215)-B(212)	53 8(32)	Au(9)-B(215)-C(216)	72 2(23)
B(113)-B(215)-C(216)	98 9(54)	B(114)-B(215)-C(216)	21 8(34)
B(117)-B(215)-C(216)	134 3(38)	B(118)-B(215)-C(216)	125 2(54)
B(211)-B(215)-C(216)	111 5(40)	B(212)-B(215)-C(216)	62 2(33)
Au(9)-B(215)-B(220)	56 4(25)	B(113)-B(215)-B(220)	91 2(54)
B(114)-B(215)-B(220)	103 4(52)	B(117)-B(215)-B(220)	38 5(25)
B(118)-B(215)-B(220)	31 4(36)	B(211)-B(215)-B(220)	61 3(34)
B(212)-B(215)-B(220)	105 9(42)	C(216)-B(215)-B(220)	123 4(43)
Au(9)-C(216)-B(111)	93 6(22)	Au(9)-C(216)-B(113)	87 1(20)
B(111)-C(216)-B(113)	52 5(22)	Au(9)-C(216)-B(114)	47 5(39)
B(111)-C(216)-B(114)	61 1(46)	B(113)-C(216)-B(114)	40 2(41)
Au(9)-C(216)-B(120)	55 1(15)	B(111)-C(216)-B(120)	51 3(19)
B(113)-C(216)-B(120)	86 9(24)	B(114)-C(216)-B(120)	60 9(48)
Au(9)-C(216)-B(212)	100 4(26)	B(111)-C(216)-B(212)	26 3(23)
B(113)-C(216)-B(212)	29 5(24)	B(114)-C(216)-B(212)	55 7(45)
B(120)-C(216)-B(212)	73 9(24)	Au(9)-C(216)-B(215)	68 8(24)
B(111)-C(216)-B(215)	80 1(31)	B(113)-C(216)-B(215)	31 1(23)
B(114)-C(216)-B(215)	35 2(47)	B(120)-C(216)-B(215)	96 0(32)
B(212)-C(216)-B(215)	60 3(30)	Au(9)-C(216)-B(217)	81 8(22)
B(111)-C(216)-B(217)	33 5(21)	B(113)-C(216)-B(217)	83 2(27)
B(114)-C(216)-B(217)	74 1(51)	B(120)-C(216)-B(217)	27 1(20)
B(212)-C(216)-B(217)	59 8(26)	B(215)-C(216)-B(217)	104 8(36)

Table 45 continued

Au(9)-B(217)-B(111)	104.7(43)	Au(9)-B(217)-B(114)	48.8(20)
B(111)-B(217)-B(114)	73.6(40)	Au(9)-B(217)-B(115)	81.6(20)
B(111)-B(217)-B(115)	65.1(39)	B(114)-B(217)-B(115)	100.4(37)
Au(9)-B(217)-B(120)	36.6(32)	B(111)-B(217)-B(120)	118.2(69)
B(114)-B(217)-B(120)	84.1(44)	B(115)-B(217)-B(120)	63.6(41)
Au(9)-B(217)-B(212)	91.5(27)	B(111)-B(217)-B(212)	22.2(31)
B(114)-B(217)-B(212)	52.7(27)	B(115)-B(217)-B(212)	79.7(31)
B(120)-B(217)-B(212)	116.6(56)	Au(9)-B(217)-B(213)	89.7(26)
B(111)-B(217)-B(213)	36.8(37)	B(114)-B(217)-B(213)	86.0(35)
B(115)-B(217)-B(213)	28.5(20)	B(120)-B(217)-B(213)	86.8(50)
B(212)-B(217)-B(213)	52.0(28)	Au(9)-B(217)-C(216)	62.7(19)
B(111)-B(217)-C(216)	85.1(39)	B(114)-B(217)-C(216)	25.4(27)
B(115)-B(217)-C(216)	125.7(36)	B(120)-B(217)-C(216)	98.4(42)
B(212)-B(217)-C(216)	63.0(26)	B(213)-B(217)-C(216)	107.9(35)
Au(9)-B(217)-B(218)	53.3(17)	B(111)-B(217)-B(218)	94.9(49)
B(114)-B(217)-B(218)	91.7(35)	B(115)-B(217)-B(218)	35.5(19)
B(120)-B(217)-B(218)	28.1(35)	B(212)-B(217)-B(218)	101.3(38)
B(213)-B(217)-B(218)	59.6(28)	C(216)-B(217)-B(218)	113.7(34)
Au(9)-B(218)-Au(9a)	25.1(4)	Au(9)-B(218)-B(111)	97.4(20)
Au(9a)-B(218)-B(111)	114.9(22)	Au(9)-B(218)-B(115)	136.3(34)
Au(9a)-B(218)-B(115)	129.6(39)	B(111)-B(218)-B(115)	57.5(28)
Au(9)-B(218)-B(120)	70.9(31)	Au(9a)-B(218)-B(120)	95.9(33)
B(111)-B(218)-B(120)	54.6(32)	B(115)-B(218)-B(120)	103.1(47)
Au(9)-B(218)-B(213)	112.0(25)	Au(9a)-B(218)-B(213)	117.4(27)
B(111)-B(218)-B(213)	31.0(25)	B(115)-B(218)-B(213)	29.7(26)
B(120)-B(218)-B(213)	85.6(39)	Au(9)-B(218)-B(214)	77.8(20)
Au(9a)-B(218)-B(214)	64.5(19)	B(111)-B(218)-B(214)	83.3(26)
B(115)-B(218)-B(214)	65.1(33)	B(120)-B(218)-B(214)	121.5(43)
B(213)-B(218)-B(214)	62.3(28)	Au(9)-B(218)-B(217)	98.1(22)
Au(9a)-B(218)-B(217)	114.3(25)	B(111)-B(218)-B(217)	30.4(22)
B(115)-B(218)-B(217)	82.5(34)	B(120)-B(218)-B(217)	26.7(29)
B(213)-B(218)-B(217)	60.5(28)	B(214)-B(218)-B(217)	118.5(30)
Au(9)-B(220)-Au(9a)	27.2(6)	Au(9)-B(220)-B(113)	108.7(31)
Au(9a)-B(220)-B(113)	126.5(32)	Au(9)-B(220)-B(114)	60.6(19)
Au(9a)-B(220)-B(114)	83.1(23)	B(113)-B(220)-B(114)	48.6(24)
Au(9)-B(220)-C(116)	103.8(21)	Au(9a)-B(220)-C(116)	85.9(18)
B(113)-B(220)-C(116)	81.2(23)	B(114)-B(220)-C(116)	98.7(26)
Au(9)-B(220)-B(117)	150.0(38)	Au(9a)-B(220)-B(117)	135.8(36)
B(113)-B(220)-B(117)	59.9(32)	B(114)-B(220)-B(117)	105.6(38)
C(116)-B(220)-B(117)	49.4(25)	Au(9)-B(220)-B(118)	78.1(41)
Au(9a)-B(220)-B(118)	103.9(43)	B(113)-B(220)-B(118)	69.3(41)
B(114)-B(220)-B(118)	54.7(45)	C(116)-B(220)-B(118)	149.1(53)
B(117)-B(220)-B(118)	117.2(50)	Au(9)-B(220)-B(211)	121.3(35)
Au(9a)-B(220)-B(211)	124.2(31)	B(113)-B(220)-B(211)	30.5(26)
B(114)-B(220)-B(211)	78.6(31)	C(116)-B(220)-B(211)	52.7(23)
B(117)-B(220)-B(211)	35.3(33)	B(118)-B(220)-B(211)	99.4(48)
Au(9)-B(220)-B(214)	82.9(24)	Au(9a)-B(220)-B(214)	67.6(20)
B(113)-B(220)-B(214)	85.2(28)	B(114)-B(220)-B(214)	86.1(31)
C(116)-B(220)-B(214)	21.0(18)	B(117)-B(220)-B(214)	69.1(30)
B(118)-B(220)-B(214)	140.8(63)	B(211)-B(220)-B(214)	62.5(26)
Au(9)-B(220)-B(215)	85.7(34)	Au(9a)-B(220)-B(215)	111.8(38)
B(113)-B(220)-B(215)	36.0(27)	B(114)-B(220)-B(215)	32.2(30)
C(116)-B(220)-B(215)	113.8(34)	B(117)-B(220)-B(215)	93.6(48)

Table 45 continued

B(118)-B(220)-B(215)	35.3(40)	B(211)-B(220)-B(215)	66.4(34)
B(214)-B(220)-B(215)	109.9(41)	P(1)-C(311)-C(312)	117.4(14)
P(1)-C(311)-C(316)	118.3(14)	C(312)-C(311)-C(316)	116.2(17)
C(311)-C(312)-C(313)	113.4(19)	C(312)-C(313)-C(314)	113.8(20)
C(313)-C(314)-C(315)	121.9(21)	C(313)-C(314)-C(316)	93.1(14)
C(315)-C(314)-C(316)	33.8(13)	C(314)-C(315)-C(316)	114.9(21)
C(311)-C(316)-C(314)	91.0(12)	C(311)-C(316)-C(315)	118.1(19)
C(314)-C(316)-C(315)	31.3(12)	P(1)-C(321)-C(322)	111.2(12)
P(1)-C(321)-C(326)	112.4(11)	C(322)-C(321)-C(326)	110.6(15)
C(321)-C(322)-C(323)	112.8(15)	C(322)-C(323)-C(324)	110.5(16)
C(323)-C(324)-C(325)	113.5(19)	C(324)-C(325)-C(326)	108.9(17)
C(321)-C(326)-C(325)	113.7(14)	P(1)-C(331)-C(332)	120.8(17)
P(1)-C(331)-C(336)	119.8(16)	C(332)-C(331)-C(336)	121.0(21)
C(331)-C(332)-C(333)	113.4(18)	C(332)-C(333)-C(334)	122.4(21)
C(332)-C(333)-C(335)	93.3(13)	C(334)-C(333)-C(335)	29.4(15)
C(333)-C(334)-C(335)	122.5(30)	C(333)-C(335)-C(334)	28.1(18)
C(333)-C(335)-C(336)	90.8(16)	C(334)-C(335)-C(336)	118.7(25)
C(331)-C(336)-C(335)	121.4(21)	P(2)-C(411)-C(412)	114.2(14)
P(2)-C(411)-C(416)	116.9(19)	C(412)-C(411)-C(416)	110.6(20)
C(411)-C(412)-C(413)	114.5(18)	C(412)-C(413)-C(414)	111.3(27)
C(413)-C(414)-C(415)	110.6(22)	C(414)-C(415)-C(416)	113.9(21)
C(411)-C(416)-C(415)	114.0(23)	P(2)-C(421)-C(422)	114.0(12)
P(2)-C(421)-C(426)	113.2(14)	C(422)-C(421)-C(426)	112.2(17)
C(421)-C(422)-C(423)	105.8(15)	C(422)-C(423)-C(424)	114.0(21)
C(422)-C(423)-C(425)	92.5(13)	C(424)-C(423)-C(425)	35.3(11)
C(423)-C(424)-C(425)	111.6(19)	C(423)-C(425)-C(424)	33.1(13)
C(423)-C(425)-C(426)	90.2(13)	C(424)-C(425)-C(426)	112.4(17)
C(421)-C(426)-C(425)	115.1(20)	P(2)-C(431)-C(432)	110.9(13)
P(2)-C(431)-C(436)	109.4(11)	C(432)-C(431)-C(436)	107.9(14)
C(431)-C(432)-C(433)	112.6(16)	C(432)-C(433)-C(434)	108.4(15)
C(433)-C(434)-C(435)	110.7(19)	C(434)-C(435)-C(436)	112.8(19)
C(431)-C(436)-C(435)	111.6(15)		

Table 46. Final fractional coordinates (x 10^4), with standard deviations in parenthesis, for [arachno-9,6,6'-Au(CB_8H_{12})$_2$] [Au(P(cyclo-C_6H_{11})$_3$)$_2$] (10).

Au(3)	4998.2(6)	3149.3(5)	2172.8(4)	58(1)*
Au(9)	42.5(12)	1081.2(9)	3250.4(8)	67(1)*
Au(9a)	-393.9(16)	1143.7(13)	2839.4(10)	67(1)*
P(1)	3528(4)	4252(3)	3045(2)	61(2)*
P(2)	6398(4)	2872(4)	1248(3)	71(2)*
B(101)	2301(22)	245(20)	1559(14)	95(12)*
B(102)	3027(25)	-673(22)	2116(13)	104(14)*
B(103)	1765(22)	-963(21)	1927(14)	96(12)*
B(104)	764(23)	304(21)	1913(15)	105(13)*
B(105)	2747(22)	766(20)	2311(13)	93(12)*
C(106)	2669(22)	-247(18)	3067(11)	122(13)*
B(107)	1919(23)	-1190(20)	2802(15)	105(13)*
B(108)	570(24)	-695(18)	2743(16)	117(13)*
B(110)	1373(23)	1371(22)	2098(16)	113(13)*
B(111)+	-1609(42)	2923(38)	4564(27)	79(13)
B(112)+	-3001(35)	2727(30)	4398(22)	64(11)
B(113)+	-2262(43)	1676(40)	4839(27)	73(13)
B(114)+	-761(45)	1628(41)	4444(29)	100(16)
B(115)+	-1873(32)	3328(28)	3630(20)	59(10)
C(116)+	-2812(28)	2399(25)	3473(18)	67(9)
B(117)+	-2877(40)	1354(35)	4129(25)	81(13)
B(118)+	-1363(36)	527(32)	4175(25)	56(10)
B(120)+	-450(38)	2706(33)	3701(27)	72(11)
B(211)+	-2720(47)	1924(42)	4442(31)	96(16)
B(212)+	-1892(47)	2408(44)	4861(38)	97(16)
B(213)+	-2148(45)	3092(38)	4147(29)	89(14)
B(214)+	-2070(38)	2170(33)	3409(24)	77(12)
B(215)+	-1420(56)	989(51)	4621(36)	128(21)
C(216)+	-359(35)	1693(31)	4677(22)	96(12)
B(217)+	-711(42)	2941(38)	4234(27)	98(14)
B(218)+	-947(38)	2845(32)	3321(24)	68(11)
B(220)+	-1750(43)	878(39)	3836(28)	85(14)
C(311)	2900(20)	3498(15)	3895(10)	97(11)*
C(312)	3515(25)	2433(18)	3997(12)	147(16)*
C(313)	2850(22)	1814(17)	4679(13)	119(14)*
C(314)	2229(27)	2464(20)	5335(12)	166(18)*
C(315)	1670(26)	3501(22)	5265(14)	152(16)*
C(316)	2243(20)	4096(16)	4603(9)	106(11)*
C(321)	4854(14)	5324(12)	3341(8)	60(7)*
C(322)	4490(15)	6051(13)	2659(9)	73(8)*
C(323)	4995(17)	6918(15)	2872(11)	94(10)*
C(324)	5890(19)	6440(17)	3263(13)	107(12)*
C(325)	5460(18)	5772(15)	3968(10)	88(10)*
C(326)	4972(15)	4908(12)	3748(9)	69(8)*
C(331)	2304(18)	4837(19)	2627(12)	119(12)*
C(332)	1371(15)	5695(13)	3025(10)	80(8)*
C(333)	513(18)	6143(20)	2582(14)	143(14)*

Table 46 continued

C(434)	524(26)	5711(26)	1955(18)	182(22)#
C(335)	1399(19)	4914(17)	1598(12)	99(11)#
C(336)	2297(21)	4468(23)	1965(13)	183(17)#
C(411)	7816(18)	2481(21)	1825(12)	110(12)#
C(412)	7800(19)	3508(19)	1229(15)	124(13)#
C(413)	9842(24)	3774(25)	1879(19)	188(22)#
C(414)	9883(21)	3459(22)	269(15)	193(18)#
C(415)	9776(21)	2325(26)	101(15)	199(20)#
C(416)	8617(19)	2137(22)	217(12)	125(13)#
C(421)	6546(18)	611(14)	1590(10)	89(9)#
C(422)	7410(19)	-197(15)	991(12)	109(11)#
C(423)	7348(19)	-1346(16)	1365(13)	118(13)#
C(424)	7584(21)	-1483(17)	2078(14)	133(15)#
C(425)	6794(20)	-675(16)	2633(13)	112(13)#
C(426)	6750(21)	448(15)	2317(10)	109(12)#
C(431)	5962(15)	2161(13)	367(9)	72(8)#
C(432)	5706(17)	3345(12)	85(10)	79(9)#
C(433)	5260(19)	3463(15)	-610(11)	95(11)#
C(434)	4145(20)	3028(16)	-407(11)	103(12)#
C(435)	4362(20)	1892(16)	-162(11)	103(12)#
C(436)	4835(16)	1717(14)	517(9)	76(9)#

Equivalent isotropic U defined as one third of the trace of the orthogonalised U tensor

+ Occupancy of these atoms is 0.5

Table 47. Interatomic distances (pm), with standard deviations in parenthesis, for $[(CB_8H_{11}Au)(AuPPh_3)_5(AuCB_8H_{12})]$ (11).

Au(1)-Au(2)	2.825(2)	Au(1)-Au(3)	2.969(2)
Au(1)-Au(5)	2.724(2)	Au(1)-Au(7)	2.932(2)
Au(1)-P(1)	2.283(10)	Au(2)-Au(3)	2.697(2)
Au(2)-Au(4)	2.883(2)	Au(2)-Au(5)	2.785(2)
Au(2)-Au(7)	2.657(2)	Au(2)-B(204)	2.231(33)
Au(2)-B(208)	2.353(36)	Au(2)-B(210)	2.356(40)
Au(3)-Au(4)	2.993(2)	Au(3)-Au(5)	2.849(2)
Au(3)-P(3)	2.284(8)	Au(3)-B(210)	2.915(34)
Au(4)-Au(5)	2.712(2)	Au(4)-Au(6)	2.858(2)
Au(4)-P(4)	2.324(9)	Au(5)-Au(6)	2.902(2)
Au(5)-Au(7)	2.939(2)	Au(5)-B(104)	2.274(31)
Au(5)-B(108)	2.383(38)	Au(5)-B(110)	2.378(36)
Au(6)-P(6)	2.297(9)	Au(6)-B(105)	2.449(33)
Au(6)-B(110)	2.254(31)	Au(7)-P(7)	2.303(10)
P(1)-C(111)	1.791(36)	P(1)-C(121)	1.811(31)
P(1)-C(131)	1.796(34)	P(3)-C(311)	1.864(38)
P(3)-C(321)	1.763(35)	P(3)-C(331)	1.778(38)
P(4)-C(411)	1.820(29)	P(4)-C(421)	1.818(34)
P(4)-C(431)	1.837(28)	P(6)-C(611)	1.835(34)
P(6)-C(621)	1.795(32)	P(6)-C(631)	1.774(42)
P(7)-C(711)	1.819(38)	P(7)-C(721)	1.818(33)
P(7)-C(731)	1.784(37)	B(101)-B(102)	1.816(61)
B(101)-B(103)	1.796(62)	B(101)-B(104)	1.785(54)
B(101)-B(105)	1.788(58)	B(101)-B(110)	1.726(46)
B(102)-B(103)	1.853(60)	B(102)-B(105)	1.761(63)
B(102)-C(106)	1.658(46)	B(102)-B(107)	1.834(64)
B(103)-B(104)	1.792(52)	B(103)-B(107)	1.934(53)
B(103)-B(108)	1.797(51)	B(104)-B(108)	1.828(61)
B(104)-B(110)	1.868(56)	B(105)-C(106)	1.896(54)
B(105)-B(110)	1.816(51)	C(106)-B(107)	1.692(58)
B(107)-B(108)	1.930(63)	B(201)-B(202)	1.768(73)
B(201)-B(203)	1.914(56)	B(201)-B(204)	1.834(57)
B(201)-B(205)	1.733(60)	B(201)-B(210)	1.775(58)
B(202)-B(203)	1.783(65)	B(202)-B(205)	1.795(61)
B(202)-C(206)	1.659(55)	B(202)-B(207)	1.792(63)
B(203)-B(204)	1.777(58)	B(203)-B(207)	1.869(60)
B(203)-B(208)	1.761(51)	B(204)-B(208)	1.962(60)
B(204)-B(210)	1.873(52)	B(205)-C(206)	1.789(63)
B(205)-B(210)	1.806(69)	C(206)-B(207)	1.707(49)
B(207)-B(208)	1.895(61)	C(111)-C(112)	1.400(51)
C(111)-C(116)	1.387(50)	C(112)-C(113)	1.443(56)
C(113)-C(114)	1.385(62)	C(114)-C(115)	1.388(80)
C(115)-C(116)	1.450(70)	C(121)-C(122)	1.341(51)
C(121)-C(126)	1.299(48)	C(122)-C(123)	1.547(49)
C(123)-C(124)	1.369(49)	C(124)-C(125)	1.381(51)
C(125)-C(126)	1.411(49)	C(131)-C(132)	1.398(46)
C(131)-C(136)	1.375(56)	C(132)-C(133)	1.324(44)
C(133)-C(134)	1.460(59)	C(134)-C(135)	1.329(58)
C(135)-C(136)	1.414(45)	C(311)-C(312)	1.315(39)

Table 47 continued

C(311)-C(316)	1.417(36)	C(312)-C(313)	1.403(43)
C(313)-C(314)	1.347(36)	C(314)-C(315)	1.339(41)
C(315)-C(316)	1.406(45)	C(321)-C(322)	1.433(44)
C(321)-C(326)	1.392(47)	C(322)-C(323)	1.320(54)
C(323)-C(324)	1.462(53)	C(324)-C(325)	1.351(53)
C(325)-C(326)	1.410(59)	C(331)-C(332)	1.389(44)
C(331)-C(336)	1.371(54)	C(332)-C(333)	1.345(44)
C(333)-C(334)	1.380(60)	C(334)-C(335)	1.430(51)
C(335)-C(336)	1.387(47)	C(411)-C(412)	1.374(39)
C(411)-C(416)	1.385(39)	C(412)-C(413)	1.379(46)
C(413)-C(414)	1.368(47)	C(414)-C(415)	1.394(52)
C(415)-C(416)	1.425(53)	C(421)-C(422)	1.318(42)
C(421)-C(426)	1.397(48)	C(422)-C(423)	1.351(54)
C(422)-C(424)	2.284(52)	C(423)-C(424)	1.297(52)
C(424)-C(425)	1.400(46)	C(425)-C(426)	1.371(53)
C(431)-C(432)	1.392(46)	C(431)-C(436)	1.374(48)
C(432)-C(433)	1.361(41)	C(433)-C(434)	1.454(54)
C(434)-C(435)	1.330(57)	C(435)-C(436)	1.403(45)
C(611)-C(612)	1.354(57)	C(611)-C(616)	1.439(58)
C(612)-C(613)	1.399(59)	C(613)-C(614)	1.322(63)
C(614)-C(615)	1.454(66)	C(615)-C(616)	1.410(63)
C(621)-C(622)	1.316(56)	C(621)-C(626)	1.394(47)
C(622)-C(623)	1.416(49)	C(623)-C(624)	1.363(53)
C(624)-C(625)	1.328(68)	C(625)-C(626)	1.316(51)
C(631)-C(632)	1.424(55)	C(631)-C(636)	1.363(45)
C(632)-C(633)	1.465(73)	C(633)-C(634)	1.352(54)
C(634)-C(635)	1.244(55)	C(635)-C(636)	1.472(60)
C(711)-C(712)	1.343(58)	C(711)-C(716)	1.389(53)
C(712)-C(713)	1.457(62)	C(713)-C(714)	1.290(64)
C(714)-C(715)	1.343(72)	C(715)-C(716)	1.423(61)
C(721)-C(722)	1.505(52)	C(721)-C(725)	2.247(65)
C(721)-C(726)	1.325(58)	C(722)-C(723)	1.395(57)
C(723)-C(724)	1.358(73)	C(724)-C(725)	1.435(77)
C(725)-C(726)	1.388(69)	C(731)-C(732)	1.385(61)
C(731)-C(736)	1.377(41)	C(732)-C(733)	1.393(79)
C(733)-C(734)	1.349(64)	C(734)-C(735)	1.454(69)
C(735)-C(736)	1.448(56)	C(1)-C(2)	1.302(110)
C(1)-C(4)	2.184(127)	C(3)-C(4)	1.348(112)

Table 48. Interbond angles (°), with standard deviations in parenthesis, for $[(CB_8H_{11}Au)(AuPPh_3)_5(AuCB_8H_{12})]$ (11).

Au(2)-Au(1)-Au(3)	55.4	Au(2)-Au(1)-Au(5)	60.2
Au(3)-Au(1)-Au(5)	59.9	Au(2)-Au(1)-Au(7)	54.9
Au(3)-Au(1)-Au(7)	104.10(10)	Au(5)-Au(1)-Au(7)	62.5
Au(2)-Au(1)-P(1)	135.8(2)	Au(3)-Au(1)-P(1)	122.8(2)
Au(5)-Au(1)-P(1)	164.5(2)	Au(7)-Au(1)-P(1)	126.1(2)
Au(1)-Au(2)-Au(3)	65.0	Au(1)-Au(2)-Au(4)	110.30(10)
Au(3)-Au(2)-Au(4)	64.80(10)	Au(1)-Au(2)-Au(5)	58.1
Au(3)-Au(2)-Au(5)	62.6	Au(4)-Au(2)-Au(5)	57.1
Au(1)-Au(2)-Au(7)	64.6	Au(3)-Au(2)-Au(7)	120.70(10)
Au(4)-Au(2)-Au(7)	107.20(10)	Au(5)-Au(2)-Au(7)	65.3
Au(1)-Au(2)-B(204)	145.9(11)	Au(3)-Au(2)-B(204)	115.2(10)
Au(4)-Au(2)-B(204)	98.6(12)	Au(5)-Au(2)-B(204)	155.1(12)
Au(7)-Au(2)-B(204)	124.8(10)	Au(1)-Au(2)-B(208)	113.5(10)
Au(3)-Au(2)-B(208)	154.7(10)	Au(4)-Au(2)-B(208)	132.1(11)
Au(5)-Au(2)-B(208)	140.2(9)	Au(7)-Au(2)-B(208)	76.8(9)
B(204)-Au(2)-B(208)	50.6(14)	Au(1)-Au(2)-B(210)	110.2(10)
Au(3)-Au(2)-B(210)	70.1(9)	Au(4)-Au(2)-B(210)	94.4(11)
Au(5)-Au(2)-B(210)	131.6(9)	Au(7)-Au(2)-B(210)	150.4(11)
B(204)-Au(2)-B(210)	48.1(13)	B(208)-Au(2)-B(210)	88.2(13)
Au(1)-Au(3)-Au(2)	59.6	Au(1)-Au(3)-Au(4)	103.50(10)
Au(2)-Au(3)-Au(4)	60.6	Au(1)-Au(3)-Au(5)	55.8
Au(2)-Au(3)-Au(5)	60.2	Au(4)-Au(3)-Au(5)	55.3
Au(1)-Au(3)-P(3)	121.8(2)	Au(2)-Au(3)-P(3)	174.6(2)
Au(4)-Au(3)-P(3)	122.3(3)	Au(5)-Au(3)-P(3)	125.2(2)
Au(1)-Au(3)-B(210)	92.7(9)	Au(2)-Au(3)-B(210)	49.4(8)
Au(4)-Au(3)-B(210)	81.6(9)	Au(5)-Au(3)-B(210)	109.8(8)
P(3)-Au(3)-B(210)	125.4(8)	Au(2)-Au(4)-Au(3)	54.6
Au(2)-Au(4)-Au(5)	59.6	Au(3)-Au(4)-Au(5)	59.7
Au(2)-Au(4)-Au(6)	105.80(10)	Au(3)-Au(4)-Au(6)	120.70(10)
Au(5)-Au(4)-Au(6)	62.8	Au(2)-Au(4)-P(4)	118.8(2)
Au(3)-Au(4)-P(4)	111.2(2)	Au(5)-Au(4)-P(4)	170.4(2)
Au(6)-Au(4)-P(4)	124.9(2)	Au(1)-Au(5)-Au(2)	61.7
Au(1)-Au(5)-Au(3)	64.30(10)	Au(2)-Au(5)-Au(3)	57.2
Au(1)-Au(5)-Au(4)	119.00(10)	Au(2)-Au(5)-Au(4)	63.2
Au(3)-Au(5)-Au(4)	65.1	Au(1)-Au(5)-Au(6)	161.30(10)
Au(2)-Au(5)-Au(6)	107.00(10)	Au(3)-Au(5)-Au(6)	124.10(10)
Au(4)-Au(5)-Au(6)	60.9	Au(1)-Au(5)-Au(7)	62.2
Au(2)-Au(5)-Au(7)	55.2	Au(3)-Au(5)-Au(7)	107.00(10)
Au(4)-Au(5)-Au(7)	104.2	Au(6)-Au(5)-Au(7)	99.20(10)
Au(1)-Au(5)-B(104)	99.2(11)	Au(2)-Au(5)-B(104)	156.5(10)
Au(3)-Au(5)-B(104)	103.5(9)	Au(4)-Au(5)-B(104)	124.8(11)
Au(6)-Au(5)-B(104)	94.9(10)	Au(7)-Au(5)-B(104)	130.5(10)
Au(1)-Au(5)-B(108)	78.2(11)	Au(2)-Au(5)-B(108)	127.5(10)
Au(3)-Au(5)-B(108)	118.3(10)	Au(4)-Au(5)-B(108)	169.3(10)
Au(6)-Au(5)-B(108)	112.4(11)	Au(7)-Au(5)-B(108)	84.8(10)
B(104)-Au(5)-B(108)	46.1(14)	Au(1)-Au(5)-B(110)	146.5(8)
Au(2)-Au(5)-B(110)	149.3(9)	Au(3)-Au(5)-B(110)	115.4(9)
Au(4)-Au(5)-B(110)	86.4(9)	Au(6)-Au(5)-B(110)	49.3(8)
Au(7)-Au(5)-B(110)	136.6(8)	B(104)-Au(5)-B(110)	47.3(13)
B(108)-Au(5)-B(110)	83.8(14)	Au(4)-Au(6)-Au(5)	56.3

Table 48 continued

Au(4)-Au(6)-P(6)	106.8(2)	Au(5)-Au(6)-P(6)	145.5(3)
Au(4)-Au(6)-B(105)	138.3(9)	Au(5)-Au(6)-B(105)	83.1(10)
P(6)-Au(6)-B(105)	122.5(9)	Au(4)-Au(6)-B(110)	85.5(9)
Au(5)-Au(6)-B(110)	53.1(10)	P(6)-Au(6)-B(110)	161.3(10)
B(105)-Au(6)-B(110)	45.2(12)	Au(1)-Au(7)-Au(2)	60.5
Au(1)-Au(7)-Au(5)	55.3	Au(2)-Au(7)-Au(5)	59.4
Au(1)-Au(7)-P(7)	126.7(2)	Au(2)-Au(7)-P(7)	163.3(2)
Au(5)-Au(7)-P(7)	137.2(2)	Au(1)-P(1)-C(111)	115.8(14)
Au(1)-P(1)-C(121)	112.1(11)	C(111)-P(1)-C(121)	106.2(16)
Au(1)-P(1)-C(131)	112.4(13)	C(111)-P(1)-C(131)	102.3(15)
C(121)-P(1)-C(131)	107.3(17)	Au(3)-P(3)-C(311)	115.7(9)
Au(3)-P(3)-C(321)	111.8(10)	C(311)-P(3)-C(321)	104.6(14)
Au(3)-P(3)-C(331)	115.9(12)	C(311)-P(3)-C(331)	104.1(14)
C(321)-P(3)-C(331)	103.4(15)	Au(4)-P(4)-C(411)	115.6(11)
Au(4)-P(4)-C(421)	114.2(9)	C(411)-P(4)-C(421)	104.8(14)
Au(4)-P(4)-C(431)	116.8(11)	C(411)-P(4)-C(431)	101.8(12)
C(421)-P(4)-C(431)	102.8(15)	Au(6)-P(6)-C(611)	110.8(10)
Au(6)-P(6)-C(621)	115.7(13)	C(611)-P(6)-C(621)	104.0(15)
Au(6)-P(6)-C(631)	114.3(11)	C(611)-P(6)-C(631)	103.4(17)
C(621)-P(6)-C(631)	107.5(16)	Au(7)-P(7)-C(711)	112.3(14)
Au(7)-P(7)-C(721)	113.2(12)	C(711)-P(7)-C(721)	107.0(16)
Au(7)-P(7)-C(731)	113.0(12)	C(711)-P(7)-C(731)	109.0(17)
C(721)-P(7)-C(731)	101.7(17)	B(102)-B(101)-B(103)	61.7(24)
B(102)-B(101)-B(104)	108.8(29)	B(103)-B(101)-B(104)	60.1(22)
B(102)-B(101)-B(105)	58.5(23)	B(103)-B(101)-B(105)	110.8(27)
B(104)-B(101)-B(105)	111.9(23)	B(102)-B(101)-B(110)	110.3(24)
B(103)-B(101)-B(110)	114.2(26)	B(104)-B(101)-B(110)	64.3(21)
B(105)-B(101)-B(110)	62.2(20)	B(101)-B(102)-B(103)	58.6(23)
B(101)-B(102)-B(105)	60.0(23)	B(103)-B(102)-B(105)	109.4(29)
B(101)-B(102)-C(106)	114.7(28)	B(103)-B(102)-C(106)	112.7(29)
B(105)-B(102)-C(106)	67.3(23)	B(101)-B(102)-B(107)	108.8(30)
B(103)-B(102)-B(107)	63.3(25)	B(105)-B(102)-B(107)	110.3(27)
C(106)-B(102)-B(107)	57.7(23)	B(101)-B(103)-B(102)	59.7(23)
B(101)-B(103)-B(104)	59.7(22)	B(102)-B(103)-B(104)	106.8(27)
B(101)-B(103)-B(107)	105.3(25)	B(102)-B(103)-B(107)	57.9(22)
B(104)-B(103)-B(107)	106.2(22)	B(101)-B(103)-B(108)	111.2(25)
B(102)-B(103)-B(108)	110.9(24)	B(104)-B(103)-B(108)	61.2(21)
B(107)-B(103)-B(108)	62.2(21)	Au(5)-B(104)-B(101)	118.5(21)
Au(5)-B(104)-B(103)	120.9(21)	B(101)-B(104)-B(103)	60.3(22)
Au(5)-B(104)-B(108)	70.1(15)	B(101)-B(104)-B(108)	110.3(27)
B(103)-B(104)-B(108)	59.5(21)	Au(5)-B(104)-B(110)	69.3(14)
B(101)-B(104)-B(110)	56.3(20)	B(103)-B(104)-B(110)	107.8(25)
B(108)-B(104)-B(110)	117.2(25)	Au(6)-B(105)-B(101)	118.6(21)
Au(6)-B(105)-B(102)	140.5(26)	B(101)-B(105)-B(102)	61.5(23)
Au(6)-B(105)-C(106)	93.1(15)	B(101)-B(105)-C(106)	105.1(27)
B(102)-B(105)-C(106)	53.8(20)	Au(6)-B(105)-B(110)	61.7(14)
B(101)-B(105)-B(110)	57.2(19)	B(102)-B(105)-B(110)	108.6(28)
C(106)-B(105)-B(110)	113.8(26)	B(102)-C(106)-B(105)	59.0(23)
B(102)-C(106)-B(107)	66.4(24)	B(105)-C(106)-B(107)	110.5(23)
B(102)-B(107)-B(103)	58.8(21)	B(102)-B(107)-C(106)	56.0(22)
B(103)-B(107)-C(106)	107.3(28)	B(102)-B(107)-B(108)	106.0(29)
B(103)-B(107)-B(108)	55.4(20)	C(106)-B(107)-B(108)	120.0(30)
Au(5)-B(108)-B(103)	115.3(26)	Au(5)-B(108)-B(104)	63.8(16)

Table 48 continued

B(103)-B(108)-B(104)	59.3(21)	Au(5)-B(108)-B(107)	108.6(23)
B(103)-B(108)-B(107)	62.4(20)	B(104)-B(108)-B(107)	104.9(28)
Au(5)-B(110)-Au(6)	77.5(9)	Au(5)-B(110)-B(101)	116.8(25)
Au(6)-B(110)-B(101)	133.2(23)	Au(5)-B(110)-B(104)	63.4(15)
Au(6)-B(110)-B(104)	136.8(22)	B(101)-B(110)-B(104)	59.4(21)
Au(5)-B(110)-B(105)	115.8(22)	Au(6)-B(110)-B(105)	73.1(15)
B(101)-B(110)-B(105)	60.6(20)	B(104)-B(110)-B(105)	106.9(25)
B(202)-B(201)-B(203)	57.8(24)	B(202)-B(201)-B(204)	104.1(30)
B(203)-B(201)-B(204)	56.6(21)	B(202)-B(201)-B(205)	61.7(26)
B(203)-B(201)-B(205)	106.3(30)	B(204)-B(201)-B(205)	107.8(26)
B(202)-B(201)-B(210)	112.9(29)	B(203)-B(201)-B(210)	109.8(26)
B(204)-B(201)-B(210)	62.5(21)	B(205)-B(201)-B(210)	62.8(24)
B(201)-B(202)-B(203)	65.2(27)	B(201)-B(202)-B(205)	58.2(26)
B(203)-B(202)-B(205)	109.4(34)	B(201)-B(202)-C(206)	112.1(30)
B(203)-B(202)-C(206)	110.6(30)	B(205)-B(202)-C(206)	62.3(24)
B(201)-B(202)-B(207)	116.6(34)	B(203)-B(202)-B(207)	63.8(25)
B(205)-B(202)-B(207)	110.8(28)	C(206)-B(202)-B(207)	59.1(23)
B(201)-B(203)-B(202)	57.8(25)	B(201)-B(203)-B(204)	59.5(22)
B(202)-B(203)-B(204)	105.9(27)	B(201)-B(203)-B(207)	106.4(25)
B(202)-B(203)-B(207)	58.7(25)	B(204)-B(203)-B(207)	112.8(24)
B(201)-B(203)-B(208)	115.5(24)	B(202)-B(203)-B(208)	111.9(28)
B(204)-B(203)-B(208)	67.4(23)	B(207)-B(203)-B(208)	62.9(23)
Au(2)-B(204)-B(201)	117.9(22)	Au(2)-B(204)-B(203)	116.6(25)
B(201)-B(204)-B(203)	64.8(23)	Au(2)-B(204)-B(208)	67.9(15)
B(201)-B(204)-B(208)	109.9(29)	B(203)-B(204)-B(208)	55.9(21)
Au(2)-B(204)-B(210)	69.4(15)	B(201)-B(204)-B(210)	57.2(20)
B(203)-B(204)-B(210)	111.5(29)	B(208)-B(204)-B(210)	117.3(27)
B(201)-B(205)-B(202)	60.1(26)	B(201)-B(205)-C(206)	107.6(29)
B(202)-B(205)-C(206)	55.1(24)	B(201)-B(205)-B(210)	60.1(24)
B(202)-B(205)-B(210)	110.1(31)	C(206)-B(205)-B(210)	118.2(30)
B(202)-C(206)-B(205)	62.6(25)	B(202)-C(206)-B(207)	64.3(24)
B(205)-C(206)-B(207)	114.3(29)	B(202)-B(207)-B(203)	58.2(24)
B(202)-B(207)-C(206)	56.5(21)	B(203)-B(207)-C(206)	104.5(27)
B(202)-B(207)-B(208)	105.5(31)	B(203)-B(207)-B(208)	55.8(21)
C(206)-B(207)-B(208)	114.1(27)	Au(2)-B(208)-B(203)	111.6(23)
Au(2)-B(208)-B(204)	61.5(14)	B(203)-B(208)-B(204)	56.7(21)
Au(2)-B(208)-B(207)	111.1(19)	B(203)-B(208)-B(207)	61.3(22)
B(204)-B(208)-B(207)	103.2(25)	Au(2)-B(210)-Au(3)	60.5(8)
Au(2)-B(210)-B(201)	114.6(23)	Au(3)-B(210)-B(201)	169.6(29)
Au(2)-B(210)-B(204)	62.4(16)	Au(3)-B(210)-B(204)	119.4(20)
B(201)-B(210)-B(204)	60.3(21)	Au(2)-B(210)-B(205)	109.4(25)
Au(3)-B(210)-B(205)	113.8(21)	B(201)-B(210)-B(205)	57.9(23)
B(204)-B(210)-B(205)	102.4(27)	P(1)-C(111)-C(112)	119.6(26)
P(1)-C(111)-C(116)	123.1(29)	C(112)-C(111)-C(116)	116.7(33)
C(111)-C(112)-C(113)	123.2(34)	C(112)-C(113)-C(114)	115.9(40)
C(113)-C(114)-C(115)	122.3(48)	C(114)-C(115)-C(116)	118.5(47)
C(111)-C(116)-C(115)	121.6(41)	P(1)-C(121)-C(122)	118.8(25)
P(1)-C(121)-C(126)	119.7(27)	C(122)-C(121)-C(126)	122.2(33)
C(121)-C(122)-C(123)	115.8(31)	C(122)-C(123)-C(124)	118.3(33)
C(123)-C(124)-C(125)	121.3(33)	C(124)-C(125)-C(126)	119.2(34)
C(121)-C(126)-C(125)	123.4(35)	P(1)-C(131)-C(132)	118.3(30)
P(1)-C(131)-C(136)	121.8(25)	C(132)-C(131)-C(136)	119.9(29)
C(131)-C(132)-C(133)	120.4(36)	C(132)-C(133)-C(134)	121.4(32)
C(133)-C(134)-C(135)	116.8(32)	C(134)-C(135)-C(136)	122.5(40)

Table 48 continued

C(131)-C(136)-C(135)	118.5(31)	P(3)-C(311)-C(312)	123.5(21)
P(3)-C(311)-C(316)	114.8(21)	C(312)-C(311)-C(316)	122.5(28)
C(311)-C(312)-C(313)	119.1(25)	C(312)-C(313)-C(314)	121.4(27)
C(313)-C(314)-C(315)	118.5(29)	C(314)-C(315)-C(316)	123.5(26)
C(311)-C(316)-C(315)	114.8(26)	P(3)-C(321)-C(322)	118.4(24)
P(3)-C(321)-C(326)	125.4(25)	C(322)-C(321)-C(326)	116.1(31)
C(321)-C(322)-C(323)	121.9(31)	C(322)-C(323)-C(324)	121.1(34)
C(323)-C(324)-C(325)	118.3(38)	C(324)-C(325)-C(326)	119.6(36)
C(321)-C(326)-C(325)	122.8(33)	P(3)-C(331)-C(332)	123.9(29)
P(3)-C(331)-C(336)	120.6(24)	C(332)-C(331)-C(336)	115.3(28)
C(331)-C(332)-C(333)	118.4(35)	C(332)-C(333)-C(334)	125.6(33)
C(333)-C(334)-C(335)	118.9(31)	C(334)-C(335)-C(336)	111.9(37)
C(331)-C(336)-C(335)	129.7(32)	P(4)-C(411)-C(412)	117.6(19)
P(4)-C(411)-C(416)	122.8(23)	C(412)-C(411)-C(416)	119.6(28)
C(411)-C(412)-C(413)	124.4(26)	C(412)-C(413)-C(414)	116.8(31)
C(413)-C(414)-C(415)	121.4(38)	C(414)-C(415)-C(416)	121.3(32)
C(411)-C(416)-C(415)	116.4(29)	P(4)-C(421)-C(422)	122.5(26)
P(4)-C(421)-C(426)	119.2(23)	C(422)-C(421)-C(426)	118.3(32)
C(421)-C(422)-C(423)	124.1(34)	C(421)-C(422)-C(424)	94.4(24)
C(423)-C(422)-C(424)	29.7(19)	C(422)-C(423)-C(424)	119.2(33)
C(422)-C(424)-C(423)	31.1(21)	C(422)-C(424)-C(425)	89.3(25)
C(423)-C(424)-C(425)	120.4(36)	C(424)-C(425)-C(426)	119.9(34)
C(421)-C(426)-C(425)	117.9(30)	P(4)-C(431)-C(432)	118.5(24)
P(4)-C(431)-C(436)	122.2(23)	C(432)-C(431)-C(436)	118.9(27)
C(431)-C(432)-C(433)	123.8(33)	C(432)-C(433)-C(434)	116.8(31)
C(433)-C(434)-C(435)	121.2(33)	C(434)-C(435)-C(436)	120.7(39)
C(431)-C(436)-C(435)	119.6(32)	P(6)-C(611)-C(612)	118.2(38)
P(6)-C(611)-C(616)	121.1(28)	C(612)-C(611)-C(616)	120.4(34)
C(611)-C(612)-C(613)	120.1(42)	C(612)-C(613)-C(614)	121.5(43)
C(613)-C(614)-C(615)	121.7(48)	C(614)-C(615)-C(616)	116.3(43)
C(611)-C(616)-C(615)	118.6(41)	P(6)-C(621)-C(622)	119.3(25)
P(6)-C(621)-C(626)	123.5(29)	C(622)-C(621)-C(626)	117.0(31)
C(621)-C(622)-C(623)	121.1(33)	C(622)-C(623)-C(624)	119.0(39)
C(623)-C(624)-C(625)	118.1(37)	C(624)-C(625)-C(626)	122.4(41)
C(621)-C(626)-C(625)	121.4(39)	P(6)-C(631)-C(632)	120.5(27)
P(6)-C(631)-C(636)	127.1(29)	C(632)-C(631)-C(636)	112.4(38)
C(631)-C(632)-C(633)	125.3(34)	C(632)-C(633)-C(634)	113.6(41)
C(633)-C(634)-C(635)	125.1(49)	C(634)-C(635)-C(636)	121.2(35)
C(631)-C(636)-C(635)	121.8(33)	P(7)-C(711)-C(712)	118.1(28)
P(7)-C(711)-C(716)	117.8(31)	C(712)-C(711)-C(716)	124.6(36)
C(711)-C(712)-C(713)	116.8(35)	C(712)-C(713)-C(714)	117.4(46)
C(713)-C(714)-C(715)	128.3(48)	C(714)-C(715)-C(716)	115.8(41)
C(711)-C(716)-C(715)	117.1(39)	P(7)-C(721)-C(722)	118.8(25)
P(7)-C(721)-C(725)	144.4(24)	C(722)-C(721)-C(725)	97.2(26)
P(7)-C(721)-C(726)	113.9(29)	C(722)-C(721)-C(726)	127.9(33)
C(725)-C(721)-C(726)	38.8(26)	C(721)-C(722)-C(723)	109.4(35)
C(722)-C(723)-C(724)	122.7(44)	C(723)-C(724)-C(725)	121.1(48)
C(721)-C(725)-C(724)	89.2(36)	C(721)-C(725)-C(726)	31.5(28)
C(724)-C(725)-C(726)	120.6(53)	C(721)-C(726)-C(725)	117.7(47)
P(7)-C(731)-C(732)	123.9(26)	P(7)-C(731)-C(736)	119.2(29)
C(732)-C(731)-C(736)	116.9(34)	C(731)-C(732)-C(733)	127.3(41)
C(732)-C(733)-C(734)	115.8(55)	C(733)-C(734)-C(735)	119.9(48)
C(734)-C(735)-C(736)	119.8(33)	C(731)-C(736)-C(735)	118.3(34)
C(2)-C(1)-C(4)	158.8(63)	C(1)-C(4)-C(3)	83.7(62)

Table 49. Final fractional coordinates (x 10^4), with standard deviations in parenthesis, for $[(CB_9H_{11}Au)(AuPPh_3)_5(AuCB_9H_{12})]$ (11).

atom	x	y	z	U
Au(1)	8631.6(8)	8161.4(6)	8844.8(10)	37(1)*
Au(2)	7632.3(8)	7082.8(6)	8646.9(9)	31(1)*
Au(3)	8920.5(8)	7095.1(6)	7195.7(10)	36(1)*
Au(4)	7382.7(8)	6764.0(6)	6888.0(9)	33(1)*
Au(5)	7781.7(7)	7942.9(6)	6766.8(9)	30(1)*
Au(6)	6311.0(8)	7691.2(6)	5980.8(10)	39(1)*
Au(7)	6893.7(8)	8111.1(6)	8716.8(10)	42(1)*
P(1)	9560(5)	8549(4)	8733(7)	42(4)*
P(3)	10062(5)	7040(4)	6082(6)	33(4)*
P(4)	7189(5)	5732(4)	6950(7)	38(4)*
P(6)	5032(6)	7265(4)	6388(7)	49(4)*
P(7)	6149(5)	8847(4)	9268(7)	45(4)*
B(101)	7701(22)	8941(17)	4354(27)	42(11)
B(102)	6988(26)	9454(21)	4790(33)	67(14)
B(103)	8022(21)	9433(17)	5039(27)	39(16)*
B(104)	8287(22)	8645(17)	5307(27)	37(10)
B(105)	6666(22)	8714(17)	4882(28)	43(17)*
C(106)	6321(17)	9118(13)	5819(24)	39(15)*
B(107)	7187(28)	9465(19)	6067(27)	65(21)*
B(108)	8047(25)	9014(17)	6331(29)	52(28)*
B(110)	7463(21)	8192(16)	5074(26)	32(10)
B(201)	8881(24)	5787(18)	10461(29)	51(12)
B(202)	8197(28)	6217(22)	11315(35)	76(15)
B(203)	7284(22)	6166(18)	11092(28)	43(11)
B(204)	7304(22)	6176(17)	9795(28)	44(11)
B(205)	8894(27)	6304(20)	10149(33)	66(14)
C(206)	8615(20)	6910(16)	10719(25)	60(11)
B(207)	7625(23)	6889(17)	11239(28)	44(11)
B(208)	6929(22)	6865(18)	10330(2	45(11)
B(210)	8379(24)	6212(18)	9169(3	51(12)
C(111)	10541(20)	8263(16)	8535(25)	62(11)
C(112)	10638(21)	7636(16)	8622(25)	68(12)
C(113)	11398(24)	7369(21)	8463(31)	113(17)
C(114)	12041(31)	7779(23)	7984(34)	136(20)
C(115)	11999(34)	8401(26)	7882(37)	150(22)
C(116)	11227(23)	8642(19)	8162(28)	86(14)
C(121)	9257(19)	8414(14)	10093(23)	39(9)
C(122)	9795(22)	8192(16)	10681(26)	67(12)
C(123)	9477(22)	8047(16)	11837(27)	68(12)
C(124)	8708(20)	8187(15)	12156(26)	59(11)
C(125)	8268(22)	8467(16)	11512(25)	72(12)
C(126)	8551(22)	8559(16)	10463(27)	74(12)
C(131)	9747(20)	9363(16)	8191(26)	62(11)
C(132)	9815(18)	9601(15)	7140(23)	44(9)
C(133)	10847(19)	10184(16)	6691(26)	58(11)

Table 49 continued

C(134)	10247(19)	10592(16)	7270(26)	60(11)
C(135)	10146(22)	10358(17)	8272(29)	81(13)
C(136)	9945(17)	9729(14)	8759(24)	46(10)
C(311)	10868(17)	6594(13)	6654(21)	31(8)
C(312)	11627(18)	6669(14)	6219(23)	46(10)
C(313)	12184(18)	6292(13)	6692(21)	37(9)
C(314)	11959(18)	5858(14)	7581(22)	44(9)
C(315)	11190(18)	5807(14)	8034(24)	50(10)
C(316)	10592(19)	6160(14)	7684(23)	46(9)
C(321)	9877(17)	6686(13)	5160(21)	33(8)
C(322)	9212(18)	6876(14)	4665(22)	48(10)
C(323)	9816(21)	6616(15)	3997(25)	60(12)
C(324)	9490(21)	6132(16)	3702(27)	75(12)
C(325)	10097(21)	5922(17)	4190(26)	77(13)
C(326)	10293(21)	6202(15)	4910(25)	67(12)
C(331)	10545(19)	7752(15)	5348(25)	53(10)
C(332)	10904(18)	7872(15)	4333(24)	52(10)
C(333)	11302(20)	8417(16)	3874(27)	69(12)
C(334)	11384(21)	8879(17)	4323(28)	73(12)
C(335)	11053(21)	8778(17)	5377(28)	74(12)
C(336)	10638(18)	8214(15)	5787(25)	51(10)
C(411)	7985(16)	5241(12)	7575(20)	24(8)
C(412)	8697(19)	5338(15)	7128(24)	51(10)
C(413)	9387(20)	5000(15)	7492(25)	53(10)
C(414)	9112(26)	4615(19)	8455(31)	103(16)
C(415)	8325(21)	4532(17)	8985(29)	79(13)
C(416)	7695(22)	4853(16)	8550(26)	69(12)
C(421)	7285(17)	5590(14)	5719(22)	37(9)
C(422)	7813(18)	5963(15)	4957(23)	48(10)
C(423)	7833(21)	5854(17)	4847(27)	77(13)
C(424)	7338(19)	5354(15)	3893(25)	59(11)
C(425)	7668(20)	4943(16)	4650(25)	67(12)
C(426)	7651(19)	5061(15)	5568(25)	63(11)
C(431)	6234(17)	5328(13)	7637(21)	34(8)
C(432)	5729(19)	5598(16)	8281(24)	57(11)
C(433)	5008(18)	5338(14)	8818(23)	49(10)
C(434)	4749(23)	4783(17)	8609(27)	72(12)
C(436)	5962(18)	4810(14)	7445(23)	49(10)
C(611)	4332(19)	7828(16)	5863(24)	51(10)
C(612)	4495(26)	8429(20)	5759(29)	94(15)
C(613)	3995(23)	8877(20)	5324(29)	95(15)
C(614)	3346(23)	8728(19)	5038(29)	96(15)
C(615)	3110(28)	8091(22)	5160(35)	127(19)
C(616)	3672(23)	7648(20)	5473(29)	99(15)
C(621)	4618(20)	7807(15)	7721(24)	58(10)
C(622)	5053(22)	7865(15)	8383(26)	63(11)
C(623)	4757(23)	6854(16)	9441(29)	76(13)
C(624)	3988(23)	6643(17)	9771(30)	83(13)
C(625)	3563(28)	6574(20)	9088(31)	118(17)
C(626)	3838(22)	6783(16)	8104(26)	69(12)
C(631)	4901(20)	6651(16)	5861(26)	55(10)
C(632)	5122(23)	6734(20)	4796(31)	94(15)

Table 49 continued

C(633)	5030(25)	6265(20)	4273(35)	110(17)
C(634)	4629(24)	5746(19)	4885(33)	91(14)
C(635)	4447(20)	5621(17)	5826(26)	68(12)
C(636)	4566(20)	6080(16)	6365(27)	64(11)
C(711)	5377(21)	9119(17)	8523(26)	59(11)
C(712)	4826(22)	8706(18)	8492(27)	73(12)
C(713)	4213(20)	8947(22)	7900(32)	108(16)
C(714)	4265(27)	9527(22)	7435(33)	103(16)
C(715)	4759(26)	9963(22)	7518(32)	104(16)
C(716)	5354(23)	9750(18)	8114(27)	76(13)
C(721)	5654(21)	8588(16)	10590(26)	55(11)
C(722)	4827(23)	8791(18)	10878(30)	82(13)
C(723)	4359(30)	8550(21)	11921(35)	127(19)
C(724)	5037(30)	8240(22)	12556(41)	140(20)
C(725)	5821(36)	8877(26)	12168(43)	186(26)
C(726)	6100(29)	8236(20)	11196(33)	119(18)
C(731)	6743(20)	9492(15)	9275(25)	48(10)
C(732)	6558(27)	9837(19)	9957(31)	100(15)
C(733)	7026(32)	10291(25)	10102(45)	160(23)
C(734)	7647(28)	10519(23)	9336(34)	115(17)
C(735)	7924(24)	10175(18)	8608(29)	83(13)
C(736)	7436(19)	9665(15)	8567(24)	54(10)
C(1)	2569(51)	6920(41)	2596(64)	109(32)
C(2)	2855(35)	6727(27)	3429(44)	39(18)
C(3)	2169(52)	7680(41)	1176(65)	110(32)
C(4)	1683(48)	7174(37)	1615(68)	92(29)

* Equivalent isotropic U defined as one third of the trace of the orthogonalised U tensor

Table 50. Interatomic distances (pm), with standard deviations in parenthesis, for [arachno-6,9,9',6'-(CB_8H_{12})Au(dppe)Au(CB_8H_{12})] (12).

Au(1)-Au(2)	2.6570(10)	Au(1)-P(1)	2.347(6)
Au(1)-B(104)	2.176(28)	Au(1)-B(108)	2.269(26)
Au(1)-B(110)	2.355(34)	Au(2)-P(2)	2.335(6)
Au(2)-B(204)	2.296(30)	Au(2)-B(208)	2.244(25)
Au(2)-B(210)	2.400(29)	P(1)-C(1)	1.834(23)
P(1)-C(111)	1.792(23)	P(1)-C(121)	1.827(31)
P(2)-C(2)	1.834(23)	P(2)-C(211)	1.790(28)
P(2)-C(221)	1.794(21)	C(1)-C(2)	1.506(38)
B(101)-B(102)	1.781(42)	B(101)-B(103)	1.869(51)
B(101)-B(104)	1.854(49)	B(101)-B(105)	1.828(53)
B(101)-B(110)	1.752(43)	B(102)-B(103)	1.718(48)
B(102)-B(105)	1.872(50)	B(102)-C(106)	1.789(42)
B(102)-B(107)	1.824(50)	B(103)-B(104)	1.828(40)
B(103)-B(107)	1.767(42)	B(103)-B(108)	1.857(46)
B(104)-B(108)	1.837(43)	B(104)-B(110)	1.765(50)
B(105)-C(106)	1.955(53)	B(105)-B(110)	1.810(52)
C(106)-B(107)	1.711(45)	B(107)-B(108)	1.828(43)
B(201)-B(202)	1.760(45)	B(201)-B(203)	1.860(51)
B(201)-B(204)	1.770(51)	B(201)-B(205)	1.776(53)
B(201)-B(210)	1.727(48)	B(202)-B(203)	1.767(54)
B(202)-B(205)	1.744(51)	B(202)-C(206)	1.739(41)
B(202)-B(207)	1.790(50)	B(203)-B(204)	1.819(38)
B(203)-B(207)	1.837(44)	B(203)-B(208)	1.895(46)
B(204)-B(208)	1.909(41)	B(204)-B(210)	1.834(44)
B(205)-C(206)	1.875(46)	B(205)-B(210)	1.818(57)
C(206)-B(207)	1.772(58)	B(207)-B(208)	1.966(46)
C(111)-C(112)	1.355(38)	C(111)-C(116)	1.396(39)
C(112)-C(113)	1.314(41)	C(113)-C(114)	1.391(59)
C(114)-C(115)	1.395(61)	C(115)-C(116)	1.352(42)
C(121)-C(122)	1.452(38)	C(121)-C(126)	1.334(39)
C(122)-C(123)	1.450(53)	C(123)-C(124)	1.232(49)
C(123)-C(125)	2.247(51)	C(124)-C(125)	1.329(58)
C(125)-C(126)	1.439(56)	C(211)-C(212)	1.395(35)
C(211)-C(216)	1.374(38)	C(212)-C(213)	1.346(47)
C(213)-C(214)	1.415(50)	C(214)-C(215)	1.417(47)
C(215)-C(216)	1.361(44)	C(221)-C(222)	1.386(32)
C(221)-C(226)	1.397(38)	C(222)-C(223)	1.366(41)
C(223)-C(224)	1.360(46)	C(224)-C(225)	1.379(41)
C(225)-C(226)	1.341(34)		

Table 51. Interbond angles (°), with standard deviations in parenthesis, for [arachno-6,9,9',6'-(CB_8H_{12})Au(dppe)Au(CB_8H_{12})] (12).

Au(2)-Au(1)-P(1)	86.1(2)	Au(2)-Au(1)-B(104)	125.4(9)
P(1)-Au(1)-B(104)	141.8(8)	Au(2)-Au(1)-B(108)	85.6(8)
P(1)-Au(1)-B(108)	169.3(8)	B(104)-Au(1)-B(108)	48.8(11)
Au(2)-Au(1)-B(110)	169.8(8)	P(1)-Au(1)-B(110)	104.1(8)
B(104)-Au(1)-B(110)	45.6(12)	B(108)-Au(1)-B(110)	84.2(12)
Au(1)-Au(2)-P(2)	89.5(2)	Au(1)-Au(2)-B(204)	131.9(8)
P(2)-Au(2)-B(204)	127.3(7)	Au(1)-Au(2)-B(208)	92.6(8)
P(2)-Au(2)-B(208)	176.9(7)	B(204)-Au(2)-B(208)	49.7(10)
Au(1)-Au(2)-B(210)	177.8(9)	P(2)-Au(2)-B(210)	92.3(11)
B(204)-Au(2)-B(210)	45.9(11)	B(208)-Au(2)-B(210)	85.5(13)
Au(1)-P(1)-C(1)	109.7(8)	Au(1)-P(1)-C(111)	115.9(8)
C(1)-P(1)-C(111)	107.5(11)	Au(1)-P(1)-C(121)	117.9(9)
C(1)-P(1)-C(121)	103.4(12)	C(111)-P(1)-C(121)	101.3(12)
Au(2)-P(2)-C(2)	105.7(7)	Au(2)-P(2)-C(211)	117.9(8)
C(2)-P(2)-C(211)	104.9(11)	Au(2)-P(2)-C(221)	121.3(8)
C(2)-P(2)-C(221)	105.4(10)	C(211)-P(2)-C(221)	100.1(11)
P(1)-C(1)-C(2)	119.3(15)	P(2)-C(2)-C(1)	114.5(15)
B(102)-B(101)-B(103)	56.1(18)	B(102)-B(101)-B(104)	102.6(23)
B(103)-B(101)-B(104)	58.8(18)	B(102)-B(101)-B(105)	62.5(18)
B(103)-B(101)-B(105)	107.2(22)	B(104)-B(101)-B(105)	105.4(22)
B(102)-B(101)-B(110)	109.0(21)	B(103)-B(101)-B(110)	107.3(24)
B(104)-B(101)-B(110)	58.5(19)	B(105)-B(101)-B(110)	60.7(19)
B(101)-B(102)-B(103)	64.5(19)	B(101)-B(102)-B(105)	60.8(19)
B(103)-B(102)-B(105)	111.9(22)	B(101)-B(102)-C(106)	112.8(20)
B(103)-B(102)-C(106)	108.3(24)	B(105)-B(102)-C(106)	64.5(18)
B(101)-B(102)-B(107)	110.8(23)	B(103)-B(102)-B(107)	59.8(19)
B(105)-B(102)-B(107)	108.5(23)	C(106)-B(102)-B(107)	56.5(18)
B(101)-B(103)-B(102)	59.4(19)	B(101)-B(103)-B(104)	60.2(17)
B(102)-B(103)-B(104)	106.3(22)	B(101)-B(103)-B(107)	109.4(23)
B(102)-B(103)-B(107)	63.1(19)	B(104)-B(103)-B(107)	104.3(20)
B(101)-B(103)-B(108)	112.3(20)	B(102)-B(103)-B(108)	113.7(21)
B(104)-B(103)-B(108)	59.8(16)	B(107)-B(103)-B(108)	60.5(17)
Au(1)-B(104)-B(101)	124.4(18)	Au(1)-B(104)-B(103)	121.7(17)
B(101)-B(104)-B(103)	61.0(18)	Au(1)-B(104)-B(108)	68.2(12)
B(101)-B(104)-B(108)	114.0(20)	B(103)-B(104)-B(108)	60.9(17)
Au(1)-B(104)-B(110)	72.5(14)	B(101)-B(104)-B(110)	57.9(18)
B(103)-B(104)-B(110)	108.6(22)	B(108)-B(104)-B(110)	118.7(20)
B(101)-B(105)-B(102)	57.5(18)	B(101)-B(105)-C(106)	103.5(25)
B(102)-B(105)-C(106)	55.7(17)	B(101)-B(105)-B(110)	57.6(19)
B(102)-B(105)-B(110)	102.7(27)	C(106)-B(105)-B(110)	107.9(27)
B(102)-C(106)-B(105)	59.8(18)	B(102)-C(106)-B(107)	62.8(18)
B(105)-C(106)-B(107)	109.6(21)	B(102)-B(107)-B(103)	57.2(18)
B(102)-B(107)-C(106)	60.7(19)	B(103)-B(107)-C(106)	109.6(25)
B(102)-B(107)-B(108)	110.2(21)	B(103)-B(107)-B(108)	62.2(18)
C(106)-B(107)-B(108)	117.7(22)	Au(1)-B(108)-B(103)	115.8(18)
Au(1)-B(108)-B(104)	63.8(12)	B(103)-B(108)-B(104)	59.3(16)
Au(1)-B(108)-B(107)	112.9(18)	B(103)-B(108)-B(107)	57.3(16)
B(104)-B(108)-B(107)	101.5(22)	Au(1)-B(110)-B(101)	119.9(22)
Au(1)-B(110)-B(104)	61.8(14)	B(101)-B(110)-B(104)	63.6(20)
Au(1)-B(110)-B(105)	117.9(20)	B(101)-B(110)-B(105)	61.7(20)

Table 51 continued

B(184)-B(110)-B(105)	110.1(24)	B(202)-B(201)-B(203)	58.3(18)
B(202)-B(201)-B(204)	106.5(23)	B(203)-B(201)-B(204)	60.1(18)
B(202)-B(201)-B(205)	59.1(18)	B(203)-B(201)-B(205)	107.4(22)
B(204)-B(201)-B(205)	109.9(23)	B(202)-B(201)-B(210)	110.7(24)
B(203)-B(201)-B(210)	112.7(24)	B(204)-B(201)-B(210)	63.3(17)
B(205)-B(201)-B(210)	62.5(19)	B(201)-B(202)-B(203)	63.7(20)
B(201)-B(202)-B(205)	60.9(20)	B(203)-B(202)-B(205)	113.3(26)
B(201)-B(202)-C(206)	116.1(24)	B(203)-B(202)-C(206)	113.8(25)
B(205)-B(202)-C(206)	65.1(19)	B(201)-B(202)-B(207)	114.0(26)
B(203)-B(202)-B(207)	62.2(20)	B(205)-B(202)-B(207)	112.5(24)
C(206)-B(202)-B(207)	60.3(19)	B(201)-B(203)-B(202)	58.0(20)
B(201)-B(203)-B(204)	57.5(18)	B(202)-B(203)-B(204)	104.1(24)
B(201)-B(203)-B(207)	107.3(25)	B(202)-B(203)-B(207)	59.5(20)
B(204)-B(203)-B(207)	109.7(21)	B(201)-B(203)-B(208)	109.2(20)
B(202)-B(203)-B(208)	110.1(22)	B(204)-B(203)-B(208)	61.8(17)
B(207)-B(203)-B(208)	63.6(17)	Au(2)-B(204)-B(201)	119.2(18)
Au(2)-B(204)-B(203)	117.4(17)	B(201)-B(204)-B(203)	62.4(19)
Au(2)-B(204)-B(208)	63.7(12)	B(201)-B(204)-B(208)	112.5(18)
B(203)-B(204)-B(208)	61.0(16)	Au(2)-B(204)-B(210)	78.0(13)
B(201)-B(204)-B(210)	57.2(19)	B(203)-B(204)-B(210)	109.7(25)
B(208)-B(204)-B(210)	114.8(20)	B(201)-B(205)-B(202)	60.0(19)
B(201)-B(205)-C(206)	108.7(25)	B(202)-B(205)-C(206)	57.3(17)
B(201)-B(205)-B(210)	57.4(18)	B(202)-B(205)-B(210)	107.3(29)
C(206)-B(205)-B(210)	116.2(27)	B(202)-C(206)-B(205)	57.6(19)
B(202)-C(206)-B(207)	61.3(18)	B(205)-C(206)-B(207)	107.3(21)
B(202)-B(207)-B(203)	58.3(19)	B(202)-B(207)-C(206)	58.5(19)
B(203)-B(207)-C(206)	109.0(23)	B(202)-B(207)-B(208)	106.0(21)
B(203)-B(207)-B(208)	59.7(17)	C(206)-B(207)-B(208)	113.9(21)
Au(2)-B(208)-B(203)	116.5(18)	Au(2)-B(208)-B(204)	66.6(11)
B(203)-B(208)-B(204)	57.1(15)	Au(2)-B(208)-B(207)	113.9(17)
B(203)-B(208)-B(207)	56.8(16)	B(204)-B(208)-B(207)	101.0(20)
Au(2)-B(210)-B(201)	116.0(23)	Au(2)-B(210)-B(204)	64.1(14)
B(201)-B(210)-B(204)	59.5(20)	Au(2)-B(210)-B(205)	112.5(22)
B(201)-B(210)-B(205)	60.1(22)	B(204)-B(210)-B(205)	105.4(29)
P(1)-C(111)-C(112)	120.7(20)	P(1)-C(111)-C(116)	121.5(20)
C(112)-C(111)-C(116)	117.3(23)	C(111)-C(112)-C(113)	123.3(30)
C(112)-C(113)-C(114)	119.4(35)	C(113)-C(114)-C(115)	120.0(31)
C(114)-C(115)-C(116)	117.7(34)	C(111)-C(116)-C(115)	122.0(30)
P(1)-C(121)-C(122)	115.2(22)	P(1)-C(121)-C(126)	121.6(21)
C(122)-C(121)-C(126)	123.0(29)	C(121)-C(122)-C(123)	113.7(28)
C(122)-C(123)-C(124)	123.1(33)	C(122)-C(123)-C(125)	93.2(23)
C(124)-C(123)-C(125)	29.9(22)	C(123)-C(124)-C(125)	122.6(40)
C(123)-C(125)-C(124)	27.5(22)	C(123)-C(125)-C(126)	94.9(26)
C(124)-C(125)-C(126)	122.4(38)	C(121)-C(126)-C(125)	115.2(27)
P(2)-C(211)-C(212)	124.8(21)	P(2)-C(211)-C(216)	119.5(20)
C(212)-C(211)-C(216)	115.4(26)	C(211)-C(212)-C(213)	124.2(27)
C(212)-C(213)-C(214)	118.4(27)	C(213)-C(214)-C(215)	119.1(32)
C(214)-C(215)-C(216)	117.9(29)	C(211)-C(216)-C(215)	124.5(28)
P(2)-C(221)-C(222)	121.8(17)	P(2)-C(221)-C(226)	122.8(16)
C(222)-C(221)-C(226)	116.1(20)	C(221)-C(222)-C(223)	122.0(24)
C(222)-C(223)-C(224)	120.7(29)	C(223)-C(224)-C(225)	118.0(27)
C(224)-C(225)-C(226)	121.9(24)	C(221)-C(226)-C(225)	121.2(21)

Table 52. Final fractional coordinates (x 10^4), with standard deviations in parenthesis, for [arachno-6,9,9',6'-(CB_8H_{12})Au(dppm)Au(CB_8H_{12})] (12).

atom	x	y	z	U
Au(1)	2403.3(7)	6189.7(5)	9697.6(4)	42(1)*
Au(2)	2994.6(7)	6236.1(5)	8475.1(4)	43(1)*
P(1)	1338(5)	7195(3)	9299(3)	44(2)*
P(2)	3986(5)	7308(3)	8817(3)	40(2)*
C(1)	2196(20)	7978(11)	9265(12)	51(10)*
C(2)	2870(19)	8005(11)	8722(12)	44(9)*
B(101)	2713(29)	5246(16)	11318(18)	64(14)*
B(102)	2239(24)	4423(16)	10898(18)	60(12)*
B(103)	3441(26)	4723(15)	10748(18)	64(13)*
B(104)	3317(24)	5698(15)	10650(16)	53(12)*
B(105)	1283(34)	5179(19)	10926(22)	95(19)*
C(106)	1236(21)	4553(15)	10116(19)	84(14)*
B(107)	2511(26)	4380(17)	10020(17)	62(13)*
B(108)	3335(24)	5144(13)	9874(16)	53(12)*
B(110)	2070(30)	5963(17)	10817(16)	71(15)*
B(201)	2886(30)	5601(14)	6766(17)	64(15)*
B(202)	3360(27)	4744(20)	7060(17)	70(14)*
B(203)	2059(31)	4959(15)	7154(18)	72(15)*
B(204)	2126(24)	5912(13)	7365(17)	56(12)*
B(205)	4242(34)	5475(17)	7204(19)	82(17)*
C(206)	4308(23)	4721(15)	7848(17)	88(13)*
B(207)	2974(31)	4457(17)	7842(15)	70(14)*
B(208)	2080(24)	5234(13)	8098(15)	53(11)*
B(210)	3466(21)	6257(27)	7351(14)	89(17)*
C(111)	461(18)	7108(13)	8455(13)	47(9)*
C(112)	-25(22)	6473(16)	8247(16)	68(12)*
C(113)	-727(22)	6391(21)	7655(18)	84(15)*
C(114)	-1043(29)	6984(27)	7228(20)	117(21)*
C(115)	-570(26)	7652(21)	7410(19)	94(16)*
C(116)	142(24)	7705(17)	8029(16)	80(14)*
C(121)	489(22)	7589(14)	9827(14)	59(7)
C(122)	910(26)	7816(15)	10501(16)	82(9)
C(123)	154(28)	8014(17)	10926(18)	93(10)
C(124)	-821(28)	7928(17)	10733(18)	88(10)
C(125)	-1266(37)	7635(21)	10128(21)	125(14)
C(126)	-644(22)	7481(14)	9628(14)	62(7)
C(211)	4825(20)	7623(12)	8311(12)	53(10)*
C(212)	4588(24)	8138(14)	7781(14)	78(12)*
C(213)	5268(26)	8342(16)	7379(15)	73(13)*
C(214)	6313(32)	8047(18)	7521(14)	97(17)*
C(215)	6567(20)	7492(21)	8026(16)	95(15)*
C(216)	5812(22)	7302(17)	8388(14)	74(13)*
C(221)	4705(18)	7422(11)	9684(11)	40(8)*
C(222)	4954(23)	8101(13)	9962(14)	71(11)*
C(223)	5621(26)	8202(18)	10681(19)	96(16)*
C(224)	6033(24)	7638(18)	11004(16)	76(14)*
C(225)	5784(22)	6951(14)	10737(15)	66(12)*
C(226)	5152(17)	6845(12)	10103(13)	46(9)*

* Equivalent isotropic U defined as one third of the trace of the orthogonalised U tensor

APPENDICES

APPENDIX I. X-RAY CRYSTALLOGRAPHY.

Because of the significant proportion of X-ray crystallographic work contained within this thesis, the following Appendix contains a brief description of the theory and practice so employed. For a more rigorous theoretical treatment of the subject, several excellent sources of information are available [237,238].

CRYSTAL SYMMETRY.

Of the various possible solid state phases, the crystalline state has long been embraced by the scientist and layman as a measure of purity. Whilst all definitions of this state allude to the high degree of internal order, a precise definition[239] is; 'Crystalline matter is matter that possesses a triperiodic structure on the atomic scale. The "ideal crystal" is an homogeneous portion of crystalline material, whether bounded by faces or not.'.

Any periodic function can be reduced to the denominator unit, and as such the atomic triperiodicity of the crystalline state can be reduced to the 'unit cell' corresponding to a parallelepiped, the contents of which are repeated within the crystal lattice, in the three directions defined by its edges. The unit cell is thus defined by six parameters, the length of the three axes (a,b,c) of the parallelepiped and the three angles (alpha, beta, gamma) between them.

The periodicity of the crystal can be more rigorously described as a three dimensional lattice. The term refers to a non-material array of identical points, and must not be confused with atoms. There are fourteen different three dimensional arrangements of an array of points, such that each and any point has an identical environment,

UNIT CELL	CRYSTAL SYSTEM	14 BRAVAIS LATTICES (14 Total)	CELL AXES & ANGLE CONSTRAINTS	AXIAL LENGTHS & ANGLES REQUIRED	SYMMETRY OF LATTICE
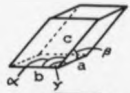	Triclinic	P	$a \neq b \neq c$ $\alpha \neq \beta \neq \gamma$	a, b, c α, β, γ	$\bar{1}$
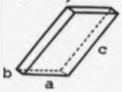	Monoclinic	P C	$a \neq b \neq c$ $\alpha = \beta = 90^\circ \neq \gamma$ (or $\alpha = \gamma = 90^\circ \neq \beta$) (or β)	a, b, c γ	2/m
	Orthorhombic	P C I, F	$a \neq b \neq c$ $\alpha = \beta = \gamma = 90^\circ$	a, b, c	mmm
	Tetragonal	P I	$a = b \neq c$ $\alpha = \beta = \gamma = 90^\circ$	a, c	4/mmm
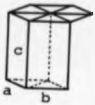	Hexagonal	P	$a = b \neq c$ $\alpha = \beta = 90^\circ$ $\gamma = 120^\circ$	a, c	6/mmm
	Rhombohedral	P	$a = b = c$ $\alpha = \beta = \gamma$ $<120^\circ \neq 90^\circ$	a α	$\bar{3}$m
	Cubic	P I, F	$a = b = c$ $\alpha = \beta = \gamma = 90^\circ$	a	m3m

Figure 1.12. The fourteen Bravais lattices and conventional unit cells (P = primative, F = face centred, I = body centred).

these are known as the Bravais Lattices.

The unit cell will conform to one of seven parallelepiped forms, as shown in Figure 112. These are the seven primative crystal systems, and are classified according to their rotational symmetry within the crystal lattice, whereby the presence of an n-fold rotation axis yields an identical unit cell after a $(360/n)^{\circ}$ rotation.

Though several choices of unit cell are possible for a given crystal lattice, the unit cell that has the full rotational and translational symmetry of the lattice is chosen.

The primitive crystal systems, with each of the vertices defined by lattice points, (one lattice point per unit cell) account for seven of the fourteen Bravais Lattices. The remainder are the non-primative lattices produced from these primitive lattices by face centering, where all faces (F) or one pair are centered (A,B,C) or body centering (I) as shown in Figure 112.

A lattice point is not required to correspond to an atom position in the crystal, though, if through the choice of the unit cell this is the case, then by definition, all lattice points must correspond to atomic positions, since lattice points are equivalent.

Within the confines of a three dimensional lattice, the seven crystal systems can posses local symmetry corresponding to one of 32 possible sets of symmetry operations, known as crystallographic point groups. These consist of combinations of rotation and inversion axes of order 1,2,3,4, and 6. The addition of translational symmetry elements to these point groups, a property obviously consistent with the repetition of the contents of a unit cell through the crystal lattice, leads to the 230 space groups, the characteristic global symmetry properties of the crystal. The additional translational

elements are the screw axes and glide plane. The former is a rotation combined with a translation, the latter a combination of a translation and mirror operation.

The space group thus reduces the necessary characterisation of the arrangement of atoms within the crystal lattice to the asymmetric unit, that portion of the unit cell that is without symmetry. Thus a unit cell containing four identical molecules packed together may be uniquely characterised by an asymmetric unit comprising one half of a molecule, the rest being symmetry related.

Examples of crystals with the space groups P1, $P\bar{1}$, $P2_1/c$ and $P2_1/n$ are those metallocarbaborane clusters characterised during the course of this work, (see Chapters 3 and 4).

THE DIFFRACTION OF X-RAYS BY A CRYSTAL.

The suitability of X-rays as a probe of crystal structure is due to the similarity in magnitude of the inter atomic spacing found in the crystal lattice and the wavelength of the radiation.

To effectively describe the principles of the diffraction of X-rays by a crystal lattice, the comparison with the diffraction of visible light by an optical grating is a useful analogy[238]. The diffraction pattern caused by simple one dimensional gratings, as shown in Figure 113, shows two important features of diffraction, in that the interspacing of the observed diffraction lines is inversely related to the interspacing of the grating. The constant K refers to the wavelength of the incident radiation. Furthermore the observed lines correspond to those diffractions that satisfy the requirement that the diffracted beam should be in phase by an integral number of wavelengths, giving an intensity that is increased by other in phase

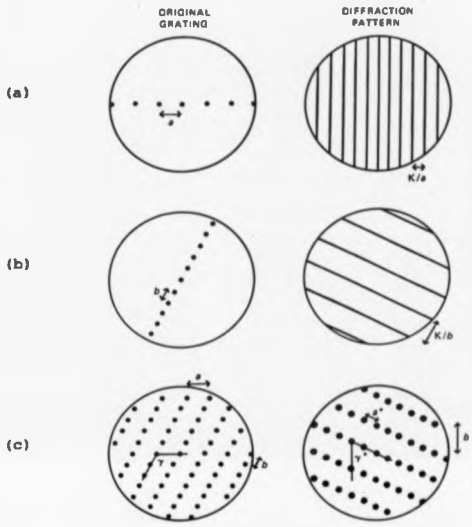

Figure 113. Diffraction patterns obtained from one (a and b) and two dimensional optical gratings (c).
(Reproduced from reference 238)

diffracted beams, so called constructive interference. Those diffracted beams which are out of phase suffer destructive interference with other out of phase beams and give substantially reduced intensities.

The diffraction pattern from the two dimensional grating (Figure 113c) illustrates another important feature of diffraction. The orientation of the diffraction is perpendicular to that of the grating, and together with the inverse ratio of the interspacing, the diffraction produced is thus a reciprocal of the original grating.

These principles of diffraction apply equally to the diffraction of X-rays by a crystal lattice, with further qualification as follows. The incident X-rays are diffracted by the electrons that surround the nuclei of the atoms within the crystal. The vector analysis of constructive interference for diffraction from a one dimensional lattice is shown in Figure 114. For the incident and diffracted beams to be in phase the following equalities have to be satisfied;

$$AB-CD = n\lambda$$

$$a(\cos X - \cos Y) = n\lambda \text{ where } n = 1,2,3,.....$$

These conditions have to be simultaneously satisfied in three dimensions (the three Laue conditions), in order to produce a diffracted beam of significant intensity, from the crystal lattice.

Another method of describing the diffraction of X-rays from crystals is that developed by W. L. Bragg. The scattering of X-rays from a crystal lattice were ascribed to their reflection from planes within the lattice, (Figure 115). The angle of the incidence and reflection of the two X-rays are equal, and the two beams will be in

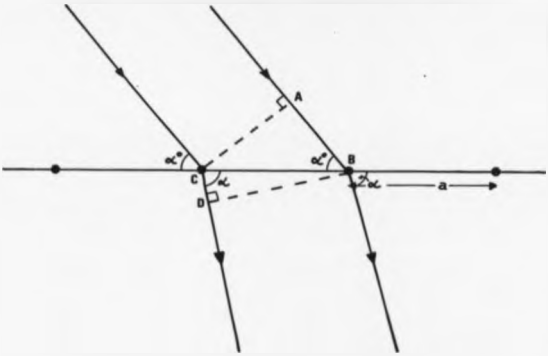

Figure 114. Diffraction from a one dimensional lattice, with constructive interference.

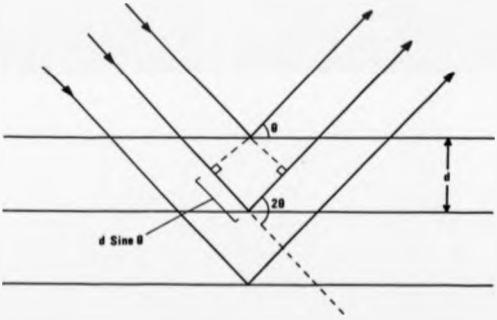

Figure 115. Bragg reflections from layers of atoms.

phase, for a given interlayer spacing d and wavelength λ, only at certain 2θ angles, where 2θ is the total deviation from the direct X-ray vector. This led to the formulation of the famous Bragg's Law;

$$n\lambda = 2\,d \sin\theta$$

From the observed 2θ reflections, the planes are conveniently labelled using the Millar indices. These are derived from the intercept of the plane with the three unit cell axes a, b and c. The Bragg equation then enables calculation of the inter-layer spacing in the crystal and the unit cell dimensions.

DIFFRACTOMETRY - DATA COLLECTION.

A single crystal X-ray crystallographic study consists of two distinct stages, namely, the experimental observation of the diffraction pattern obtained from a given crystal (diffractometry or data collection) and the interpretation of the observations (structure solution). The following description of data collection is of that employed at the University of Warwick, though the principles involved are universal.

Data collection consists of the systematic observation of two parameters of the diffracted / reflected X-rays, these being the 2θ angle of scattering and the intensity of the diffracted beam. The former allows the calculation of unit cell size and shape, whilst the latter characterises the contents of the asymmetric unit.

A Syntex $P2_1$ four circle diffractometer is used to aquire the necessary angular and intensity data (see Figure 116). The crystal, suitably mounted on a quartz fibre on the Goniometer, is positioned on the phi axis then manually centered in the X-ray beam. The three

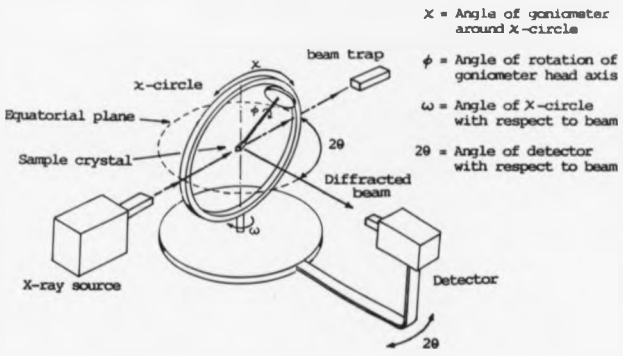

Figure 116. The four circle diffractometer.

independent rotation axes of this instrument, allow the movement of the crystal to almost any orientation. For convenience, the X-ray source and detector are kept in the equatorial 2θ circular plane concentric with the omega circle. Combinations of rotations of the phi, khi and omega circles then allow the crystal to be orientated so that the diffractions are brought into the equatorial plane and detected at varing 2θ angles.

Whilst detection is normally achieved with a scintillation counter, preliminary investigation of the single crystal specimen is carried out more conveniently by photographic methods. Deterioration of the crystal through loss of solvent or on exposure to air, can be corrected by encapsulation of the crystal in a thin quartz tube

containing either an inert or solvent atmosphere. Because of the relative air sensitivity of the metallocarbaboranes prepared during the course of this work, all of the crystals examined by X-ray diffraction were encapsulated.

After an initial location and centering of 6-8 diffraction intensities obtained from a rotation photograph of the crystal, the unit cell is identified from a computer generated list of indexed crystal planes. Axial photographs are then obtained for each of the cell axes, and used to confirm the expected dimensions and symmetry of the chosen unit cell, and to identify any apparent crystal twinning. In a similar manner to that described earlier for optical gratings, those diffractions recorded conform to the reciprocal lattice and consequently the reciprocal unit cell. This is readily appreciated when measuring the axial lengths of the axial photograph, when a reciprocal scale has to be used. A more rigorous description of the relationship between real space and the reciprocal lattice was made by P. P. Ewald, the so called 'Ewald Construction'.

A subsequent rapid data collection provides 15 high 2θ angle reflections which are then centered on and used to accurately determine by a least-squares fit, the unit cell parameters and an orientation matrix. At this point, these parameters are entered into a cell reduction program which produces the transformation matrices for any alternative unit cells, which may show higher symmetry elements. Adjustment to the parameters stored in the computer for the unit cell can then be made as appropriate.

An automatic data collection over an appropriate 2θ range is then carried out. The minimum and maximum values of h, k and l are selected and the computer systematically advances through the Miller

indices range specified, scanning at the angles computed for the particular reflection, recording the intensity of diffraction. Three standard reflections are checked every 200 reflections in order to monitor the crystal stability. Numerous adjustments can be made to the diffraction detection parameters, though for most crystals the default settings of scan speed, range and background intensity measurement suffice. In the event of a very weakly diffracting crystal being examined these parameters have to be appropriately adjusted. The 2θ angle, indices and intensities for each observed diffraction are recorded onto magnetic tape.

Either before or after the X-ray diffraction study the crystal is measured using a optical travelling microscope and a absorption correction of the diffraction data made. The density of the crystals can be obtained by flotation methods, though in certain instances this may not be possible, for example air sensitive or easily solubilised compounds.

STRUCTURE SOLUTION.

The majority of effort expended in the structure solution stage is focused on the successful employment of a number of crystallographic computer programs. These function on a number of important crystallographic theories, discussed below. The first step is to get the raw diffractometry data into a computer data handling system.

The raw data obtained from the diffractometry consists of the reflection indices, 2θ angles and intensities for a range of reflections, obtained for a unit cell of known size and symmetry.

The remaining unknown is the space group, which is essential for structure solution. The translational symmetry elements of a space group give rise to absences in the observed diffraction pattern, that is, zero or near-zero intensity for a given reflection. The systematic absences, those for which a general expression describes their absence, for example when 0k0 when k is odd, are indicative of the translational symmetry of the space group. In this way, a number of space groups are uniquely identifiable, as in the case of $P2_1/n$, where the h0l and 0k0 reflections are absent when h+l and k are odd respectively.

Whilst systematic absences can be detected by inspection of the recorded reflection data, a simple computer program can speedily tabulate the observed reflections into intensity groups for appraisal. Unfortunately some space groups have the same translational symmetry elements and will therefore give rise to the same systematic absences. In these cases each space group is used, the correct one ultimately yielding a resolvable structure.

The intensities of any given diffraction depend primarily upon the type and distribution of atoms within the crystal. Given that an X-ray is diffracted by the electrons associated with an atom, the observed intensity is the sum of the scattering of many atoms with constructive interference. The larger the atomic number of an atom and hence greater complement of electrons the larger the contribution of the atom in the gross scattering process. The diffraction has an associated amplitude and phase angle, the combination of which is known as the structure factor F or F(hkl). This quantity can be expressed as an exponential or a complex number;

$$F(hkl) = |F(hkl)|e^{i\alpha(hkl)} = A(hkl) + iB(hkl)$$

where $|F(hkl)|$ is the amplitude and $\alpha(hkl)$ the phase. The intensity is proportional to the square of the amplitude $|F(hkl)|^2$. The vector representation of the structure factor is shown in Figure 117, known as an Argand diagram. The structure factor is the summation of the scattering amplitude, f_j, and phase angle, $2\pi(hx_j+ky_j+lz_j)$, of diffraction from each individual atom at fractional cell coordinates x, y and z, towards the reciprocal lattice point hkl.

$$F(hkl) = \sum f_j \ (\cos [2\pi(hx_j+ky_j+lz_j)] + i \sin(2\pi(hx_j+ky_j+lz_j)]$$

$$F(hkl) = \sum f_j \ e^{i2\pi(hx_j+ky_j+lz_j)}$$

Knowing the amplitude and phase components of each observed diffraction would enable direct structure solution. Unfortunately the phase information is lost in the recording of the diffraction pattern, (the so called 'Phase Problem'), with the observed intensity, $|F|^2$ allowing only calculation of the amplitude $|F|$.

The observed diffraction intensities are also dependent on several other features modifying the diffraction of X-rays by atoms in a crystal,

$$I_{obs} = K \ |F(hkl)|^2 \ L(hkl) \ P(hkl) \ A(hkl)$$

where I_{obs} is the observed intensity, K is a scaling factor, and L, P and A correction factors for Lorentz, polarisation and absorption effects. The absorption factor is a correction for absorption of some of the X-ray intensity within the crystal lattice and is dependent on the symmetry, size and contents of the unit cell. The other

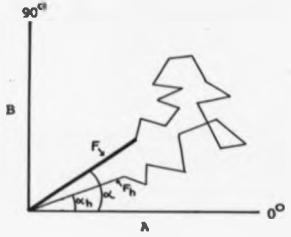

Figure 117. Vector analysis of individual F_j components to yield the resultant F(hkl).

corrections account for the observed reduction in scattering power with increasing 2θ. All three corrections are accounted for in the computer analysis of the observed data.

The interpretation of the observed diffraction intensities to yield a molecular structure involve the use of approximate phase angles. The combination of the observed amplitudes and approximate phases allows the deduction of a trial structure by computation of the fractional coordinates x, y and z of the individual atoms contributing to the observed X-ray diffraction.

From these approximate atomic positions the calculated structure factor amplitudes |Fcalc| are computed. The comparison of these to the observed structure factor amplitudes |Fobs| enables a set of improved approximate phase angles to be obtained. These are then substituted back into the |Fcalc| : |Fobs| comparison to yield a further improved set of phases. This recycling is the basis of the 'Fourier Synthesis',

a convergent process leading to a refined structure solution. The refinement process is monitored by the residual factor R, where

$$R = \frac{\sum (|Fobs| - |Fcalc|)}{\sum (|Fobs|)}$$

The R-factor is a measure of fit between the observed and trial structure amplitudes, and though not equated to the correctness of the structure, with a few exceptions, this normally proves to be the case.

Whilst the method of structure solution and refinement outlined appears to be reasonably straightforward, the initial choice of approximate phase angles that lead to the trial structure is of paramount importance. The methods available for this purpose include the 'Direct Methods' and 'Patterson Heavy Atom' techniques. The former is mainly of use in interpretation of data derived from the analysis of organic materials, in which all atoms are of a roughly similar mass. The heavy atom technique is used in cases where one or more significantly heavier atoms are present in the crystal lattice, and is therefore used to obtain structures of inorganic compounds, especially those containing a transition metal atom.

The basic reason behind the success of the Patterson method is the domination of the X-ray scattering by the heavy atom. Referring back to the Argand diagram of the structure factor, Figure 117, it is easily seen that the amplitude and phase angle of a diffraction that includes that of the heavy atom (F,α) will have a phase very nearly that expected from an isolated heavy atom (Fh,αh).

Patterson devised a method of determining the position of the heavy atom by evaluation of a series that does not rely on phase

information, only the $|F|^2$ and indices of each diffraction.

$$P(u,v,w) = 1/V_c \sum\sum\sum |F|^2 \cos 2\pi(hu + kv + lw)$$

The resultant vector map produced corresponds to a set of N^2 peaks representing all of the interatomic vectors between N atoms. The intensity of each peak is proportional to the product of the atomic numbers of the atoms concerned, hence, this will also be dominated by the heavy atom vectors, particularly the self vectors, which are coincident at the origin. A simple two dimensional Patterson map for a three atom system is shown in Figure 118, (h and l refer to heavy and light atoms).

Once any heavy atom positions have been found by a Patterson analysis, the phase angle of the heavy atom dominated diffractions are calculable. These phase angles are then used in the Fourier refinement described earlier, with the lighter atoms being revealed in subsequent Fourier maps.

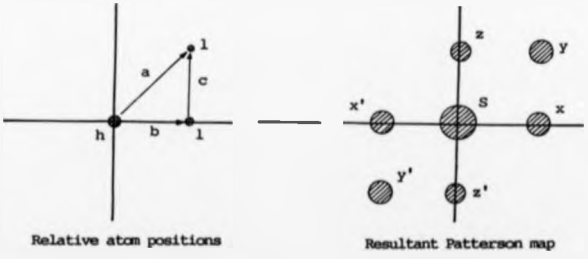

Figure 118. Two dimensional Patterson map for a three atom system.

APPENDIX II. NUCLEAR MAGNETIC RESONANCE SPECTROSCOPY.

Though X-ray crystallography is the definitive method of structural analysis, boron-11 and proton n.m.r. spectroscopy provides a quick and convenient method of obtaining structural information, particularly using recently developed 2D n.m.r. techniques[156,157,158].

With a nuclear spin quantum number (I) of 3/2 and 1/2 for ^{11}B and ^{1}H respectively, the BH cluster unit produces a four line resonance in the ^{1}H spectrum and a two line resonance in the ^{11}B spectrum. Typical coupling constants are found to be $J(B\text{-}H_{(terminal)})$ - 80 - 190 Hz. Further coupling is found where bridging hydrogens are present, $J(B\text{-}H_{(bridging)})$ - 50 Hz. For a boron with one terminal and one bridging hydrogen attached the expected boron resonance is therefore a doublet with doublet fine structure, whilst the proton spectrum should reveal a septet (from 2 B's) for the bridging hydrogen with fine structure due to any coupling to the terminal hydrogen. The magnitude of boron-boron and long range proton-proton couplings are significantly less than than the couplings observed between boron and attached hydrogen atoms, with typical values of J(B-B), $J(B\text{-}H_{(terminal)})$ and $J(H_{(terminal)}\text{-}H_{(bridging)})$ ranging from - 20 to 5 Hz.

Because the ^{11}B nucleus has a large electric quadrupole moment, spin lattice relaxation is rapid causing line broadening for resonances in both ^{11}B and ^{1}H n.m.r. spectra of boron clusters. Typical half height linewidths are 30 to 60 Hertz compared to a few Hertz in the proton n.m.r. organic compounds. The large linewidths hinder the interpretation of ^{11}B spectra due to the overlapping of many of the observed resonances. Comparing the magnitude of the linewidths with the various coupling constants for boron clusters it

is clear that the only coupling expected to be resolved in a normal resolution n.m.r. spectrum is that between boron and the attached hydrogens. Whilst the ^{10}B isotope with I = 3 and 20% abundance should be considered, it is found to give coupling constants of one-third the magnitude of ^{11}B coupling constants. The combination of higher multiplicites, lower abundance and smaller coupling constants give rise to negligible impact on the observed spectra due to ^{10}B and is normally disregarded.

The successful extraction of structural information from the boron-11 and proton spectra of boron cluster molecules relies on the interpretion of the number of observed resonances and their multiplicities, with regard to the symmetry they imply. There are no generally applicable empirical correlations between chemical shift of boron resonances and the chemical environment of the boron atoms that can be used to predict or confirm the precise ^{11}B n.m.r. spectrum. Advances in this area are however being made, with some very useful correlations having been developed for the prediction of the relative positions of the resonances in the n.m.r. spectra for closo boranes and hetaro-boranes[240].

Several of the techniques available for the simplification of proton spectra in organic compounds are equally useful in clarifying the often complex ^{11}B n.m.r. spectra of boranes and carboranes. The most important of these are, increasing magnetic field strength, proton decoupling and most recently 2-Dimensional n.m.r. Along with assumed use of Fourier Transform collection of data, the use of increased field strength and both proton and boron decoupling have the expected effect of improving resolution of the observed resonances and simplification of their multiplicities respectively. These effects

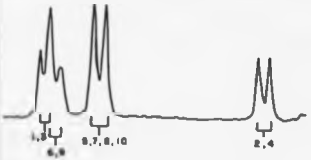

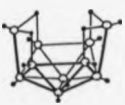

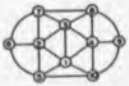

(a) 62.4 MHz, proton coupled[11].

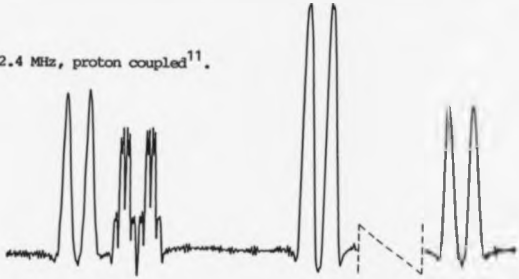

(b) 128.8 MHz, proton coupled[241].

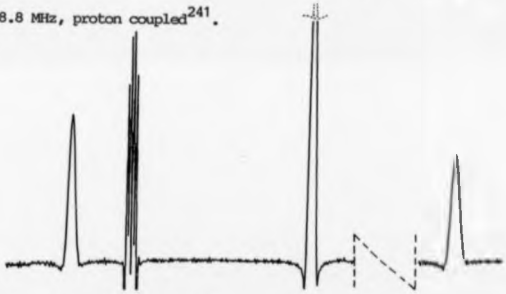

(c) 128.8 MHz, proton decoupled[241].

Figure 119. ^{11}B n.m.r. spectra of decaborane(14).

are illustrated in the ^{11}B spectra of decaborane(14) shown in Figure 119. The structure and topological description are also given to aid interpretation.

Though the original application of 2D n.m.r. was in heteronuclear ^{13}C - ^{1}H systems, it has now been developed[158] for application in both heteronuclear ^{11}B - ^{1}H and homonuclear ^{1}H - ^{1}H and ^{11}B - ^{11}B studies and has been used to provide structural information for a number of boranes, carbaboranes and metalla derivatives[158,159, 184,242-5]. Of these techniques the latter gives the more important information, though all are extremely useful in the elucidation of borane cluster structure.

In the heteronuclear ^{11}B - ^{1}H 2D n.m.r. experiment, the spectra obtained show correlations between the ^{11}B resonances and the attached hydrogen atoms which enables the assignment of proton resonances, both bridging and terminal, to specific boron atoms.

The homonuclear ^{11}B - ^{11}B 2D n.m.r. experiment detects scalar spin-spin coupling between adjacent boron atoms, enabling the connectivity of the polyhedral framework to be mapped and the boron resonances to be assigned unambiguously (in most cases). The 2D n.m.r. spectrum is obtained by recording 256 F.I.D's at a constant time interval t1, and as a function of t2. The pulse sequence used is relatively simple compared to the heteronuclear experiment, 90^{o}-t1-90^{o}. The 256 x 512 point data matrix is subjected to Fourier Transforms in both directions yielding a 2D frequency map. Those peaks on the diagonal represent the resonances in which no modulation of their precession frequency by other resonances has occured during the second 90^{o} mixing pulse, i.e. the normal ^{11}B spectrum. Those peaks off the diagonal (cross-peaks) represent modulation of one resonance by

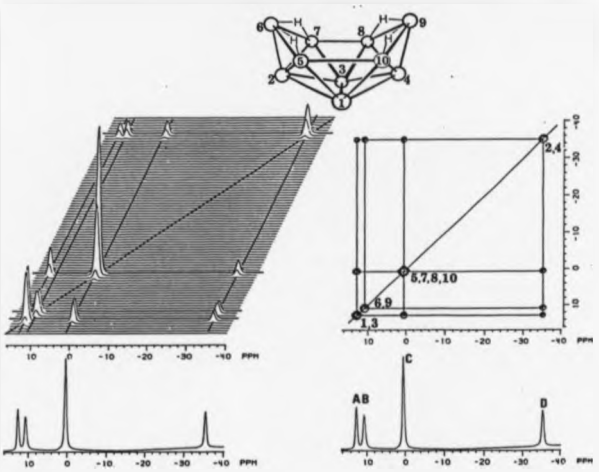

$^{11}B - {}^{11}B$ cosy plots and assignments

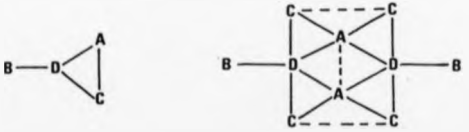

Fundamental connectivity Complete connectivity

Figure 120. $^{11}B-{}^{11}B$ COSY plots for decaborane(14) and connectivities.

(Reproduced from reference 158)

another via scalar coupling during the mixing pulse, indicating adjacent nuclei. Detection of coupling is dependant on factors such as reasonable separation of resonances in the 1D spectrum and sufficiently long relaxation times. Whilst the intensity of the cross peak is not solely related to the magnitude of J(B-B) it is an aproximate guide, such that low intensity indicates long boron-boron bonds. In most instances those boron atoms connected by a bridging hydrogen do not give rise to cross peaks. This reflects the M.O. description of such bonds as having little electron density along the B-B vector. In the 2D n.m.r. of carbaboranes prepared during this work (see Chapter 3) coupling has been observed between boron atoms connected by bridging hydrogens, though in most instances it is of low intensity.

In a review of homonuclear ^{11}B 2D n.m.r. Grimes *et al*[158] outlined the following approach to the deduction of structure from the so called 'COSY' plots. By considering all of the observed couplings in the ^{11}B-^{11}B COSY of decaborane(14) illustrated in Figure 120, the fundamental connectivity of the four sets of boron atoms in decaborane(14) can be deduced as shown. Translation to the complete structure is made by taking into account the relative weightings (A(2), B(2), C(4), D(2) from the integration and molecular formula, giving the connectivity of the complete framework. The boron atoms 1 to 10 are therefore assigned to the resonances A to D as shown in Figure 120.

REFERENCES

REFERENCES

1. A. Stock, 'Hydrides of Boron and Silicon', Cornell University Press, Ithaca, New York, 1933.
2. R. N. Grimes, 'Carboranes', Academic Press, New York, 1971.
3. T. Onak, 'Boron Hydride Chemistry' Chapter 10, Edited by E. L. Muetterties, Academic Press, New York, 1975.
4. R. Hoffmann, Les Prix Nobel, 1981, Almqvist and Wilsell, Stockholm, 1982.
5. K. Base, B. Stibr, J. Dolanski and J. Duben, Collect. Czech. Chem. Commun., 1981, 46, 2345.
6. W. R. Hertler, F. Klanberg and E. L. Muetterties, Inorg. Chem., 1967, 6, 1969.
7. A. R. Kane, L. J. Guggenberger and E. L. Muetterties, J. Am. Chem. Soc., 1970, 92, 2571.
8. R. E. Williams, Inorg. Chem., 1971, 10, 210 and Adv. Inorg. Chem. and Radiochem., 1976, 18, 67.
9. R. N. Grimes, Adv. Inorg. Chem. and Radiochem., 1983, 26, 55.
10. R. W. Rudolph and W. Pretzer, Inorg.Chem., 1972, 11, 1974.
11. G. B. Dunks and M. F. Hawthorne, 'Boron Hydride Chemistry' Chapter 11, Edited by E. L. Muetterties, Academic Press, New York, 1975.
12. R. N. Grimes, 'Metal Interactions with Boron Clusters', Plenum Press, New York, 1982.
13. K. P. Callahan and M. F. Hawthorne, Adv. Organomet. Chem., 1976, 14, 145.
14. L. J. Todd and A. R. Siedle, Prog. Nucl. Magn. Reson. Spectrosc., 1979, 13, 87.
15. H. C. Longuet-Higgins, J. Chem. Phys., 1949, 46, 275.
16. H. C. Longuet-Higgins, Quart. Revs., 1957, 11, 121.

17. W. H. Eberhardt, B. L. Crawford(Jnr), and W. N. Lipscomb, J. Chem. Phys., 1954, 22, 989.
18. R. E. Dickerson and W. N. Lipscomb, J. Chem. Phys., 1957, 27, 212.
19. W. N. Lipscomb, 'Boron Hydrides', Benjamin, New York, 1963.
20. H. D. Johnson, R. A. Geanangel and S. G. Shore, Inorg. Chem., 1970, 9, 908.
21. V. T. Bruce, H. D. Johnson and S. G. Shore, J. Am. Chem. Soc., 1973 95, 6629.
22. D. Marynick and W. N. Lipscomb, J. Am. Chem. Soc., 1972, 94, 8699.
23. W. N. Lipscomb, 'Boron Hydride Chemistry' Chapter 2, Edited by E. L. Muetterties, Academic Press, New York, 1975.
24. K. Wade, 'Electron Deficient Compounds', Nelson, London, 1971.
25. K. Wade, Inorg. Nucl. Chem. Lett., 1972, 8, 823.
26. D. M. P. Mingos, Nature, 1972, 236, 99.
27. K. Wade, J. Chem. Soc., Chem. Commun., 1971, 792.
28. K. Wade, Chem. Br., 1975, 11, 177.
29. K. Wade, Adv. Inorg. Chem. and Radiochem., 1976, 18, 1.
30. M. E. O'Neil and K. Wade, 'Metal Interactions with Boron Clusters' Chapter 1, Edited by R. N. Grimes, Plenum Press, New York, 1982.
31. K. Callahan, W. Evans, F. Lo, C. E. Strouse and M. F. Hawthorne, J. Am. Chem. Soc., 1975, 97, 296.
32. E. Nishimura, Inorg. Nucl. Lett., 1981, 17, 269.
33 J. Duban, S. Hermanek and B. Stibr, J. Chem. Soc., Chem. Commun., 1978, 287.
34. A. J. Stone, Polyhedron, 1984, 23, 1299, and Inorg. Chem., 1981, 20, 563.
35. D. M. P. Mingos and M. I. Forsyth, J. Chem. Soc., Dalton Trans., 1977, 610.

36. D. M. P. Mingos, J. Chem. Soc., Chem. Commun., 1983, 706.

37. B. T. Kao, Inorg. Chem., 184, 23, 1251; 1257.

38. N. N. Greenwood, 'The Chemistry of Boron', Pergamon Press, 1975.

39. A. D. Norman and W. L. Jolly, Inorg. Synth., 1968, 11, 15.

40. L. H. Long, Progr. Inorg. Chem., 1971, 15, 1.

41. E. Groszek, J. B. Leach, G. T. F. Wong, C. Ungermann and T. Onak, Inorg. Chem., 1971, 10, 2770.

42. R. Wilczynski and L. G. Sneddon, Inorg. Chem., 1981, 20, 3955, and J. Am. Chem. Soc., 1980, 102, 420.

43. T. Onak, P. Mattachai and E. Groszek, J. Chem. Soc. (A), 1969, 1990.

44. W. Knoth, Inorg. Chem., 1971, 10, 598, and J. Am. Chem. Soc., 1967, 89, 1274.

45. J. Plesek, T. Jelinek, E. Drakova, S. Hermanek and B. Stibr, Collect. Czech. Chem. Commun., 1984, 49, 1559.

46. J. F. Ditter, E. B. Klusmann, J. D. Oakes and R. E. Williams, Inorg. Chem., 1970, 9, 889.

47. T. Onak, R. P. Drake and G. B. Dunks, Inorg. Chem., 1964, 3, 1686.

48. R. R. Raitz, and R. Schaaffer, J. Am. Chem. Soc., 1971, 89, 1263; 1973, 95, 6254.

49. F. N. Tebbe, P. M. Garrett and M. F. Hawthorne, J. Am. Chem. Soc., 1968, 90, 869.

50. P. M. Garrett, G. S. Ditta and M.F. Hawthorne, J. Am. Chem. Soc., 1971, 93, 1265.

51. A. P. Fung, E. W. Distefano, K. Fuller, G. Siwapinyoyos, T. Onak and R. E. Williams, Inorg. Chem., 1979, 18, 372.

52. M. P. Brown, A. K. Holliday, G. M. Way, R. B. Whittle and C. M. Woodward, J. Chem. Soc., Dalton Trans., 1977, 1862.

53. T. Onak and E. Wan, J. Chem. Soc., Dalton Trans., 1974, 665.

54. J. Plesek, B. Stibr and S. Hermanek, Chem. Ind., (London), 1980, 626.

55. H. M. Colquhoun, T. J. Greenhough, M. G. H. Wallbridge, S. Hermanek and J. Plesek, J. Chem. Soc., Dalton Trans., 1978, 944.

56. J. S. Plotkin, R. J. Astheimer and L. G. Sneddon, J. Am. Chem. Soc., 1979, 101, 4155.

57. T. L. Heying, J. W. Agar, S. L. Clark, D. J. Mangold, H. L. Goldstein, M. Hillman, R. J. Polak and J. W. Szymanski, Inorg. Chem., 1963, 2, 1089.

58. H. Baal, Inorg. Chem., 1972, 11, 637.

59. D. Graftstein and J. Dvorak, Inorg. Chem., 1963, 2, 1128.

60. S. Papetti, B. B. Schaeffer, H. J. Troscianiec and T. L. Heying, Inorg. Chem., 1964, 3, 1444.

61. M. Thompson and R. N. Grimes, J. Am. Chem. Soc., 1971, 93, 6677.

62. T. Onak and G. Wong, J. Am. Chem. Soc., 1970, 92, 5226.

63. R. N. Grimes, Acc. Chem. Res., 1978, 11, 420.

64. R. B. Maynard and R. N. Grimes, J. Am. Chem. Soc., 1982, 104, 5983.

65. R. Koster, G. Seidel and B. Wrackmeyer, Angew. Chem., Int. Ed. Engl., 1984, 23, 512.

66. Z. Janousek, S. Hermanek, J. Plesek and B. Stibr, Collect. Czech. Chem. Commun., 1974, 39, 2363.

67. R. J. Astheimer and L. G. Sneddon, Inorg. Chem., 1983, 22, 1928.

68. E. L. Anderson, R. L. Dekock and T. P. Fehlner, J. Am. Chem. Soc., 1980, 102, 2644.

69. T. P. Fehlner, J. Am. Chem. Soc., 1980, 102, 3424; 1977, 99, 8355.

70. M. F. Hawthorne, D. C. Young and P. A. Wegner, J. Am. Chem. Soc., 1965, 87, 1818.

71. M. F. Hawthorne and R. L. Pilling, J. Am. Chem. Soc., 1965, 87, 3987.

72. A. Zalkin, D. H. Templeton and T. E. Hopkins, J. Am. Chem. Soc., 1965, 87, 3988.

73. J. B. Dunitz, L. E. Orgel and A. Rich, Acta Crystallogr., 1956, 9, 373.

74. E. B. Moore, L. L. Lohr and W. N. Lipscomb, J. Chem. Phys., 1961, 35, 1329.

75. W. Moffit, J. Am. Chem. Soc., 1954, 76, 3386.

76. D. St. Clair, A. Zalkin and D. H. Templeton, Inorg. Chem., 1971, 10, 2587.

77. A. Zalkin D. H. Templeton and T. Hopkins, J. Am. Chem. Soc., 1965, 87, 1911.

78. F. V. Hansen, R. G. Hazell, C. Hyatt and G. D. Stuckey, Acta Chem. Scand., 1973, 27, 1210.

79. A. Zalkin D. H. Templeton and T. Hopkins, Inorg. Chem., 1967, 6, 1911.

80. R. M. Wing, J. Am. Chem. Soc., 1967, 89, 5599; 1968, 90, 4828; 1970, 92, 1187.

81. L. F. Warren and M. F. Hawthorne, J. Am. Chem. Soc., 1970, 92, 1157.

82. P. A. Wang, Inorg. Chem., 1975, 14, 212.

83. H. M. Colquhoun, T. J. Greenhough and M. G. H. Wallbridge, J. Chem. Soc., Chem. Commun., 1976, 1019.

84. T. A. George and M. F. Hawthorne, J. Am. Chem. Soc., 1968, 90, 1661; 1969, 91, 5475.

85. D. St. Clair, A. Zalkin and D. H. Templeton, Inorg. Chem., 1972, 11, 377.

86. R. W. Rudolph, R. L. Voorhees and R. E Cochoy, J. Am. Chem. Soc., 1970, 92, 3351.

87. V. Choudry, W. R. Pretzer, D. N. Rai, and R. W. Rudolph, J. Am. Chem. Soc., 1973, 95, 4560.

88. G. B. Dunks and M. F. Hawthorne, J. Am. Chem. Soc., 1970, 92, 7213.

89. W. J. Evans, G. B. Dunks and M. F. Hawthorne, J. Am. Chem. Soc., 1973, 95, 4565.

90. E. L. Hoel, C. E. Strouse and M. F. Hawthorne, Inorg. Chem., 1974, 13, 1388.

91. G. B. Dunks, M. M. McKown and M. F. Hawthorne, J. Am. Chem. Soc., 1971, 93, 2541.

92. D. F. Dustin, G. B. Dunks and M. F. Hawthorne, J. Am. Chem. Soc., 1973, 95, 1109.

93. M. R. Churchill and B. G. DeBoer, Inorg. Chem., 1974, 13, 1411.

94. W. J. Evans and M. F. Hawthorne, J. Chem. Soc., Chem. Commun., 1974, 38.

95. J. R. Pipal and R. N. Grimes, Inorg. Chem., 1978, 17, 6.

96. W. J. Evans and M. F. Hawthorne, J. Chem. Soc., Chem. Commun., 1972, 611.

97. W. J. Evans and M. F. Hawthorne, J. Chem. Soc., Chem. Commun., 1973, 706.

98. W. J. Evans and M. F. Hawthorne, Inorg. Chem., 1974, 13, 869.

99. D. F. Dustin, W. J. Evans and M. F. Hawthorne, J. Chem. Soc., Chem. Commun., 1973, 805.

100. K. P. Callahan, A. L. Sims, C. B. Knobler, F. Y. Lo, and M. F. Hawthorne, Inorg. Chem., 1978, 17, 1658.

101. J. L. Spencer, M. Green and F. G. A. Stone, J. Chem. Soc., Chem. Commun., 1972, 1178.

102. M. Green, J. L. Spencer, F. G. A. Stone, and A. J. Welch, J. Chem. Soc., Dalton Trans., 1975, 179.

103. J. L. Spencer, M. Green, F. G. A. Stone and A. J. Welch, J. Chem. Soc., Chem. Commun., 1974, 571

104. A. J. Welch, J. Chem. Soc., Dalton. Trans., 1975, 1473.

105. M. Green, J. L. Spencer and F. G. A. Stone, J. Chem. Soc., Dalton Trans., 1979, 1679.

106. M. Green J. L. Spencer, F. G. A. Stone, and A. J. Welch, J. Chem. Soc., Chem. Commun., 1974, 794.

107. G. Hardy, K. Callahan, M. F. Hawthorne, Inorg. Chem., Chem. Commun., 1978, 1178.

108. G. K. Barker, M. Green, F. G. A. Stone, A. J. Welch and W. C. Wolsey, J. Chem. Soc., Chem. Commun., 1980, 627.

109. G. K. Barker, M. Green, T. P. Onak, G. Swipanyoyos, F. G. A. Stone and A. J. Welch, J. Chem. Soc., Dalton Trans., 1979, 1687.

110. G. K. Barker, M. Green, T. P. Onak, F. G. A. Stone, C. B. Ungermann and A. J. Welch, J. Chem. Soc., Chem. Commun., 1978, 169.

111. G. K. Barker, M. Green, F. G. A. Stone and A. J. Welch, J. Chem. Soc., Dalton Trans., 1980, 1186.

112. G. K. Barker, M. P. Garcia, M. Green, G. N. Pain, F. G. A. Stone, S. K. R. Jones and A. J. Welch, J. Chem. Soc., Chem. Commun., 1981, 652.

113. M. Green, J. A. K. Howard, J. L. Spencer and F. G. A. Stone, J. Chem. Soc., Chem. Commun., 1974, 153.

114. M. Green, J. A. K. Howard, J. L. Spencer and F. G. A. Stone, J. Chem. Soc., Dalton Trans., 1975, 2274.

115. G. K. Barker, M. P. Garcia, M. Green, F. G. A. Stone , J. M. Bassett and A. J. Welch, J. Chem. Soc., Chem. Commun., 1981, 653.

116. C. J. Jones, J. N. Francis and M. F. Hawthorne., J. Chem. Soc., Chem. Commun., 1972, 900.

117. D. F. Dustin and M. F. Hawthorne, Inorg. Chem., 1973, 12, 1380.

118. D. F. Dustin and M. F. Hawthorne, J. Am. Chem. Soc., 1974, 96, 3462.

119. W. J. Evans and M. F. Hawthorne, J. Am. Chem. Soc., 1974, 96, 301.

120. J. L. Spencer, M. Green and F. G. A. Stone, J. Chem. Soc., Chem. Commun., 1972, 1178.

121. L. G. Sneddon, D. C. Beer and R. N. Grimes, J. Am. Chem. Soc., 1973, 95, 6623.

122. P. A. Wegner, L. J. Guggenberger and E. L. Muettertiea, J. Am. Chem. Soc., 1970, 92, 3473.

123. R. Weiss, J. Bowser and R. N. Grimes, J. Am. Chem. Soc., 1978, 17, 1522.

124. P. L. Timms, Adv. Inorg. Chem. Radiochem., 1972, 14, 121.

125. G. J. Zimmerman, R. Wilcynski and L. G. Sneddon, J. Organomet. Chem., 1978, 154, C29.

126. R. P. Micciche, J. J. Briguglio and L. J. Sneddon, Organometallics, 1984, 3, 1396.

127. G. J. Zimmerman, L. W. Hall and L. G. Sneddon, Inorg. Chem., 1980, 19, 3642.

128. G. K. Barker, M. P. Garcia, M. Green, G. N. Pain, F. G. A. Stone, S. K. R Jones and A. J. Welch, J. Chem. Soc., Chem. Commun., 1981, 652.

129. R. E. Williams, 'Progress in Boron Chemistry', Vol 2, Chapter 2, Pergamon Press, Oxford, 1969.

130. C. C. S. Chaung, R. A. Beaudet and G. A. Segal, J. Am. Chem. Soc., 1970, 92, 4158.

131. E. D. Jemmis, J. Am. Chem. Soc., 1982, 104, 7017.

132. H. V. Hart and W. N. Lipscomb, Inorg. Chem., 1967, 7, 1070.

133. R. Hoffman and W. N. Lipscomb, J. Chem. Phys., 1962, 36, 3489.

134. E. L. Muettertiea and W. H. Knoth, 'Polyhedral Boranes', Marcel Dekker, New York, 1968.

135. A. J. Welch, J. Chem. Soc., Dalton Trans., 1977, 962.

136. A. J. Welch, J. Chem. Soc., Dalton Trans., 1975, 2270.

137. F. G. A. Stone, J. Organomet. Chem., 1975, 100, 257.

138. C. W. Jung, R. T. Baker, C. B. Knobler and M. F. Hawthorne, J. Am. Chem. Soc., 1980, 102, 5782.

139. C. W. Jung, R. T. Baker, M. F. Hawthorne, J. Am. Chem. Soc., 1981, 103, 810.

140. J. E. Crook, M. Elrington, N. N. Greenwood, J. D. Kennedy, and J. D. Woollins, Polyhedron, 1984, 3 (7), 901.

141. J. Bould, J. E. Crook, N. N. Greenwood, J. D. Kennedy, W. S. McDonald, J. Chem. Soc., Chem. Commun., 1982, 346.

142. J. D. Kennedy, Inorg. Chem., 1986, 25, 111.

143. R. T. Baker, Inorg. Chem., 1986, 25, 109.

144. R. C. Johnstone and D. M. P. Mingos, Inorg. Chem., 1986, 25, 3323.

145. W. H. Knoth, J. L. Little and L. J. Todd, Inorg. Synth., 1968, 11, 41.

146. B. Stibr, E. Jancousek, K. Base, J. Plesek, K. A. Solntsev, L. A. Butman, I. I. Kuznetsov, and N. T. Kuznetsov, Collect. Czech. Chem. Commun., 1984, 49, 1660.

147. B. Stibr, E. Jancousek, K. Base, J. Dolansky, S. Hermanek, K. A. Solntsev, L. A. Butman, I. I. Kuznetsov and N. T. Kuznetsov, Polyhedron, 1982, 1, 833.

148. C. G. Salentine, R. R. Rietz, and M. F. Hawthorne, Inorg. Chem., 1974, 13, 3025.

149. N. W. Alcock, J. G. Taylor and M. G. H. Wallbridge, J. Chem. Soc., Chem. Commun., 1983, 1168.

150. K. Base, B. Stibr and I. Zakharova, Synth. React. Inorg. Metal Org. Chem., 1980, 10, 509.

151. K. Base, B. Stibr, G. A. Kukina and I. A. Zakharova, 8th Proc. Conf. Coord. Chem., Slovak Chem. Soc., Bratislava, Czechoslovakia, December, 1980, 17.

152. B. Stibr, K. Base, J. Plesek, S. Hermanek, J. Dolansky and Z. Janousek, Pure and Applied Chem., 1977, 49, 803.

153. W. H. Knoth, J. L. Little and J. R. Lawrence, F. R. Scholer and L. J. Todd, Inorg. Synth., 1968, 11, 33.

154. T. Jelinek, B. Stibr, J. Plesek and S. Hermanek, J. Organomet. Chem., 1986, 307, C13.

155. G. R. Eaton and W. N. Lipscomb, 'NMR Studies of Boron Hydrides and Related Compounds', Benjamin, New York, (1969).

156. A. Bax and R. Freeman, J. Magn. Reson., 1981, 42, 164; 1981, 44, 542.

157. A. Bax and L. Lerner, Science, 1986, 232, 960.

158. T. Venable, W. Hutton and R. N. Grimes, J. Am. Chem. Soc., 1982, 104, 4716; 1984, 106, 29.

159. D. Read, J. Chem. Research, 1984, 198.

160. D. E. Hyatt, D. A. Owen and L. J. Todd, Inorg. Chem., 1966, 5, 1749.

161. D. E. Hyatt, F. R. Scholer, L. J. Todd and J. L. Warner, Inorg. Chem., 1967, 6, 2229.

162. J. Dolansky, S. Hermanek and R. Zahradnik, Collect. Czech. Chem. Commun., 1981, 46, 2479.

163. S. Hermanek and J. Plesek, Z. Anorg. Allg. Chem., 1974, 409, 115.

164. J. D. Kennedy, Prog. Inorg. Chem., 1984, 32, 519; 1986, 34, 211.

165. M. A. Beckett, N. N. Greenwood, J. D. Kennedy, and M. Thornton-Pett, J. Chem. Soc., Dalton Trans., 1986, 795.

166. M. A. Beckett, N. N. Greenwood, J. D. Kennedy, and M. Thornton-Pett, J. Chem. Soc., Dalton Trans., 1985, 1119.

167. S. K. Boocock, J. Bould, N. N. Greenwood, J. D. Kennedy, and W. S. McDonald, J. Chem. Soc., Dalton Trans., 1982, 713.

168. J. W. Lott and D. F. Gaines, Inorg. Chem., 1974, 13, 2261.

169. V. R. Miller and R. N. Grimes, J. Am. Chem. Soc., 1973, 95, 5078.

170. V. R. Miller, R. Weiss and R. N. Grimes, J. Am. Chem. Soc., 1977, 99, 5646.

171. R. Wilczynski and L. G. Sneddon, Inorg. Chem., 1979, 18, 864.

172. M. Bown, X. L. R. Fontaine, N. N. Greenwood, J. D. Kennedy and P. Mackinnon, J. Chem. Soc., Chem. Commun., 1987, 817.

173. N. N. Greenwood, M. J. Hails, J. D. Kennedy, and W. S. McDonald, J. Chem. Soc., Dalton Trans., 1985, 953.

174. T. L. Venable, E. Sinn and R. N. Grimes, Inorg. Chem., 1982, 21, 895.

175. S. K. Boocock, N. N. Greenwood, M. J. Hails, J. D. Kennedy, and W. S. McDonald, J. Chem. Soc., Dalton Trans., 1981, 1415.

176. C. J. Jones, J. N. Francis and M. F. Hawthorne, J. Am. Chem. Soc., 1972, 94, 8391.

177. B. Stibr, S. Hermanek, J. Plesek, K. Base and I. Zakharova, Chem. Ind., (London), 1980, 468.

178. T. P. Hanusa, J. C. Huffman, T. L. Curtis and L. J. Todd, Inorg. Chem., 1985, 24, 787.

179. J. J. Briguglio and L. G. Sneddon, Organometallics, 1986, 5, 327.

180. J. E. Crooks, N. N. Greenwood, J. D. Kennedy, and W. S. McDonald, J. Chem. Soc., Chem. Commun., 1981, 933.

181. K. A. Solntsev, L. A. Butman, I. Yu. Kuznetsov, N. T. Kuznetsov, B. Stibr, E. Jancusek and K. Base, Koord. Khim., 1983, 9(7), 586.

182. C. G. Salentine and M. F. Hawthorne, J. Am. Chem. Soc., 1975, 97, 6382.

183. G. E. Hardy, K. P. Callahan and M. F. Hawthorne, Inorg. Chem., 1978, 17, 1662.

184. O. W. Howarth, M. J. Jaszta1 and M. G. H. Wallbridge, Polyhedron, 1985, 4, 1461.

185. N. N. Greenwood, J. D. Kennedy, M. Thornton-Pett and J. D. Woolins, J. Chem. Soc., Dalton Trans., 1985, 2397.

186. O. W. Howarth, M. J. Jaszta1 and M. G. H. Wallbridge, unpublished work.

187. K. P. Callahan, F. Y. Lo, C. E. Strouse, A. L. Sims and M. F. Hawthorne, Inorg. Chem., 1974, 13, 2842.

188. J. Bould, J. E. Crook, N. N. Greenwood and J. D. Kennedy, J. Chem. Soc., Dalton Trans., 1984, 1903.

189. N. N. Greenwood, J. D. Kennedy, M. Thornton-Pett and J. D. Woolins, J. Chem. Soc., Dalton Trans., 1987, 275.

190. R. F. Sprecher, B. E. Aufderheide, G. W. Luther and J. C. Carter, J. Am. Chem. Soc., 1974, 96, 4404.

191. R. F. Sprecher and B. E. Aufderheide, Inorg. Chem., 1971, 10, 1096.

192. R. E. Williams and T. P. Onak, J. Am. Chem. Soc., 1964, 86, 3159.

193. R. D. Dobrott and W. N. Lipscomb, J. Chem. Phys, 1962, 37, 1779.

194. R. Hoffmann, Angew. Chem., Int. Ed. Engl., 1982, 21, 771.

195. J. W. Lauher and K. Wald, J. Am. Chem. Soc., 1981, 103, 7648.

196. B. F. G. Johnson, D. A. Kaner, J. Lewis, P. R. Raithby and M. J. Taylor, J. Chem. Soc., Chem. Commun., 1982, 314.

197. L. J. Farrugia, A. K. Howard, P. Mitrprachachon, J. L.Spencer, F. G. A. Stone and P. Woodward, J. Chem. Soc., Chem. Commun., 1978, 260.

198. L. W. Bateman, M. Green, K. A. Mead, R. M. Mills, I. D. Slater. F. G. A. Stone and P. Woodward, J. Chem. Soc., Chem. Commun., 1983, 2599.

199. N. W. Alcock, L. Parkhill and M. G. H. Wallbridge, Acta Cryst., 1985, C41, 716.

200. L. F. Warren and M. F. Hawthorne, J. Am. Chem. Soc., 1968, 90, 4823.

201. H. M. Colquhoun, T. J. Greenhough and M. G. H. Wallbridge, J. Chem. Soc., Dalton Soc., 1978, 303.

202. A. J. Wynd, S. E. Robins, D. A. Walch and A. J. Walch, J. Chem. Soc., Chem. Commun., 1985, 819.

203. T. J. Bargendahl and J. H. Waters, Inorg. Chem., 1975, 14, 2556.

204. A. J. Wynd, A. J. McLennan, D. Read and A. J. Walch, J. Chem. Soc., Dalton Trans., 1987, 2761.

205. A. J. Wynd and A. J. Walch, J. Chem. Soc., Chem. Commun., 1987, 1174.

206. J. W. A. Van der Velden, P. T. Beurskens, J. J. Bour, W. P. Bosman, J. H. Noordik, M. Kolenbrander, and J. A. K. M. Buskes, Inorg. Chem., 1984, 23 (2), 146.

207. M. I. Bruce and B. K. Nicholson, J. Chem. Soc., Chem. Commun., 1982, 1141.

208. C. A. Tolman, Chem. Rev., 1977, 77, 313.

209. D. M. P. Mingos, Inorg. Chem., 1982, 21, 464.

210. E. A. McNeill and F. R. Scholer, J. Am. Chem. Soc., 1977, 99, 6243.

211. J. E. Ellis, J. Am. Chem. Soc., 1981, 103, 6106.

212. D. M. P. Mingos, J. Chem. Soc., Dalton Trans., 1976, 1163.

213. K. P. Hall and D. M. P. Mingos, Prog. Inorg. Chem., 1984, 32, 237.

214. P. Jennische, H. Anacker-Eickhoff and A. Wahlberg, Acta Crystallogr., 1975, A31, 5143.

215. A. R. Sangar, J. Chem. Soc., Chem. Commun., 1975, 893.

216. W. S. Crane and H. Basil, Inorg. Chim. Acta, 1978, L469, 31.

217. J. W. A. van der Velden, J. J. Bour, J. J. Steggarda, P. T. Beurskens, M. Roseboom and J. H. Noordik, Inorg. Chem., 1982, 4321.

218. F. Cariati, L. Naldini, G. Simonetta and L. Maltesta, Inorg. Chim. Acta., 1967, 1, 315.

219. F. Cariati, L. Naldini, G. Simonetta and L. Maltesta, J. Chem. Soc., Chem. Commun., 1966, 647.

220. J. G. M. van der Linden, M. L. Paulissen and J. E. J. Schmitz, J. Am. Chem. Soc., 1983, 105, 1903.

221. B. Lorenz, R. Kirmse and E. Hoyer, Z. Anorg. Allg. Chem., 1970, 378, 144.

222. S. J. Barnars-Price, M. A. Mazid and P. J. Sadler, J. Chem. Soc., Dalton Trans., 1984, 969.

223. L. F. Warren and M. A. Bennett, Inorg. Chem., 1976, 15, 3126.

224. D. D. Perrin, W. L. F. Armarego and D. R. Perrin, 'Purification of Laboratory Chemicals', 2nd Ed., Pergamon Press, Oxford, 1980.

225. W. C. Still, M. Kahn and A. Mitra, J. Org. Chem., 1978, 43, 2923.

226. N. Ahmad, J. J. Levison, S. D. Robinson and M. F. Uttley, Inorg. Synth., 1974, 15, 45.

227. L. Vaska, J. Am. Chem. Soc., 1964, 86, 1942.

228. M. I. Bruce, C. Hameister, A. G. Swincar and T. C. Wallis, Inorg. Synth., 1982, 21, 78.

229. C. Kowala and J. M. Swan, Aust. J. Chem., 1966, 19, 547.

230. G. Calvin, G. E. Coates and P. S. Dixon, Chem. Ind. (London), 1959, 1628.

231. K. Issleib, A. Brack, Z. Anorg. Allg. Chem., 1954, 277, 258.

232. J. Bailey, J. Inorg. Nucl. Chem., 1973, 35, 1921.

233. N. W. Alcock, in 'Crystallographic Computing,' ed. F. Ahmed, Munksgaard, Copenhagen, 1970.

234. G. M. Sheldrick, SHELTEX User Manual, Nicolet Instrument Co., Wisconsin, 1981.

235. 'International Tables for X-Ray Crystallography,' Kynoch Press, Birmingham, 1974, Vol. 4.

236. J. M. M. Smits, P. T. Beurskens and J. J. Steggerda, J. Cryst. Spec. Res., 1983, 13, 381.

237. 'X-Ray Structure Determination - A Practical Guide', G. H. Stout and L. H. Jensen, Macmillan, New York, 1968.

238. 'Crystal Structure Analysis - A Primer', J. P. Glusker and K. N. Trueblood, Oxford University Press, Oxford, New York, 1972.

239. Handbook of Chemistry and Physics, 65th Edition, CRC Press, Florida, 1984.

240. F. Teixidor, C. Vinas and R. Rudolph, Inorg. Chem., 1986, 25, 3339.

241. O. W. Howarth, M. J. Jaastal, J. G. Taylor and M. G. H. Wallbridge, unpublished work.

242. X. L. Fontaine and J. D. Kennedy, J. Chem. Soc., Chem. Commun., 1986, 799.

243. S. Hermanek, J. Fusek, B. Stibr, J. Plesek and T. Jelinek, Polyhedron, 1986, 5(11), 1873.

244. B.Stibr, T. Jelinek, J. Plesek and S. Hermanek, J. Chem. Soc., Chem. Commun., 1987, 963.

245. X. L. R. Fontaine, H. Fowkes, N. N. Greenwood, J. D. Kennedy and M. Thornton-Pett, J. Chem. Soc., Dalton Trans., 1987, 2417.

TITLE ..... A STUDY OF MONOCARBON CARBABORANES AND SOME METALLA DERIVATIVES .....

AUTHOR ..... Michael John Jasstal .....

INSTITUTION and DATE ..... University of Warwick 1988 .....